



**Max-Planck-Institut für Metallforschung**  
Stuttgart

---

# **Thermochemistry and Constitution of Precursor-Derived Si-(B-)C-N Ceramics**

Jianqiang Peng

Dissertation  
an der  
**Universität Stuttgart**

---

Bericht Nr. 123  
Juli 2002

# **Thermochemistry and Constitution of Precursor-Derived Si-(B-)C-N Ceramics**

Von der Fakultät Chemie der Universität Stuttgart  
zur Erlangung der Würde eines Doktors der  
Naturwissenschaften (Dr. rer. nat.) genehmigte Abhandlung

vorgelegt von

**Jianqiang Peng**

aus Baotou, China

Hauptberichter:	Prof. Dr. rer. nat. F. Aldinger
Mitberichter:	Prof. Dr. rer. nat. Dr. h. c. mult. G. Petzow
Mitprüfer:	Prof. Dr. Ir. E. J. Mittemeijer
Prüfungsvorsitzender :	Prof. Dr. Ir. E. J. Mittemeijer
Tag der mündlichen Prüfung:	10.07.2002

Institut für Nichtmetallische Anorganische Materialien der Universität Stuttgart  
Max-Planck-Institut für Metallforschung  
Pulvermetallurgisches Laboratorium / Abteilung Aldinger

Stuttgart 2002

献给我的爱妻田鑫及家人朋友

## Acknowledgements

This Ph. D work has been carried out from November 1997 to March 2001 in the Max-Planck-Institute for Metals Research, Stuttgart and University of Stuttgart. Financial support of the German Research Foundation (DFG) is gratefully acknowledged.

I would like to thank my advisor, Prof. Dr. F. Aldinger for the opportunity to work on the interesting project and for the support during my work on this thesis. I particularly appreciated his teachings on many aspects of scientific research, many fruitful discussions and providing the possibility to present the results at international conferences. Without the encouragement and continual support from Prof. Dr. F. Aldinger, this work would not have been possible.

My special thanks to my group leader Dr. H. J. Seifert. This thesis is greatly marked by his fingerprints and is the fruit of several years of our close scientific collaboration. It was a nice experience. During that time, I have learnt much from his serious attitude towards scientific work.

I would like to thank Prof. Dr. G. Petzow, who friendly helped me and agreed to become the “Mitberichter” (co-examiner) for my examination.

I am grateful to Dr. I. Arpshofen for many useful discussions and for his suggestions to improve the quality of this manuscript.

There were many people in MPI-PML who taught me and helped me. Dr. H. L. Lukas and Dr. J. Golczewski taught me phase diagram calculations. With Dr. J. Bill, Dr. M. Weinmann and Dr. A. Müller I had many intensive discussions. Ms. M. Thomas helped to do XRD analyses. Dr. Y. Cai and Dr. A. Zimmermann helped to do TEM observations. Mr. H. Kummer helped to do DTA/TG and dilatometry investigations. Mr. H. Labitzke helped to do SEM observations. Mr. D. Matusch helped me to operate the high-temperature furnace. Dr. T. Ludwig helped me to operate DSC. Mr. E. Bruckner provided computer services. Mr. P. Gerstel, Dr. J. Seitz and Ms. S. Prinz provided samples. Dr. O. Fabrichnaya helped me by checking the thermodynamic data set. With Ms. S. Wagner and Mr. R. Weiland I had interesting discussions. My new group leader Dr. M. Zinkevich supported me. I would like to take this opportunity to express my sincere thanks to them.

There were many other people in PML who made my work and life easier and full of fun. Ms. S. Paulsen and Ms. J. Weber-Bock always knew how to help me out and always with a smile. Ms. C. Garcia and Ms. U. Demko helped me so much. Dr. A. Rosinus, Mr. S.-H. Lee, Mr. G. Stieger, Mr. R. Kumar, Dr. S.-J. Jia and Mr. X.-B. Yu are nice people to share an office. With my Chinese colleagues Mr. J.-H. Yang, Dr. Y. Zeng, Dr. L. Wang and Dr. H. Ye, I had also many interesting discussions. There were many other people I can not list all but I would like to thank all of them who have ever helped me.

Many German friends outside our institute helped me also so much, e. g. Mr. W. Ahl, Dr. H. Kockelmann, Family Dr. Richter and Family Hartmann, they invited my family to have dinner with them and introduced to German culture and encouraged me. Thank you very much.

My Family has always been behind me and always been a source of support in many forms. My parents and my parents in law encouraged me. My daughter Ruiqi and my son Jiaqi made me very happy. The biggest support was from my lovely wife: Xin. Thank you very much.

Jianqiang Peng

# Contents

<b>Abstract.....</b>	<b>3</b>
<b>1 Introduction .....</b>	<b>6</b>
<b>2 Literature Review.....</b>	<b>8</b>
2.1 Precursor-Derived Si-(B-)C-N Ceramics .....	8
2.2 Fundamentals of Thermodynamic Calculations (The CALPHAD method).....	11
2.3 Thermodynamic Data .....	18
2.3.1 The Si-B-C-N system.....	18
2.3.2 The Si-C-N-H System.....	22
<b>3 Experimental Procedures .....</b>	<b>26</b>
3.1 Sample preparation.....	26
3.2 Sample analyses .....	31
3.2.1 X-ray diffraction analysis (XRD), scanning electron microscopy (SEM) and high-resolution transmission electron microscopy (HRTEM).....	31
3.2.2 Differential thermal analysis (DTA) and thermogravimetric analysis (TGA).....	31
3.2.3 Chemical analysis.....	31
3.2.4 Dilatometry (thermal expansion).....	32
3.2.5 Laser-Flash method (thermal conductivity).....	34
<b>4 Phase Equilibria, Phase Reactions and Thermal Stability of Precursor-Derived Si-(B-)C-N Ceramics .....</b>	<b>37</b>
4.1 Si-C-N System.....	37
4.1.1 Thermodynamic calculations.....	37
4.1.2 Experimental investigations and discussion.....	47
4.1.3 Conclusion.....	54
4.2 Si-B-C-N System.....	56
4.2.1 Thermodynamic calculations.....	56
4.2.1.1 Isothermal sections.....	56
4.2.1.2 Isothermal sections at constant boron contents.....	59
4.2.1.3 Temperature composition sections (isopleths).....	65

4.2.1.4 Scheil's reaction scheme.....	68
4.2.1.5 Phase fraction diagrams.....	68
4.2.1.6 Partial pressure diagrams.....	73
4.2.2 Experimental investigations.....	74
4.2.2.1 T2-1 precursor-derived ceramic.....	74
4.2.2.2 MW33 precursor-derived ceramic and MW36 precursor-derived ceramic.....	78
4.2.2.3 BNCP precursor-derived ceramic and T2-1 (NH <sub>3</sub> /Ar) precursor-derived ceramic.....	79
4.2.2.4 BVT50 precursor-derived ceramic.....	81
4.2.3 Discussion and Summary.....	83
<b>5 Phase Equilibria and Constitution in the Si-C-N-H System .....</b>	<b>93</b>
<b>6 Thermophysical Properties of Precursor-Derived Amorphous Si-(B-)C-N Ceramics .....</b>	<b>103</b>
6.1 Thermal expansion .....	103
6.2 Heat capacity .....	110
6.3 Thermal conductivity .....	111
6.4 Conclusion.....	115
<b>Zusammenfassung (Extended abstract in German) .....</b>	<b>116</b>
<b>References .....</b>	<b>124</b>

## Abstract

The synthesis of Si-(B-)C-N ceramics from precursor polymers is a novel way to produce ceramics for high temperature use. For the development and application of precursor ceramics, their thermal stabilities, crystallization behavior and their thermophysical properties are of crucial importance.

The thermal stability and the crystallization behavior of precursor-derived ceramics have important consequences with regard to the physico-chemical properties of the polycrystalline ceramics and to the maximum application temperature of the amorphous ceramics. A deep understanding of the multicomponent phase equilibria and phase reactions in the underlying Si-(B-)C-N system is required. Therefore, within the scope of the present work the phase equilibria and phase reactions of Si-C-N and Si-B-C-N precursor ceramics, respectively, were studied by means of CALPHAD method combined with experimental studies: e. g. DTA/TG, XRD, HRTEM and SEM. Thermodynamic calculations of different types of phase diagrams, phase fraction diagrams and phase composition diagrams in regard to the reaction behavior of Si-C-N and Si-B-C-N precursor ceramics were carried out using softwares such as THERMOCALC/PARROT and BINGSS/BINFKF. Consistent Scheil's reaction schemes for the ternary system Si-C-N and the quaternary system Si-B-C-N are presented. The constitution of the system Si-(B-)C-N is comprehensively disclosed. DTA was combined with TG to investigate the phase reactions and the thermal stability of precursor-derived Si-(B-)C-N ceramics. The materials were characterized up to a temperature of 2200°C. XRD, HRTEM and SEM were used to determine the microstructures and the phase compositions of the as-thermolyzed materials and the heat treated products. TEM study shows that the phase reactions are significantly influenced by specific nanocrystalline microstructures. A large variety of different types of samples were investigated systematically. On this basis, the thermal decomposition of Si-C-N ceramics as well as the high temperature stability of specific Si-B-C-N ceramics are explained and physico-chemical criteria for the development of high-temperature stable precursor ceramics are derived.

The thermal degradation of precursor-derived Si-C-N ceramics has been characterised quantitatively by taking into account the endothermic phase reactions  $\text{Si}_3\text{N}_4 + 3\text{C} = 3\text{SiC} + 2\text{N}_2$  (1484°C) and  $\text{Si}_3\text{N}_4 = 3\text{Si} + 2\text{N}_2$  (1841°C). Because of the first reaction the thermal stability of the Si-C-N ceramics is limited to some 1550°C to 1600°C. Both reactions influence the



crystallization behavior of the metastable amorphous as-thermolyzed materials. The results of thermodynamic calculations are in good agreement with the experimental results and describe very well quantitatively the high temperature behavior of the ceramics.

The incorporation of boron in Si-C-N ceramics can increase the thermal stability up to much higher temperatures. The XRD patterns of individual precursor-derived Si-B-C-N ceramics after DTA/TG with the highest temperature of 2200°C show that the material still consists of  $\beta$ -Si<sub>3</sub>N<sub>4</sub> besides  $\beta$ -SiC. The HRTEM images of these ceramics show Si<sub>3</sub>N<sub>4</sub> grains “encapsulated” by a metastable matrix phase composed of BN and carbon with varying compositions (BNC<sub>x</sub>). Ceramics with compositions located in the center of the four-phase equilibrium Si<sub>3</sub>N<sub>4</sub>+SiC+BN+graphite and close to the three-phase equilibrium SiC+BN+graphite have shown to have this kind of microstructure in a marked way and therefore being thermally so stable. Thus a minimum of boron seems to be necessary to form this metastable matrix phase by which the activity of the carbon not bond to silicon is obviously substantively reduced with respect to its reaction with silicon bond to nitrogen. By calculation of carbon activity versus temperature diagrams and nitrogen partial pressure versus temperature diagrams the influence of decreasing carbon activity and intrinsic pressure increases (encapsulation effects) on the phase equilibria are described quantitatively. It can be concluded that both effects, i. e. (1) significantly decreased carbon activity and (2) encapsulation effect cause the high temperature stability of precursor-derived Si-B-C-N ceramics, if materials gross composition and the microstructure are controlled. A model for the phase formation was developed which can describe qualitatively the thermal stability in dependence of material composition. It can be suggested that amorphous ceramics that exhibit a composition within the four-phase equilibrium space Si<sub>3</sub>N<sub>4</sub>+SiC+C+BN consist of Si<sub>3+y/4</sub>C<sub>y</sub>N<sub>4-y</sub> that can be derived from the structural units of silicon nitride (SiN<sub>4</sub>) and carbide (SiC<sub>4</sub>) as well as of a matrix phase BCN<sub>x</sub> present in sp<sup>2</sup> graphite and hexagonal BN. Crystallization of the Si<sub>3+y/4</sub>C<sub>y</sub>N<sub>4-y</sub> phase results in a demixing into SiN<sub>4</sub> and SiC<sub>4</sub> units. Further growth of these nuclei leads to the formation of Si<sub>3</sub>N<sub>4</sub> and SiC nanocrystallites within the surrounding BNC<sub>x</sub> matrix. The calculated B:N:C atomic ratio of BNC<sub>x</sub> turbostratic layers is in good agreement with EELS investigations.

In addition, phase reactions of polymer-precursors of the system Si-C-N-H and resulting compositions were calculated also by the CALPHAD method. The results were compared to experimentally derived compositions and gaseous products formed by thermolysis at

temperatures up to 1050°C. The comparison shows that a semi-quantitative description of the thermolysis process by the CALPHAD method is possible.

The thermal expansion behavior of some precursor-derived amorphous Si-C-N and Si-B-C-N ceramics, which were shaped by plastic forming after crosslinking, were studied applying high-temperature differential dilatometry. The thermal expansion coefficient of VT50-derived amorphous Si-C-N ceramic increases from  $1.98 \times 10^{-6}/\text{K}$  at 400°C to  $3.09 \times 10^{-6}/\text{K}$  at 1000°C, of NCP200-derived amorphous Si-C-N ceramic increases from  $2.35 \times 10^{-6}/\text{K}$  at 400°C to  $3.45 \times 10^{-6}/\text{K}$  at 1000°C, and of T2-1-derived amorphous Si-B-C-N ceramic increases from  $2.08 \times 10^{-6}/\text{K}$  at 400°C to  $3.18 \times 10^{-6}/\text{K}$  at 1000°C, which are comparable with those of crystallized  $\text{Si}_3\text{N}_4$ . No glass transition for these amorphous ceramic materials was detected, indicating that as-thermolized precursor-derived Si-(B-)C-N ceramic materials are amorphous solids, but not glasses in the term of definition of glasses.

Measurements of the thermal diffusivity of precursor ceramics were carried out using the laser flash method. From these data the thermal conductivity has been derived by calculating the heat capacities of the ceramics and measuring their densities. The thermal conductivities are between 0.77 and 1.43 W/mK in the temperature range from 100 until 1200°C.

# 1 Introduction

Ceramics of the system Si-B-C-N are suitable candidates for high temperature applications because of their thermal, chemical and mechanical high temperature stability [83Lan, 87Gre, 87Zie, 91Lan, 93Hof]. Materials such as  $\text{Si}_3\text{N}_4$ , SiC, BN,  $\text{B}_{4+\delta}\text{C}$  and  $\text{Si}_3\text{N}_4/\text{SiC}$  composites are conventionally prepared by powder technology. Densification of the powder compact is commonly performed by sintering, which requires high temperatures as well as the use of sintering aids to overcome the low self-diffusion coefficients of such highly covalent bonded ceramic materials. These sintering aids form oxide-type secondary phases with increased atomic mobility substantially degrading the thermal, chemical and mechanical high temperature stability.

An alternative approach that recently has attracted wide attention is the use of precursor polymers [85Tak, 90Peu, 92Rie, 95Bil1, 96Rie1, 97Bal, 98Ald, 00Wei], which offers a number of advantages compared to classic powder technology. Novel ceramics with high temperature stability and with good oxidation resistance can be obtained from molecular units without sintering aids. These ceramics have a homogeneous chemical distribution on an atomic scale and controllable microstructures and properties. For several applications such as the preparation of ceramic coatings, ceramic fibres, and fibre-reinforced composites of ceramic matrices, the precursor route is the practical way [95Bil1, 99Bal].

According to this route, precursor polymers are synthesized from monomer units. Then these polymers are thermally transformed into metastable amorphous covalent ceramic materials via cross-linking and thermolysis. During further heat treatments at higher temperatures these amorphous ceramic materials are transformed into crystalline ceramics consisting of thermodynamically stable and metastable phases. Since the pyrolysis products can be used both as amorphous and crystalline materials, the understanding of the high temperature behavior of the ceramics, the phase reactions and the crystallization behavior as well as the accompanying materials thermal degradation are of great importance with respect to the physico-chemical properties of the polycrystalline ceramics and to the maximum application temperature of the amorphous ceramics.

Thus thermal stability has been recognized as a key aspect with respect to the development and application of precursor-derived ceramics. Thermal stability of the precursor-derived amorphous ceramics should cover several implications, such as chemical

stability which is related to the decomposition of the materials (high temperature mass stability), structure stability which is associated with crystallization and phase transition processes (amorphous state up to high temperatures), and good resistance against oxidation. The Si-C-N materials remain amorphous up to 1500°C and resist oxidation and thermal decomposition at temperatures up to 1600°C [92Rie]. The addition of boron to Si-C-N materials increases their thermal stability and the temperature of crystallization. Some Si-B-C-N materials remain amorphous up to temperatures of 1700°C and do not decompose significantly up to 2000°C [95Rie, 97Bal, 00Wei]. However, some Si-B-C-N ceramics decompose already at temperatures between 1600°C and 1800°C [00Pen2, 00Wei].

Up to now, understanding of these phenomena has been scarcely developed, especially on the quantitative explanation of the thermal stability of these amorphous ceramics. The main goal of this work is to systematically study chemical stability (the high temperature mass stability) and structure stability with respect to the phase equilibria and phase reactions of the Si-B-C-N ceramics. A first approach to understand these multicomponent materials is the treatment of the ternary Si-C-N ceramics. To explain in detail the high temperature behavior of these ceramics, various types of phase diagrams and phase fraction diagrams were calculated using the datasets of the Si-B-C-N system developed by Kasper et al. [96Kas1, 96Kas2, 02Sei]. By combining these calculations with results of microstructure investigations by high resolution transmission electron microscopy (HRTEM) a model for the explanation of the high temperature behavior of these ceramics is proposed.

Additionally, the understanding of the transformation of precursor polymers into amorphous Si-(B-)C-N ceramics is important to develop efficiently the ceramics according to the precursor route. To understand this thermolysis process phase equilibrium calculations in the Si-C-N-H system were carried out by taking into account recent thermodynamic data.

Finally, the thermophysical properties (e.g. thermal expansion, specific heat and thermal conductivity) of precursor-derived Si-(B-)C-N ceramics are important for the determination of the fabrication process and the choice of composites when these materials are used in high-temperature applications. In the present work, thermal expansion behavior and thermal conductivity of some precursor-derived Si-(B-)C-N amorphous ceramics were measured and specific heats of these materials were calculated. It was discussed, whether these precursor-derived amorphous ceramics are glasses.

## 2 Literature Review

### 2.1 Precursor-Derived Si-(B-)C-N Ceramics

The synthesis of Si-(B-)C-N ceramics from precursor polymers is an ideal way to control the materials structure and properties in order to achieve an architectural design for advanced ceramics based on atomic or molecular units. Since the pioneering work of Popper [67Pop] as well as Verbeek and Winter [74Ver] in addition to Yajima's work [76Yaj] in the mid 1970's, a wide variety of precursors have been developed for the preparation of different non-oxide Si-(B-)C-N ceramics [85Tak, 90Sey, 92Rie, 93Su, 94Bal, 96Rie1, 97Lüc, 97Wei, 98Sri, 99Jün, 99Wei, 00Wei] and the results have been reviewed recently in several articles [90Pai, 91Tor, 95Bil1, 95Bir, 96Rie2, 97Ald, 97Jan, 98Ald, 98Lai, 00Rie].

The preparation of ceramics from organometallic compounds containing precursor substances can be started via solid state thermolysis (SST), chemical vapor deposition (CVD) or chemical liquid deposition (CLD) [99Bil]. The general idea of these processes is that the initial molecules already contain structural units of the produced ceramic material. This is illustrated in Fig. 2-1 [95Bil1, 98Ald] giving an overview of the different types of organosilicon polymers which can be used for the preparation of silicon-containing ceramics. Si can be lined with Si-, C-, and N-containing units to form polymers with a variety of molecular structures. Moreover, polymers containing further elements like B, Al, Ti or P can be synthesized.

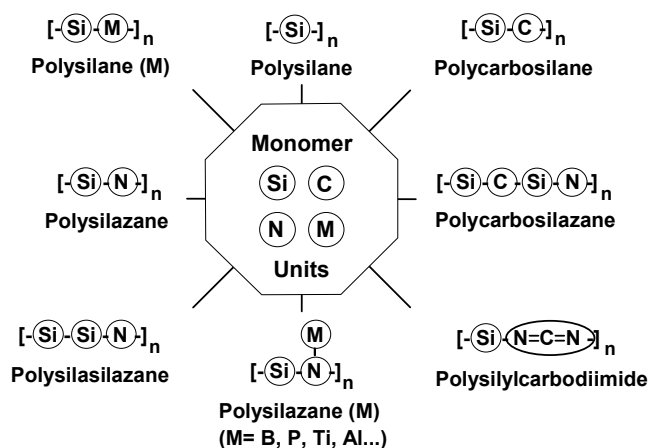


**Fig. 2-1** Formation of organosilicon polymers from monomer units [95Bil, 98Ald].

The preparation of Si-(B-)C-N ceramics from organometallic compounds consists of the following steps (Fig. 2-2): Synthesis of polymers from monomer units according to the monomer route and the polymer route, cross-linking of these precursors to form unmeltable preceramic networks, thermolysis of the networks into amorphous covalent ceramics and crystallization of the amorphous ceramics into thermodynamically stable crystalline materials with micro-nanostructures (Fig. 2-3). The main advantage of this process is that high purity novel amorphous covalent materials with high temperature stability can be produced, which is not obtainable with conventional methods. Depending on heat treatment conditions the pyrolysis products can be produced as amorphous or as crystalline materials. By precursor processing many products such as ceramic monoliths, ceramic matrixes, powders, fibers, infiltration, coatings and other types of performs can be manufactured. Of special interest is the production of dense bulk materials, fibers and coatings for high-temperature engine applications. Fig. 2-4 shows as examples carbon fiber reinforced silicon carbide (C/C-SiC) coated with a precursor-derived Si-B-C-N ceramic by means of dip-coating [95Bil, 95Hei] and Si-B-C-N ceramic fibers prepared by melt-spinning [99Bal].

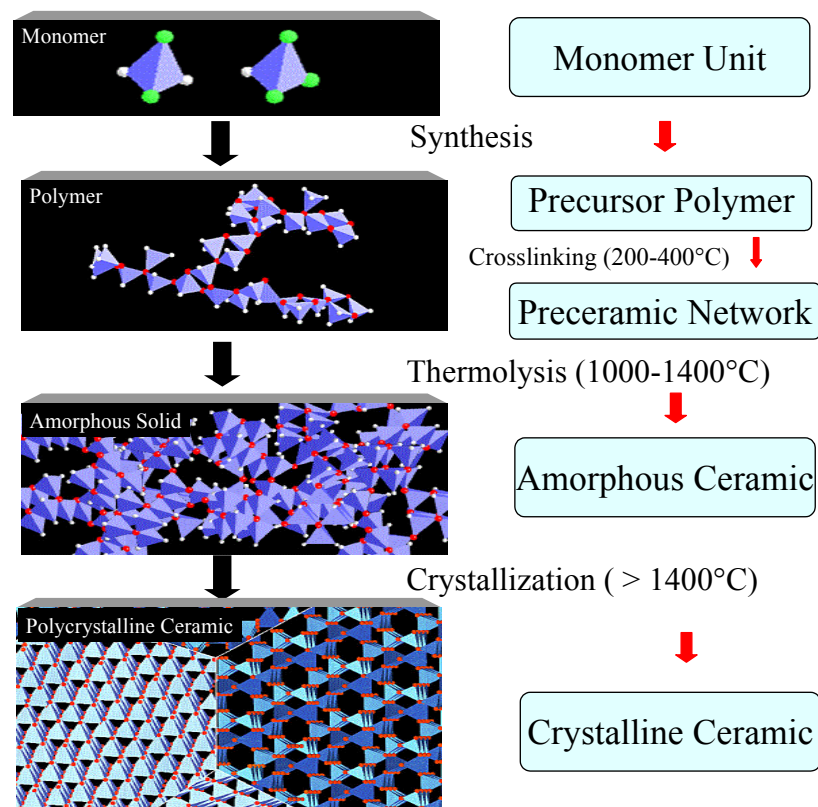


**Fig. 2-2** Process of precursor-derived Si-(B-)C-N ceramics [97Ald].

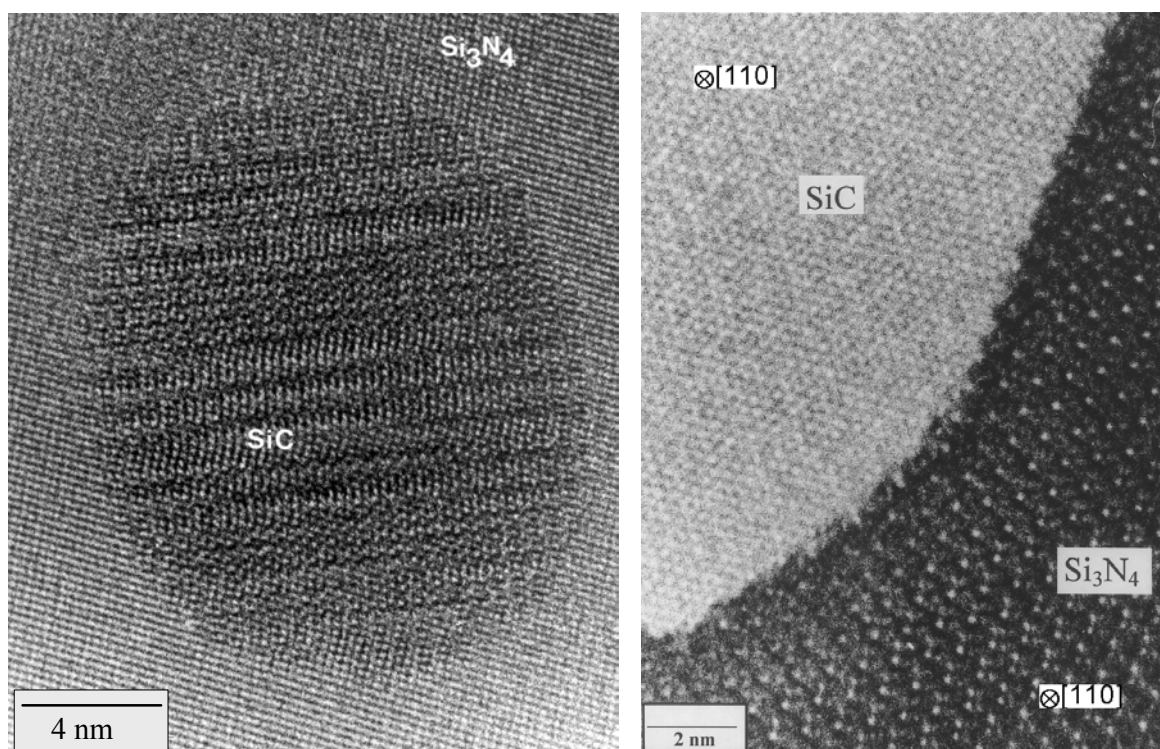


**Fig. 2-3** HRTEM images showing a nano SiC inclusion within a matrix made of  $\text{Si}_3\text{N}_4$ , completely clean grain boundaries between the  $\text{Si}_3\text{N}_4$  and SiC crystals are formed. The material is NCP200-derived Si-C-N ceramic, annealed at 1800°C for 50 h in a nitrogen atmosphere [00Bil1].

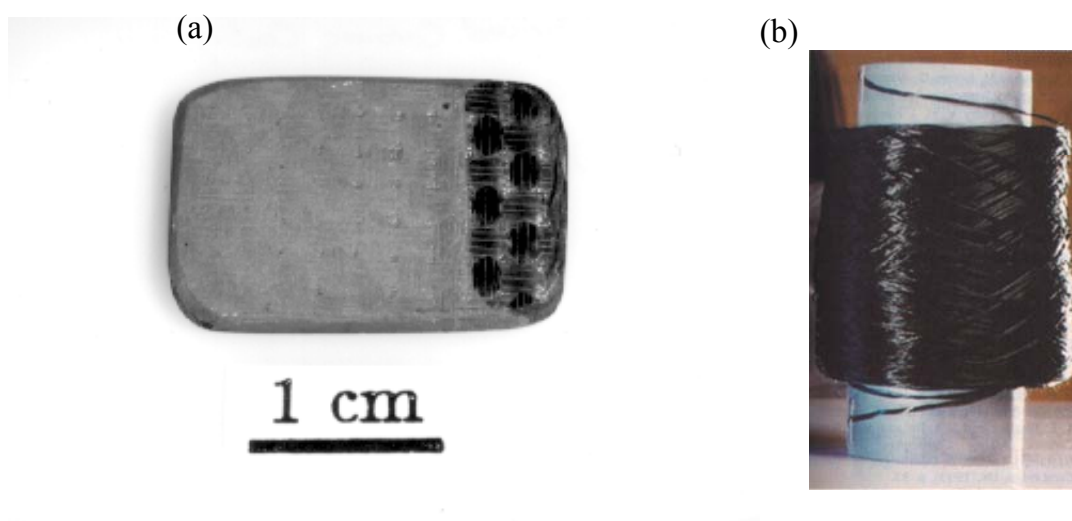


**Fig. 2-4** Materials for applications made from precursor-derived Si-B-C-N ceramics. (a) Carbon fiber reinforced silicon carbide coated with a precursor-derived Si-B-C-N ceramic [95Bil, 95Hei]; (b) Si-B-C-N ceramic fibers [99Ba].

## 2.2 Fundamentals of Thermodynamic Calculations (The CALPHAD method)

### 2.2.1 The CALPHAD method

CALPHAD is an acronym for the CALculation of PHase Diagrams but it is also well defined by the sub-title of the CALPHAD journal, *The Computer Coupling of Phase Diagrams and Thermochemistry* [98Sau]. The major achievement of the CALPHAD method is the calculation of phase equilibria, phase reactions and thermodynamic functions under physico-chemical conditions not sufficiently subjected to experimental investigations. Especially with this method, it is possible to extrapolate by calculation the phase behavior of multicomponent systems from their lower-order binary and ternary systems.

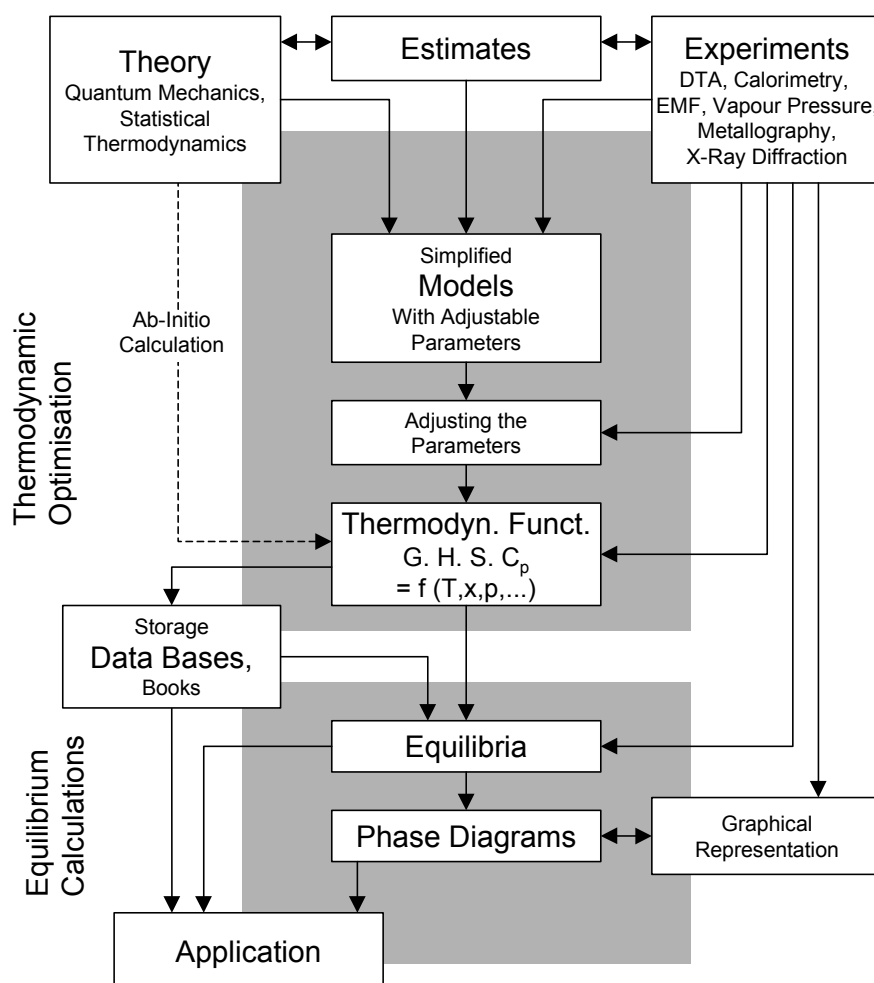


**Fig. 2-5** A scheme of the CALPHAD method [96Sei1].



A scheme of the CALPHAD method is shown in Fig. 2-5 [96Sei1]. Receiving reliable results from extrapolating calculations requires self-consistent high quality analytical descriptions of all thermodynamic functions of state. Therefore, analytical formulae describing the Gibbs energies for all stable phases and gas species of the particular system have to be provided. In the course of the so-called “thermodynamic optimization” model parameters are adjusted to various types of experimental data, using the least squares method after Gauss. The experimental data used for optimization may comprise all kinds of quantitative phase equilibrium data, and of course results of measurements of the calorimetric heat, of emf and of vapour pressure data due to chemical potentials. In case of insufficient experimental data, estimates could be taken into account, if available ab-initio data can also be used for optimization. The thermodynamic data are stored in a computer database and binary and ternary system descriptions can then be combined to extrapolate to multicomponent phase diagrams, if no further phases exist and if the higher order excess parameters are assumed to be zero. The determination of the thermodynamic equilibrium is based on the minimization of the Gibbs energy of a multicomponent system with consideration of the phase rule. Experimentally unexplored regions of temperature, concentration and pressure can be calculated and further key-experiments can be planned on this basis in order to prove previous assumptions or to improve the quality of the data.

Well-established CALPHAD software packages are available and used in this work such as BINGSS/BINFKT developed by Lukas [77Luk, 92Luk] and THERMO-CALC of Sundman et al. [85Sun]. Especially the Poly-3 program from the THERMO-CALC set was used for phase diagram calculations according to the method of minimization of the Gibbs energy. For the success of the CALPHAD method when applied to a practical problem it is crucial that the most appropriate diagrams for the particular case in consideration are calculated. Using software packages as THERMO-CALC any kind of section can be calculated in multicomponent systems. In this work different types of phase diagrams (isothermal sections, temperature-composition sections, potential phase diagrams), phase fraction and phase composition diagrams are used to simulate and understand the phase reactions and the crystallization behaviour of precursor-derived Si-(B-)C-N ceramics and the decomposition reactions of elemental organic polymers containing Si, C, N and H.

## 2.2.2 Analytical description of Gibbs energy and models

For a phase  $\phi$  the Gibbs energy is given by the general formula

$$G^\phi = {}^0G + {}^{\text{id}}G^\phi + {}^{\text{ex}}G^\phi, \quad (2.1)$$

where  ${}^0G$  is the contribution of the pure components of the phases to the Gibbs energy,  ${}^{\text{id}}G^\phi$  is the ideal mixing contribution and  ${}^{\text{ex}}G^\phi$  is the contribution due to non-ideal interactions between the components, also known as the Gibbs excess energy of mixing. Thermodynamics describe the stability of phase, as functions of macroscopic variables such as temperature, chemical composition and pressure. In this work, the dependence of the Gibbs energy of condensed phases on pressure has been neglected as well as the influence of other variables as electromagnetic field, surface energy etc. The equilibrium state corresponds to a minimum of the Gibbs energy at constant temperature and pressure as well as at constant concentrations of elements.

### 2.2.2.1 Temperature dependence

The Gibbs energy of elements or a stoichiometric phase is a function of only the temperature. At temperatures above the Debye temperature, the specific heat at constant pressure  $C_p$  can be well represented by the polynomial after the suggestion of Kubaschewski et al.[67Kub]:

$$C_p = -c - 2dT - 6eT^2 - 2fT^{-2}, \quad (2.2)$$

where  $c$  comes from the harmonic lattice vibrations,  $d$  and  $e$  are due to the anharmonic and electronic corrections, respectively, and  $f$  is a correction term for lower temperatures.

The Gibbs energy is defined by  $G = H - TS$  and can be obtained by integrating  $C_p$  from the reference state to the desired temperature  $T$ :

$$G = \int_{298}^T C_p dT - T(S_{298} + \int_{298}^T \frac{C_p}{T} dT) . \quad (2.3)$$

According to the standards prescribed by Scientific Group Thermodata Europe (SGTE) [87Ans, 91Din] the Gibbs energy is referred to the enthalpy of the elements at 25°C (298 K) (SER = Stable Element Reference). The Gibbs energy can be written as

$${}^0G_i^\phi(T) - H_i^{\text{SER}}(298.15\text{K}) = a + bT + cT \ln(T) + dT^2 + eT^{-1} + fT^3 . \quad (2.4)$$

### 2.2.2.2 Pressure dependence

Most of the calculations of phase diagrams have been made at a total pressure of 1 bar. The influence of nitrogen partial pressure on phase equilibria and phase reactions has been calculated. It is supposed that the gas phase has an ideal mixing behavior and can add a term of  $-RT \ln(p/p_0)$  to its description.

### 2.2.2.3 Composition dependence

When considering an ideal mixing of  $i$  components, after Equation (2.1) the term  ${}^{\text{ex}}G^\phi$  is equal to zero. Then the Gibbs energy of such an ideal solution can be written as:

$$G^\phi = \sum x_i \cdot {}^0G_i^\phi + R \cdot T \cdot \sum x_i \ln x_i , \quad (2.5)$$

where  $x_i$  are the mole fractions of the components  $i$  in the phase  $\phi$ .  $R$  is the universal gas constant. However, in real solutions, interactions between the species give rise to deviations from the ideal behavior. These deviations are taken into account by the excess term  ${}^{\text{ex}}G^\phi$  in Equation (2.1), which, in the case of a simple binary solution of compound A and B, such as liquid and disordered solid solutions, are described as random mixtures of the elements by a regular-solution type model. Most commonly this can be written as Redlich-Kister [48Red] polynomials:

$${}^{\text{ex}}G_{AB}^\phi = x_A \cdot x_B \cdot \sum_{v=0} L_{AB}^v \cdot (x_A - x_B)^v . \quad (2.6)$$

The interaction parameter  $L_{AB}^V$  characterizes the Gibbs energy of mixing. The first term of the polynomials is  $x_i x_j L_{ij}$  which is a regular solution parameter based on random mixing. Furthermore, each  $L$  term can be written as the sum of an enthalpy and entropy of mixing, i.e.  $L = a + bT$ . Although other polynomials have been used in the past, in most cases they can be converted to Redlich-Kister polynomials.

The Gibbs energy of a binary stoichiometric phase is given by

$$G^\phi = x_A \cdot {}^0G_A + x_B \cdot {}^0G_B + \Delta^f G, \quad (2.7)$$

where  $x_A$  and  $x_B$  are mole fractions of elements A and B and are given by the stoichiometry of the compound,  ${}^0G_A$  and  ${}^0G_B$  are the respective reference states of elements A and B, and  $\Delta^f G$  is the Gibbs energy of formation. The first two terms correspond to  ${}^0G$ , and the third term corresponds to  ${}^{ex}G^\phi$  in Equation (2.1).  ${}^{id}G^\phi$  of Equation (2.1) is zero for a stoichiometric phase, since there is no random mixing.

For ordered solid phases, Wagner and Schottky [30Wag] introduced the concept of defects of the crystal lattice in order to describe deviations from stoichiometry. The most complex and general model is the sublattice model frequently used to describe ordered binary solution phases, which was introduced by Schmalzried [65Sch] and later refined by Sundman and Ågren [81Sun] and deduced by Andersson et al. [86And, 01Hil] as “Compound Energy Formalisms”. The basic premise for this model is that a sublattice is assigned for each distinct site in the crystal structure. The structure of a phase is represented simply by the formula, e. g.  $(A,B)_p(D, E, F)_q$  where A and B mix on the first sublattice and D, E and F mix on the second one. The coefficients  $p$  and  $q$  are the stoichiometric coefficients and one mole of a formula units thus contains  $p+q$  moles of atoms. The constitution of the phase is described by the site fraction,  $y_j^i$  where  $i$  defines the sublattice and  $j$  represents any type of species, i.e. atom, molecule, ion or vacancy. The summation over each sublattice yields 1. In order to illustrate the Compound Energy Formalism it is convenient to use the simple case, for example  $(A, B)_p(B, A)_q$ , which consists of two sublattices, each one of which is occupied by A atoms or B

atoms. The Gibbs energy of this binary solution phase  $\phi$  (for 1 mol of phase = (A, B)<sub>p</sub>(B, A)<sub>q</sub>, that is for (p+q) mole of atoms) can be described by the expression:

$$\begin{aligned}
G^\phi = & y_A^1 \cdot y_B^2 \cdot {}^0G_{A_p B_q}^\phi + y_A^1 \cdot y_A^2 \cdot {}^0G_{A_p A_q}^\phi + y_B^1 \cdot y_B^2 \cdot {}^0G_{B_p B_q}^\phi + y_B^1 \cdot y_A^2 \cdot {}^0G_{B_p A_q}^\phi \\
& + R \cdot T \cdot \left[ p \cdot (y_A^1 \cdot \ln y_A^1 + y_B^1 \cdot \ln y_B^1) + q \cdot (y_B^2 \cdot \ln y_B^2 + y_A^2 \cdot \ln y_A^2) \right] \\
& + y_A^1 \cdot y_B^1 \cdot (y_A^2 \cdot {}^0L_{A,B:A}^\phi + y_B^2 \cdot {}^0L_{A,B:B}^\phi) \\
& + y_A^2 \cdot y_B^2 \cdot (y_A^1 \cdot {}^0L_{A:B,A}^\phi + y_B^1 \cdot {}^0L_{B:B,A}^\phi) \\
& + y_A^1 \cdot y_B^1 \cdot (y_A^1 - y_B^1) \cdot (y_A^2 \cdot {}^1L_{A,B:A}^\phi + y_B^2 \cdot {}^1L_{A,B:B}^\phi) \\
& + y_A^2 \cdot y_B^2 \cdot (y_A^2 - y_B^2) \cdot (y_A^1 \cdot {}^1L_{A:B,A}^\phi + y_B^1 \cdot {}^1L_{B:B,A}^\phi)
\end{aligned} \tag{2.8}$$

where  $y_A^1$  is site fraction of atom A on sublattices 1,  $G_{A_p B_q}^\phi$  is the Gibbs energy of one mole of the “compound”  $A_p B_q$ ,  ${}^0L_{A,B:A}^\phi$  is the Redlich-Kister term of zero degree for one sublattice is occupied by A and B atoms and another only by A atom. The first four terms correspond to  ${}^0G$ , and the fifth term corresponds to  ${}^{id}G^\phi$  in Equation (2.1). The remaining terms are the excess Gibbs energy term,  ${}^{ex}G^\phi$ , in Equation (2.1).

A higher component system can be calculated from thermodynamic extrapolation of the thermodynamic excess quantities of the constituent subsystems. Several methods exist to determine the weighting terms used in such an extrapolation formula. Hillert [80Hil] analyzed various extrapolation methods and recommended the use of Muggianu's method [75Mug] since it can easily be generalized. The usual strategy for assessment of a multicomponent system is the following one: First, the thermodynamic descriptions of the constituent binary systems are derived. Thermodynamic extrapolation methods are then used to extend the thermodynamic functions of the binaries into ternary and higher order systems. The results of such extrapolations can then be used to design critical experiments. The results of the experiments are compared to the extrapolation, and, if necessary, interaction functions are added to the thermodynamic description of the higher order system.

### 2.2.3 Calculation of phase equilibria

For the calculation of phase equilibria in a multicomponent system, it is necessary to minimize the total Gibbs energy of all the phases that take part in this equilibrium for a given temperature, pressure, and composition. From this condition Gibbs derived the well-known equilibrium conditions that the chemical potential,  $\mu_i^\phi$ , of each component  $i$ , is the same in all phases (I, II, III,... $\phi$ ),

$$\mu_i^I = \mu_i^{II} = \mu_i^{III} = \dots = \mu_i^\phi. \quad (2.9)$$

This equation results in nonlinear equations that can be used in numerical calculations. All of the CALPHAD-type software tools use methods like the two-step method of Hillert [81Hil] or the one-step method of Lukas et al.[82Luk1] to minimize the Gibbs energy.

### 2.2.4 Optimization

The coefficients of the Gibbs energy functions are determined from experimental data for each system. In order to obtain an optimized set of coefficients, it is desirable to take into account all types of experimental data (e.g., phase diagram, chemical potential, and enthalpy data). The coefficients can be determined from the experimental data by mathematical methods or by a trial-and-error method. The trial-and-error method is only feasible if few different data types are available. This method becomes increasingly cumbersome as the number of components or the number of data types increases. In this case, mathematical methods, such as the least squares method of Gauss are more efficient.

## 2.3 Thermodynamic Data

### 2.3.1 The Si-B-C-N system

To predict and control the production and application conditions such as temperature, pressure and atmosphere of non-oxide ceramics (e.g.  $\text{Si}_3\text{N}_4$ ,  $\text{SiC}$ ,  $\text{BN}$ ,  $\text{B}_{4+\delta}\text{C}$ ) thermodynamic calculations and thermochemical analyses in the system Si-(B-)C-N have been performed in a number of studies [66Ras, 68Gug, 81Wei, 82Luk2, 88Nic, 88Wad, 91Mis, 93Jha, 94Nei, 96Kas1, 96Kas2, 98Sei1, 99Sei1]. Most of these publications take into account the influence of the nitrogen partial pressure and the activity of carbon on phase equilibria. The results provided guidelines for the developing of the ceramic materials. The CALPHAD method can be used to understand the phase reactions and the crystallization behavior of precursor ceramics [98Sei1, 00Pen1, 00Pen2, 01Sei1, 01Sei2]. The present work takes into account most recent thermodynamic data for the Si-(B-)C-N system which are used for the calculation of phase equilibria and phase reactions in precursor derived Si-(B-)C-N ceramics. The phase diagrams were calculated with a consistent set of thermodynamic data [96Kas1, 96Kas2, 02Sei], which is containing 11 crystalline solid phases as well as 38 distinct gas species (Table 2-1).

The unary phase data for the pure elements and the descriptions for the gaseous species (mainly  $\text{N}_2$ ,  $\text{Si}$ ,  $\text{Si}_2$ ,  $\text{Si}_2\text{C}$ ,  $\text{SiC}_2$ ,  $\text{CN}$ ,  $\text{C}_2\text{N}_2$ ) were taken from the SGTE substance database [SGTE]. Ideal mixing of species is assumed for the gas phase. The solid phases  $\beta$ -boron, graphite and silicon were taken into account as stable phases. In the binary B-N system the data for  $\alpha$ -BN as stable phase was accepted from [SGTE], whereas  $\beta$ -BN and  $\gamma$ -BN are stable only under conditions at high pressures. The postulated compound  $\text{C}_3\text{N}_4$  [95Fan] was not found as a solid stable phase until now. Datasets for the binary Si-B system were thermodynamically optimized within the work [95Lim] and verified in the works [96Kas1, 96Kas2], where  $\text{B}_3\text{Si}$ ,  $\text{B}_6\text{Si}$ , and  $\text{B}_n\text{Si}$  were taken into account.  $\text{B}_{4+\delta}\text{C}$  is the only solid phase with a significant homogeneity range in the Si-B-C-N system. Based on experimental crystallographic information [76Wil, 94Kuh] using the compound energy formalism with the sublattice occupation  $(\text{B}_{11}\text{C}, \text{B}_{12})(\text{CBC}, \text{CBB}, \text{BVaB})$  phase  $\text{B}_{4+\delta}\text{C}$  was optimized in the work [96Kas2]. The thermodynamic data for the binary system Si-C used in this work was taken from [96Grö]. The descriptions for the binary system Si-N was used from literature [92Hil].

**Table 2-1** Solid phases and gas species used in the calculations  
(in brackets are metastable or unstable phases).

Crystalline solid phases	Gas species	
$\beta$ -boron	Ar	$C_3N$
Graphite	B	$C_4$
Silicon	$BC_1$	$C_4N$
$B_{4+\delta}C$	$BC_2$	$C_4N_2$
$\alpha$ -BN	BN	$C_5$
$B_3Si$	$B_2$	$C_5N$
$B_6Si$	$B_2C$	$C_6N$
$B_nSi$	C	$C_6N_2$
$\beta$ -SiC	CN	$C_7N$
$\alpha$ -SiC	$CN_2$ -CNN	$C_9N$
$\beta$ - $Si_3N_4$	$CN_2$ -NCN	He
( $\alpha$ - $Si_3N_4$ )	Csi	N
( $\beta$ -BN)	$CSi_2$	NSi
( $\gamma$ -BN)	$C_2$	$NSi_2$
( $C_3N_4$ )	$C_2N$ -CCN	$N_2$
( $BC_2N$ , $BC_4N$ , $BC_xN$ )	$C_2N$ -CNC	$N_3$
( $B_5Si_2C_2$ , $B_3Si_2C_2$ )	$C_2N_2$	Si
( $SiC_2N_4$ , $Si_2CN_4$ )	$C_2Si$	$Si_2$
	$C_3$	$Si_3$

Because of only small energetic differences a single analytical Gibbs- energy description was used to describe  $\alpha$ - and  $\beta$ -SiC, as well as  $\alpha$ - and  $\beta$ - $Si_3N_4$ , respectively ( $\alpha$ - $Si_3N_4$  is generally accepted to be a metastable phase [99Lia]). More recent discussions on the experimental information on the thermodynamics of  $\alpha$ - and  $\beta$ -SiC were provided recently by [98Kle, 95Roc] and  $\alpha$ - and  $\beta$ - $Si_3N_4$  by [99Lia] and [99Har]. These publications confirm the analytical descriptions used in the present work. For example, the standard enthalpy of formation of SiC at 25°C (298.15 K) was measured by P. Rocabois [95Roc] to be  $-69.35 \pm 1.20$  KJ mol<sup>-1</sup>, which is in good agreement with the calculated one of -70.533 KJ mol<sup>-1</sup> using this database. The six binary phase diagrams calculated using the data above are shown in Fig. 2-6. The corresponding calculated invariant reactions for these binary systems are given in Table 2-2, respectively.

The ternary system Si-B-C was optimized in the work [95Lim, 96Kas1, 96Kas2] in consideration of the silicon solubility in  $B_{4+\delta}C$  and the boron solubility in SiC [69Sha, 88Car,



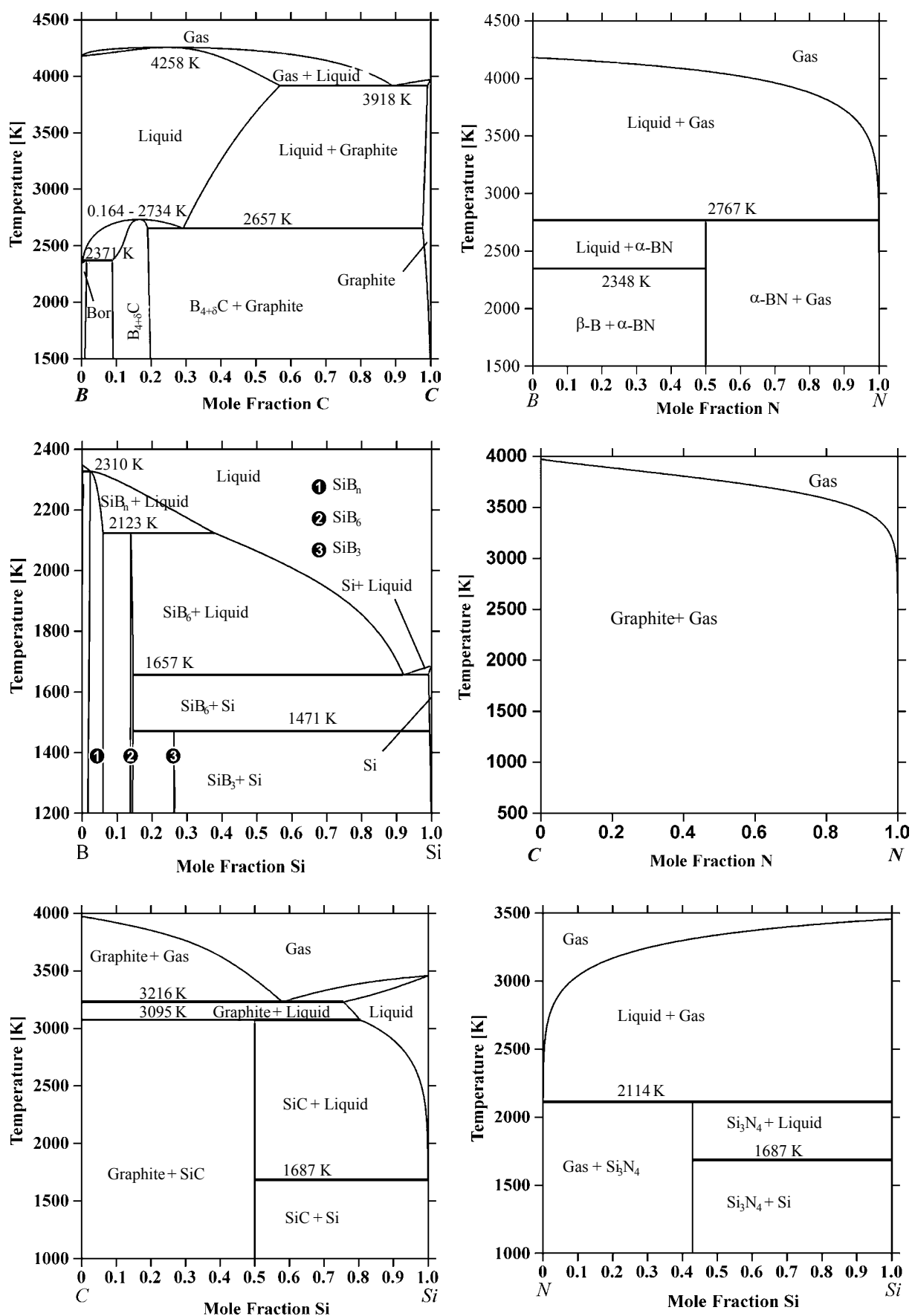


Fig. 2-6 Calculated phase diagrams of the six binary subsystems of the Si-B-C-N system.

**Table 2-2** Invariant reactions in the binary systems.**B-C system**

Reaction	Composition at.% C	Composition at.% C	Composition at.% C	Temperature (K)
$G = L$	24.9	24.9		4258
$G = L + \text{graphite}$	89.1	56.9	99.1	3918
$L = B_4C$	17.1	17.1		2734
$L = B_4C + \text{graphite (e)}$	29.1	18.9	97.7	2657
$L + B_4C = (B) (p)$	0.35	1.47	8.8	2371

**B-N system**

Reaction	Composition at.% N	Composition at.% N	Composition at.% N	Temperature (K)
$G + L = \alpha\text{-BN}$	100.0	0	50.0	2767
$L = \beta(B), \alpha\text{-BN (d)}$	0	0	50.0	2348

**Si-B system**

Reaction	Composition at.% Si	Composition at.% Si	Composition at.% Si	Temperature (K)
$L + (B) = SiB_n (p)$	7.4	2.1	3.3	2310
$L + SiB_n = SiB_6 (p)$	37.9	5.9	13.8	2123
$L = (Si) + SiB_6 (e)$	91.9	99.1	14.6	1657
$(Si) + SiB_6 = SiB_3 (p)$	99.5	26.2	14.5	1471

**Si-C system**

Reaction	Composition at.% Si	Composition at.% Si	Composition at.% Si	Temperature (K)
$G = L + C$	58.4	78.7	0	3216
$L + C = SiC (p)$	82.7	0	50.0	3095
$L = Si, SiC (d)$	100.0	100.0	50.0	1687

**Si-N system**

Reaction	Composition at.% Si	Composition at.% Si	Composition at.% Si	Temperature (K)
$G + Si(l) = Si_3N_4$	0	100.0	42.9	2114
$L = Si, Si_3N_4 (d)$	100.0	100.0	42.9	1687

90Tel, 94Wer]. These solubilities were modelled using the sublattice descriptions ( $B_{11}C$ ,  $B_{12}$ )(CBC, CBB, BVaB, SiSi) and (Si)(C, B), respectively. Their homogeneity ranges were calculated by a trial and error method corresponding to the experimental information. The ternary phases  $B_5Si_2C_2$ ,  $B_3Si_2C_2$  reported by [60Por] were not taken into account. The evaluation has been performed by the Lukas program. Fig. 2-7 shows the calculated isothermal section at 1127°C in the Si-B-C system and the isopleth SiC-B, respectively.

The other three ternary systems (Si-B-N, Si-C-N, B-C-N) could be calculated comprehensively by thermodynamic extrapolation. Comparison with experimental data shows that the adjustment of ternary parameters is not necessary [96Kas2]. The ternary phases  $SiC_2N_4$  and  $Si_2CN_4$  reported by [97Rie] are not stable under conditions treated here ( $p = 1$  bar,  $T > 1000^\circ C$ ). In the B-C-N system numerous graphite-like layered materials ( $BNC_2$ ,  $BC_4N$ ,  $BC_xN$ ) have been synthesized by chemical vapor deposition (CVD) [87Kan, 89Kou] and by pyrolysis of amine borane-derived polymers [92Bil1, 92Bil2]. They were not included in the calculation because it is not clear yet, whether these phases are stable. Another reason is that detailed crystal structures have not yet been conclusively determined for them.

The ternary descriptions were combined in a database to simulate the phase equilibria in the quaternary Si-B-C-N system. Table 2-3 gives the optimized parameters of the Gibbs free energy functions for the phases in this system.

### 2.3.2 The Si-C-N-H System

For this system the thermodynamic description for the phases and gaseous species of the Si-C-N system as described above has been applied together with the thermodynamic descriptions for the hydrogen containing gaseous species (e.g.  $H_2$ ,  $CH_2$ ,  $CH_3$ ,  $CH_4$ ,  $C_2H_4$ ,  $NH_3$ ,  $SiH$ ,  $SiH_2$ ,  $SiH_3$ ,  $SiH_4$ ,  $Si_2H_2$ ) included in the SGTE-database [SGTE]. No hydrogen containing solid compounds are known in this system. Therefore the quaternary system Si-C-N-H could be calculated by extrapolation.

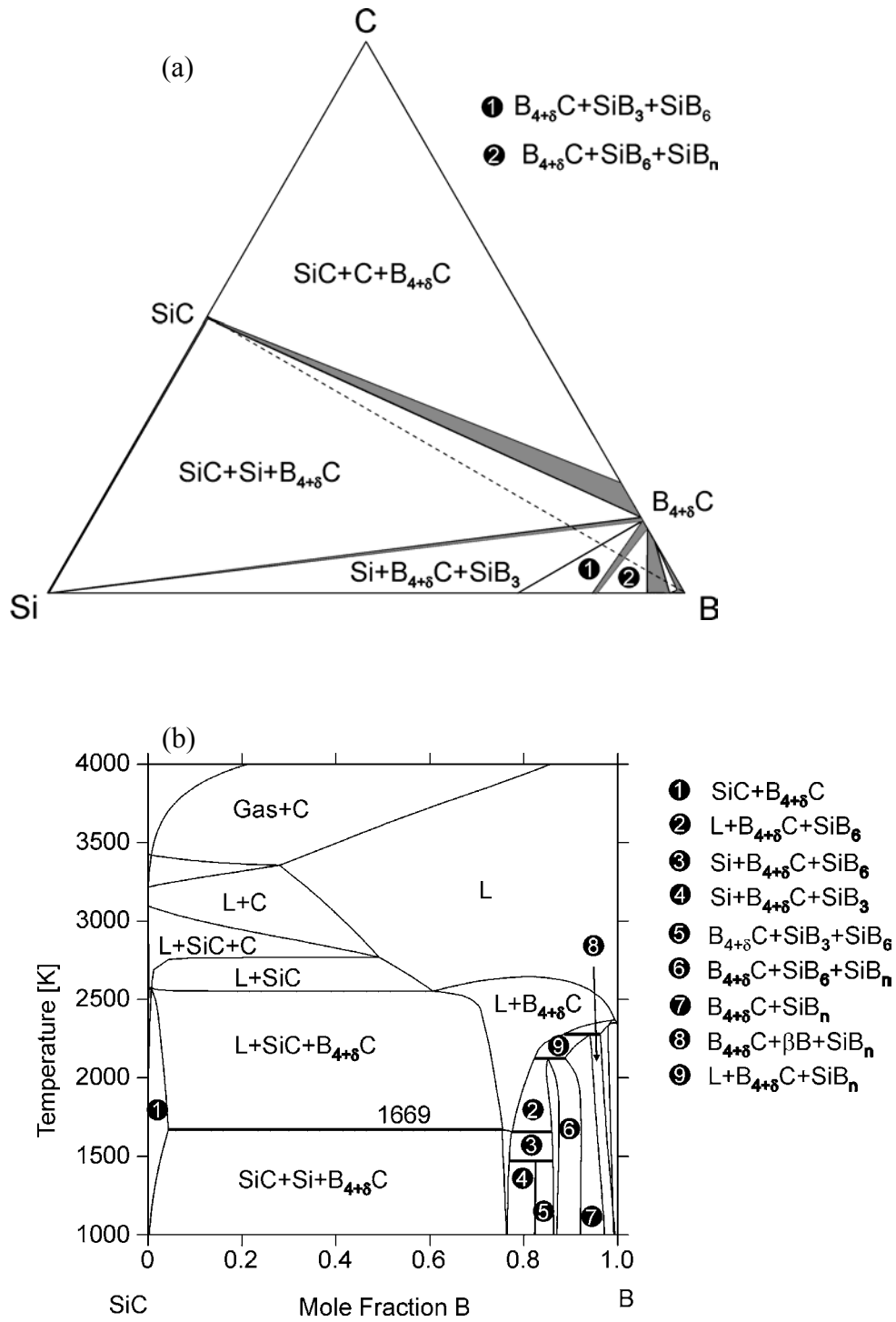


**Fig. 2-7** Calculated phase diagrams of the Si-B-C system, (a) isothermal section at 1127°C (1400 K) and (b) isopleth SiC-B. (The dashed line in (a) indicates the trace of the isopleth shown in (b))

**Table 2-3** Optimized parameters (J/mol) for the phases in the system Si-B-C-N. Unary descriptions were taken from [91Din].

Phase and model	Parameter	$a$	$b$	$c$	$d$ $10^{-3}$	$e$ $10^6$	$f$ $10^{-6}$
<b>Liquid</b> (Redlich-Kister-Muggianu)	${}^0L_{B,C}^{liq}$	-67045.16	4.47				
	${}^1L_{B,C}^{liq}$	-36682.57	2.45				
	${}^0L_{B,Si}^{liq}$	-2389700	238.97				
	${}^1L_{B,Si}^{liq}$	-15715636	1571.56				
	${}^2L_{B,Si}^{liq}$	-281573.6	28.16				
	${}^0L_{Si,C}^{liq}$	25645.0	-6.38				
<b><math>\beta</math>-boron</b> (compound energy formalism)	$G_{B:C}^{\beta\text{-boron}} - 93 \cdot {}^0G_B^{\beta\text{-boron}} - 12 \cdot {}^0G_C^{\text{graphite}}$	10000	-				
	$G_{B:Si}^{\beta\text{-boron}} - 93 \cdot {}^0G_B^{\beta\text{-boron}} - 12 \cdot {}^0G_{Si}^{\text{diam}}$	-6160.245	-0.62				
	${}^0L_{B:B,C}^{\beta\text{-boron}}$	-1636713.01	-				
<b>Graphite</b> (Redlich-Kister-Muggianu)	$G_B^{\text{graph}} - {}^0G_B^{\beta\text{-boron}}$	10000	-2				
	$G_N^{\text{graph}} - {}^0G_N^{N_2}$	-2423.05	28.19				
	${}^0L_{C,B}^{\text{graph}}$	34385.95	8.68				
<b>Diamond</b> (Redlich-Kister-Muggianu)	${}^0L_{B,Si}^{\text{diam}}$	57978.16					
	${}^0L_{Si,C}^{\text{diam}}$	93386.8					
<b><math>B_{4+\delta}C</math></b> (compound energy formalism)	$G_{B_{11}C:CBC}^{B_{4+\delta}C} - 12 \cdot {}^0G_B^{\beta\text{-boron}} - 3 \cdot {}^0G_C^{\text{graphite}}$	-311207.416	11.53				
	$G_{B_{11}C:CBB}^{B_{4+\delta}C} - 13 \cdot {}^0G_B^{\beta\text{-boron}} - 2 \cdot {}^0G_C^{\text{graphite}}$	-293453.353	11.53				
	$G_{B_{11}C:BVaB}^{B_{4+\delta}C} - 13 \cdot {}^0G_B^{\beta\text{-boron}} - {}^0G_C^{\text{graphite}}$	-148993.047	11.53				
	$G_{B_{12}C:CBC}^{B_{4+\delta}C} - 13 \cdot {}^0G_B^{\beta\text{-boron}} - 2 \cdot {}^0G_C^{\text{graphite}}$	-283453.45	11.53				
	$G_{B_{12}C:CBB}^{B_{4+\delta}C} - (14 + \frac{1}{14}) \cdot {}^0G_B^{\beta\text{-boron}} - {}^0G_C^{\text{graphite}}$	-138993.047	11.53				

Phase and model	Parameter	$a$	$b$	$c$	$d$ $10^{-3}$	$e$ $10^6$	$f$ $10^{-6}$
2	$G_{B_{12}:BVaB}^{B_{4+\delta}C} - 14 \cdot {}^0G_B^{\beta\text{-boron}}$	10000	11.53				
	$G_{B_{11}C:SiSi}^{B_{4+\delta}C} - 11 \cdot {}^0G_B^{\beta\text{-boron}} - {}^0G_C^{graphite} - 2 \cdot {}^0G_{Si}^{diam}$	74000	-129				
	$G_{B_{11}C:SiSi}^{B_{4+\delta}C} - 12 \cdot {}^0G_B^{\beta\text{-boron}} - 2 \cdot {}^0G_{Si}^{diam}$	112000					
$\alpha$ -BN (stoichiometric)	$G_{B:N}^{\alpha\text{-BN}} - (H_B^{SER} + H_N^{SER})$ $298.15\text{ K} < T < 700\text{ K}$	-254468.02	-2.0167	2.0213	-46.6240	0.0687	8.4686
	$700\text{ K} < T < 1200\text{ K}$	-252837.33	31.8461	-4.7738	-29.6618	0.4645	3.4429
	$1200\text{ K} < T < 1900\text{ K}$	-305197.77	485.7227	-68.6456	5.5660	7.7129	0.2646
	$1900\text{ K} < T < 6000\text{ K}$	-276126.05	333.5054	-48.9528	-4.0585E-6	17.7193E-6	3.8409E-7
SiC (compound energy formalism)	$G_{Si:C}^{SiC} - (H_{Si}^{SER} + H_C^{SER})$	-88584.0	271.1462	-41.2785	-4.3627	0.8	0.2
	${}^0G_{Si:B}^{SiC} - {}^0G_{Si:C}^{SiC}$	120000	-12.0				
SiB <sub>3</sub> (compound energy formalism)	$G_{B:Si:B}^{SiB_3} - 12 \cdot {}^0G_B^{\beta\text{-boron}} - 2 \cdot {}^0G_{Si}^{diam}$	112000	0				
	$G_{B:Si:Si}^{SiB_3} - 6 \cdot {}^0G_B^{\beta\text{-boron}} - 8 \cdot {}^0G_{Si}^{diam}$	1120000	0				
SiB <sub>6</sub> (compound energy formalism)	$G_{B:Si:B}^{SiB_6} - 258 \cdot {}^0G_B^{\beta\text{-boron}} - 23 \cdot {}^0G_{Si}^{diam}$	729824.4	-72.98244				
	$G_{B:Si:Si}^{SiB_6} - 258 \cdot {}^0G_B^{\beta\text{-boron}} - 23 \cdot {}^0G_{Si}^{diam}$	5454561	-545.46				
SiB <sub>n</sub> (compound energy formalism)	$G_{B:Si}^{SiB_n} - 69 \cdot {}^0G_B^{\beta\text{-boron}} - {}^0G_{Si}^{diam}$	-89819.86	8.98				
	$G_{B:Si:Si}^{SiB_n} - 61 \cdot {}^0G_B^{\beta\text{-boron}} - 9 \cdot {}^0G_{Si}^{diam}$	-176659.7	17.67				
Si <sub>3</sub> N <sub>4</sub> (stoichiometric)	$G_{Si:N}^{Si_3N_4} - (H_{Si}^{SER} + H_N^{SER})$	-936805.62	1066.0398	-158.4527	8.2264	10.8858	-
		-7.730173E+08 T <sup>-2</sup>					

Parameter =  $a + b T + c T \ln(T) + d T^2 + e / T + f T^3 + \dots$  (in J / mol)

## 3 Experimental Procedures

### 3.1 Sample preparation

The polymers, which were used to produce different types of amorphous Si-C-N and Si-B-C-N ceramics, and the chemical compositions of these amorphous ceramics are shown in Table 3-1. Details about the ceramic preparation including polymer synthesis may be drawn from the corresponding publications [95Bil2, 96Sei2, 96Sei3, 96Rie1, 98Ald, 00Wei, 00Bil1, 00Wan].

The ternary Si-C-N ceramics were derived from polyvinylsilazane (PVS; VT50, Hoechst AG, Germany) or polyhydridomethylsilazane (PHMS; NCP200, Nichimen Corp., Tokyo, Japan), as described in detail elsewhere [96Sei2, 96Sei3]. The structural formula of the precursors PVS and PHMS are  $[(CH=CH_2)(NH)_{0.5}SiNH]_n$  and  $[(CH_3)(H)SiNH]_n$ , respectively. The as-thermolyzed compositions were  $Si_1C_{1.6}N_{1.33}$  and  $Si_1C_{0.6}N_{1.02}$ , respectively (Table 3-1). Both polysilazanes were crosslinked between 200°C and 400°C under vacuum and Ar atmosphere, and then pyrolysed at a temperature of 1050°C under Ar atmosphere into the amorphous ceramics. The pyrolyses of the samples were carried out in tubes of quartz using the Schlenk technique, (this preparative method is based on experiments developed by the German chemist Wilhelm Schlenk). Some of the products were ball milled to powders with grain sizes of about 10 µm for the investigation by differential thermal analysis (DTA) and thermogravimetry (TG). Some of them were directly used for DTA / TG experiments.

The various types of amorphous Si-B-C-N ceramics were derived from T2-1, MW33, MW36, BNCP, T2-1(NH<sub>3</sub>/Ar) and BVT50, respectively (Table 3-1), as described in detail elsewhere [95Bil2, 96Rie1, 96Sei2, 00Wei, 00Wan]. These polymers were synthesized according to the so-called monomer route or polymer route [95Bil1, 98Ald, 00Wie]. In the monomer route (m) commercially available monomers are functionalized and subsequently polymerized. An example is the attachment of boron by hydroboration of vinylsilanes. This is

**Table 3-1** The polymers which were used to produce the amorphous ceramics and the chemical compositions of the amorphous ceramics.

Laboratory name	Polymers <sup>b</sup>	Structural formula of polymers	Pyrolysis (in Ar or in NH <sub>3</sub> )	Chemical compositions of the amorphous ceramics (at.%) <sup>a</sup>				References
				Si	B	C	N	
<b>VT50</b>	PVS	$[(CH=CH_2)(NH)_{0.5}SiNH]_n$	1050°C, 4 h, Ar	25.4	-	40.7	33.8	[96Sei2]
<b>NCP200</b>	PHMS	$[(CH_3)(H)SiNH]_n$	1050°C, 4 h, Ar	38.2	-	22.9	38.9	[96Sei3]
<b>T2-1</b>	B-PMVS(m)	$[B\{(C_2H_4)(CH_3)SiNH\}_3]_n$	1400°C, 4 h, Ar	24.1	8.3	44.9	22.6	[96Rie1]
<b>MW33</b>	B-PHVS(p)	$[B\{(C_2H_4)(H)SiNH\}_3]_n$	1400°C, 4 h, Ar	25.1	9.1	38.9	26.9	[00Wei]
<b>MW36</b>	B-PMVS(p)	$[B\{(C_2H_4)(CH_3)SiNH\}_3]_n$	1400°C, 4 h, Ar	26.9	9.3	41.8	22.0	[00Wei]
<b>BNCP</b>	B-PHMS	---	1400°C, 4 h, Ar	39.2	0.72	21.8	38.2	[95Bil2]
<b>T2-1(NH<sub>3</sub>/Ar)</b>	B-PMVS	$[B\{(C_2H_4)(CH_3)SiNH\}_3]_n$	500°C, 4 h, NH <sub>3</sub> and 1050°C, 4 h, Ar	28.0	10.0	15.0	47.0	[00Wan]
<b>BVT50</b>	B-PVS	---	1400°C, 4 h, Ar	17.6	26.8	28.9	26.6	[95Bil2]

<sup>a</sup> Oxygen values were determined to be < 2 at. %, hydrogen < 0.5 at. %.

<sup>b</sup> B- means boron containing, P: poly, M: methyl, V: vinyl, S: silazane, H: hydro, m: monomer route, p: polymer route. For details see [98Ald] [95Bil1] and [00Wei].



the initial step in the preparation of several precursors such as T2-1 [96Rie1]. In contrast, the polymer route (p) uses commercially available multi-functional monomers which are first transformed into polymers followed by incorporation of additional elements. An example for this is the hydroboration of oligovinylsilazanes in the synthesis of the Si-B-C-N polymer MW33 [00Wei]. After the synthesis both types of polymers were crosslinked at temperatures between 200°C and 400°C in vacuum and then thermolysed in alumina tubes using the Schlenk technique. For T2-1(NH<sub>3</sub>/Ar) ceramic a stepwise thermolysis was carried out. The samples were heated up with 5°C/min to 550°C in ammonia atmosphere, isothermally annealed at this temperature for 4 hours and then in Ar atmosphere heated with 5°C/min up to 1050°C and annealed at this temperature for 4 hours. For other ceramics T2-1, MW33, MW36, BNCP, and BVT50, one step thermolyses were carried out in Ar atmosphere by heating with 5°C/min up to 1400°C, and subsequent annealing also for 4 hours.

To study in detail the thermal stability of precursor-derived Si-B-C-N amorphous ceramics, beside samples investigated experimentally in this work numerous other Si-B-C-N ceramics as reported in the literature were taken into account. They are summarized in Table 3-2. Sample Nr. 1, 2, 3, 12, 13, and 14 were investigated in this work.

For investigations of the thermal expansion and thermal conductivity, bulk amorphous ceramics were produced. To get them, after cross-linking polymers were ground and shaped into cylinders with a diameter of 18 mm and a thickness of about 5 mm by plastic forming (warm pressing) [96Sei3, 99Hau] or by cold isostatic pressing [92Rie, 96Sei2]. The cylindrical specimens were then thermolysed in a quartz tube or in an alumina tube by heating at the rate of 10°C/min up to 1050°C, (for Si-B-C-N ceramics 1400°C) and then holding at 1050°C (1400°C) for 4 hours in argon. Thermolysis resulted in black and crack-free bulk bodies.

Small bars for measuring the thermal expansion and disk samples for the measuring the thermal conductivity were cut from the specimens using a low speed diamond saw. Typically, the bars were 3.5 mm wide, 3.5 mm thick and 10 mm long and the disk samples were about

**Table 3-2** Summary of the Si-B-C-N precursor-derived ceramics from the literature and this work.

No.	Ceramics Laboratory name	Polymers <sup>(a)</sup>	Remarks <sup>(b)</sup>	As-thermolyzed Composition (at. %)				Decomposition. Temperatures <sup>(c)</sup> (°C)	References
				Si	B	C	N		
1	<b>T2-1</b>	B-PMVS(m)	T2(1)	24.1	8.3	44.9	22.6	2000	[96Rie, this work]
2	<b>MW36</b>	B-PMVS(p)	3P, T2-1 (inv)	26.5	9.3	42.5	21.7	2000	[00wie, this work]
3	<b>MW33</b>	B-PHVS(p)	1P	25.1	9.1	38.9	26.9	2000	[00Wei, this work]
4	<b>MW26</b>	B-PHVS(m)	1M, T2-1(H)	24.5	10.0	40.0	25.5	2000	[00Wei]
5	<b>Wang</b>	B-PMVS		23.9	8.9	45.1	22.1	1950	[00Wan]
6	<b>AM2 k</b>			29.4	11.4	43.0	16.3	2000	[00Mül]
7	<b>KSiH2</b>	B-PCS	K241, H2Me/K	27.1	4.6	53.0	15.3	1950	[98Kam, 99Wei]
8	<b>K269A</b>	B-PCS		24.6	5.7	53.4	16.3	2000	[98Kam, 99Wei]
9	<b>K269B</b>	B-PCS		25.8	4.9	52.6	16.8	1950	[98Kam, 99Wei]
10	<b>K270A</b>	B-PCS		30.6	5.5	57.2	6.7	2000	[98Kam, 99Wei]
11	<b>K270B</b>	B-PCS		28.7	4.6	44.7	22.1	2000	[98Kam, 99Wei]
12	<b>BVT50</b>	B-PVS(p)		17.6	26.8	28.9	26.6	7% to 2000	[95Bil, this work]
13	<b>T2-1(Ar/NH<sub>3</sub>)</b>	B-PMVS(m)		28.0	10.0	15.0	47.0	1800	[00Wan, this work]
14	<b>BNCP</b>	B-PHMS(p)		36.3	1.9	23.4	38.5	1620	[this work]
15	<b>AMFH4k</b>			27.2	4.1	39.9	27.5	1600	[00Mül]
16	<b>MW60</b>		2P, T2-1(N)i	27.0	9.5	27.0	36.0	1550	[00Wei]
17	<b>MW18AMC</b>	B-PSCD(m)	2b	17.5	6.8	45.4	30.3	1550	[97Wei, 98Wei]
18	<b>HyVT50</b>			24.7	8.9	28.6	37.8	1600	
19	<b>HPZ3</b>	B-HPZ		34.4	7.5	15.0	43.1	1550	[93Su]
20	<b>MW25</b>	B-PSCD(m)	2a	22.2	7.8	40.4	29.6	1500	[97Wei, 98Wei]
21	<b>vT2(1)1</b>			31.3	5.3	35.4	27.9	1600	[95Bil]
22	<b>HPZ2</b>	B-HPZ		38.2	3.6	16.9	41.3	1600	[93Su]
23	<b>MW31</b>		2c, Vi/Hbis(inv)	19.1	6.9	41.3	32.8	1500	[97Wei, 98Wei]
24	<b>HPZ4</b>	B-HPZ		18.8	25.0	9.7	46.5	1680	[93Su]
25	<b>NH<sub>3</sub>TADB</b>	TADB(m)		23.3	23.5	0,0	53.3	1700	[92Bal]
26	<b>TADB94</b>	TADB(m)	Jansen-Polymer	23.4	14.9	14.3	47.4	1780	[94Bal]
27	<b>TSDE99</b>	TSDE(m)	Jansen-Polymer	15.4	15.4	30.8	38.5	12% to 2000	[99Jün, 98Jün]

<sup>a</sup> P means poly, V: vinyl, S: silazane, B-: boron containing, H: hydro, M: methyl, m: monomer route, p: polymer route, C: carbo, D: di-imide. For details see [98Ald] [95Bil] and [00Wei]. <sup>b</sup>Other names in the literature. <sup>c</sup>Mass loss at this temperature is lower than 4%.

12 mm in diameter and 1 mm thick. The faces of the bars were ground smooth and parallel vertically to the longitudinal axis of the sample.

Additionally, different powder mixtures of  $\alpha$ -Si<sub>3</sub>N<sub>4</sub> (UBE, Japan) or  $\beta$ -Si<sub>3</sub>N<sub>4</sub>: (Denka, Japan, includes ca. 10 mass%  $\alpha$ -Si<sub>3</sub>N<sub>4</sub>), amorphous carbon (Degussa AG, Hanau, gas soot for oxygen determining), and BN (HCS) were prepared, the specifications of the starting powders of which are given in Table 3-3.

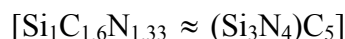
**Table 3-3** The specifications of starting powder.<sup>a</sup>

Powder	manufacturers	S m <sup>2</sup> /g	$\bar{d}$ μm	C (free)	O	N	Al	Ca	Fe
$\alpha$ -Si <sub>3</sub> N <sub>4</sub>	UBE	7.5	0.64	0.2	1.00	-	-	0.002	0.01
$\beta$ -Si <sub>3</sub> N <sub>4</sub>	Denka	16	0.8	0.25	0.8	-	0.005	0.01	0.005
Carbon	Degussa	-	-	-	0.69	-	-	-	-
BN	HCST	5.9		0.02	1.0	-			

<sup>a</sup> The amount of impurities are in mass %, “-” means not specified.

Three different powder samples were prepared:

1:  $\alpha$ -Si<sub>3</sub>N<sub>4</sub> + C with the same chemical composition as VT50 amorphous ceramic



2:  $\beta$ -Si<sub>3</sub>N<sub>4</sub> + C also with the same chemical composition as VT50 amorphous ceramic

3:  $\alpha$ -Si<sub>3</sub>N<sub>4</sub> + C + BN with chemical composition equivalent to  $[\text{Si}_3\text{B}_1\text{C}_5\text{N}_5 = (\text{Si}_3\text{N}_4)\text{C}_5 + \text{BN}]$

For homogenization the powder mixtures milled in methanol with ethanol for ca. 1 h. After drying, the homogenized mixtures were cold isostatically pressed at 800 kN (673 MPa).

## **3.2 Sample analyses**

### **3.2.1 X-ray diffraction analysis (XRD), scanning electron microscopy (SEM) and high-resolution transmission electron microscopy (HRTEM)**

The phase composition was analysed by X-ray diffractometry (XRD) (Siemens Diffractometer D5000/Kristalloflex) using Cu-K $\alpha_1$  radiation ( $\lambda = 1.5418 \text{ \AA}$ ) and a graphite monochromator. Diffractograms of the samples were taken in the  $2\theta$  range of  $20^\circ - 80^\circ$ . The step size was  $0.02^\circ$ , and the time per step was 10 s. For phase analysis, the program DIFFRAC AT was used.

The microstructure and the phase composition were investigated by scanning electron microscopy (SEM) (Zeiss DSM982 GEMINI) coupled with EDX (Oxford – Instrument ISIS 300) and the high-resolution transmission electron microscopy (HRTEM) (JEOL 4000 FX).

### **3.2.2 Differential thermal analysis (DTA) and thermogravimetric analysis (TGA)**

Differential thermal analysis (DTA) and thermogravimetry (TG) were carried out simultaneously (nitrogen or argon atmosphere, BN crucibles, Simultaneous Thermal Analysis, STA Bähr STA501 with graphite heating element). The heating rate was 10 K/min up to  $1000^\circ\text{C}$ , 5 K/min up to  $1800^\circ\text{C}$ ,  $2000^\circ\text{C}$  and  $2200^\circ\text{C}$ , respectively.

### **3.2.4 Chemical analysis**

Silicon and boron in ceramics were analysed by optical emission spectrometry with inductively coupled plasma excitation (OES-ICP, JY 70 Plus, Instruments S.A., France) and in polymers were determined by fluorine combustion with subsequent fourier transformed infrared spectroscopy (Nicolet, IR Magna 560, USA). Carbon in ceramic materials was determined by combustion in flowing oxygen in a HF furnace (CS-800, Eltra, Neuss, Germany). Carbon, nitrogen and hydrogen in polymers were analysed by combustion in oxygen in a quartz furnace at  $1100^\circ\text{C}$ , (Vario EL, Elementar, Hanau Germany). Carrier gas hot extraction method was used in a resistance furnace at  $T > 2500^\circ\text{C}$ , (TC-436 DR, Leco, USA) to determine oxygen and nitrogen contents in ceramic materials and oxygen in polymers.

### 3.2.5 Dilatometry

The thermal expansion of solids is well understood from the fundamental perspective of the anharmonic effects on the equilibrium bond distances [72Yat, 96Wal]. It is usually characterized by the linear coefficient of thermal expansion  $\alpha$ , which is defined at constant pressure [89DIN] by the following equation:

$$\alpha(T) = \frac{1}{L_0} \frac{\partial L}{\partial T}. \quad (3.1)$$

The mean linear thermal expansion coefficient for a temperature range is defined according to:

$$\alpha(T_0; T) = \frac{1}{L_0} \cdot \frac{L_T - L_0}{T - T_0} = \frac{\Delta L}{L_0 \Delta T}, \quad (3.2)$$

where  $T_0$  is the reference temperature, generally 20°C,  $T$  is the measurement temperature,  $L_0$  is the sample length at  $T_0$ ,  $L_T$  is the sample length at the measurement temperature  $T$  and  $\Delta L$  the true length change at the temperature change  $\Delta T$ .

The change of the sample length due to the total temperature variation is often expressed by the relative length change  $\varepsilon$  according to the following equation:

$$\varepsilon = \frac{\Delta L}{L_0}(T) = \frac{L_T - L_0}{L_0}(\%). \quad (3.3)$$

There are many measurement methods to determine the thermal expansion [96Wal]. In all cases the accurate measurement of the linear expansion coefficient requires a symmetrical heating of the sample, as well as a reliable measurement of the temperature and of the length change. Differential dilatometry [74Plu, 89Hem] is often used in practice for determining length changes during a controlled temperature program in order to obtain information about the sintering behavior, phase transformations or thermal expansion [98Lei]. In this work, the measurement was carried out using a high temperature differential dilatometer (Bähr dilatometer type 802, Germany), as schematically presented in Fig. 3-1. The equipment consists of two push-rods, an inductive displacement transducer, a ferrite kernel, a protecting

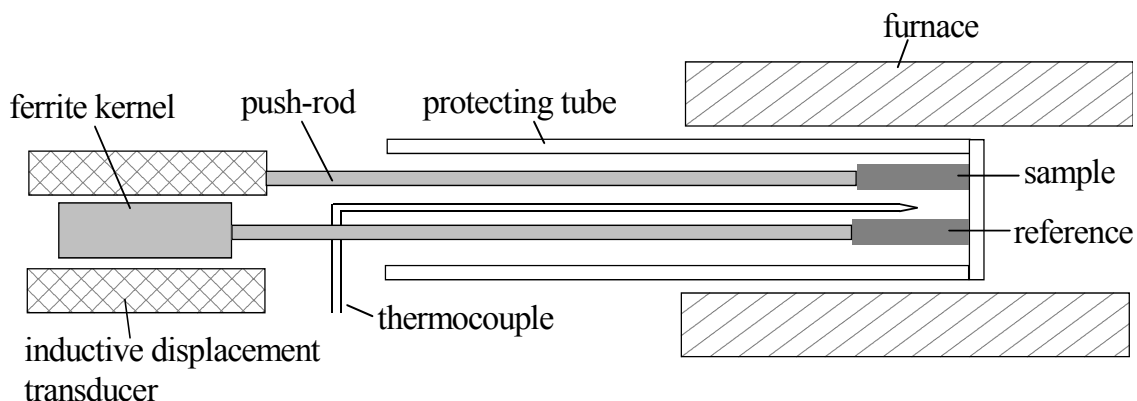


**Fig. 3-1** A schematic presentation of the principle of the high temperature differential dilatometer.

tube, a furnace and a thermocouple. The sample and the reference sample are placed within a tube in the center of the furnace. This tube can be evacuated or charged with inert gases such as  $N_2$ , Ar or He and gas mixtures (e. g. air). The principle of the measurement is to record an elongation difference between the measured sample and a reference sample. The choice of the reference is depending on the measurement temperature and the expansion behavior of the test sample. Normally, the reference should have similar dimensional and thermal behavior as the measuring sample. Table 3-4 gives frequently used reference materials for dilatometric measurements, of which sapphire is used in the present work. The expansion of sample and reference are transmitted through two push-rods. The differential expansion is measured by means of a differential transformer (Linear Variable Differential Transformator (L.V.D.T.)), which contains a movable ferrite kernel and can yield a dissolution of 30 nm. The two push-rods for the sample and the reference with a displacement transducer enable the measurement of the relative change of the sample length.

**Table 3-4** Frequently used reference materials.

	Frequently used reference materials	Temperature range ( $^{\circ}C$ )	$\alpha$ ( $10^{-6} K^{-1}$ )
1	platinum	20 - 1620	10
2	sapphire	20 - 1727	9.5
3	quartz glass	-193 - 727	0.5
4	copper	-253 - 527	17
5	tungsten	-196 - 1527	4
6	borosilicate glass	-193 - 407	4

Table 3-5 gives often used thermocouples for dilatometry of which types 2 and 3 were used. Thermocouples ought to be fixed to a suitable place and to be well in contact with both sample and reference.

**Table 3-5** Frequently used thermocouples in the dilatometer.

Type	Thermocouple	Suitable using temperature (°C)
1	NiCr-Ni	-200 - 1100
2	Pt-PtRh10	20 - 1550
3	PtRh6—PtRh30	120 - 1750
4	W/Re5-W/Re26	20°C - 2050

### 3.2.6 Laser-Flash method (thermal diffusivity)

The thermal conductivity  $\kappa$  of a material is the rate at which heat is conducted across an unit of cross-sectional area when there is an unit temperature gradient perpendicular to this area [76Ber]. The determination of the thermal conductivity is increasingly accomplished by measurements of the thermal diffusivity  $\alpha$ , using the relation for the diffusivity  $\alpha$ :

$$\kappa = \alpha C_p \rho, \quad (3.4)$$

where  $C_p$  is the specific heat and  $\rho$  the density of the material under investigation.

The laser flash method, as developed by Parker et al. [61Par, 62Par], has become one of the most customary methods in measuring thermal diffusivity of solid materials because of its basic simplicity, the small sample size required, the rapidity of the measurements and the suitability of the used technique from low to high temperatures. A schematic diagram of the laser flash method is shown in Fig. 3-2. The front side of the thin flat sample is heated by a short laser pulse. The heat absorbed is transported by thermal diffusion processes described by Fourier's equation to the sample's rear side. The resulting temperature rise of the rear side

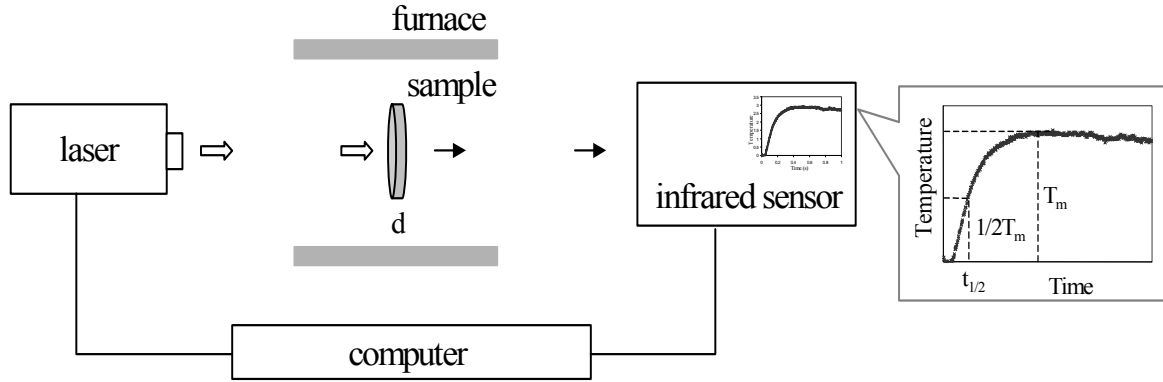


**Fig. 3-2** A schematic diagram of the laser flash method and temperature rise on the rear face.

vs. time is recorded and subsequently analyzed to yield the thermal diffusivity. Usually the thermal diffusivity is derived using the following well-known relation [61Par]:

$$\alpha = 1.36975 \, d^2 / (\pi^2 t_{1/2}), \quad (3.5)$$

where  $d$  is the sample thickness,  $t_{1/2}$  the time required to reach at the rear surface half of the maximum temperature rise. This relation is valid only when the pulse-duration time is sufficiently short as compared with  $t_{1/2}$ , there are no heat losses from the surface, and heat flow is one dimensional. If these preconditions are not fulfilled, the determination of the thermal diffusivity should be fitting the theoretical solution of Fourier's equation with heat losses [73Hec, 75Cla] and a finite pulse length correction [67Lar, 74Tay, 81Azu] to the measured temperature rise vs. time curve.

In this work, the thermal diffusivities of VT50- and NCP200-derived amorphous Si-C-N ceramics as well as of T2-1-derived amorphous Si-B-C-N ceramics were measured with the laser flash method over the temperature range from 25°C to 1200°C under a vacuum of ca.  $10^2$  Pa or less. A Neodym-YAG glass laser (Lasermetric. INC firm) with 1.06  $\mu\text{m}$  wavelength and ca. 1 ms pulse-duration time, as well as an infrared detector (Computherm firm) were used. The computer software Computherm firm has been employed to control the measurement and calculate the time required to reach half the maximum temperature rise of the rear surface  $t_{1/2}$  and the thermal diffusivity.



Details about the bulk amorphous ceramics preparation were described in Chapter 3.1. Both sides of the disc samples were coated with black thin carbon layers to enhance the absorption of the laser beam energy. Then the sample was fixed in the furnace (Theta-Industries firm) and thermal diffusivity measurements were carried out in the temperature range indicated above using 50-100°C steps (intervals).

## 4 Phase Equilibria, Phase Reactions and Thermal Stability of Precursor-Derived Si-(B-)C-N Ceramics

### 4.1 Si-C-N System

#### 4.1.1 Thermodynamic calculations

Fig. 4-1 shows the calculated isothermal sections in the ternary system Si-C-N for the temperatures  $1414^{\circ}\text{C} < T < 1484^{\circ}\text{C}$  (Fig. 4-1a),  $1484^{\circ}\text{C} < T < 1841^{\circ}\text{C}$  (Fig. 4-1b),  $T = 1850^{\circ}\text{C}$  (Fig. 4-1c) and  $T = 2727^{\circ}\text{C}$  (Fig. 4-1d). At temperatures lower than  $1414^{\circ}\text{C}$ , Si exists as solid

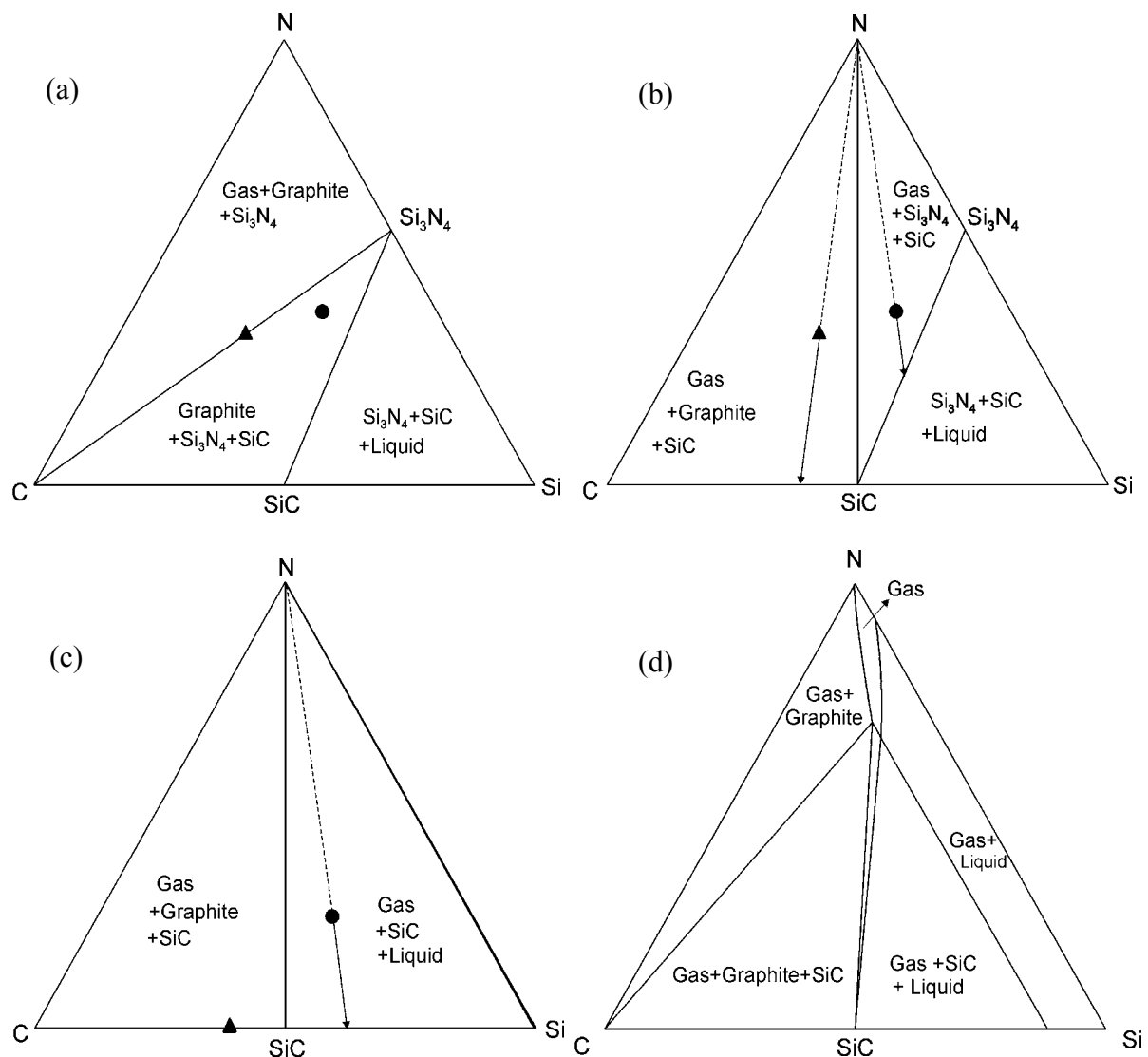
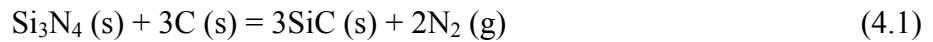


**Fig. 4-1** Isothermal sections in the Si-C-N system at a total pressure of 1 bar. The compositions of the amorphous VT50- and NCP200-derived ceramics (▲, ●) and reaction paths (arrows) are indicated: (a)  $1414^{\circ}\text{C} < T < 1484^{\circ}\text{C}$ ; (b)  $1484^{\circ}\text{C} < T < 1841^{\circ}\text{C}$ ; (c)  $T = 1850^{\circ}\text{C}$ ; (d)  $T = 2727^{\circ}\text{C}$ .

phase. For the calculations a constant total pressure of 1 bar was used. From the experimental point of view nitrogen escapes at 1 bar, but for the calculation it is in the gas phase and still part of the system (included in the mole fraction). The gas phase exists only in areas where there is excess nitrogen. The phase equilibria, the compositions of the as-thermolysed amorphous ceramics made from VT50 or NCP200 and the correlated reaction paths are shown (arrows in Figs. 4-1b and 1c). The reaction paths [99Sei2] indicate the change of the gross composition of the solid samples due to the loss of nitrogen according to the reaction of  $\text{Si}_3\text{N}_4$  with graphite (Fig. 4-1b) and decomposition of  $\text{Si}_3\text{N}_4$  (Fig. 4-1c) (reactions 4.1 and 4.2, respectively).

The calculated isothermal sections in Fig 4-1a and b are similar to the results presented by Weiss et al. [81Wei] but with improved reaction temperature data and related mostly to precursor-derived ceramics. At temperatures between 1414°C and 1484°C (Fig. 4-1a), the following three phase fields are present: (1) gas+graphite+ $\text{Si}_3\text{N}_4$ , (2) graphite+ $\text{Si}_3\text{N}_4$ +SiC, and (3)  $\text{Si}_3\text{N}_4$ +SiC+liquid. The liquid phase consists of nearly pure silicon. The composition of the VT50-derived ceramic is almost located on the tie line between graphite and  $\text{Si}_3\text{N}_4$ . Under the assumption of a complete crystallization of the materials, it consists of these both phases and only a very small amount of SiC. At a temperature of 1484°C,  $\text{Si}_3\text{N}_4$  and graphite react according to the nonvariant reaction

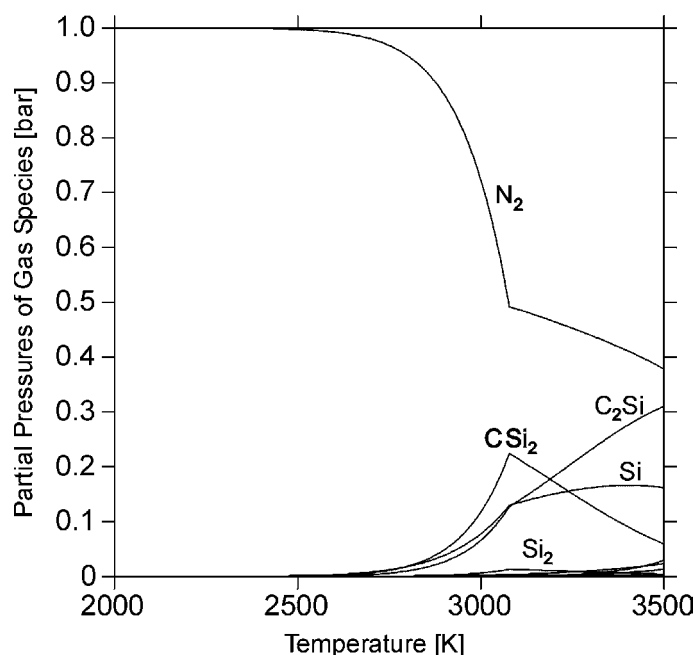


and at temperatures between 1484°C and 1841°C (Fig. 4-1b), the phase equilibria (1) gas+graphite+SiC (2) gas+ $\text{Si}_3\text{N}_4$ +SiC and (3)  $\text{Si}_3\text{N}_4$ +SiC+liquid occur. In connection with reaction (1) the VT50 ceramic with a ratio C:Si > 1 releases nitrogen until the indicated reaction path ends on the tie line graphite-SiC (Fig. 1b), whereas the ceramic NCP200 with a ratio C:Si < 1 loses nitrogen and changes the composition to the SiC- $\text{Si}_3\text{N}_4$  tie line. At temperatures above 1841°C the NCP200-derived ceramic again loses nitrogen (Fig. 4-1c) because the residual  $\text{Si}_3\text{N}_4$  dissociates into liquid silicon and nitrogen gas according to the reaction



At higher temperatures only two three-phase fields, (1) gas+graphite+SiC and (2) gas+SiC+liquid, remain. These phase fields exist up to very high temperatures. Fig. 4-1d

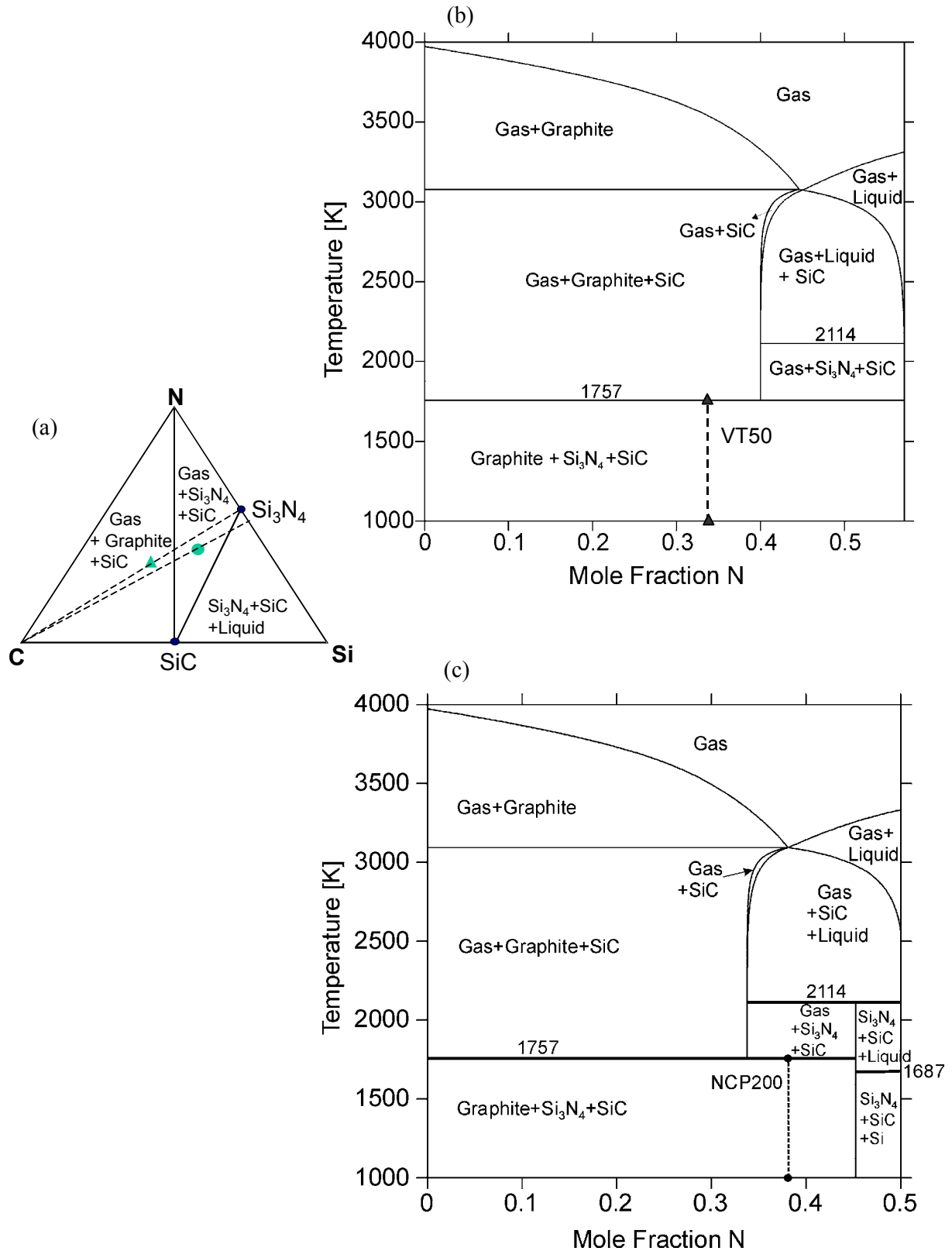
shows the calculated isothermal section in the Si-C-N system at a temperature of 2727°C. At such high temperatures, liquid silicon dissolves some carbon and the ternary gas phase region is significantly extended. The gas phase does not only consist of  $N_2$  but as well of other gaseous species such as Si,  $Si_2$ ,  $SiC_2$ ,  $Si_2C$ , CN and  $C_2N_2$  as given in Fig. 4-2, which shows the calculated partial pressure of different gaseous of the gas phase related to the VT50-derived ceramic at a total pressure of 1 bar.



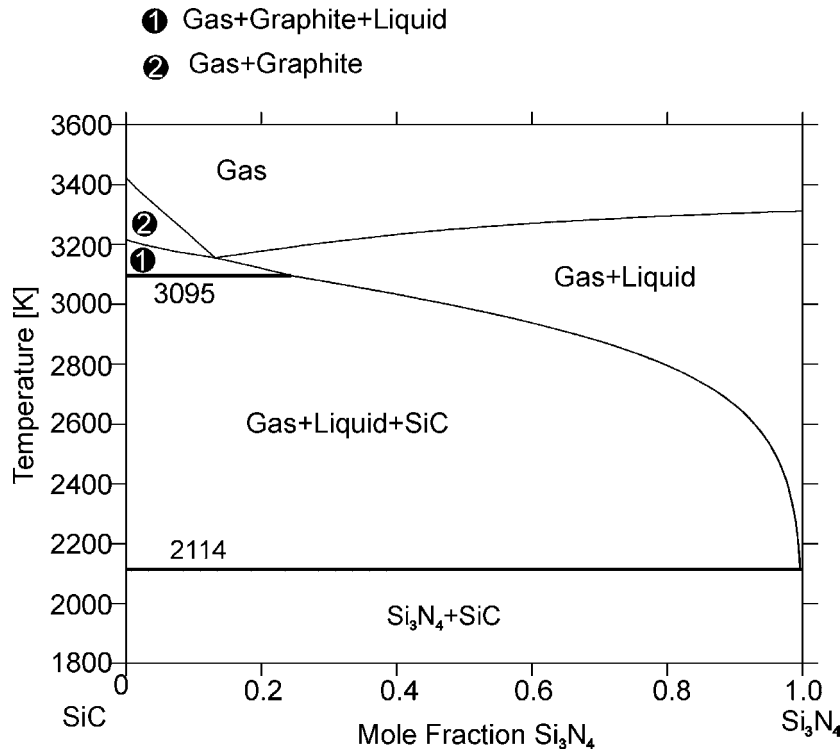
**Fig. 4-2** Partial pressures of different gaseous species of the gas phase in equilibrium with VT50-derived ceramic.

Fig. 4-3a shows the isothermal section at temperatures between 1484°C and 1841°C. The two dashed lines are the composition lines of isopleths shown in Figs. 4-3b and c ( $C - Si_{42.9}N_{57.1}$ ;  $C - Si_{49.5}N_{50.5}$ ) including the compositions of the VT50- and NCP200-derived ceramics. At temperatures below 1484°C (1757 K) both materials consist of graphite,  $Si_3N_4$  and SiC. The composition of the VT50-derived material is very close to the tie line between graphite and  $Si_3N_4$  thus it contains only very low amounts of SiC. At 1484°C reaction (4.1) occurs and the samples loose nitrogen. Hence, at higher temperatures the sample compositions are located outside the indicated composition lines of the isopleths (see reactions paths in Fig. 4-1b). In accordance with the isothermal section at  $T > 1484^\circ C$  the condensed materials consist of graphite and SiC (VT50) or of  $Si_3N_4$  and SiC (NCP200), respectively.

The isopleth between SiC and  $Si_3N_4$  in the Si-C-N system was calculated and is shown in Fig. 4-4. It can be seen that at a temperature 1841°C of (2114 K)  $Si_3N_4$  dissociates into liquid silicon and nitrogen gas and at a temperature of 2822°C (3095 K) SiC into graphite and gas.



**Fig. 4-3** Isoleths in the Si-C-N system. Compositions of VT50- and NCP200-derived ceramics are indicated: (a) Isothermal section for the temperature range  $1484^{\circ}\text{C} < T < 1841^{\circ}\text{C}$  with indicated composition lines of isopleths shown in Figs. 4-3(b) and (c); (b) Isoleth C - Si<sub>42.9</sub>N<sub>57.1</sub>; (c) Isoleth C - Si<sub>49.5</sub>N<sub>50.5</sub>.



**Fig. 4-4** Isopleth between SiC and Si<sub>3</sub>N<sub>4</sub> in the Si-C-N system.

Based on these calculations and the binary Si-N, Si-C and C-N phase diagrams (Fig. 2-6), Scheil's reaction scheme [36Sch, 60Geb] of the Si-C-N system (valid for  $p=1$  bar) was derived (Fig. 4-5). The scheme is similar to the one presented by Weiss et al. [81Wei] but with improved reaction temperatures. The reactions (4.1) and (4.2) are indicated as  $U_2$  and  $p_2$ , respectively. The melting point of Si is indicated by the reaction  $D_2$ . Because of lack of data the transformation  $\beta$ -SiC /  $\alpha$ -SiC was not taken into account. The  $\alpha$ -Si<sub>3</sub>N<sub>4</sub> /  $\beta$ -Si<sub>3</sub>N<sub>4</sub> transformation also was not considered, as  $\alpha$ -Si<sub>3</sub>N<sub>4</sub> is assumed to be a metastable phase [99Lia].

The influence of the gas phase on the phase reactions is shown in Fig. 4-6 by the calculated potential phase diagrams for  $C:Si > 1$  (Fig. 4-6a, valid for e.g. the VT50 ceramic) and  $C:Si < 1$  (Fig. 4-6b, valid for e.g. the NCP200 ceramic). The way of calculation of such diagrams is described elsewhere [98Sei1]. Here the gas phase is considered to be outside of the system, but may exchange nitrogen with it. Along the line identical in both figures the three phases graphite, SiC, and Si<sub>3</sub>N<sub>4</sub> are in equilibrium and show the reaction (4.1). Below the line, either the two phase fields SiC+C ( $C:Si > 1$ ) or SiC+Si<sub>3</sub>N<sub>4</sub> ( $C:Si < 1$ ) exist.

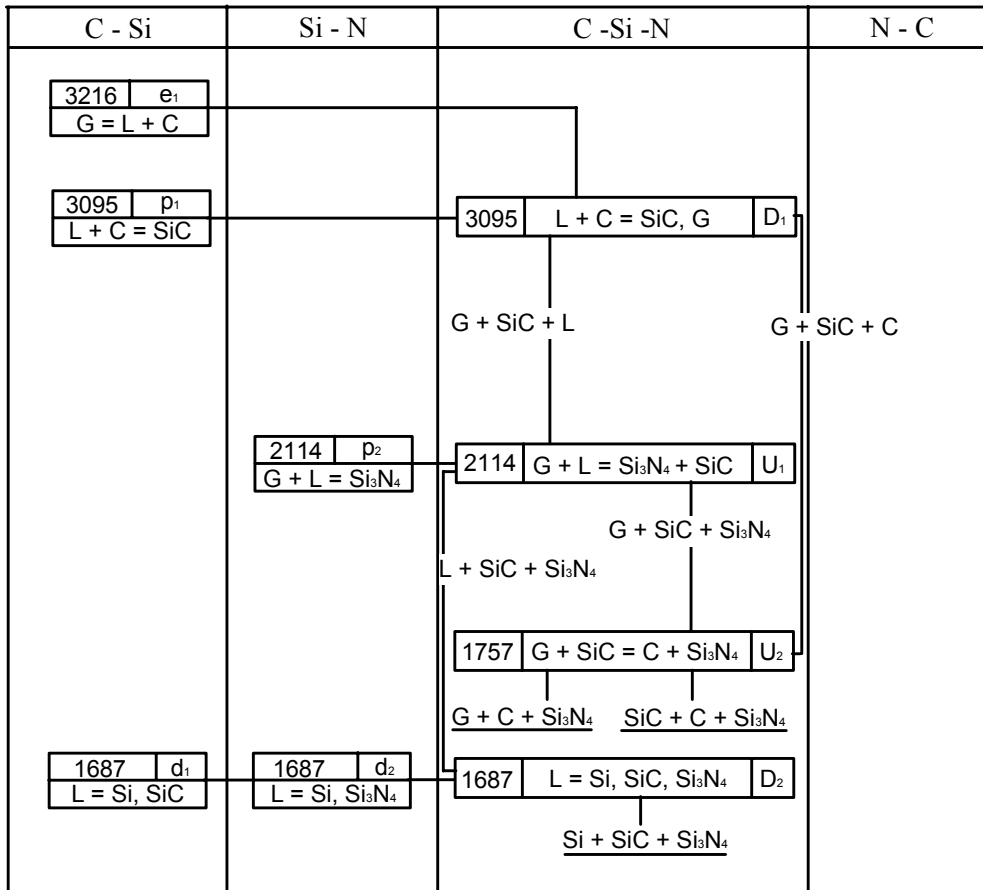


**Fig. 4-5** Scheil's reaction scheme for the Si-C-N system, temperature in K. ( $\beta$ -SiC/ $\alpha$ -SiC and  $\alpha$ -Si<sub>3</sub>N<sub>4</sub>/ $\beta$ -Si<sub>3</sub>N<sub>4</sub> transformations not indicated).

Of major interest is the nitrogen–pressure dependence of reaction (4.1). The reaction temperature increases with increasing partial pressure of nitrogen. The reaction temperatures given in the Scheils reaction scheme (Fig. 4-5) are valid for a total pressure of 1bar. At  $p(\text{N}_2) = 1$  bar the temperature of reaction (4.1) is 1484°C (1757 K), whereas at  $p(\text{N}_2) = 10$  bar this temperature is shifted to 1700°C (1973 K) (Fig. 4-6). Assuming a pressure of e. g. only  $p(\text{N}_2) = 10^{-4}$  bar, the reaction should occur at a much lower temperature of 954°C (1227 K).

Another important point is the N<sub>2</sub>-pressure dependence of the decomposition temperature of Si<sub>3</sub>N<sub>4</sub> according to reaction (4.2) into nitrogen and liquid or solid Si (which is in equilibrium with SiC). From Fig. 4-6b it can be seen that at  $p(\text{N}_2) = 1$  bar Si<sub>3</sub>N<sub>4</sub> decomposes at 1841°C (2114 K) into liquid silicon and nitrogen. At  $p(\text{N}_2) = 10$  bar the pertinent value is 2034°C (2307 K). Assuming a N<sub>2</sub> partial pressure of 10<sup>-4</sup> bar, the decomposition of Si<sub>3</sub>N<sub>4</sub> should occur at 1299°C (1572 K).

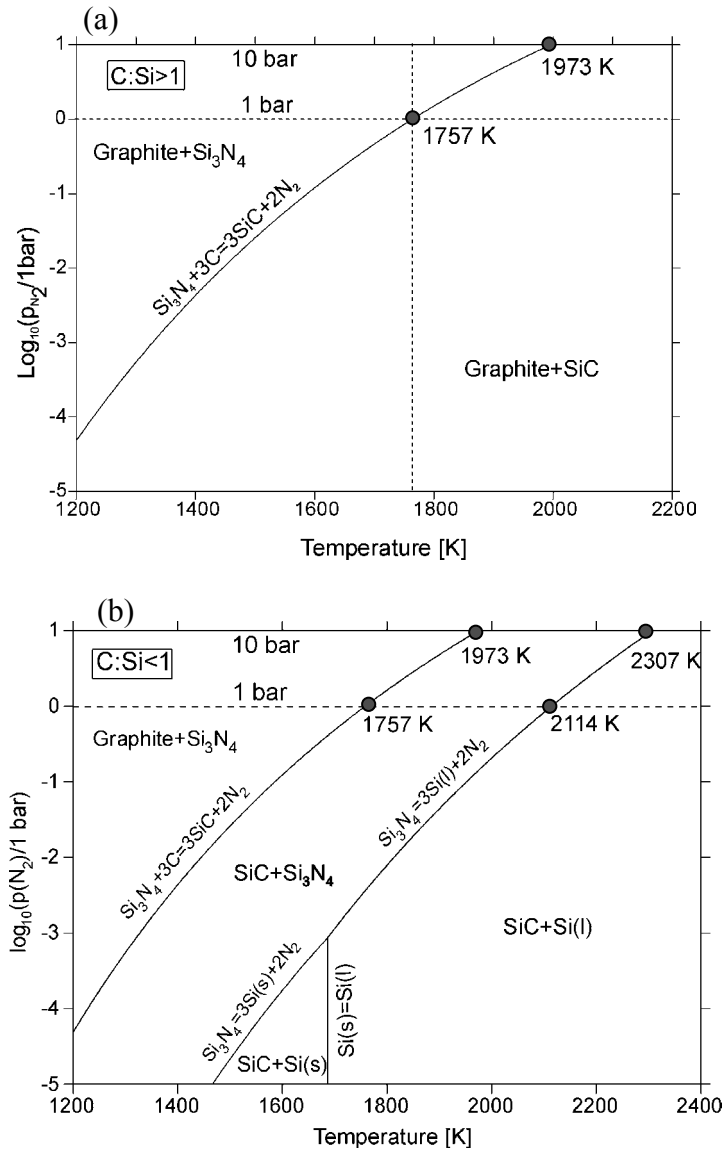


**Fig. 4-6** Potential phase diagrams for the Si-C-N system [98Sei1]: (a)  $C:Si > 1$ ; (b)  $C:Si < 1$ .

The diagrams give advice for the sintering of precursor ceramics and  $Si_3N_4$ -SiC samples. If the  $N_2$ -partial pressure is above the line of reaction (4.1), the sample is stable at the sintering temperature. For the sintering of SiC+ $Si_3N_4$ , there are temperature dependent upper and lower limits for the  $N_2$ -pressure for the stability range. During cooling from the sintering temperature of such samples the  $N_2$ -pressure has to be lowered simultaneously to keep the composition of the sample in the SiC+ $Si_3N_4$  phase field (Fig. 4-6b). For more details see references [88Nic, 91Mis, 98Sei1].



Additionally, quantitative mass balances and the enthalpies of phase reactions can be calculated for the ceramics. To achieve this, phase fraction diagrams were calculated for individual materials compositions. Fig. 4-7a shows this type of diagram at a total pressure of

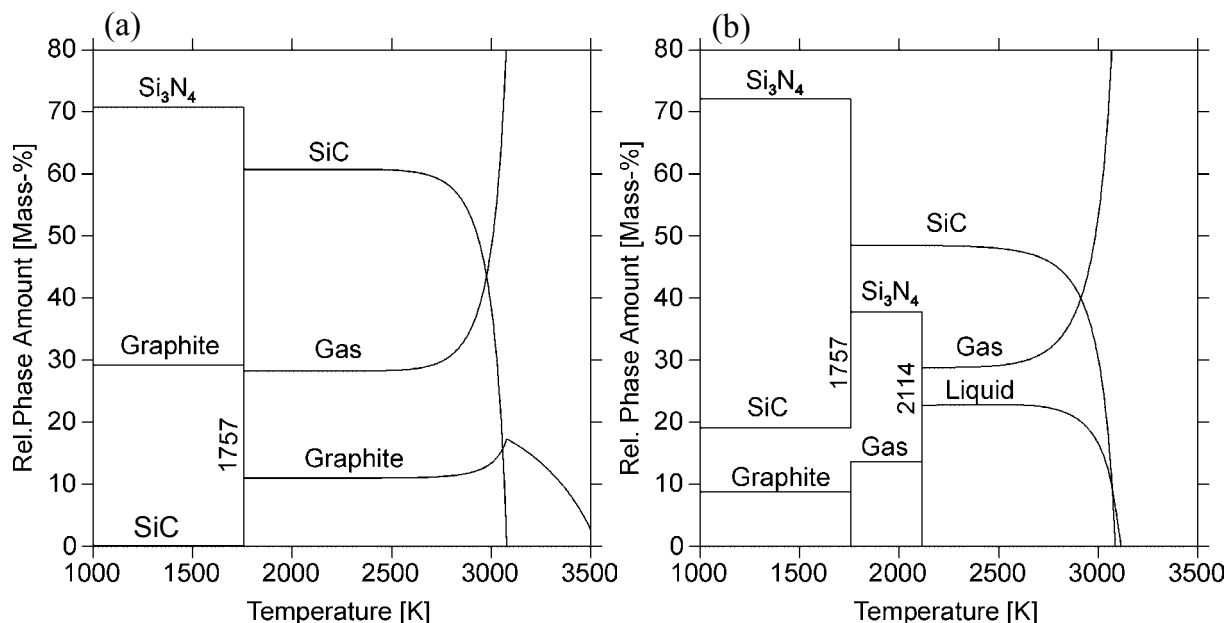


**Fig. 4-7** Calculated phase fraction diagrams in the Si-C-N system: (a) VT50-derived ceramics (C:Si > 1); (b) NCP200-derived ceramics (C:Si < 1).

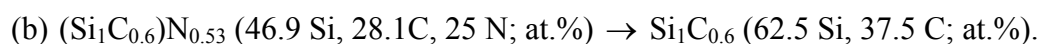
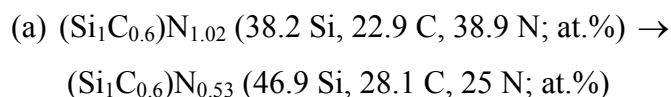
1 bar for the composition of the VT50-derived ceramic (C:Si > 1), where at the aforementioned temperature of 1484°C (1757 K) according to reaction (4.1) 70.7 mass%  $\text{Si}_3\text{N}_4$ , 29.2 mass% graphite and a negligible amount of SiC form 60.7 mass% of SiC, 11 mass% graphite and 28.3 mass% of nitrogen gas. The predicted sample mass loss due to nitrogen evaporation is 28.3 %. The gas phase in calculation still belongs to the system but appears as “mass loss” in TG experiments. After reaction (4.1) excess graphite remain. In VT50-derived ceramics, no  $\text{Si}_3\text{N}_4$  is found any longer. The changing gas phase composition with different gaseous species constituting the gas phase at different temperatures is shown in the calculated diagram of Fig. 4-2.

For NCP200-derived ceramic (Fig. 4-7b) with a ratio C:Si < 1 due to reaction (4.1) all free carbon is consumed and there is a mass loss of 13.7 %. After the reaction, excess  $\text{Si}_3\text{N}_4$  remains beside SiC. At temperatures higher than 1841°C (2114 K), this residual  $\text{Si}_3\text{N}_4$  decomposes according to reaction (4.2) causing a further mass loss of 15.1 %. Note that the balanced reaction equation (4.1) is only valid for a ratio C: $\text{Si}_3\text{N}_4$  defined by the intersection of

the inner tie-lines C-Si<sub>3</sub>N<sub>4</sub> and N-SiC of the four phase reaction (4.1) (79.6 mass% Si<sub>3</sub>N<sub>4</sub>, 20.4 mass% graphite).

Figs. 4-7a and 4-7b show that at temperatures higher than 2600 K the SiC fraction decreases, whereas the fraction of the gas phase increases. This results from the formation of the gaseous species CSi<sub>2</sub> and C<sub>2</sub>Si at such high temperatures as shown for the composition of the VT50-derived ceramic in Fig. 4-2.

The lengths of the arrows indicating the reaction paths in Fig. 4-1b and c, respectively, give the values of the relative changes of the nitrogen content of the solid samples. In the case of VT50-derived ceramic a direct comparison with the result of the calculated phase fraction diagram is possible. The composition of this ceramic changes according to the sequence Si<sub>1</sub>C<sub>1.6</sub>N<sub>1.33</sub> (25.4 Si, 40.7 C, 33.8 N; at.%) → Si<sub>1</sub>C<sub>1.6</sub> (38.5 Si, 61.5 C; at.%). The final solid sample lost the complete nitrogen content of 33.8 at.%. This value can be found from the indicated reaction path (arrow) for VT50-derived ceramics in Fig. 4-1b and corresponds to the 28.3 mass% calculated in the phase fraction diagram (Fig. 4-7a). The relationship between the reaction paths and the calculated phase fraction diagram for the NCP200-derived ceramic is not as obvious as for the VT50-derived ceramics. The composition of that ceramic changes during the reactions (4.1) and (4.2) according to the following sequence:



The lengths of the corresponding two arrows (reaction paths in Fig. 4-1b and c, respectively) give only the relative changes of the nitrogen content of the solid samples. After the first step (a) the nitrogen content of the solid sample is 25 at.%. The phase fraction diagram gives a mass loss of 13.7% which corresponds to 18.5 at.%. At a first glance this value does not agree with the value of nitrogen loss derived from the length of the arrow in Fig. 4-1b which is 13.9 at.%. The data of the phase fraction diagram calculation refer to the total system including the gas phase which was released during the reaction at 1484°C (1757 K), whereas the 25 at.% are referring to the solid residue after this reaction. The calculation assumes that the gas phase is always a part of the system. On the other hand, the data from the indicated reaction paths refer only to the composition of the solid phases without taking into account the released gas

phase. The calculated mass loss of the second step is 15.1 mass% (20.4 at.%) of the initial sample or 25.0 at.% referred to the residue of step 1.

The DTA experiments can be simulated by calculating enthalpy-temperature diagrams (Fig. 4-8). The calculated enthalpy-temperature diagram shows for the VT50-derived ceramic an endothermic heat effect of +52.3 kJ/mol (moles of atoms of total sample) for reaction (4.1). The enthalpy of phase reaction (4.1) for the ceramic NCP200 is +28 kJ/mol and of phase reaction (2) is +49 kJ/mol. Both phase reactions are endothermic.

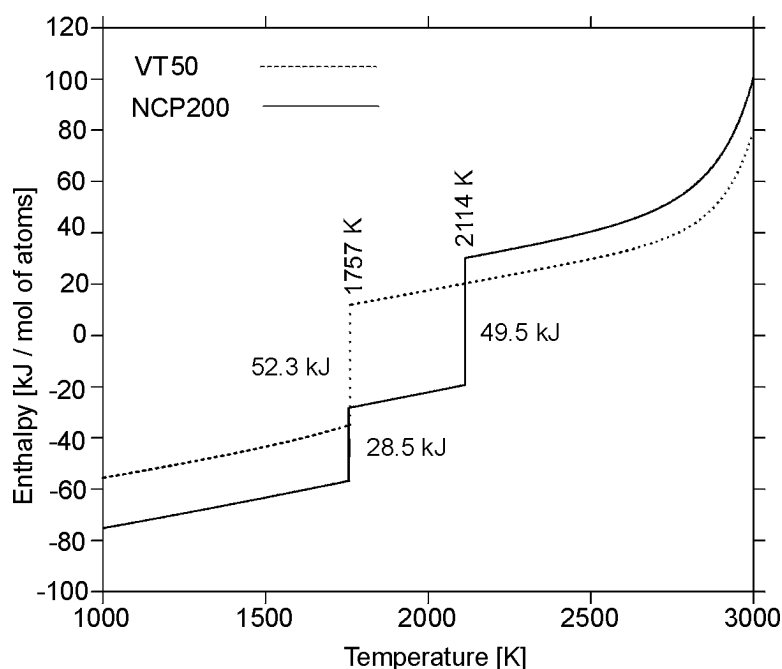


**Fig. 4-8** Calculated enthalpy-temperature diagrams for the VT50- and NCP200-derived ceramics.

It has to be decided which crucible material is suitable for the heat treatment and thermal analyses of the ceramic samples. Graphite crucibles are not adequate because they react with  $\text{Si}_3\text{N}_4$ . A suitable crucible material is BN. The reaction of VT50-derived ceramics of the composition  $\text{Si}_1\text{C}_{1.6}\text{N}_{1.33}$  with BN was simulated. The result is shown as phase fraction diagram in Fig. 4-9. The calculation shows that BN does not take part in reaction (1) (i.e. U2 in Fig. 4-5). According to the equilibrium calculation, BN is formed at temperatures lower than 727°C (1000 K) and remains inert until the reaction of BN, graphite and SiC is starting at the temperature of 2313°C (2586 K). Based on this result, BN crucibles were used for thermal analyses.

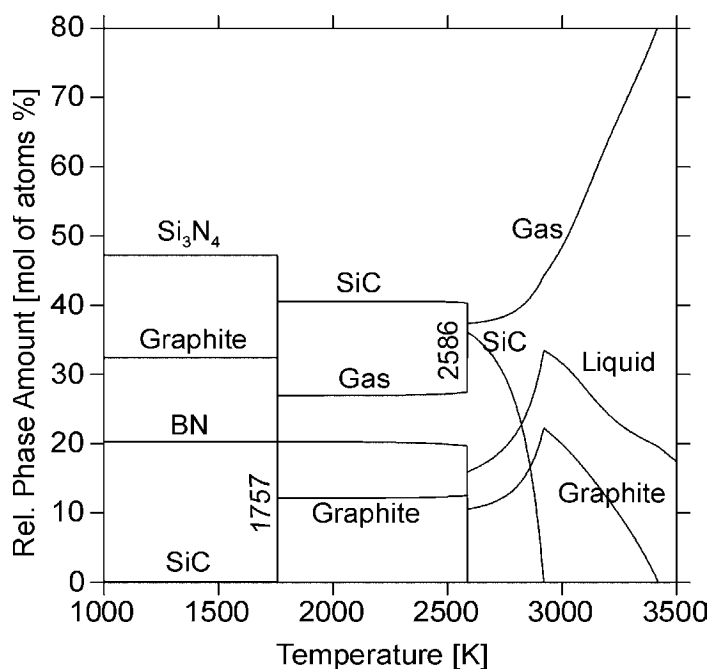


**Fig. 4-9** Phase fraction diagram for the combination of VT50-derived ceramic with BN.

#### 4.1.2 Experimental investigations and discussion

Figs. 4-10a and b show the DTA/TG measurement curves in N<sub>2</sub> atmosphere (1 bar) with a heating rate of 5 K/min, and BN-crucible for the VT50-derived and the NCP200-derived ceramic, respectively. The TG analysis of VT50 ceramic shows a mass loss of 29% between 1600°C (1873 K) and 1690°C (1963 K). Simultaneously, an endothermic reaction peak was found by DTA. This mass loss and the endothermic reaction peak can be explained by reaction (4.1) (Figs. 4-1b, 4-7a), although the reaction temperature is somewhat higher than the calculated one due to this “dynamic” experiment and kinetic influences.

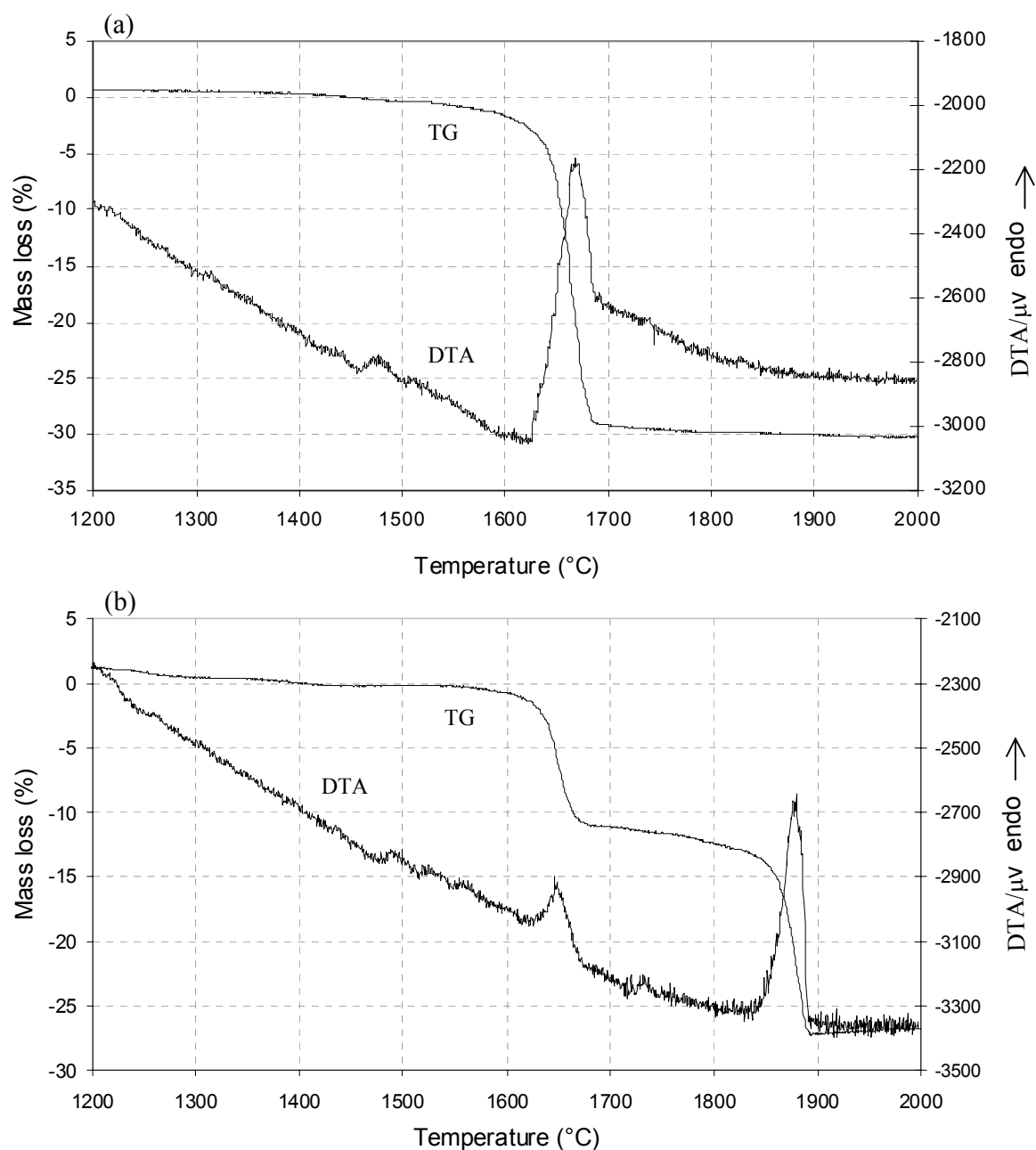


**Fig. 4-10** DTA/TG measurements (STA) for precursor-derived ceramics;  $\text{N}_2$  atmosphere (flowing, 1 bar), BN crucible, 10K/min up to 1000 $^{\circ}\text{C}$  (1273 K), 5K/min up to 2000 $^{\circ}\text{C}$  (2273 K): (a) VT50-derived ceramics; (b) NCP200-derived ceramics.

In the case of the NCP200 ceramic, the two steps of mass loss with accompanied endothermic reactions could be disclosed as predicted by the thermodynamic calculations (Figs. 4-1b and 4-7b). In the temperature range from 1600 $^{\circ}\text{C}$  (1873 K) to 1690 $^{\circ}\text{C}$  (1963 K) 12% mass loss and an endothermic reaction peak were detected, and between 1840 $^{\circ}\text{C}$  (2113

K) and 1900°C (2173 K) 15% mass loss and an endothermic reaction peak were determined. The first endothermic peak can be attributed to reaction (4.1), although its temperature is higher than calculated because of the influence of the kinetics. The second endothermic peak is due to the decomposition of residual  $\text{Si}_3\text{N}_4$  according to reaction (4.2). The temperature of reaction (4.2) is in agreement with the calculated result. According to the present assessment,  $\text{Si}_3\text{N}_4$  should decompose into liquid Si and gaseous  $\text{N}_2$  of 1 atm at 1841°C (2114 K). The two steps of mass loss agree quantitatively with the calculated results. The ratios of the three experimentally derived enthalpy values (the area of the endothermic peaks) are similar to the ratio of the calculated enthalpies (Fig. 4-8).

No DTA measurement of Si-C-N precursor-derived ceramic has been documented in the literature. The TG measurements for the VT50-derived ceramic and the NCP200-derived ceramic were carried out by Kamphowe [99Kam]. But the run of curve for the measurement of the NCP200-derived ceramic did not fit well the calculated one because graphite crucible was used in the measurement and graphite reacts with  $\text{Si}_3\text{N}_4$  as mentioned in Chapter 4.1.1.

XRD and SEM combined with EDX were used to confirm the results obtained by DTA / TG (STA) and the thermodynamic calculations. Fig. 4-11 shows the XRD patterns of the

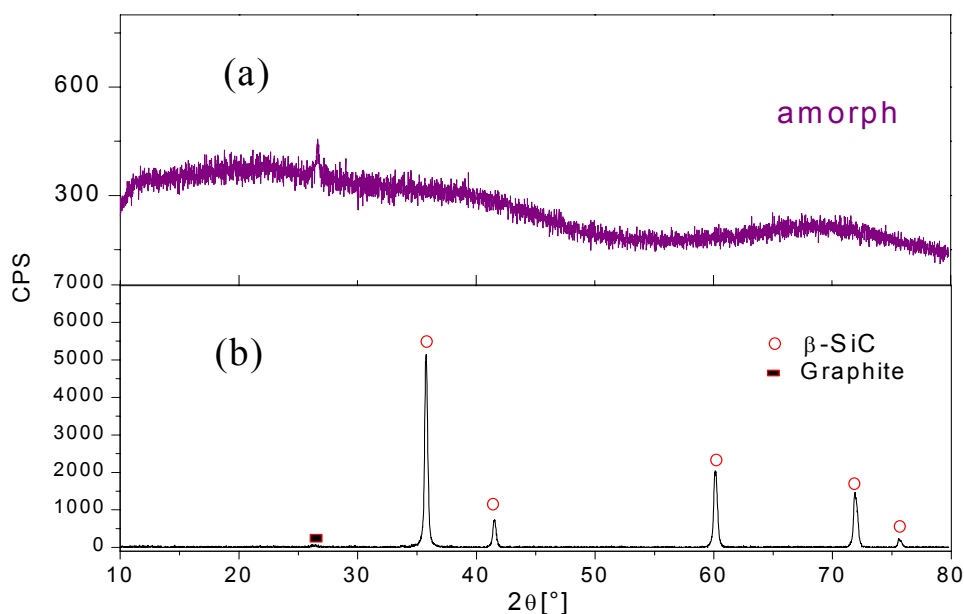


**Fig. 4-11** XRD patterns of the VT50-derived ceramic: (a) Before STA; (b) After STA up to 2000 °C (2273 K).

VT50-derived ceramic. As shown in Fig. 4-11a the structure of this material before STA is typically amorphous as reported in the work [97Ja]. After STA with an upper temperature of 2000°C (2273 K, Fig. 4-10a) the material consists of crystalline  $\beta$ -SiC and graphite (Fig. 4-11b), which is in accordance with the calculations (Figs. 4-1a, 4-1b and 4-7a). The carbon is formed mainly in amorphous form and only a small crystallized amount is detectable by X-ray analysis. In the case of the NCP200-derived ceramic, after STA up to 1800°C (2073 K, Fig. 4-12b) the phase configuration changes to  $\beta$ -SiC/ $\alpha$ -Si<sub>3</sub>N<sub>4</sub> or to  $\beta$ -SiC/Si(liquid), if the STA is continued up to 2000°C (2273 K, Fig. 4-12c). Comparing the XRD patterns of the

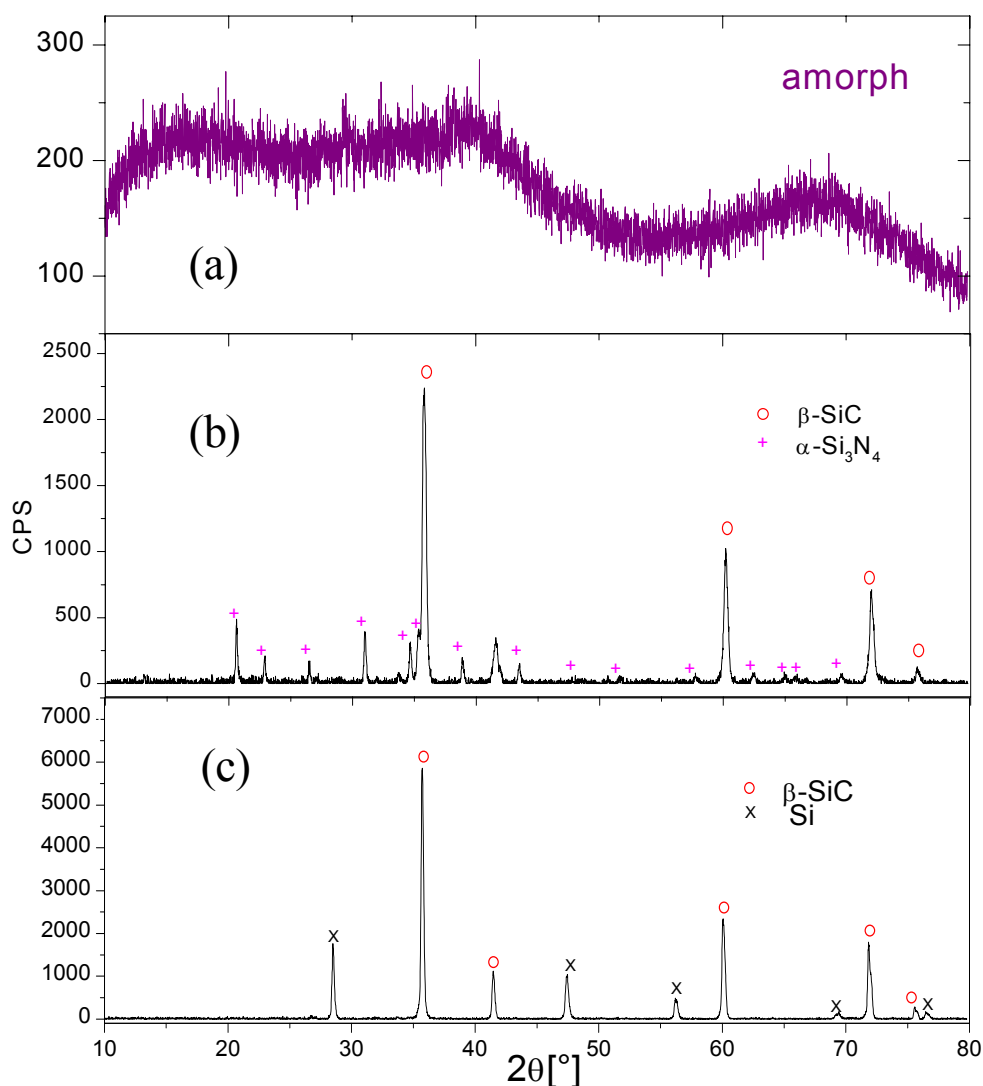


**Fig. 4-12** XRD pattern of the NCP200-derived ceramic: (a) Before STA; (b) After STA up to 1800 °C (2073 K); (c) After STA up to 2000 °C (2273 K).

NCP200-derived ceramics in Figs. 4-12a-c with Figs. 4-1a-c and 7b shows that the experimental results are also correctly simulated by the calculation.

Fig. 4-13 shows SEM images of the NCP200-derived ceramic. Heating up to 1800°C (2073 K, Fig. 4-13a) clearly  $\beta$ -SiC/ $\alpha$ -Si<sub>3</sub>N<sub>4</sub> can be recognized, whereas after heating up to 2000°C (2273 K, Fig. 4-13b) besides  $\beta$ -SiC silicon can be seen, which still has the shape of solidified droplets. The phase compositions were confirmed by EDX analyses.

The high temperature behavior of VT50-derived ceramic in different atmospheres is shown in Fig. 4-14. It was found that the atmosphere has a strong influence on the temperature of reaction (4.1). The temperature of beginning of reaction (4.1) shifts from 1560°C in nitrogen atmosphere to ca. 1500°C in argon atmosphere.

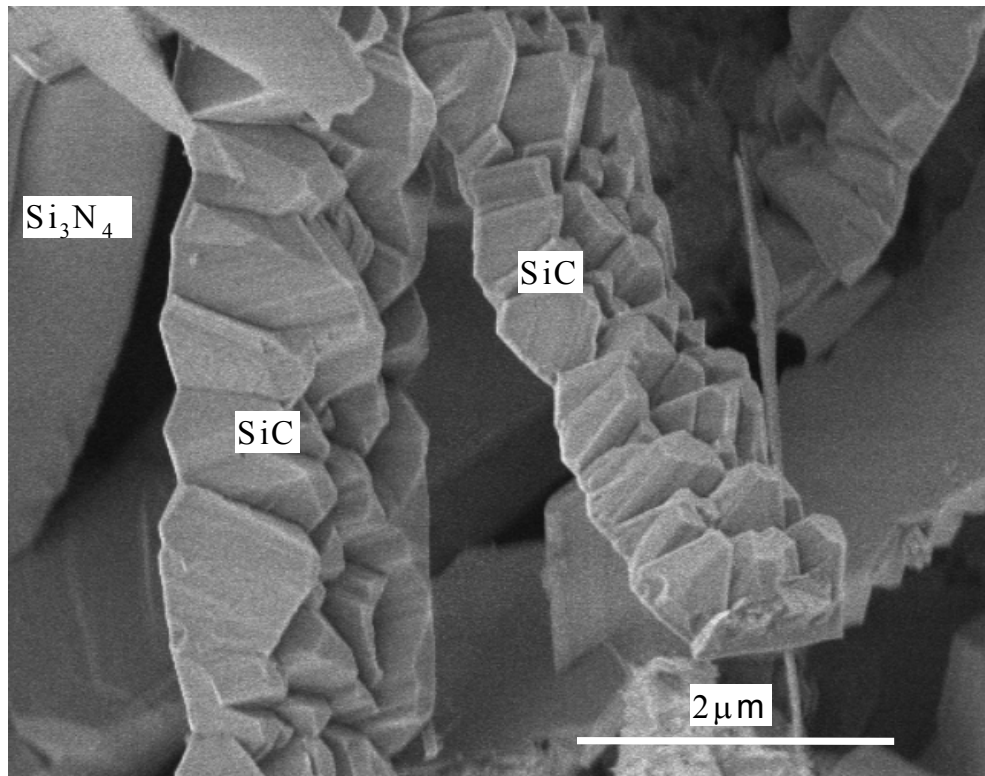
In order to derive the influence of the heating rate on the temperatures of reaction (4.1) and (4.2), different rates were used for carrying out DTA/TG measurements for NCP200-derived ceramic. The TG curves are shown in Fig. 4-15 and the onset temperatures at different heating rates obtained from these curves are given in Table 4-1. As can be seen, the higher the heating rate is, the higher is the onset temperature of the reactions (4.1) and (4.2).

**Table 4-1** Extrapolated onset temperatures of reaction (4.1) and (4.2) at different heating rates.

Heating rate	2 K/min	5 K/min	10 K/min	15 K/min
Onset temperature of reaction (4.1)	1597°C	1625°C	1625°C	1628°C
Onset temperature of reaction (4.2)	1864°C	1864°C	1872°C	1878°C



(a)



(b)

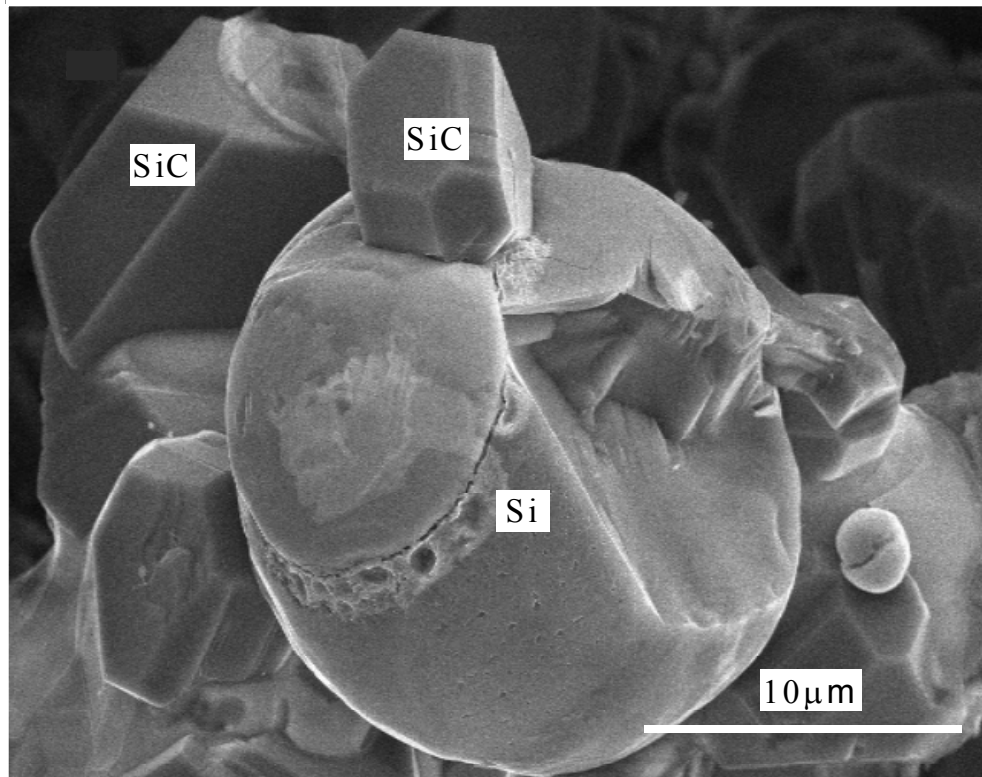


**Fig. 4-13** SEM images of NCP200-derived ceramics: (a) After STA up to 1800°C (2073 K); (b) After STA up to 2000°C (2273 K).

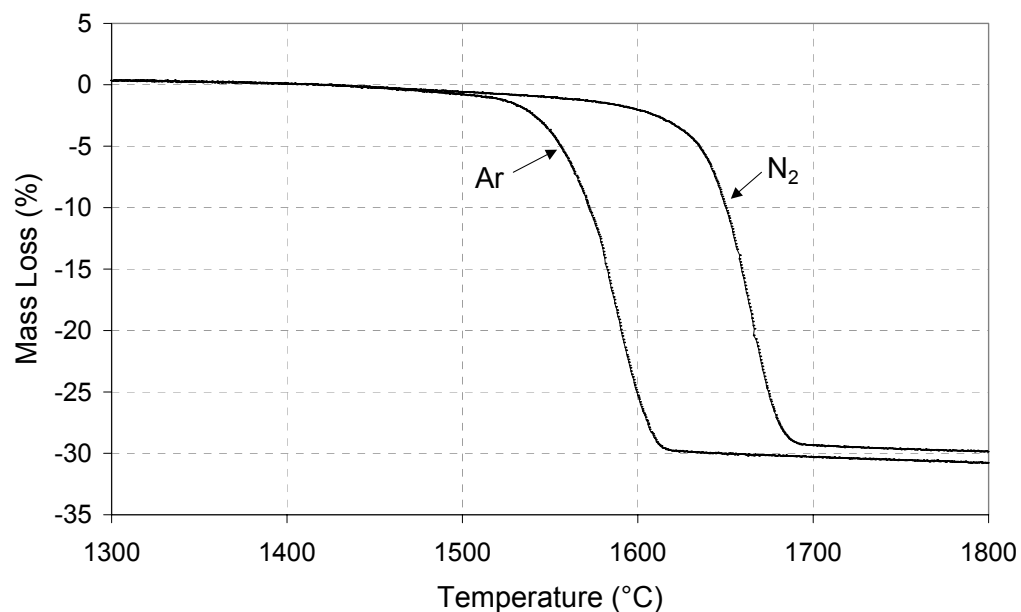


**Fig. 4-14** TG measurements curves for VT50-derived ceramic carried out under argon and nitrogen atmosphere (flowing, 1 bar), BN crucible, 10 K/min up to 1000°C (1273 K), 5K/min up to 2000°C (2273 K).

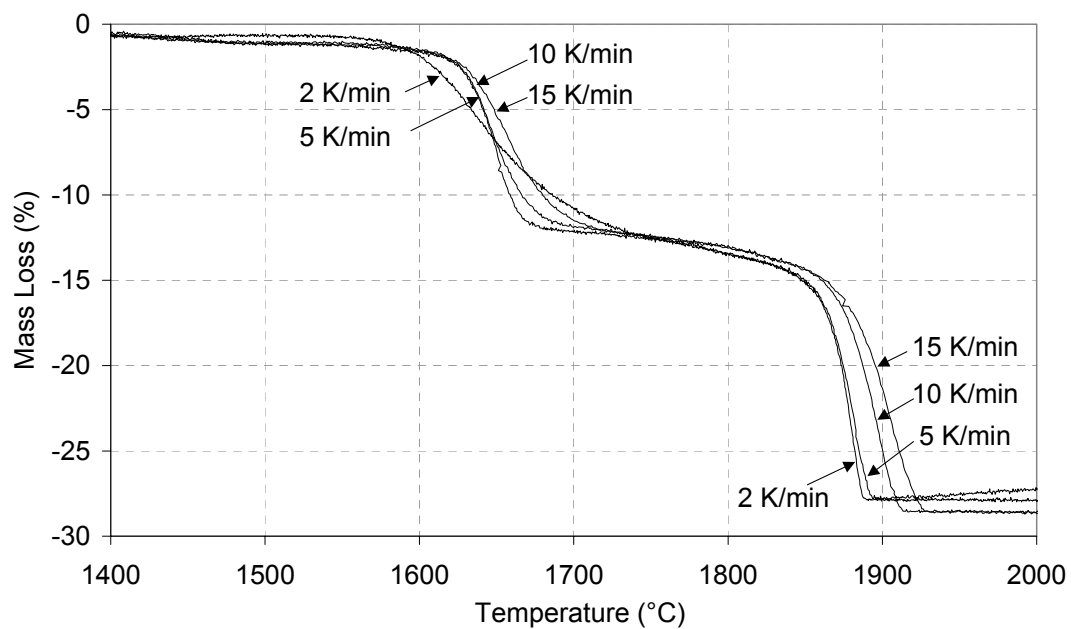


**Fig. 4-15** The TG measurements of NCP200-derived ceramic carried at different heating rates (2 K/min, 5 K/min, 10 K/min and 15 K/min), N<sub>2</sub> atmosphere (flowing, 1 bar), BN crucible.

DTA/TG measurements for VT50-derived ceramic and for samples of powder mixtures of  $\alpha$ - $\text{Si}_3\text{N}_4$  and C,  $\beta$ - $\text{Si}_3\text{N}_4$  and C and of  $\alpha$ - $\text{Si}_3\text{N}_4$ , C and BN were also carried out in nitrogen atmosphere with a heating rate of 5 K/min, as shown in Fig. 4-16. Because the grain sizes of the powder mixtures  $\alpha$ - $\text{Si}_3\text{N}_4$  + C,  $\beta$ - $\text{Si}_3\text{N}_4$  + C are greater than that of VT50-derived amorphous ceramic, the reaction temperatures of the two powder mixtures are slightly higher than of the VT50-derived amorphous ceramic. In contrast to that, the reaction temperature of the powder mixture  $\alpha$ - $\text{Si}_3\text{N}_4$  and C is significantly higher when BN was added to it, this result will be discussed in Chapter 4.2.

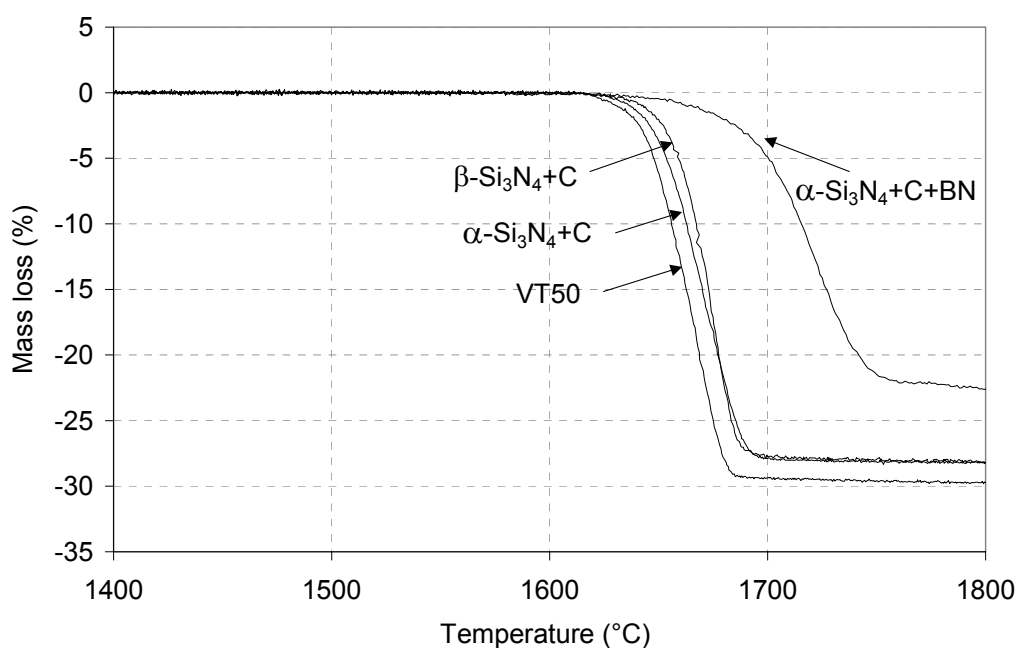


**Fig. 4-16** DTA/TG measurements of VT50-derived ceramic and of samples of powder mixtures  $\alpha$ - $\text{Si}_3\text{N}_4$  + C,  $\beta$ - $\text{Si}_3\text{N}_4$  + C and  $\alpha$ - $\text{Si}_3\text{N}_4$  + C + BN carried out in nitrogen atmosphere with a heating rate of 5 K/min.

### 4.1.3 Conclusion

The phase reactions, the crystallization behavior and the thermal degradation of two Si-C-N ceramics derived from precursor VT50 and NCP200, respectively, were studied by means of CALPHAD type thermodynamic calculations, DTA / TG , XRD and SEM/EDX. The thermal degradation of both ceramics have been characterized quantitatively by taking into account

the endothermic phase reactions  $\text{Si}_3\text{N}_4 + 3\text{C} = 3\text{SiC} + 2\text{N}_2$  and  $\text{Si}_3\text{N}_4 = 3\text{Si} + 2\text{N}_2$ . The thermal degradation behaviour of these two ceramics is different. The endothermic phase reaction 4.1: ( $\text{Si}_3\text{N}_4 + 3\text{C} = 3\text{SiC} + 2\text{N}_2$ ) proceeds during the thermal degradation of both ceramics. The phase reaction 4.2: ( $\text{Si}_3\text{N}_4 = 3\text{Si} + 2\text{N}_2$ ) occurs only during the thermal degradation of the ceramic derived from NCP200. Both phase reactions have been quantitatively characterized. To explain quantitatively the high temperature behaviour of Si-C-N ceramics reaction scheme, isothermal sections, isopleths, phase fraction diagrams and phase composition diagrams (for gas partial pressures) were calculated. The studies of DTA /TG, X-ray diffraction and SEM are in good agreement with the calculated results. The computer simulations were confirmed by the experiments for both ceramics.

The results of the experimental investigation of VT50- and NCP200-derived ceramics show that CALPHAD-type simulations can quantitatively predict their high-temperature behaviour. The present work shows that thermodynamic calculations can be used successfully to support the development of Si-C-N ceramics using the powder technology and the precursor route, respectively. From these calculations the phase equilibria, phase compositions, phase reactions and the accompanied microstructure development can be derived. Such information provides guidelines for favorable sintering and processing conditions and the understanding of the materials reactions during application. Additionally, kinetic effects (e.g. during crystallization of amorphous ceramics) and the formation of metastable phases (e.g.  $\alpha\text{-Si}_3\text{N}_4$ ) have to be taken into account.

The composition of most of the precursor-derived amorphous Si-C-N ceramics documented in literature are located within the three-phase field graphite+ $\text{Si}_3\text{N}_4$ +SiC (see also Chapter 5). After crystallization such materials are most frequently composed of  $\text{Si}_3\text{N}_4$ , SiC and graphite. Therefore, the high temperature stability of these ceramics is limited because reaction (4.1) takes place during these conditions. Recent results [01Wei] point out that it is possible to obtain stoichiometric  $\text{Si}_3\text{N}_4$ /SiC composites directly by thermolyzing proper precursors with compositions resulting in material free of carbon and a higher temperature stability until reaction (4.2) takes place.

## 4.2 Si-B-C-N System

### 4.2.1 Thermodynamic calculations

#### 4.2.1.1 Isothermal sections

The addition of boron to Si-C-N materials leads to additional stable phases, i.e. BN,  $B_{4+\delta}C$ ,  $B_3Si$ ,  $B_6Si$ , and  $B_nSi$ , according to the boron content in the materials. Clear information on phase equilibria in the Si-B-C-N system at constant temperatures were derived from calculated quaternary isothermal sections [98Ald, 99Sei1, 01Sei2]. Resulting isothermal sections at 25°C (298 K), 1400°C (1673 K), 1600°C (1873 K) and 2000°C (2273 K), respectively, are shown in Figs. 4-17a, b, c, and d. In these cases different irregular tetrahedra indicating the four-phase equilibria at the specific temperature separate the regular concentration tetrahedron. At temperatures between 25°C (298 K) and 1198°C (1471 K) nine four-phase equilibria 1a-9a exist as shown in Fig. 4-17a. At temperatures above 1198°C (1471 K) the phase  $SiB_3$  is not stable and decomposes into Si and  $SiB_6$ . The eutectic temperature between  $SiB_6$  and silicon was calculated to be 1384°C (1657 K). At the temperature of 1396°C (1669 K),  $B_{4+\delta}C$  and Si react according to the reaction (4.3):



Therefore, at the temperature 1673 K (1400°C) nine different four-phase equilibria 1a-6a and 7b-9b exist as shown in Fig 4-17b. Above a temperature of 1414°C (1687 K), Si exists as liquid phase and at a temperature of 1484°C (1757 K)  $Si_3N_4$  and graphite react according to the nonvariant reaction (4.1). So at 1600°C (1873 K), there are the other eight four-phase equilibria (Fig. 4-17c).  $Si_3N_4$  dissociates into liquid silicon and nitrogen gas according to the reaction (4.2) at temperatures above 1841°C (2114 K). At a temperature of 1850°C (2123 K), the phase  $SiB_6$  separates into the phase  $SiB_n$  and liquid. In Fig. 4-17d there are six possible four-phase equilibria at the temperature of 2000°C (2273 K).

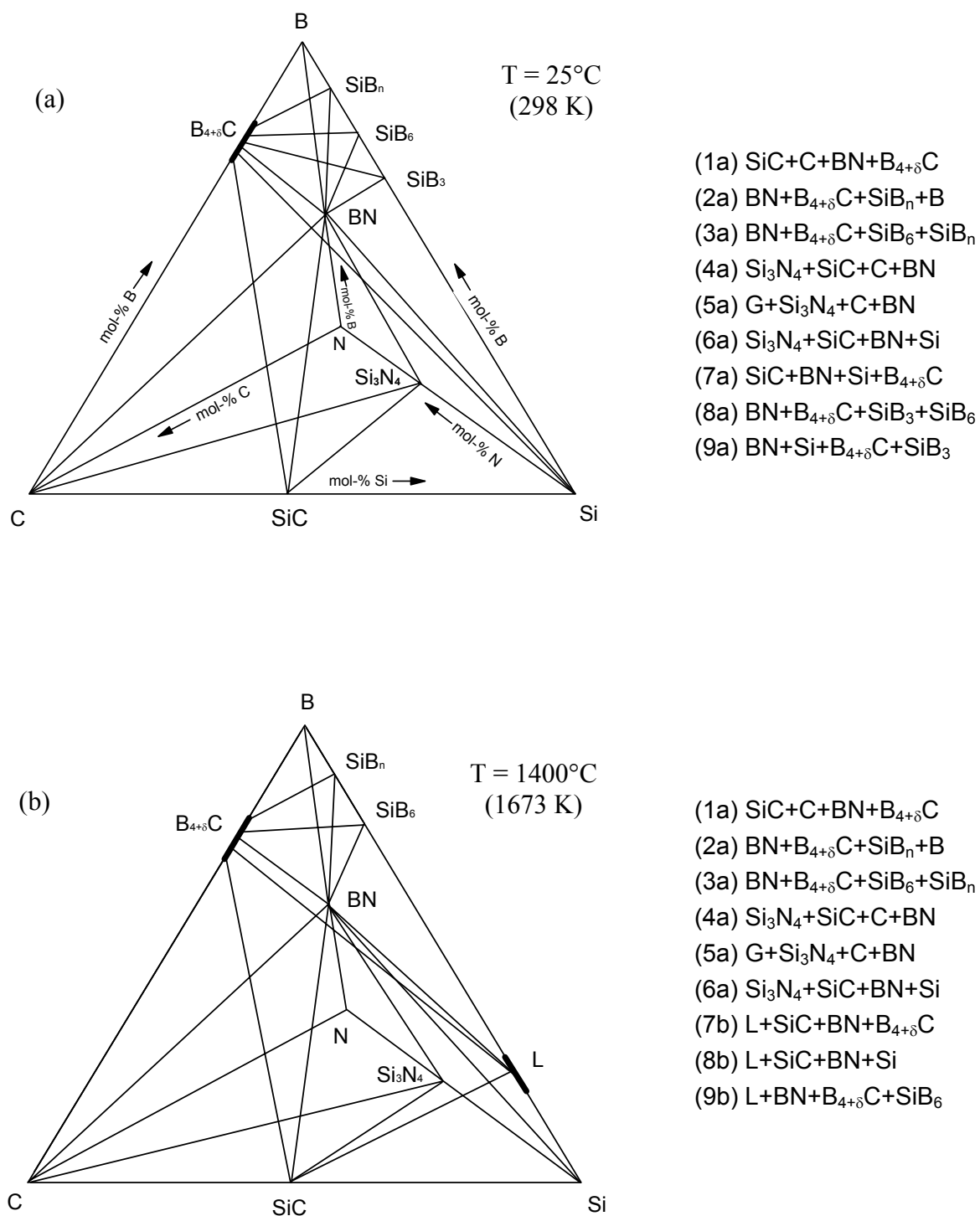


**Fig. 4-17** Calculated quaternary isothermal sections in Si-B-C-N system, the existing four-phase equilibria at each temperature are also indicated: (a)  $T = 25^{\circ}\text{C}$  (298 K) (or  $T < 1198^{\circ}\text{C}$  (1471 K)); (b)  $1400^{\circ}\text{C}$  (1673 K).

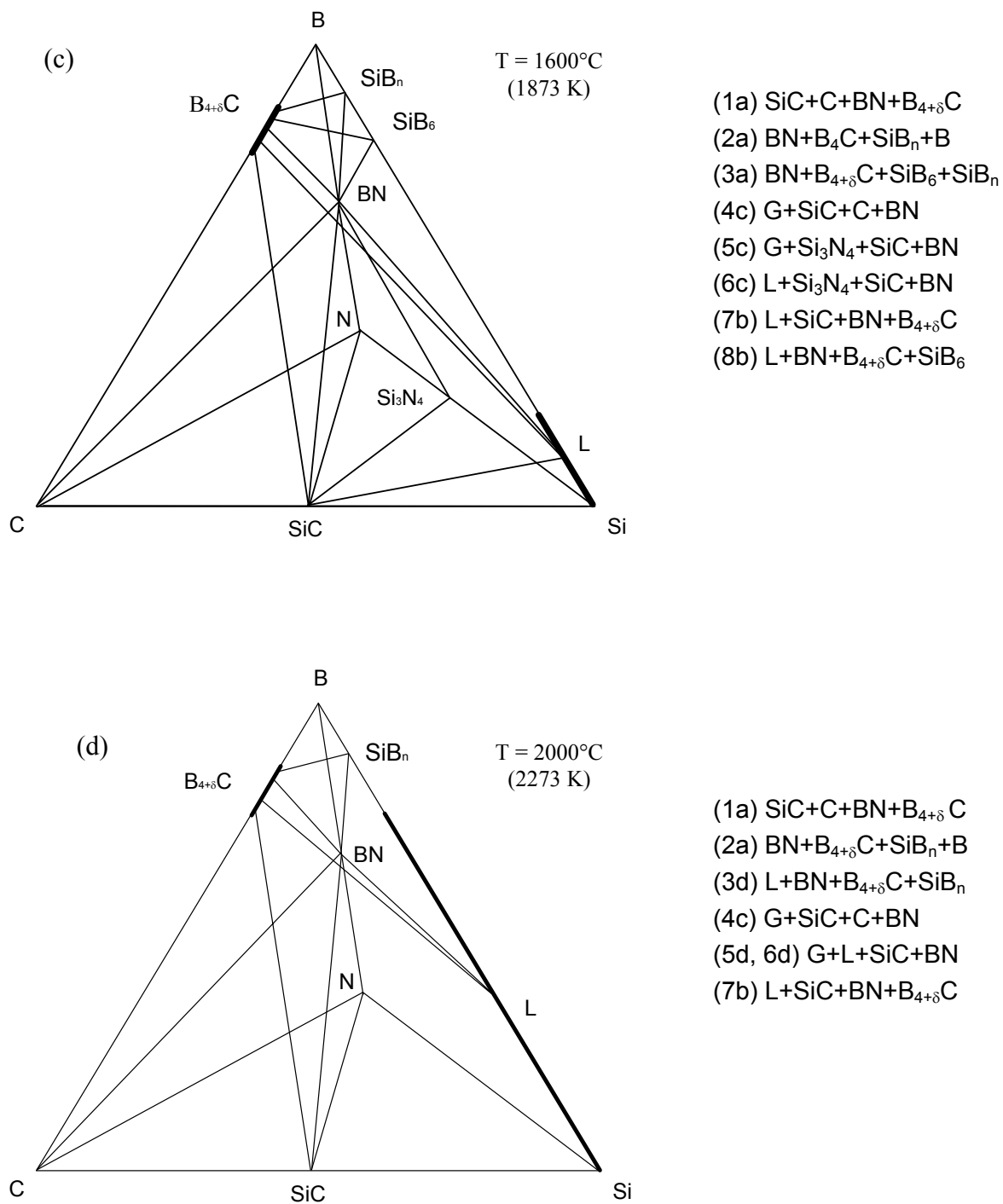


**Fig. 4-17** Calculated quaternary isothermal sections in Si-B-C-N system, the existing four-phase equilibria at each temperature are also indicated: (c)  $1600^{\circ}\text{C}$  (1873 K); (d)  $2000^{\circ}\text{C}$  (2273 K).

#### 4.2.1.2 Isothermal sections at constant boron contents

From Table 3-2 it can be seen that the boron content of all precursor derived Si-B-C-N amorphous ceramics listed is less than 27 at.% and that the boron content of these ceramics may fall roughly into four groups of about 5 at.%, 10 at.%, 15 at.% and 25 at.% boron, respectively. In order to analyze the phase equilibria of these materials, isothermal sections at these four boron contents were calculated. For reference Fig. 4-18 shows the isothermal section at 1400°C (1673 K), at a constant boron content of 25 at. %. To clarify the appearance of phase equilibria some dotted lines are added.

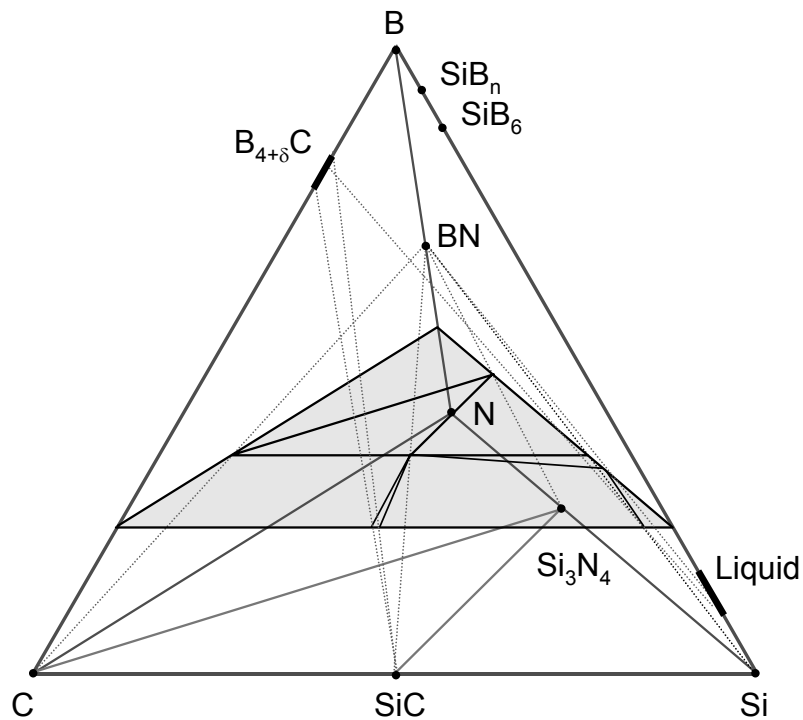


**Fig. 4-18** Stable phases and an isothermal section at 1400°C (1673 K) at a constant boron content of 25 at.% of the system Si-B-C-N.



The calculated isothermal sections of the four selected boron contents at temperatures of 25°C (298 K), 1400°C (1673 K), 1600°C (1873 K) and 2000°C (2273 K) are shown in Figs. 4-19, 4-20, 4-21 and 4-22, respectively. In the sections at 25°C (Figs. 4-19a, 20a, 21a, 22a) the six four-phase equilibria (4a)  $\text{Si}_3\text{N}_4+\text{SiC}+\text{C}+\text{BN}$ , (5a)  $\text{Gas}+\text{Si}_3\text{N}_4+\text{C}+\text{BN}$ , (6a)  $\text{Si}_3\text{N}_4+\text{SiC}+\text{Si}+\text{BN}$ , (1a)  $\text{SiC}+\text{C}+\text{BN}+\text{B}_{4+\delta}\text{C}$ , (7a)  $\text{SiC}+\text{BN}+\text{B}_{4+\delta}\text{C}+\text{Si}$  and (9a)  $\text{BN}+\text{Si}+\text{B}_{4+\delta}\text{C}+\text{SiB}_3$  and one three-phase equilibrium ( $\text{SiC}+\text{BN}+\text{B}_{4+\delta}\text{C}$ ) appear as triangles or squares, respectively, dependent on the way how the plane is intersecting the tetrahedron. Note that with increasing boron content the extensions of the four-phase equilibria fields (4a), (5a), (6a) shrink and those of (1a), (7a), (9a) expand. For a boron contents of more than 50 at.%, the four-phase equilibria of (4a) (5a) (6a) will disappear.

In all diagrams the compositions of the relevant precursor-derived Si-B-C-N amorphous ceramics are inserted. As can be seen from the diagrams at temperatures of 25°C and 1400°C all considered compositions are located within the four-phase equilibrium (4a)  $\text{Si}_3\text{N}_4+\text{SiC}+\text{C}+\text{BN}$ . The materials can be grouped into those with compositions located in the center of this four-phase equilibrium (No. 1-12; Table 3-2, p. 29) and those with compositions more or less close to the edge of this phase field and near to the equilibrium phase containing either gas or free silicon (No.13-27; Table 3-2, p. 29). This phase equilibrium remains stable as high as 1484°C (1757 K), where  $\text{Si}_3\text{N}_4$  reacts with carbon and the ceramics are expected to lose nitrogen as described above for the Si-C-N ceramics.

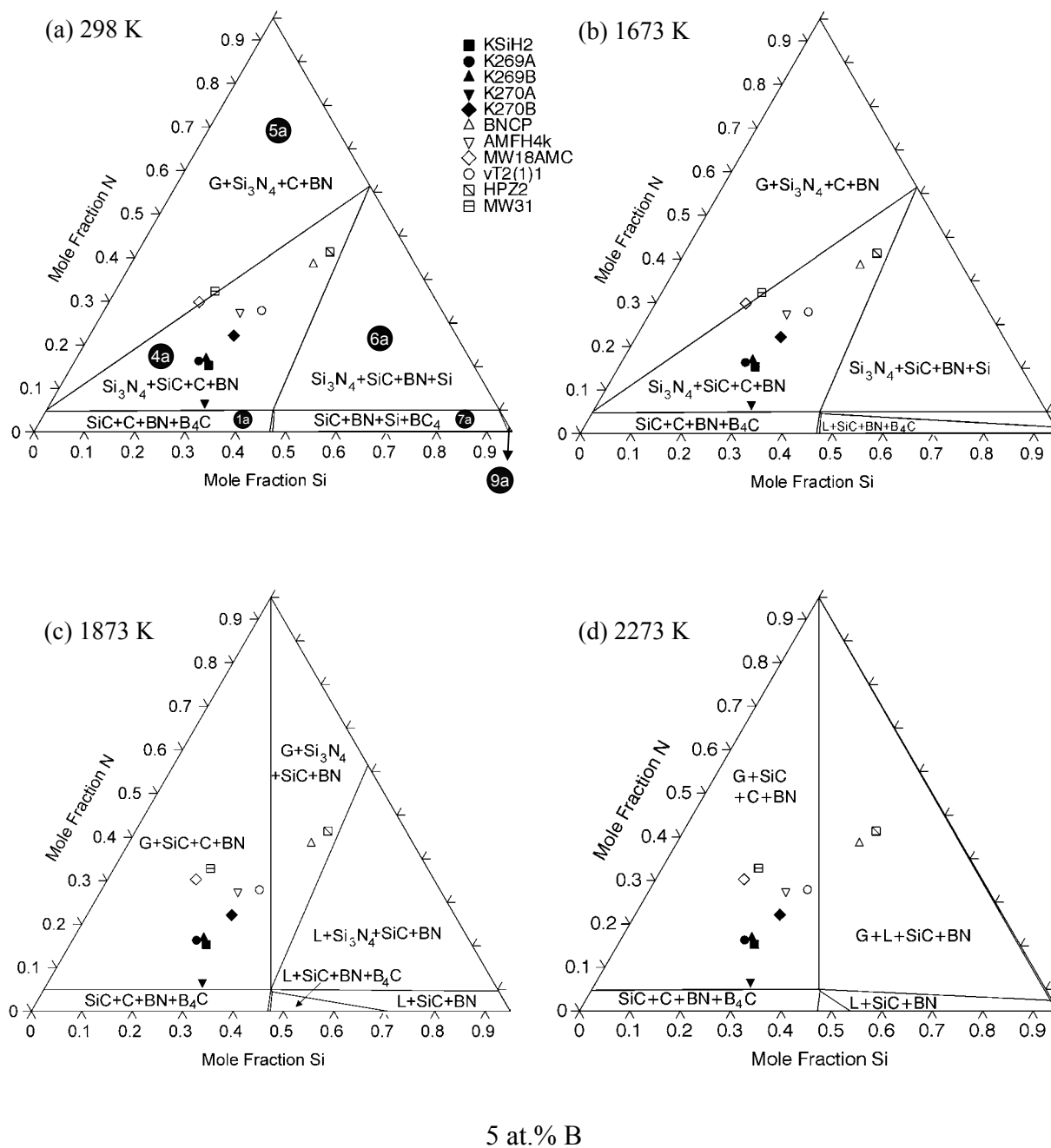


**Fig. 4-19** Calculated isothermal sections at 5 at.% boron at temperatures of (a) 25°C (298 K); (b) 1400°C (1673 K); (c) 1600°C (1873 K); (d) 2000°C (2273 K). The compositions of the relevant precursor derived Si-B-C-N amorphous ceramics are inserted; for details see Table 3-2 (p. 29).

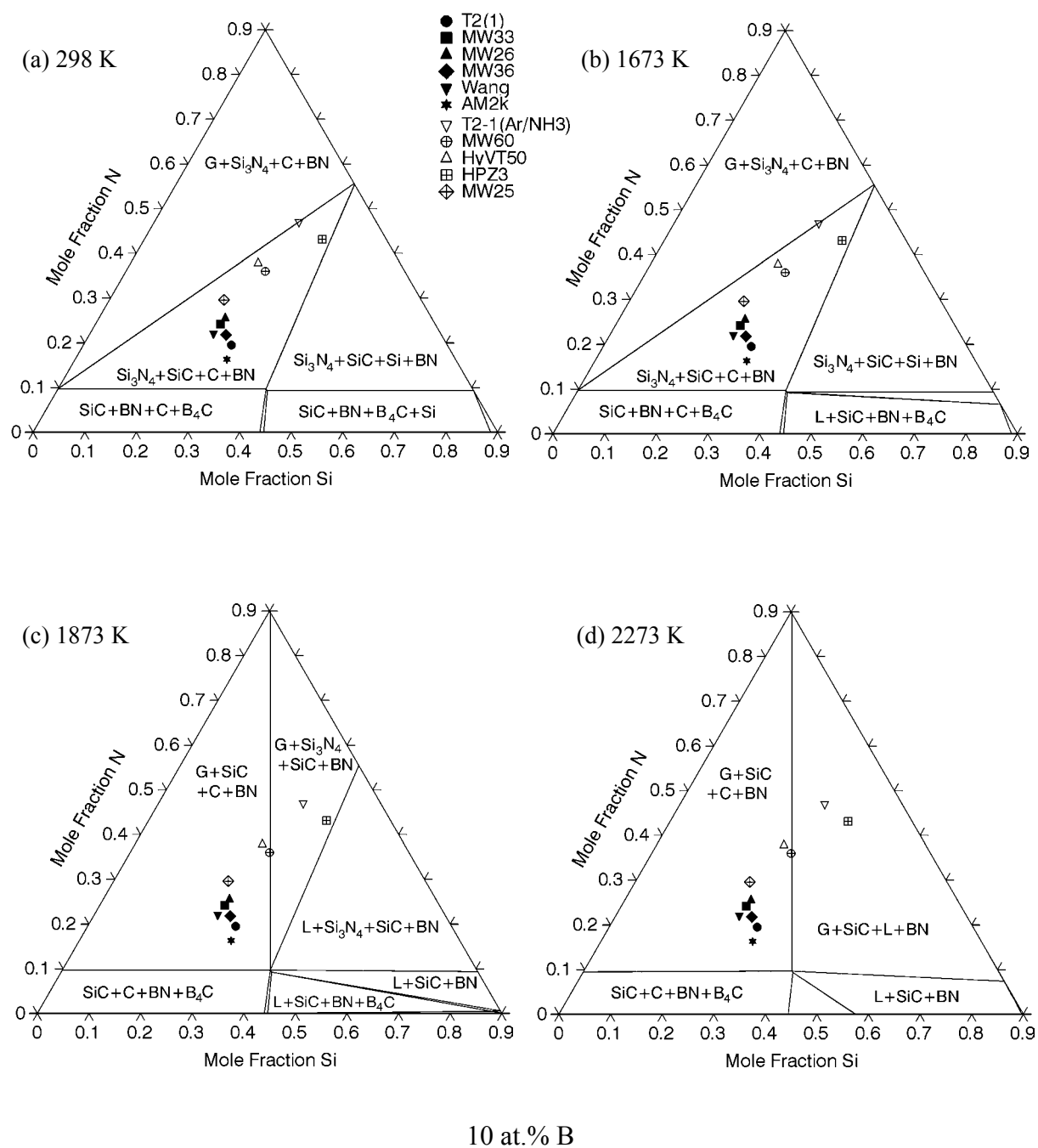


**Fig. 4-20** Calculated isothermal sections at 10 at.% boron at temperatures of (a) 25°C (298 K); (b) 1400°C (1673 K); (c) 1600°C (1873 K); (d) 2000°C (2273 K). The compositions of the relevant precursor derived Si-B-C-N amorphous ceramics are inserted; for details see Table 3-2 (p. 29).

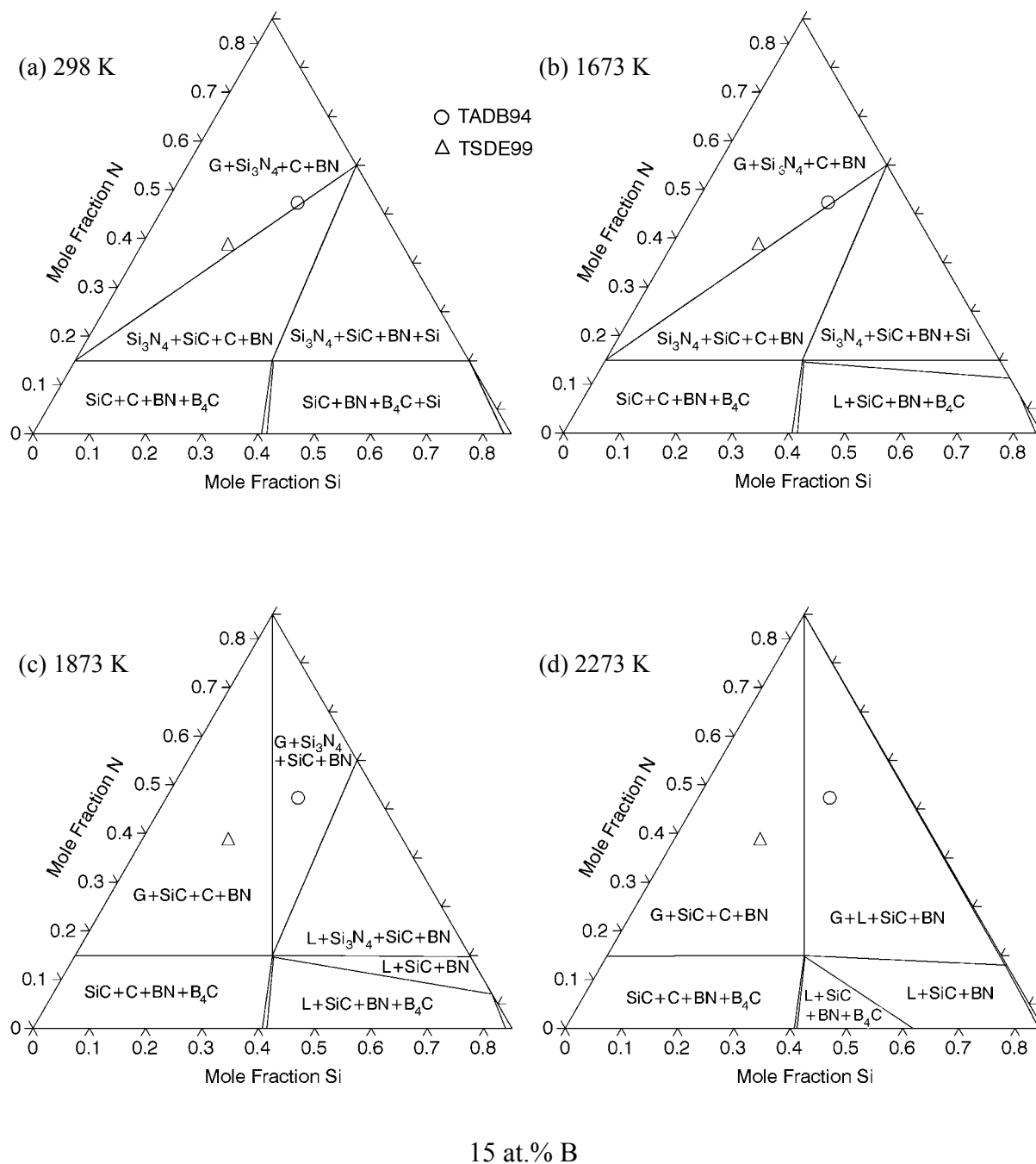


**Fig. 4-21** Calculated isothermal sections at 15 at.% boron at temperatures of (a) 25°C (298 K); (b) 1400°C (1673 K); (c) 1600°C (1873 K); (d) 2000°C (2273 K). The compositions of the relevant precursor derived Si-B-C-N amorphous ceramics are inserted; for details see Table 3-2 (p. 29).

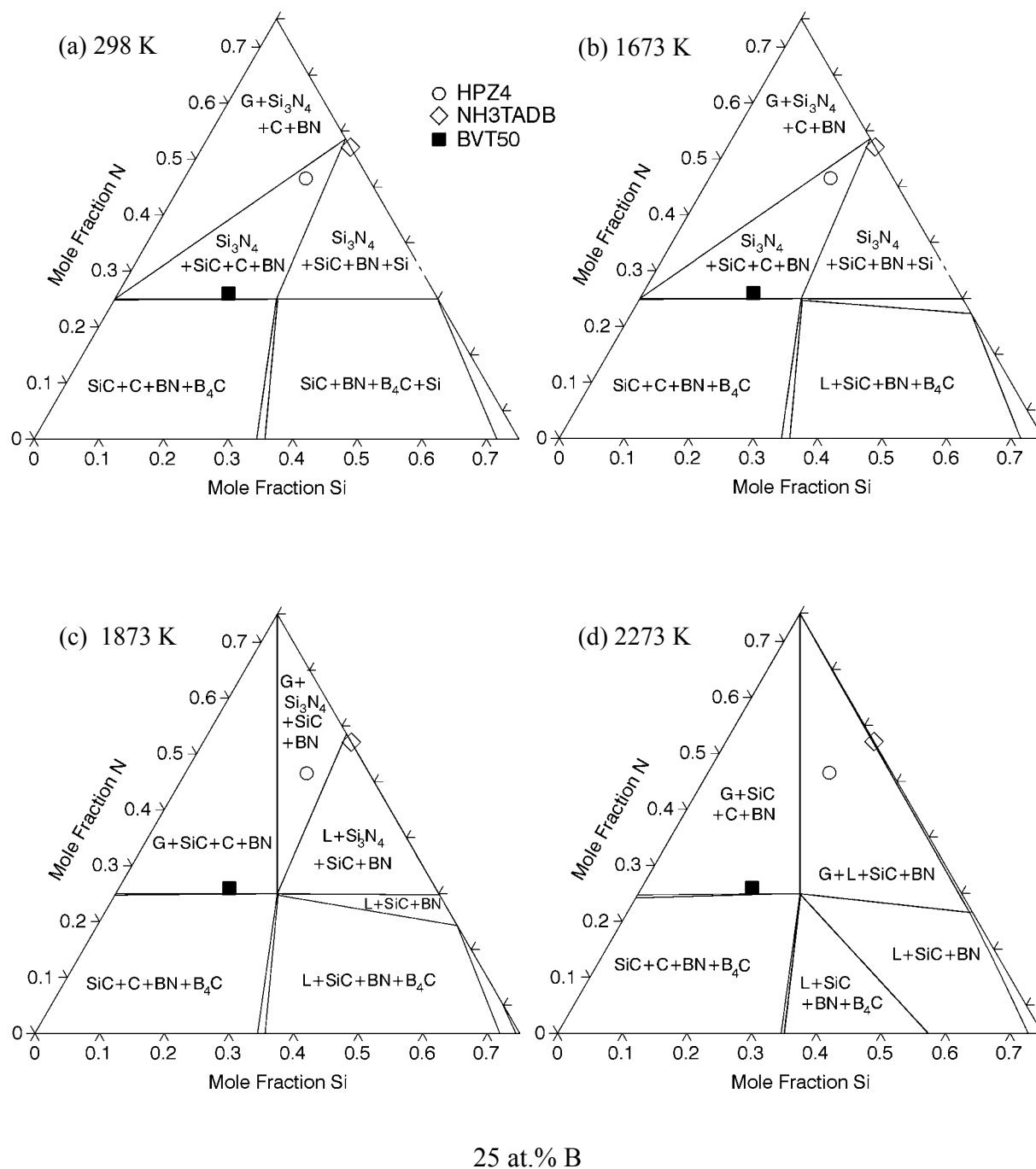


**Fig. 4-22** Calculated isothermal sections at 25 at.% boron at temperatures of (a) 25°C (298 K); (b) 1400°C (1673 K); (c) 1600°C (1873 K); (d) 2000°C (2273 K). The compositions of the relevant precursor derived Si-B-C-N amorphous ceramics are inserted; for details see Table 3-2 (p. 29).

### 4.2.1.3 Temperature composition sections (isopleths)

To explain the phase equilibria in more details and give more information on the development on precursor-derived Si-B-C-N ceramics, some temperature composition sections (isopleths) were calculated. Fig. 4-23 gives the calculated temperature composition section (isopleth) between  $\text{Si}_{1.0}\text{C}_{1.6}\text{N}_{1.33}$  and boron. ( $\text{Si}_{1.0}\text{C}_{1.6}\text{N}_{1.33}$  is the composition of the amorphous VT50-derived Si-C-N ceramic, see Table 3-1, p. 27). As can be seen from this diagram, the incorporation of boron into the VT50 leads besides  $\text{Si}_3\text{N}_4$ , SiC and C to additional stable phases, i.e. BN,  $\text{B}_{4+\delta}\text{C}$ ,  $\text{B}_3\text{Si}$ ,  $\text{B}_6\text{Si}$ , and  $\text{B}_n\text{Si}$ , according to content of boron. If the boron content is less than 25.3 at.%, only the phase BN is additionally appearing in the material, so that this material contains the phases:  $\text{Si}_3\text{N}_4+\text{SiC}+\text{C}+\text{BN}$  below 1484°C (1757 K). If the addition of boron is between 25.3 at. % and 48.7 at. %, the material should be composed of  $\text{SiC}+\text{C}+\text{BN}+\text{B}_{4+\delta}\text{C}$ , and show high-temperature stability (chemical stability) up to 2295°C

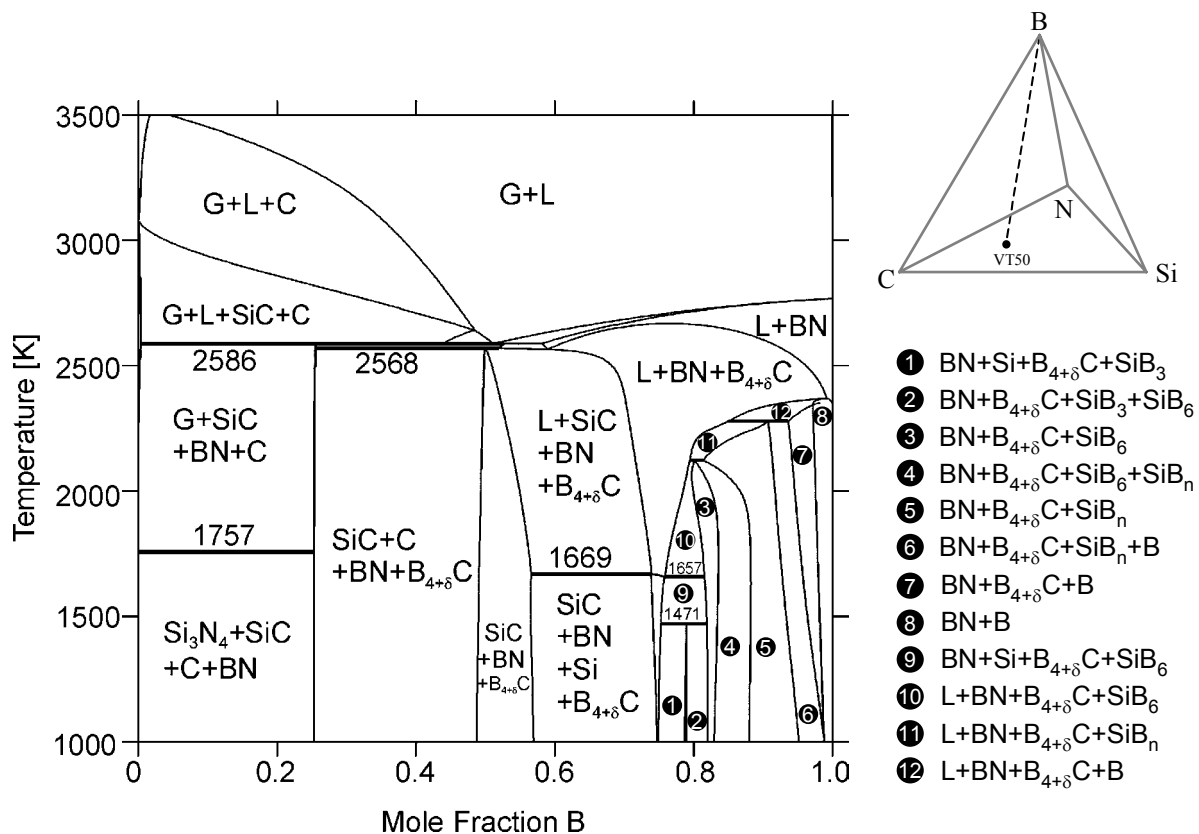


**Fig. 4-23** Calculated temperature composition section (isopleth) between  $\text{Si}_{1.0}\text{C}_{1.6}\text{N}_{1.33}$  and boron. ( $\text{Si}_{1.0}\text{C}_{1.6}\text{N}_{1.33}$  is the composition of the amorphous VT50-derived Si-C-N ceramic).

(2568 K), according to the thermodynamic calculation. The silicon borides ( $\text{SiB}_3$ ,  $\text{SiB}_6$ ,  $\text{SiB}_n$ ) will appear in the materials only if the boron content is more than 70 at. %. This diagram gives also seven of total nine four-phase equilibria the system at temperatures below 1198°C (1471 K) in Fig. 4-17a.

Fig. 4-24a, b and c show the calculated isopleths (a) between  $\text{B}_{0.1}\text{C}_{0.65}\text{Si}_{0.25}$  and  $\text{B}_{0.1}\text{N}_{0.65}\text{Si}_{0.25}$  at constant 10 at.% B and 25 at. % Si, (b) between  $\text{B}_{0.1}\text{C}_{0.65}\text{N}_{0.25}$  and  $\text{B}_{0.1}\text{N}_{0.25}\text{Si}_{0.65}$  at constant 10 at.% B and 25 at.% N, (c) between  $\text{B}_{0.1}\text{C}_{0.85}\text{Si}_{0.05}$  and  $\text{B}_{0.1}\text{N}_{0.05}\text{Si}_{0.85}$  at constant 10 at.% B and 5 at.% N. Dashed lines in the inserted isothermal sections indicate the corresponding composition lines of the individual isopleths. The dashed lines in the isopleths (Fig. 4-24a, b) pass through areas in which the compositions of many important precursor-derived Si-B-C-N ceramics materials such as MW33, MW26, T2-1 and MW36 are located. At temperatures below 1484°C (1757 K) these materials consist of  $\text{Si}_3\text{N}_4$ , SiC, graphite and BN. At temperatures above 1484°C (1757 K) these materials should be

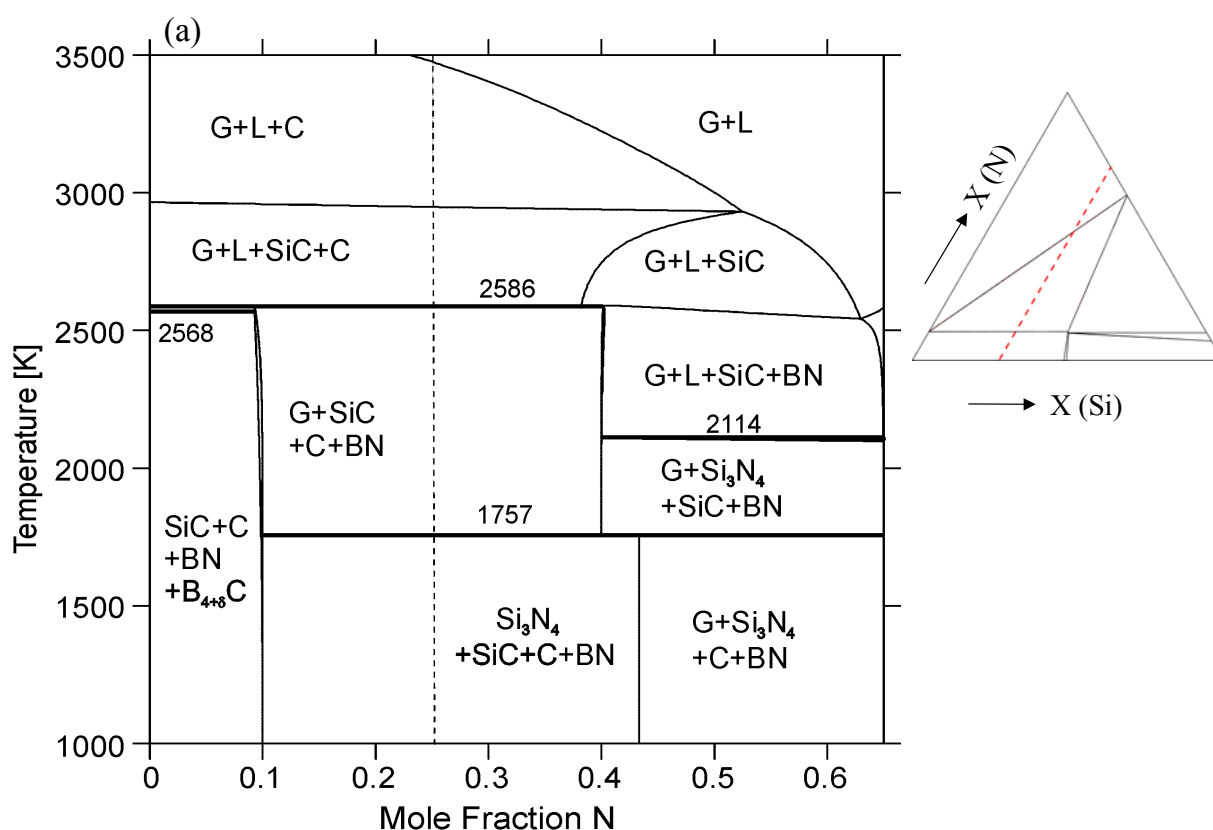


**Fig. 4-24** Isopleths in the Si-B-C-N system: (a) between  $\text{B}_{0.1}\text{C}_{0.65}\text{Si}_{0.25}$  and  $\text{B}_{0.1}\text{N}_{0.65}\text{Si}_{0.25}$  (at 10 mol-% B and 25 mol-% Si).

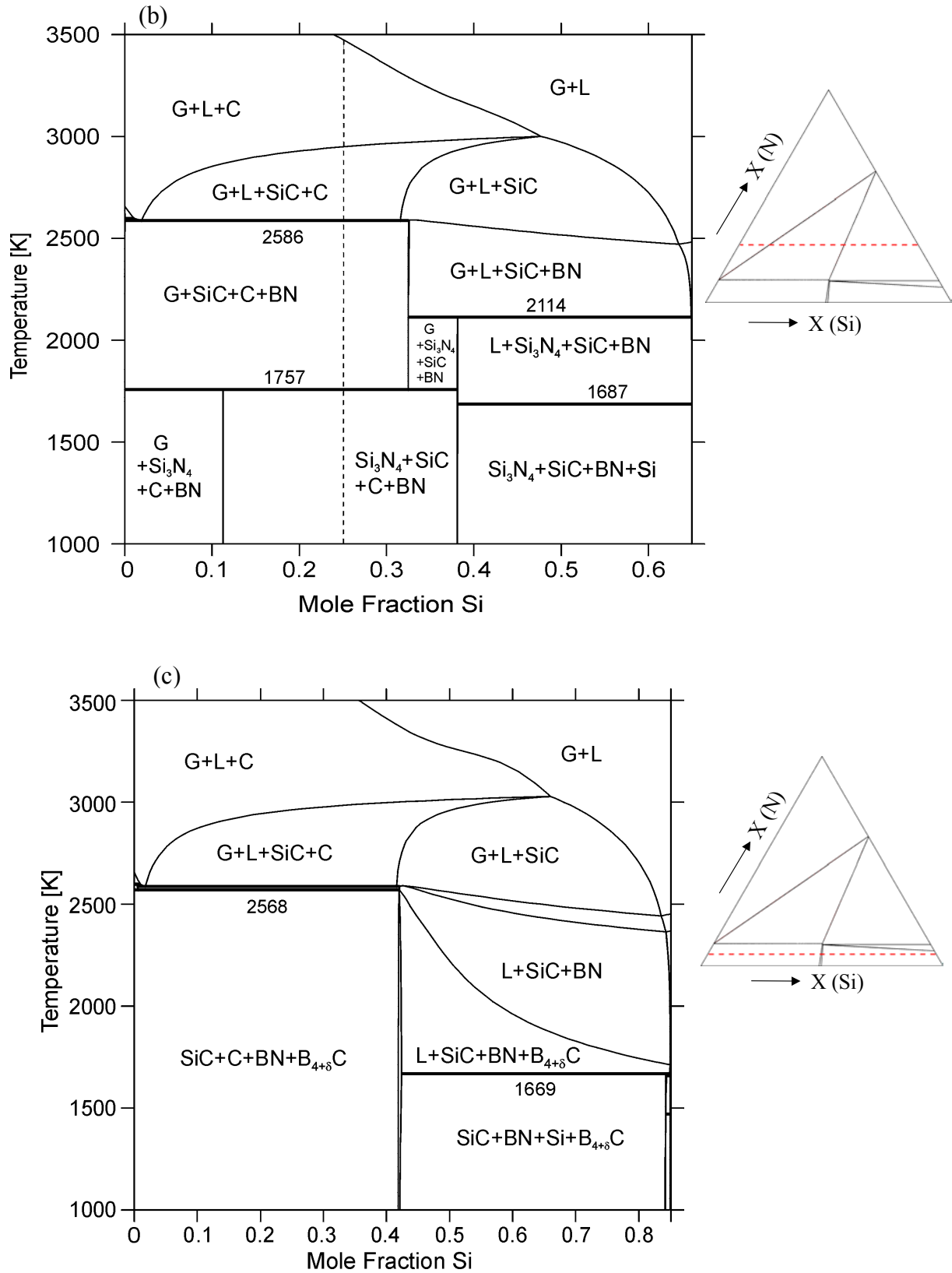
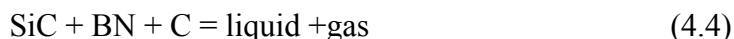


**Fig. 4-24** Isoleths in the Si-B-C-N system: (b) between  $B_{0.1}C_{0.65}N_{0.25}$  and  $B_{0.1}N_{0.25}Si_{0.65}$  in the Si-B-C-N System (at 10 mol-% B and 25 mol-% N); (c) between  $B_{0.1}C_{0.85}N_{0.05}$  and  $B_{0.1}N_{0.05}Si_{0.85}$  in the Si-B-C-N System (at 10 mol-% B and 5 mol-% N).



composed of SiC , graphite and BN because  $\text{Si}_3\text{N}_4$  reacts with graphite according to the reaction (4.1) as shown above for the system Si-C-N. If temperature approaches  $2313^\circ\text{C}$  (2586 K) SiC, C and BN react according to the reaction



and at temperatures higher than  $2313^\circ\text{C}$  (2586 K) the four-phase equilibrium gas+liquid+SiC+graphite prevails.

#### 4.2.1.4 Scheil's reaction scheme

The Scheil's reaction scheme for the Si-B-C-N system was inferred based on the above calculations (Fig. 4-25). It is valid for total pressure of 1 bar. Twelve quaternary invariant reactions occur. Nine four-phase equilibria existing at temperatures below  $1198^\circ\text{C}$  (1471 K) are indicated with underlines. The reactions (4.1), (4.2), (4.3) and (4.4) are indicated as  $u_9$ ,  $u_8$ ,  $u_{10}$  and  $U_2$ , respectively.

#### 4.2.1.5 Phase fraction diagrams

In order to explain and predict the crystallization behavior and phase relationships of precursor-derived ceramics, phase fraction diagrams were calculated, which are very suitable for better understanding of the manifold chemistry in higher component ceramic materials. Regarding the phase fraction diagrams it can be quantitatively predicted, at which temperatures the phases are co-existing in equilibrium. Mass losses during phase reactions can be easily derived [98Sei2, 00Pen1]. Fig. 4-26 shows calculated phase fraction diagrams of ceramics derived from (a) T2-1, (b) MW33, (c) BNCP and (d) T2-1 (Ar/NH<sub>3</sub>) (e) TADB94 (f) TSDE99 precursors (Compositions see Table 3-2, p. 29) The total pressure was fixed at 1 bar. It can be concluded that at temperatures below  $1484^\circ\text{C}$  (1757 K) all these ceramics should be composed of  $\text{Si}_3\text{N}_4$ , (SiC), BN and graphite. At  $1484^\circ\text{C}$  (1757 K) the free carbon should react with  $\text{Si}_3\text{N}_4$  to form SiC and gas. In all cases the total mass of the ceramic should decrease due to the loss of gaseous  $\text{N}_2$ . For the T2-1 ceramic material e. g., the calculation of the phase fraction diagram (Fig. 4-26a) gives a composition of  $\text{Si}_3\text{N}_4$  (25.0 at. %), SiC (26.8 at. %), BN (16.6 at. %) and graphite (31.5 at. %) at temperatures below  $1484^\circ\text{C}$  (1757 K). The MW33 ceramic material should be composed of  $\text{Si}_3\text{N}_4$  (31.2 at. %), SiC (23.5 at. %), BN (18.2 at. %)

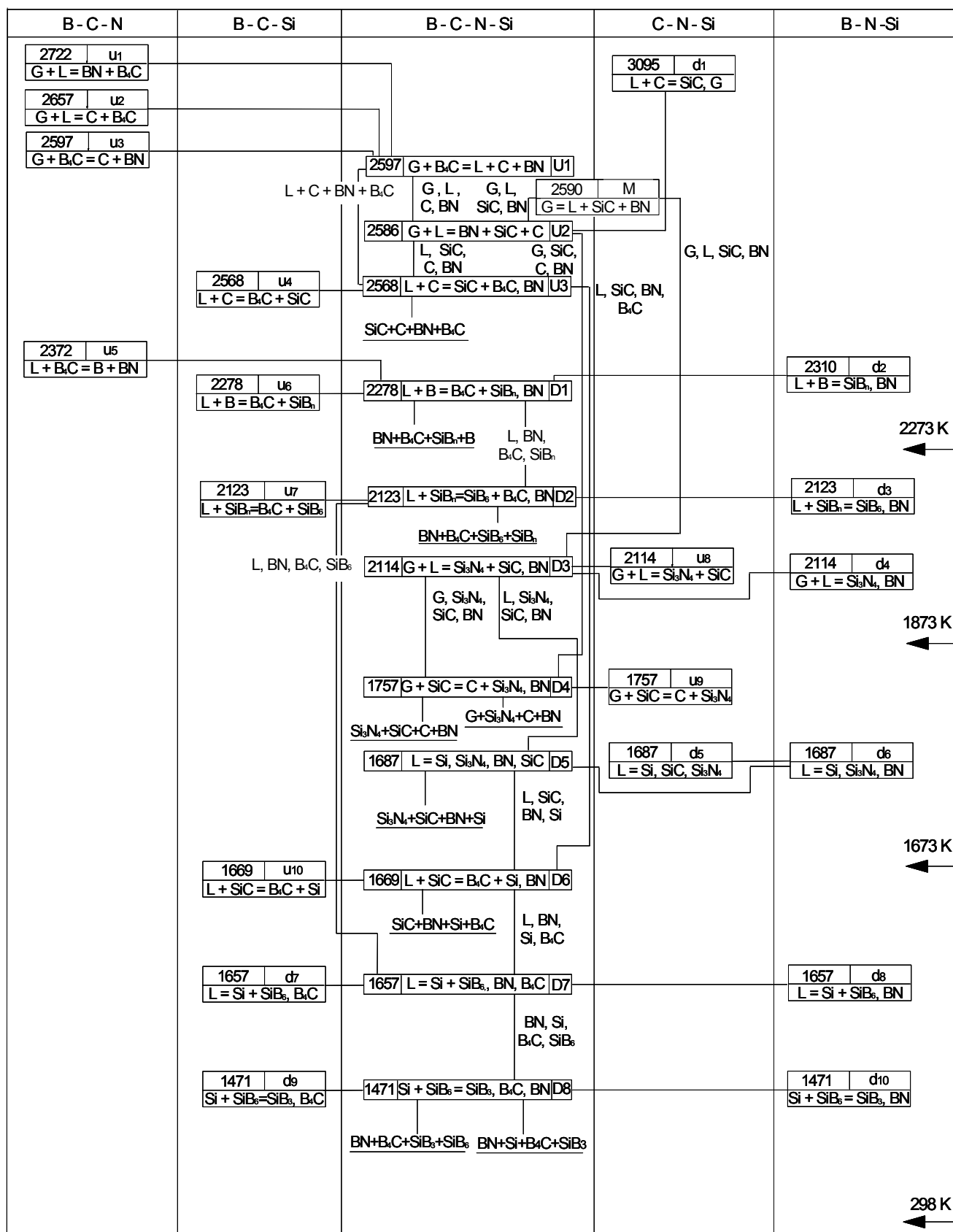
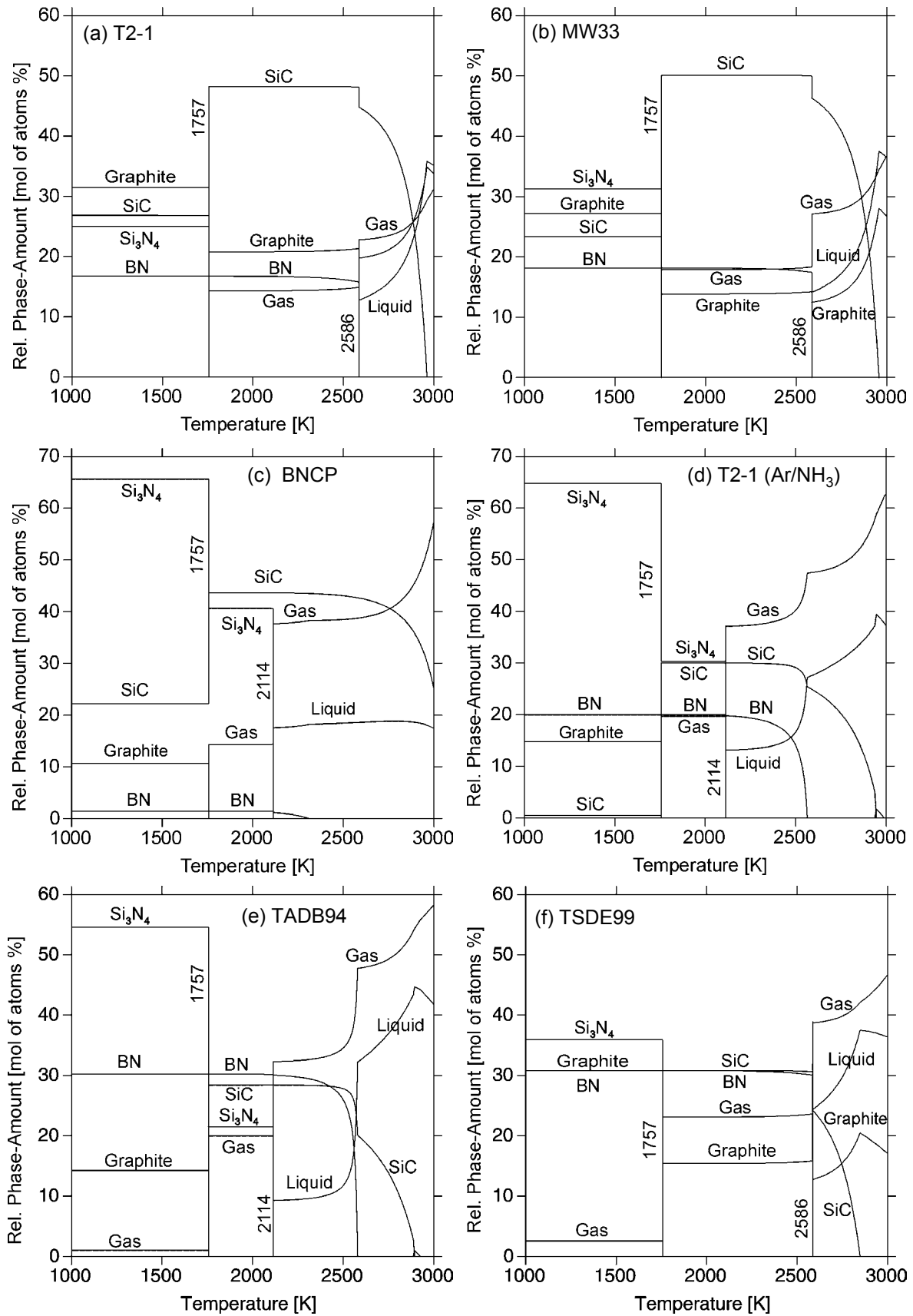


Fig. 4-25 The Scheil's reaction scheme of the Si-B-C-N system, temperature in K.



**Fig. 4-26** Calculated phase fraction diagrams of ceramics derived from (a) T2-1, (b) MW33, (c) BNCP and (d) T2-1 (Ar/ $\text{NH}_3$ ) (e) TADB94 (f) TSDE99 precursors.

**Table 4-2** Summary of the calculated phase fractions for Si-B-C-N ceramics.

No.	Ceramics Laboratory name	Calculated phase fractions (mole of atoms %) at T<1484°C				(SiC+BN+C)/Si <sub>3</sub> N <sub>4</sub>	Si <sub>3</sub> N <sub>4</sub> /(Si <sub>3</sub> N <sub>4</sub> +SiC)	BN/(BN+C)	(BN+C)/(Si <sub>3</sub> N <sub>4</sub> +SiC+BN+C)
		Si <sub>3</sub> N <sub>4</sub>	SiC	BN	C				
1	<b>T2-1</b>	25.0	26.8	16.6	31.5	<b>3.0</b>	0.48	0.35	0.48
2	<b>MW36</b>	21.7	34.4	18.6	25.3	<b>3.6</b>	0.39	0.42	0.44
3	<b>MW33</b>	31.2	23.5	18.2	27.2	<b>2.2</b>	0.57	0.40	0.45
4	<b>MW26</b>	27.1	25.8	20.0	27.1	<b>2.7</b>	0.51	0.42	0.47
5	<b>Wang</b>	23.1	28.0	17.8	31.1	<b>3.3</b>	0.45	0.36	0.49
6	<b>AM2 k</b>	8.6	51.5	22.8	17.3	<b>10.7</b>	0.14	0.57	0.40
7	<b>KSih2</b>	18.7	38.2	9.2	33.9	<b>4.3</b>	0.33	0.21	0.43
8	<b>K269A</b>	18.6	33.3	11.4	36.8	<b>4.4</b>	0.36	0.24	0.48
9	<b>K269B</b>	20.8	33.8	9.8	35.7	<b>3.8</b>	0.38	0.22	0.45
10	<b>K270A</b>	2.10	59.4	11.0	27.5	<b>46.6</b>	0.03	0.29	0.39
11	<b>K270B</b>	30.6	31.2	9.2	29.1	<b>2.3</b>	0.50	0.24	0.38
12	<b>BVT50</b>	0	35.5	53.6	11.2	-	0	0.82	0.65
13	<b>T2-1(Ar/NH<sub>3</sub>)</b>	64.7	0.5	20.0	14.8	<b>0.5</b>	0.99	0.57	0.35
14	<b>BNCP</b>	64.1	17.7	3.8	14.6	<b>0.6</b>	0.78	0.21	0.18
15	<b>AMFH4k</b>	41.0	19.3	8.2	30.3	<b>1.4</b>	0.71	0.18	0.41
16	<b>MW60</b>	46.4	14.3	19.0	19.9	<b>1.1</b>	0.76	0.49	0.39
17	<b>MW18A</b>	40.8	0.0	13.6	45.4	<b>1.4</b>	1.00	0.23	0.59
18	<b>HyVT50</b>	50.6	6.1	17.8	25.6	<b>1.0</b>	0.89	0.41	0.43
19	<b>HPZ3</b>	62.3	15.4	15.0	7.3	<b>0.6</b>	0.80	0.67	0.22
20	<b>MW25</b>	38.2	11.7	15.6	34.6	<b>1.6</b>	0.77	0.31	0.50
21	<b>vT2(1)1</b>	39.6	28.7	10.6	21.1	<b>1.5</b>	0.58	0.33	0.32
22	<b>HPZ2</b>	66.0	19.9	7.2	7.0	<b>0.5</b>	0.77	0.51	0.14
23	<b>MW31</b>	44.6	0.0	13.8	41.3	<b>1.2</b>	1.00	0.25	0.55
24	<b>HPZ4</b>	37.6	5.4	50.0	7.0	<b>1.7</b>	0.87	0.88	0.57
25	<b>NH<sub>3</sub>TADB</b>	52.2	0.0	47.0	0.0	<b>0.9</b>	1.00	1.00	0.47
26	<b>TADB94</b>	54.6	0.0	29.8	14.3	<b>0.8</b>	1.00	0.68	0.45
27	<b>TSDE99</b>	35.9	0.0	30.8	30.8	<b>1.7</b>	1.00	0.50	0.63

and graphite (27.2 at. %). For all materials listed in Table 3-2 the phase fraction diagrams were calculated. Those phase fractions at temperatures below 1484°C are summarized in Table 4-2. Table 4-2 gives also the ratios of  $(\text{SiC}+\text{BN}+\text{C})/\text{Si}_3\text{N}_4$ ,  $\text{Si}_3\text{N}_4/(\text{Si}_3\text{N}_4+\text{SiC})$ ,  $\text{BN}/(\text{BN}+\text{C})$  and  $(\text{BN}+\text{C})/(\text{Si}_3\text{N}_4+\text{SiC})$ . (“SiC” means the relative phase fraction of phase SiC, etc.). As can be seen, from phase fraction diagrams the crystallization behavior of Si-B-C-N precursor-derived ceramics materials can be predicted quantitatively.

Fig. 4-27 shows another type of phase fraction diagram, which represents the relative phase amount as a function of the chemical composition of one element (boron) at a fixed temperature ( $T = 1400^\circ\text{C}$ ). When calculating this phase diagram the atomic ratio Si:C:N was fixed to 1:1.6:1.33, similar to the composition of amorphous VT50-derived ceramics ( $\text{Si}_{1.0}\text{C}_{1.6}\text{N}_{1.33}$ ). As can be seen from the diagram the incorporation of boron into the VT50-derived Si-C-N ceramic leads to additional stable phases, i.e. BN,  $\text{B}_{4+\delta}\text{C}$ ,  $\text{B}_3\text{Si}$ ,  $\text{B}_6\text{Si}$ , and  $\text{B}_n\text{Si}$ , according to the boron content in the materials, as shown as in Fig. 4-23. Increasing the boron content in the material from 0 to 25.3 at. %, the relative phase amounts of  $\text{Si}_3\text{N}_4$  and graphite are decreased from 59 at. % and 41 at. % to 0 at. % and 12 at. %, whereas the relative phase amounts of SiC and BN are increased from 0.3 at. % and 0 at. % to 38 at. % and 50 at. %, respectively. A boron content of less than 25.3 at. % is necessary for the existence of the  $\text{Si}_3\text{N}_4$  phase in the material. If the boron content is more than 25.3 at. %,  $\text{B}_{4+\delta}\text{C}$  appears as additional phase.

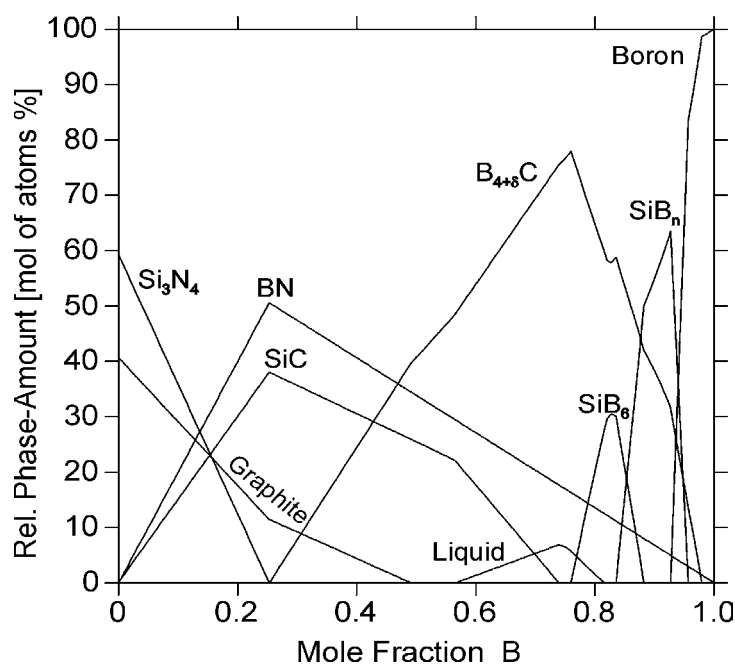


**Fig. 4-27** Calculated relative phase amount as a function of boron contents at a temperature of 1400°C (1673 K).

#### 4.2.1.6 Partial pressure diagrams

As in the Si-C-N system, the nitrogen partial pressure diagrams were calculated in the Si-B-C-N system. To calculate such diagrams a particular Si:B:C ratio is fixed and the chemical potential of nitrogen and the temperature are changed systematically, as described in detail elsewhere [98Sei1]. Fig. 4-28a gives the resulting  $\log(P(N_2))$ -temperature diagram for the specific composition  $Si_{25.1}B_{9.1}C_{38.9}$  (MW33-derived ceramic). This diagram represents also the general behavior of other high-temperature Si-B-C-N ceramic materials with  $Si:C < 1$  e.g. T2-1, MW36, MW26. Along the upper line,  $Si_3N_4$ , SiC, graphite, BN and gas are in equilibrium. Upon crossing this line,  $Si_3N_4$  disappears by the reversible reaction with graphite to SiC and nitrogen gas. In comparison with the calculated phase fraction diagrams (Fig. 4-26b, a) the solid phase SiC is missing in the equilibrium because no limit for the quantity of nitrogen is given by the calculation. Increasing the  $N_2$  pressure from 1 bar to 10 bar, the reaction temperature of  $Si_3N_4$  and graphite is increased from a temperature of 1484°C (1757 K) to 1700°C (1973 K), as in the Si-C-N system (Fig. 4-6).

The lower line represents the two reactions i. e. the reaction (4.4) or  $U_2$  (Fig. 4-25) if  $P(N_2) > 0.78$  bar ( $\log(P(N_2)) > -0.1074$ ) and the reaction (4.5) or  $u_3$



if  $P(N_2) < 0.78$  bar ( $\log(P(N_2)) > -0.1074$ ). At the normal pressure of 1 bar the temperature of reaction (4.5) ( $u_3$ ) is 2324°C (2597 K) and reaction (4.4) is 2313°C (2586 K) as shown in Fig. 4-25. Here the reaction (4.5) occurs at a temperature of 2065°C (2338 K) at  $P(N_2) = 0.1$  bar. Underneath this lower line, if the  $N_2$  pressure is higher than 0.78 bar, gas, graphite and liquid are in equilibrium, (as this is also the case for  $T > 2295^\circ\text{C}$  (2568 K) because of the reaction  $U_3$  (Fig. 4-25)), whereas at pressures  $< 0.78$  bar, gas, SiC, graphite and  $B_4C$  are in equilibrium.

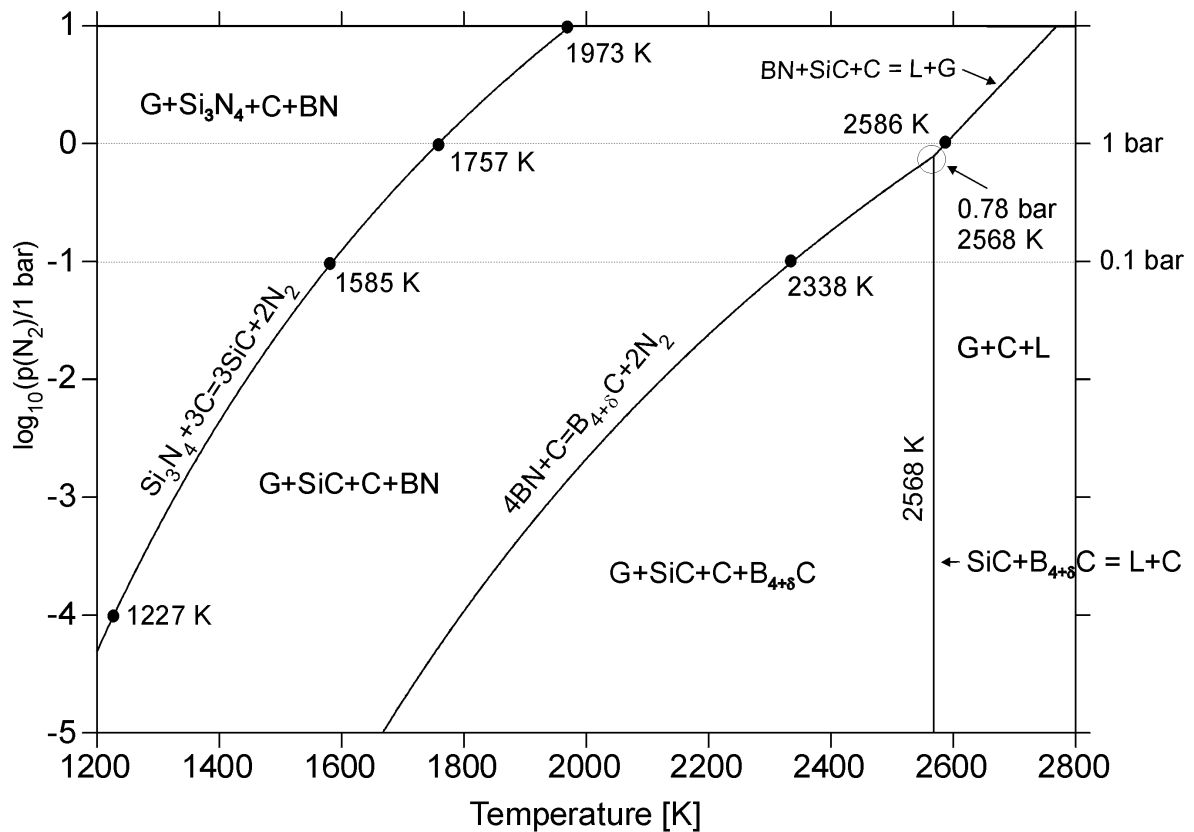
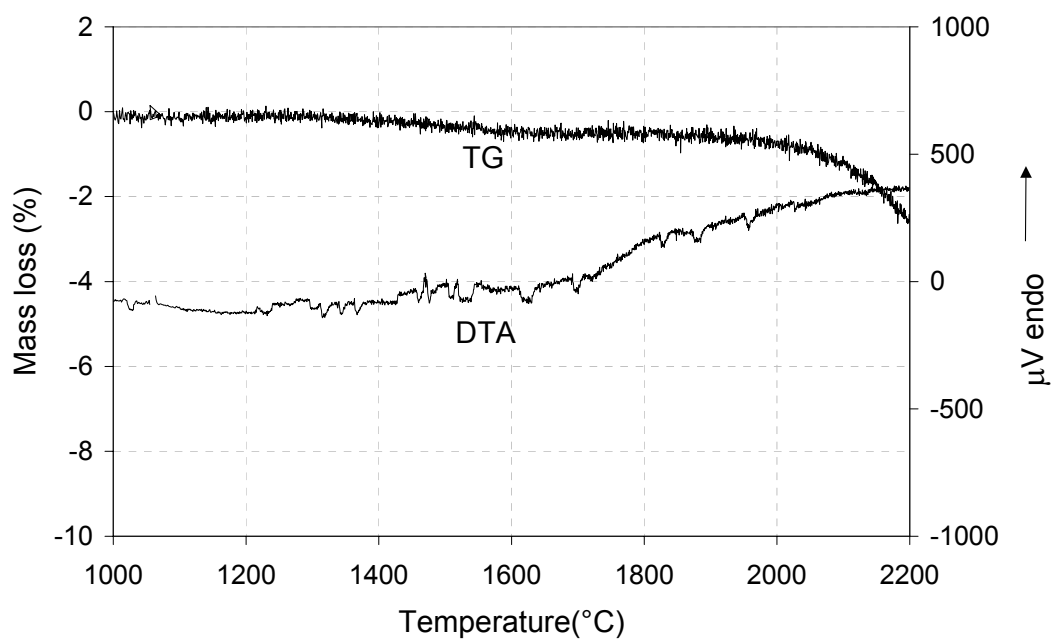


Fig. 4-28 Calculated nitrogen partial pressure diagrams in Si-B-C-N system.

## 4.2.2 Experimental Investigations

### 4.2.2.1 T2-1 precursor-derived ceramic

Fig. 4-29 shows the DTA/TG measurement curves in  $N_2$  atmosphere with a heating rate of 5 K/min, (BN crucible) for T2-1-derived ceramic material. As can be seen from this diagram, there is no significant mass loss up to temperatures above 2000°C (2273 K). The material shows only ca. 2 % mass loss when it is heated up to 2200°C (2473 K), indicating a thermal stability up to this temperature. No clear endothermic or exothermic reaction peak was found by DTA. After DTA/TG of T2-1 precursor-derived ceramic with the highest temperature of 2200°C, the sample was analyzed by X-ray diffractometry (XRD), the scanning electron microscopy (SEM) and the high-resolution transmission electron microscopy (HRTEM). Fig. 4-30 shows the XRD pattern. In contradiction to the calculated results (Fig. 4-20, 26), the



**Fig. 4-29** DTA/TG measurements curves in N<sub>2</sub> atmosphere with a heating rate of 5 K/min, and BN-crucible for T2-1 ceramic material.

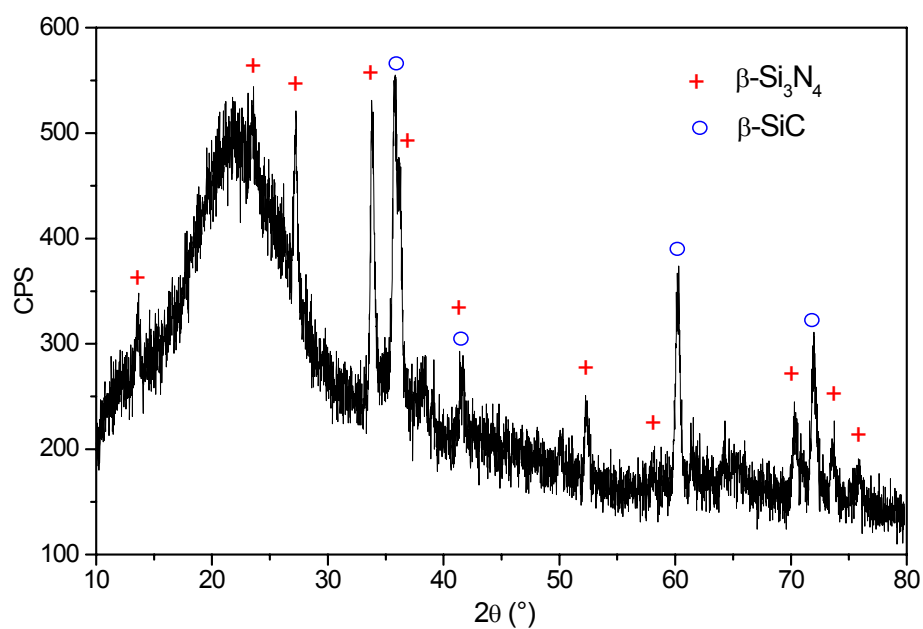


**Fig. 4-30** The XRD pattern of the T2-1 precursor-derived ceramic after DTA/TG with the highest temperature of 2200°C.



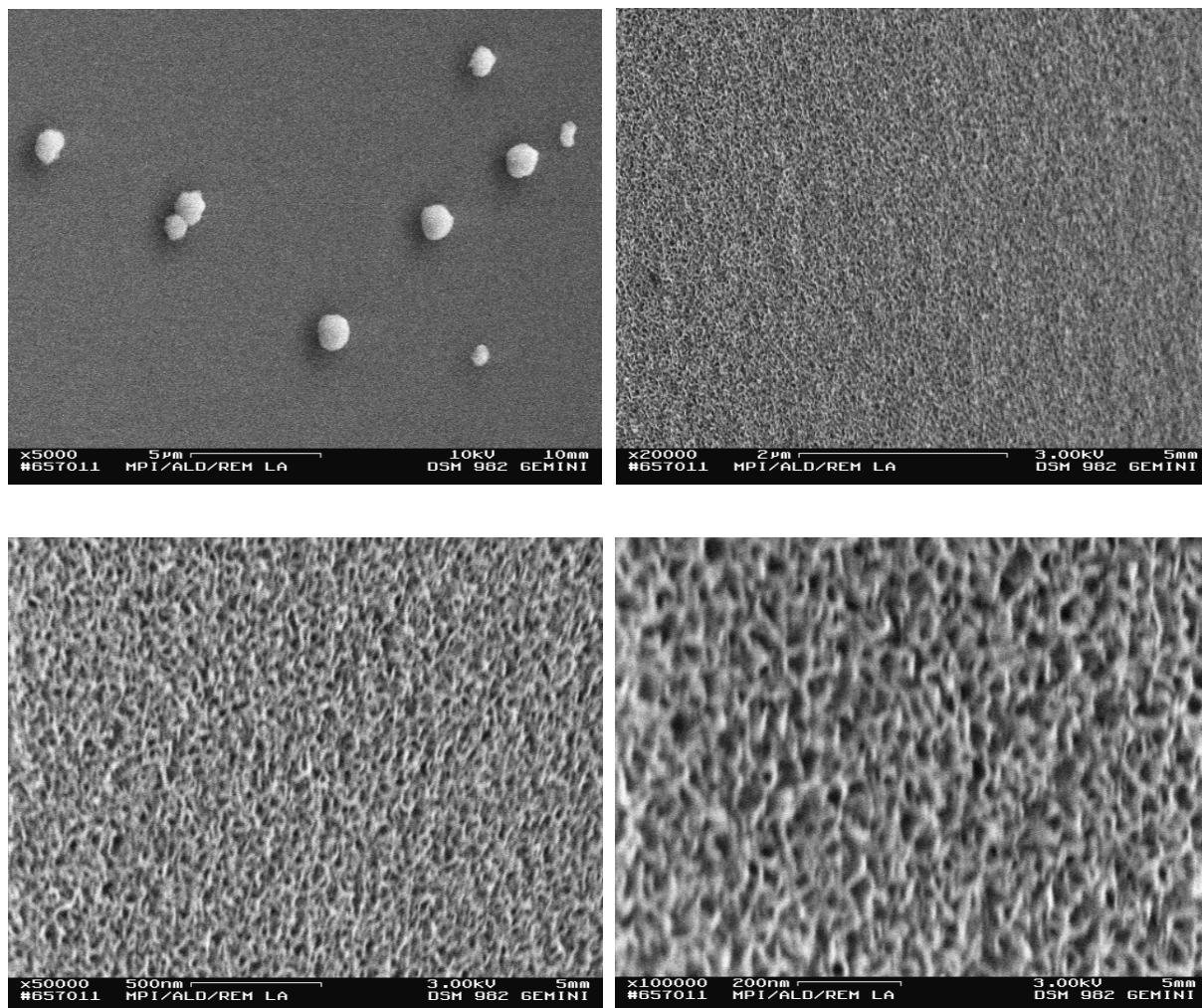


**Fig. 4-31** SEM images of the T2-1 precursor-derived ceramic after DTA/TG with the highest temperature of 2200°C (resolutions 5000, 20000, 50000, 100000).

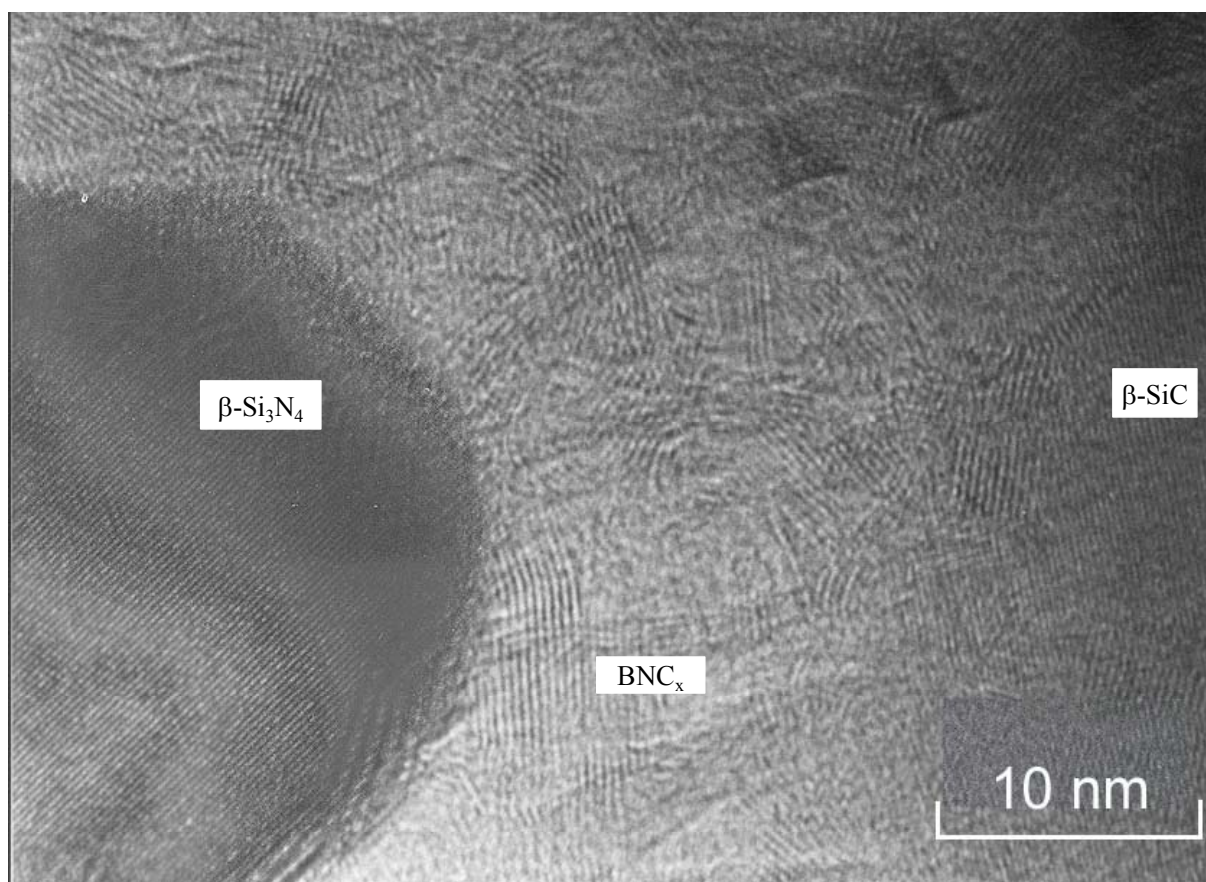


**Fig. 4-32** HRTEM image of the T2-1 precursor-derived ceramic after DTA/TG up to 2200°C.

material still consists of  $\beta$ - $\text{Si}_3\text{N}_4$  besides  $\beta$ -SiC (Note that  $\text{Si}_3\text{N}_4$  should react with carbon at 1484°C and eventually residual amounts should decompose quantitatively at 1841°C (2114 K) at  $p=1\text{bar}$ ). The SEM micrographs of the surface of this sample (Fig. 4-31) show a very fine and closely packed structure. The investigation of the HRTEM indicates that nanocrystalline  $\beta$ - $\text{Si}_3\text{N}_4$  besides turbostratic  $\text{BNC}_x$  layers and nanocrystalline  $\beta$ -SiC (Fig. 4-32) exist in the material. It can be seen that the turbostratic  $\text{BNC}_x$  matrix encloses nanocrystalline  $\beta$ - $\text{Si}_3\text{N}_4$  besides  $\beta$ -SiC.

#### 4.2.2.2 Ceramics derived from MW33 and MW36

The DTA/TG investigations for the amorphous ceramics materials MW33 and MW36 show similar results as for the T2-1-derived material. Fig. 33 gives DTA/TG measurement curves for both materials. As can be seen, both materials have a similar high-temperature stability up to temperatures above 2000°C (2273 K). The phase analysis by XRD for both materials after DTA/TG with the highest temperature of 2200°C (2473 K) (Fig. 4-34) shows that both materials also consist of  $\beta$ -Si<sub>3</sub>N<sub>4</sub> and  $\beta$ -SiC as it is the case with T2-1-derived material.

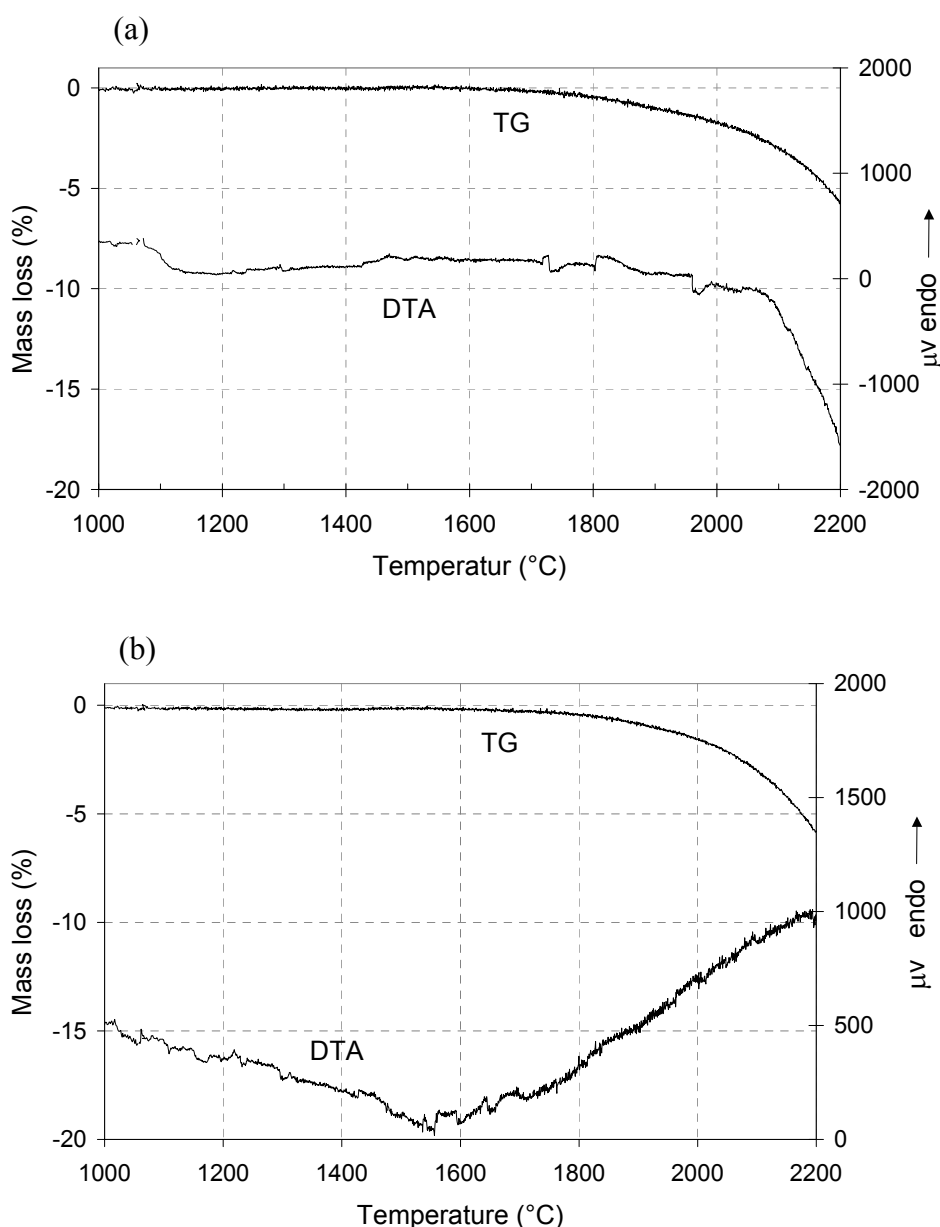


**Fig. 4-33** DTA/TG measurement curves in N<sub>2</sub> atmosphere with a heating rate of 5 K/min, and in BN-crucibles for (a) MW33-derived and (b) MW36-derived ceramic material.

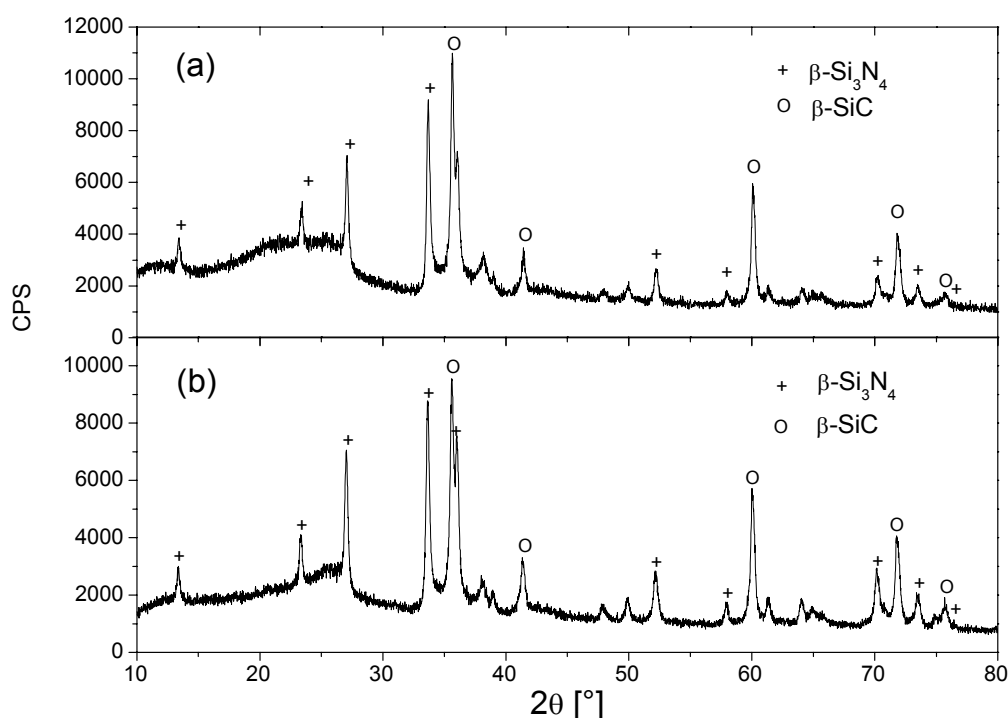


**Fig. 4-34** The XRD patterns of the (a) MW33 and (b) MW36 precursor-derived ceramic after DTA/TG with the highest temperature of 2200°C.

#### 4.2.2.3 Ceramic derived from BNCP and ceramic derived from T2-1 (NH<sub>3</sub>/Ar)

The DTA/TG measurement curves in N<sub>2</sub> atmosphere with a heating rate of 5 K/min, (BN crucible) of the ceramic derived from BNCP and the ceramic derived from T2-1 (NH<sub>3</sub>/Ar) are illustrated in Fig. 4-35a, b, separately. For the ceramic derived from BNCP, a two step mass loss as predicted by the thermodynamic calculation (Figs. 4-19, 4-20, 4-26) has been affirmed. In the temperature range from 1620°C (1893 K) to 1860°C (2133 K) a 13% mass loss and between 1880°C (2153 K) and 1910°C (2183 K) a 15% mass loss were determined. The first mass loss can be attributed to the reaction (4.1) and the second mass loss to the decomposition of residual Si<sub>3</sub>N<sub>4</sub> according to reaction (4.2). Only the latter one is combined with an endothermic reaction peak, whereas reaction (4.1) runs slowly, due to the fact that “free” carbon is soluted in BN and obviously does not react with Si<sub>3</sub>N<sub>4</sub>. Therefore no reaction peak was detected. For the T2-1 (NH<sub>3</sub>/Ar)-derived ceramic only one single step mass loss of 30% accompanied by an endothermic reaction peak in the temperature range from 1880°C (2153 K) to 1920°C (2193 K) could be detected. This can be attributed to the decomposition of Si<sub>3</sub>N<sub>4</sub> according to reaction (4.2). Additionally, exothermic reaction peaks between 1720°C

and 1760°C for the BNCP-derived ceramic and between 1740°C and 1780°C for the T2-1 (NH<sub>3</sub>/Ar)-derived ceramic were determined. They could be attributed to the crystallization of both materials.

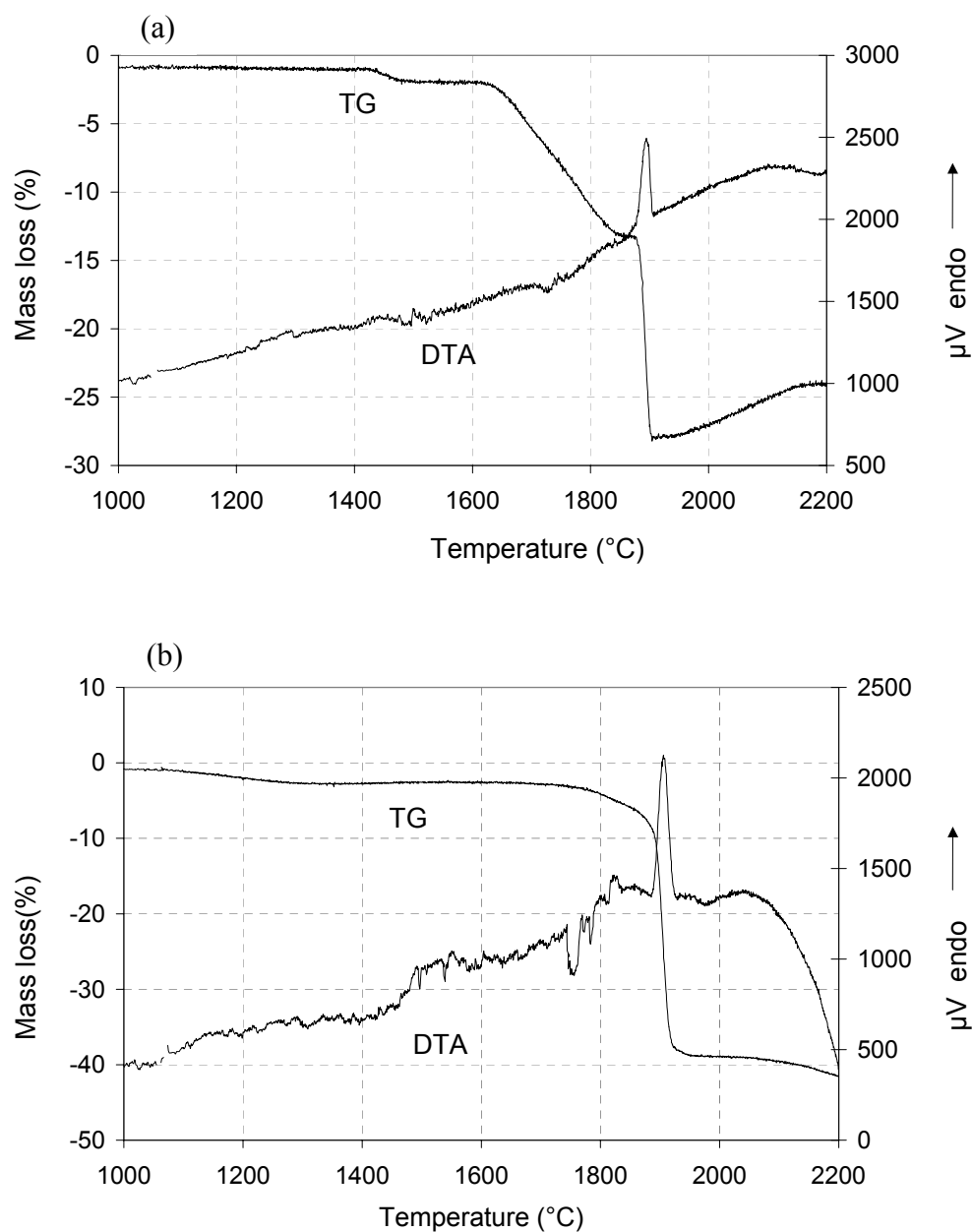


**Fig. 4-35** The DTA/TG measurement curves in N<sub>2</sub> atmosphere with a heating rate of 5 K/min, and in BN-crucibles for (a) BNCP-derived ceramic and (b) T2-1(Ar/NH<sub>3</sub>)-derived ceramic.

After DTA/TG with the highest temperature of 2200°C (2473 K) both samples were analyzed by X-ray diffractometry (XRD) and the results are presented in Fig. 4-36a, b. It can

be seen that the BNCP-derived ceramic consists of the phases SiC, Si, Si<sub>3</sub>N<sub>4</sub> and SiO<sub>2</sub>, as well as the T2-1 (Ar/NH<sub>3</sub>)-derived ceramic consists of SiC, Si and very small contents of Si<sub>3</sub>N<sub>4</sub>, SiO<sub>2</sub>.

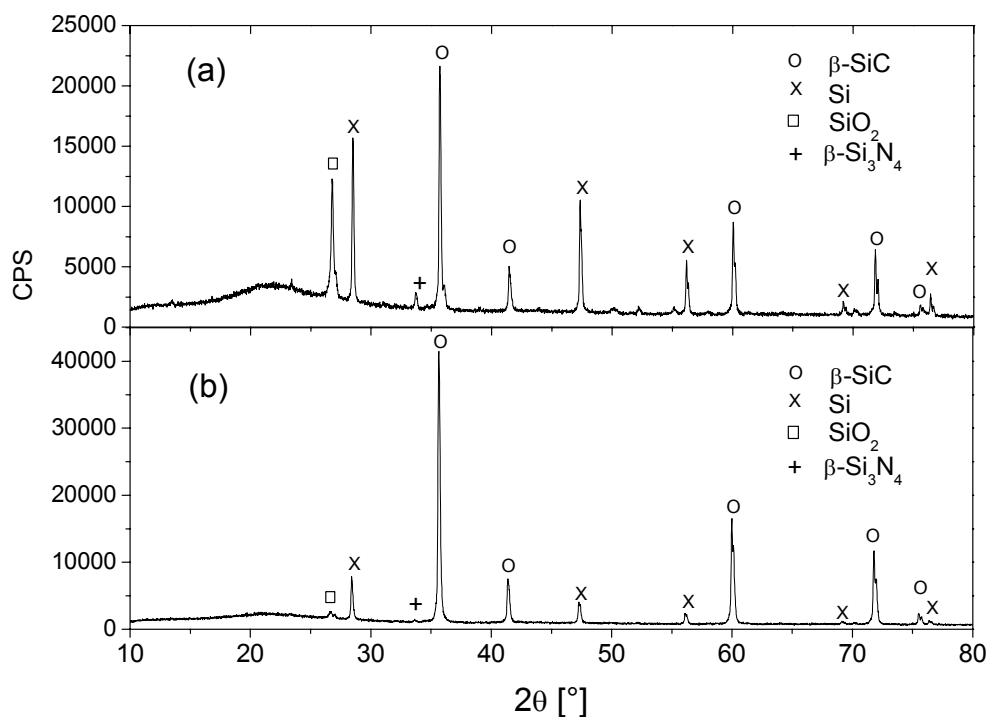


**Fig. 4-36** The XRD analysis of (a) BNCP-derived ceramic and (b) T2-1(Ar/NH<sub>3</sub>)-derived ceramic after DTA/TG with the highest temperature of 2200°C.

#### 4.2.2.4 Ceramic derived from BVT50

The DTA/TG curve of BVT50-derived ceramic illustrated in Fig. 4-37 shows that the material has 7% mass loss when it has been heated up to 2000°C (2273 K) and no clear endothermic or exothermic reaction peaks were detected by DTA. Fig. 4-38 presents the phase formation characterized by XRD for this amorphous ceramic after DTA/TG with the highest temperature of 2200°C. Besides the diffraction lines of β-SiC a reflection located at  $2\theta = 25.8^\circ$  could be found. This value is smaller than the  $2\theta$  values of the (002) diffraction peaks of graphite and α-BN. Therefore, it could be identified as belonging to a graphite-like turbostratic BNC<sub>x</sub> phase.

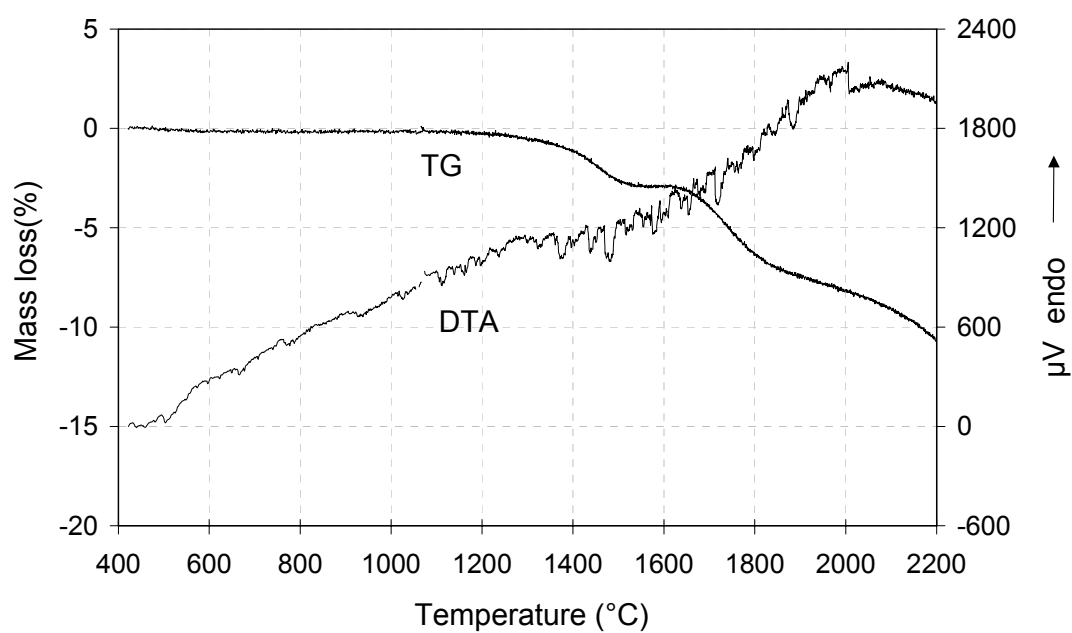


**Fig. 4-37** The DTA/TG measurement curves in N<sub>2</sub> atmosphere with a heating rate of 5 K/min, and in BN-crucibles of BVT50-derived ceramic.

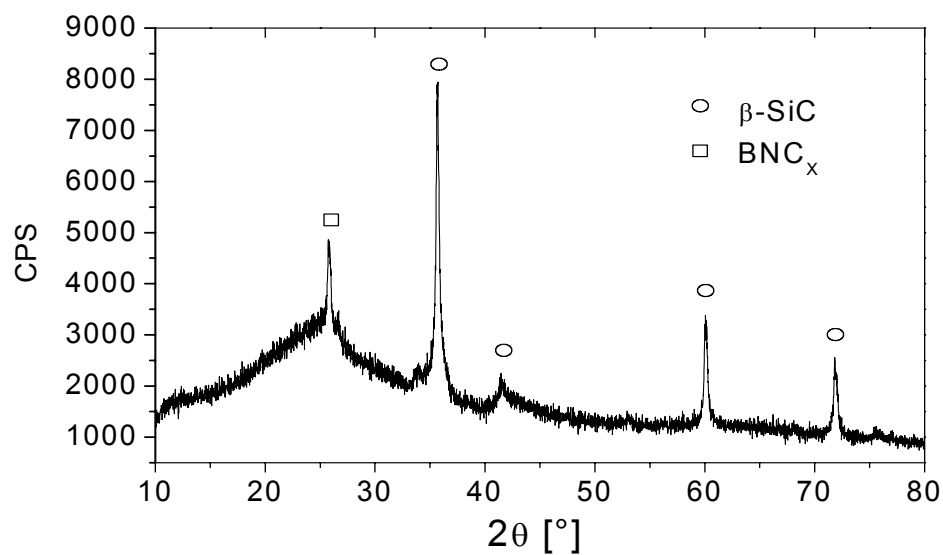


**Fig. 4-38** The phase formation characterized by XRD for BVT50 amorphous ceramic after DTA/TG with the highest temperature of 2200 °C.

### 4.2.3 Discussion and Summary

Thermodynamic calculations (Figs. 4-19, 20, 21, 22, 4-26) show that most of the ceramics investigated should be composed of  $\text{Si}_3\text{N}_4$ ,  $\text{SiC}$ ,  $\text{BN}$  and graphite at temperatures below  $1484^\circ\text{C}$  ( $1757\text{ K}$ ). Above  $1484^\circ\text{C}$  ( $1757\text{ K}$ )  $\text{Si}_3\text{N}_4$  should react with graphite to form  $\text{SiC}$  and gas and the total mass of the ceramic should decrease due to the loss of gaseous  $\text{N}_2$ . However, the T2-1-, MW33- and MW36-derived ceramics exhibit no major mass loss up to temperatures around  $2000^\circ\text{C}$  or even higher, as can be seen from Fig. 4-39, in which the TG curves of these materials together with some others mentioned above (Fig. 4-29, 33, 35, 37) are compiled. And XRD patterns of the T2-1-derived ceramic (Fig. 4-30) show that the material still consists of  $\beta\text{-Si}_3\text{N}_4$  besides  $\beta\text{-SiC}$  and  $\text{BNC}_x$  even after heating up to  $2200^\circ\text{C}$ , although it should decompose under this condition according to the calculated results. Obviously reaction (4.1) does not occur and reaction (4.2) is prevented or at least shifted to substantial higher temperatures.

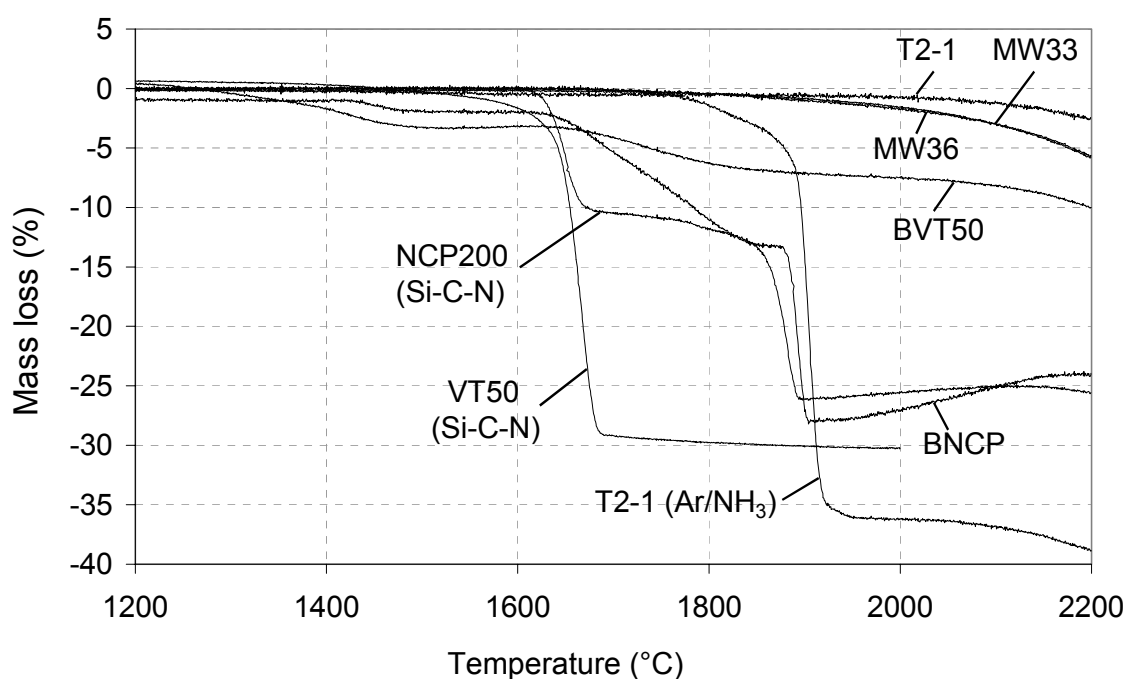


**Fig. 4-39** Thermogravimetric (TG) analysis of selected precursor-derived Si-C-N and Si-B-C-N ceramics.



To understand these conflicting results, the microstructure of the materials has to be taken into account. The investigation of the HRTEM for the ceramic derived from T2-1 indicate that nanocrystalline  $\beta$ - $\text{Si}_3\text{N}_4$  grains are embedded in a turbostratic  $\text{BNC}_x$  matrix (Fig. 4-32). This type of microstructure is in accordance with earlier results of HRTEM investigations [96Jal], in which layers of turbostratic  $\text{BNC}_x$  were found along grain boundaries between nanocrystalline  $\text{Si}_3\text{N}_4$  and  $\text{SiC}$  (Fig. 4-40). In neither case free carbon was detected. Carbon not bond to silicon is dissolved in a turbostratic phase ( $\text{BNC}_x$ ), which contains also BN. Because of this structure the carbon is passivated, i.e. its activity is significantly reduced and its reaction with  $\text{Si}_3\text{N}_4$  inhibited. Besides that the “encapsulation” of  $\text{Si}_3\text{N}_4$  within the  $\text{BNC}_x$  matrix phase has been assumed to stabilize  $\text{Si}_3\text{N}_4$  to higher temperatures since it acts as a diffusion barrier for nitrogen promoting a pressure stabilization of  $\text{Si}_3\text{N}_4$  [98Sei1].

To derive quantitative information on the effect of a decreased carbon activity, the activity vs. temperature diagram was calculated (Fig. 4-41). At a pressure of 1 bar  $\text{N}_2$  the temperature of the reaction between  $\text{Si}_3\text{N}_4$  and carbon is increased from  $1484^\circ\text{C}$  (1757 K) to  $1841^\circ\text{C}$  (2114 K) by decreasing carbon activity from 1 to 0.1. At even lower carbon activities  $\text{Si}_3\text{N}_4$

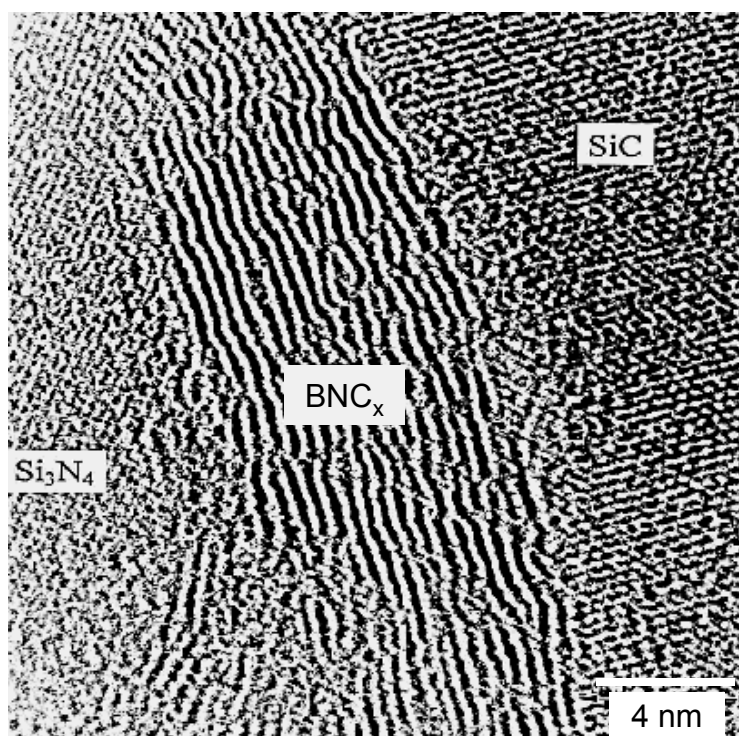


**Fig. 4-40** HRTEM images of high temperature stable Si-B-C-N ceramics [96Jal].

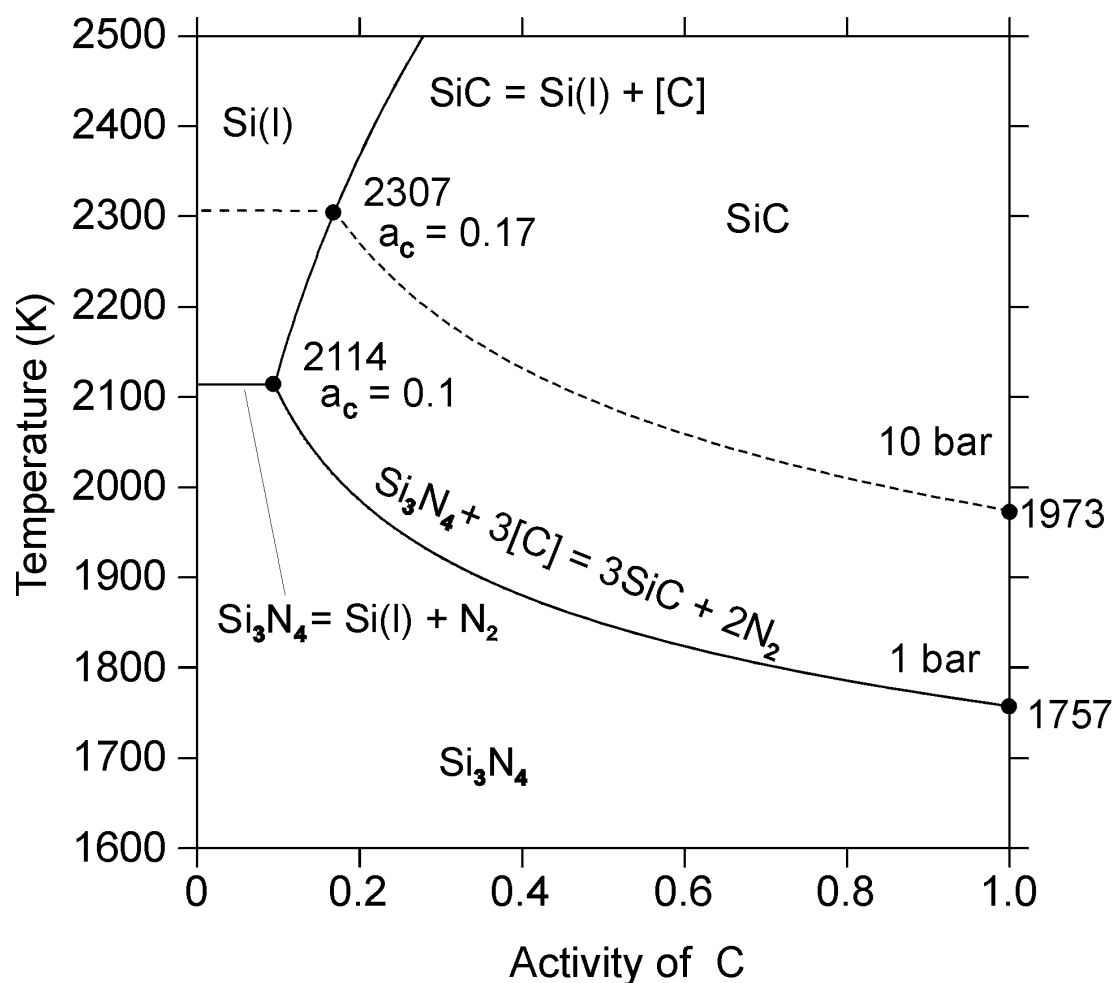
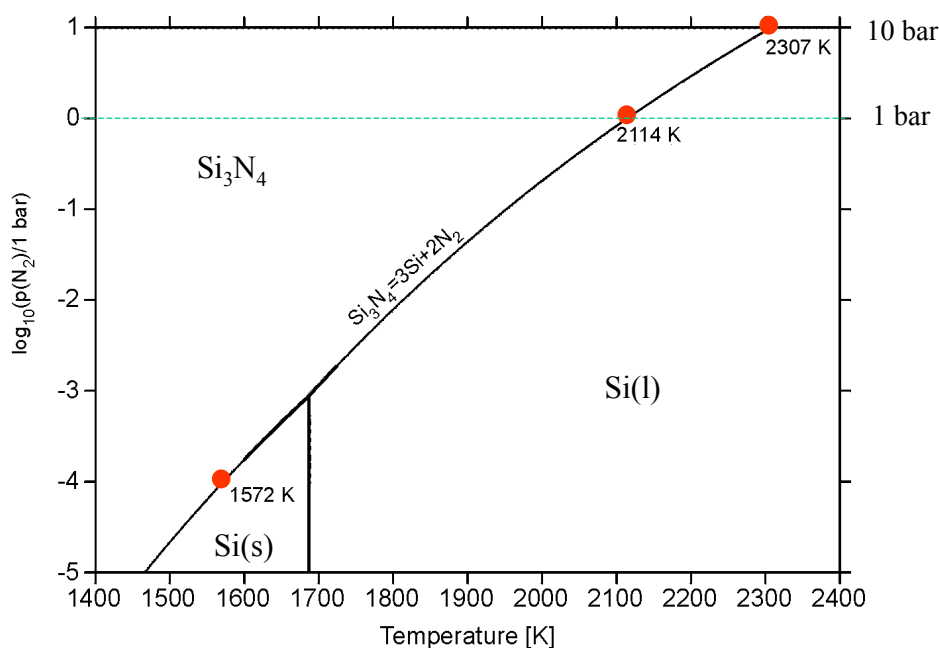


Fig. 4-41 Carbon activity vs. temperature diagram.

decomposes into liquid silicon and nitrogen as indicated by the horizontal line. Calculated nitrogen partial pressure vs. temperature diagrams (Fig. 4-6, 4-28, 4-42) can be used to describe quantitatively the “encapsulation” effect. If the pressure of nitrogen increases from 1 bar to 10 bar, the reaction temperature between  $\text{Si}_3\text{N}_4$  and carbon will be shifted from 1484°C (1757 K) to 1700°C (1973 K), as well as the  $\text{Si}_3\text{N}_4$  decomposition temperature from 1841°C (2114 K) to 2043°C (2307 K). Combining these two effects, at a nitrogen pressure of 10 bar the carbon activity-temperature diagram was calculated (the dashed lines in Fig. 4-41). The reaction temperature between  $\text{Si}_3\text{N}_4$  and carbon at a nitrogen pressure of 10 bar increases from 1700°C (1973 K) at  $a_c=1$  to 2034°C (2307 K) at  $a_c=0.17$ . It has to be emphasized that the absolute pressure values and activities in the Si-B-C-N ceramics are not known exactly but the diagram shows quantitatively the increase of stability of  $\text{Si}_3\text{N}_4$  by pressure and carbon activity variation influenced by the specific microstructure. Estimating a carbon activity of 0.2 because of the formation of the  $\text{BNC}_x$  phase and a pressurizing of the nitrogen of 10 bar



**Fig. 4-42** Nitrogen partial pressure vs. temperature diagram for  $\text{Si}_3\text{N}_4$ .

because of the embedding of the  $\text{Si}_3\text{N}_4$  into the  $\text{BNC}_x$  matrix, it can be concluded that the thermal stability of the T2-1, MW33, MW36 precursor-derived ceramics is increased to about 2000°C.

In contrast to the T2-1, MW33- and MW36-derived ceramics, the ceramics derived from BNCP and T2-1 (Ar/ $\text{NH}_3$ ) show different behaviors (Figs. 4-35, 39). From the calculation of phase fraction diagrams (Fig. 4-26) it can be seen, that the most remarkable differences between the T2-1, MW33- and MW36-derived ceramics on the one hand and the BNCP and T2-1(Ar/ $\text{NH}_3$ )-derived ceramics on the other hand are the relatively low phase amount of BN in the BNCP-derived ceramic and the relatively high amount of  $\text{Si}_3\text{N}_4$  in BNCP- and T2-1( $\text{NH}_3$ /Ar)-derived ceramics. It can be concluded that in BNCP-derived ceramic there is some residual free carbon, since the amount of BN is not sufficient to enable a complete “dissolution” of carbon. Therefore, reaction (4.1) occurs at least slowly in the BNCP-derived ceramic. The relatively high amount of  $\text{Si}_3\text{N}_4$  in both BNCP- and T2-1(Ar/ $\text{NH}_3$ )-derived ceramics is the reason for an insufficient encapsulation of  $\text{Si}_3\text{N}_4$  grains by the turbostratic  $\text{BNC}_x$ , thus reaction (4.2) may occur at higher temperature by that reducing the thermal stability of both materials to some 1880°C (which is still higher than the 1840°C of NCP200 derived Si-C-N ceramic).

For the sake of finding an universal relationship of the thermal stability and the compositions, other Si-B-C-N ceramics reported in the literature have been taken also into account. In Table 3-2 the information on 27 Si-B-C-N ceramics is listed. Materials No. 1-12 reveal minor mass losses up to some 2000°C under the condition of TG analyses whereas all other ones (No. 13-27) don't exhibit such a behavior. The calculated isothermal sections (Figs. 4-19, 4-20, 4-21, 4-22) contain the compositions of these ceramics given in Table 3-2. Symbols of the ceramics No. 1-12 are black (full) and the other ones No. 13-27 are blank (empty). As can be seen from the diagrams the compositions of the most stable ceramics No. 1-12 are located in the more or less center of the four-phase equilibrium field  $\text{Si}_3\text{N}_4 + \text{SiC} + \text{C} + \text{BN}$  and tentatively close to the three-phase equilibrium  $\text{SiC} + \text{C} + \text{BN}$ , while the compositions of the less stable ceramics No. 13-27 are located close to the three-phase equilibrium  $\text{Si}_3\text{N}_4 + \text{C} + \text{BN}$  ( $\text{Si}_3\text{N}_4$ -enriched area). The compositions of all stable materials are located within the overlap area of the four-phase equilibrium fields  $\text{Si}_3\text{N}_4 + \text{SiC} + \text{C} + \text{BN}$  and  $\text{G}(\text{N}_2) + \text{SiC} + \text{C} + \text{BN}$ .

Structural stability which is associated with crystallization and phase transition processes of precursor-derived ceramics materials is of great importance with respect to possible applications for these amorphous materials and for the final properties of the polycrystalline ceramics materials. Riedel et. al. [96Rie3] and Jansen et al. [Jan97] summarized a selection of synthetic routes to amorphous ceramics and their crystallization temperature and concluded that the starting temperatures of crystallization is lowest for binary Si or B nitrides and carbides (1200-1300°C or less), and increases with a growth in the number of constituent elements except for the B-C-N system. The Si-C-N amorphous ceramics materials remain in the amorphous state up to 1400°C, and the addition of boron is connected with an increased thermal stability of the amorphous state. Some Si-B-C-N materials remain in the amorphous state up to 1700°C [96Rie1, 00Wei]. Some authors reported stability even up to 1900-2000°C [99Jün, 94Bal], but this value is obtained from the sample after TGA measurement with a heating rate of 5 K/min. In this work an exothermic reaction peak between 1720°C and 1760°C for the BNCP-derived ceramic as well as an exothermic reaction peak between 1740°C and 1780°C for the T2-1 ( $\text{NH}_3/\text{Ar}$ )-derived ceramic were determined, which could be perhaps attributed to the crystallization of the materials. But the crystallization temperatures for other materials, such as T2-1, MW33, MW36 could not be detected in this work by DTA/TG experiments because of the sluggishness of the process of crystallization. It is difficult to give relationships between structure stability and chemical compositions because

of the lack of crystallization temperature data for some material. The thermodynamic modeling of the metastable amorphous state in order to describe in detail its transformation into the stable phases needs further investigations before generalizations can be carried out. But certainly boron and carbon are responsible for the increase in crystallization temperature and turbostratic BNC<sub>x</sub> play a major role for thermal stability of Si-B-C-N materials.

Detailed structure and phase analyses by X-ray and neutron scattering and by solid state NMR spectroscopy of some of the ceramics considered here revealed that in all of them in the as-thermolyzed stable phase separation and short range ordering occur [96Sei5, 98Dür, 98Sch, 98Bil, 00Bil, 01Bil, 01Hau]. It was concluded that the structural units of the thermodynamically stable crystalline phases are already preformed within the amorphous state. Ternary Si-C-N materials with a composition within the concentration triangle Si<sub>3</sub>N<sub>4</sub>+SiC+C are demixed in two phases, amorphous sp<sup>2</sup>-type carbon and an amorphous sp<sup>3</sup>-type network of Si(CN)<sub>4</sub> tetrahedra. The phase composition of the latter one can be described as Si<sub>3+y/4</sub>C<sub>y</sub>N<sub>4-y</sub> where y varies due to the overall composition and is zero in the case, when the composition is somewhere along the tie line between C and Si<sub>3</sub>N<sub>4</sub>. At higher Si contents the N deficit with respect to Si will be balanced by carbon resulting in mixed coordination of C and N to Si. As-thermolyzed quaternary Si-B-C-N materials with compositions within the four-phase equilibria Si<sub>3</sub>N<sub>4</sub>+SiC+C+BN are similarly demixed into two amorphous phases, namely Si<sub>3-y/4</sub>C<sub>y</sub>N<sub>4-y</sub> and BNC<sub>x</sub>. The latter phase can be considered as an atomic mixture of sp<sup>2</sup> carbon and sp<sup>2</sup> BN. The relative amounts of both structure units depend on the overall composition of the material. The absolute amount of BN depends on the boron content and that of sp<sup>2</sup> carbon on the silicon content, i.e. on the amount of C, which is not bonded to Si within the Si<sub>3-y/4</sub>C<sub>y</sub>N<sub>4-y</sub> phase.

Even if kinetic effects are significantly influencing the crystallization behavior, calculation of phase fraction diagrams can quantitatively predict the crystallization behavior of Si-B-C-N precursor-derived ceramics materials. The composition of the BNC<sub>x</sub> turbostratic layers can be derived from calculated phase fraction diagrams (Fig. 4-26, Table 4-2). For T2-1 ceramic material e. g. the calculated relative phase amounts are 16.6 at. % BN and 31.5 at. % carbon (graphite) (mole of atoms), which are equivalent to an atomic ratio B:N:C = 1:1:3.8 for the BNC<sub>x</sub> phase. For MW33 ceramic material the calculated atomic ratio B:N:C of BNC<sub>x</sub> is 1:1:3.0. These calculated results are in very good agreement with investigations by the quantitative evaluation of the energy loss spectra (EEL), as shown in Fig. 4-43 [00Wic].

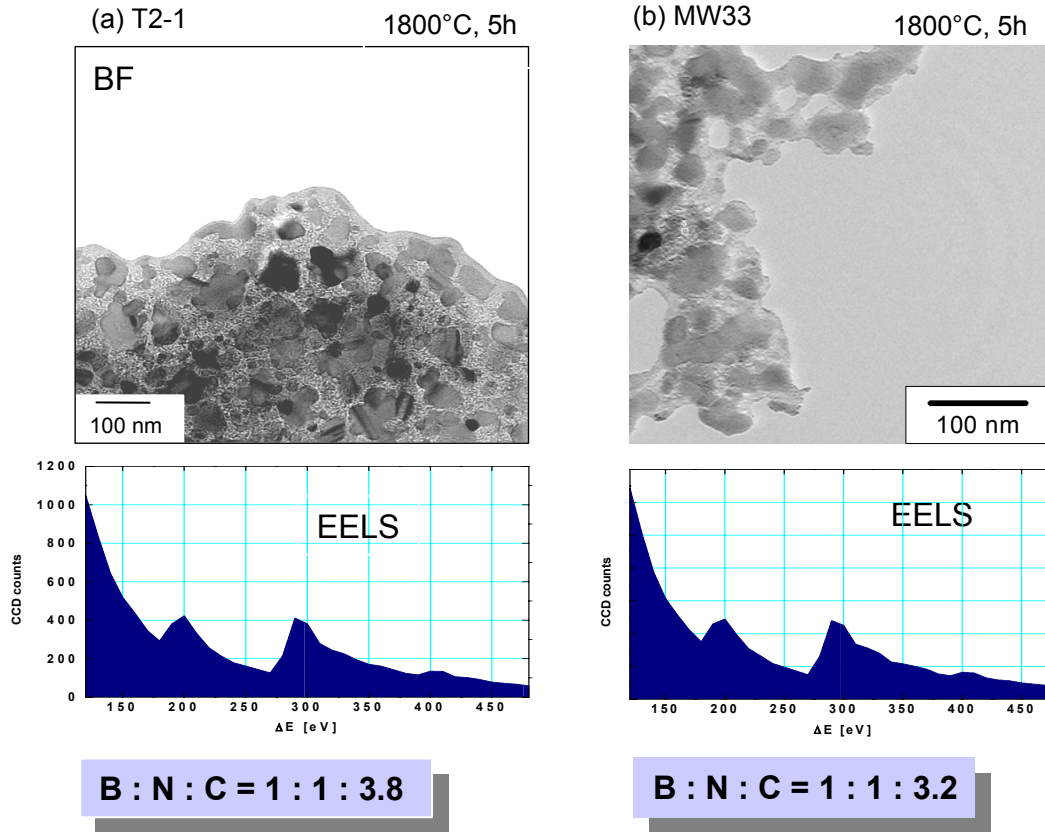


**Fig. 4-43** TEM bright field image of (a) T2-1-derived; (b) MW33-derived ceramic material after annealing at 1800°C (2073 K) (5 h, Ar) and corresponding EEL spectra of the BNC<sub>x</sub> turbostratic layers. The average atomic ratio B:N:C was determined 1:1:3.8 for T2-1 derived ceramic and 1:1:3.2 for MW33 derived ceramic [00Wic].

In summary Si-(B-)C-N materials with compositions within the four-phase equilibrium Si<sub>3</sub>N<sub>4</sub>+SiC+C(+BN) demix during thermolyses of precursor polymers into two metastable amorphous phases according to the general equation



This was confirmed by Schumacher [00Sch] as an example for a ceramic thermolyzed from T2-1. In the case of ternary Si-C-N precursor the right side of equation simplifies to a-C+a-Si<sub>3+y/4</sub>C<sub>y</sub>N<sub>4-y</sub> (e.g. with NCP200, s. Fig. 4-1 and Table 5-2) and in the case of compositions at the tie line between carbon and Si<sub>3</sub>N<sub>4</sub> to a-C+a-Si<sub>3</sub>N<sub>4</sub> ( e.g. with VT50, s. Fig. 4-1 and Table 5-2).

Since any composition of  $a\text{-BNC}_x$  is located at the edge C-BN and any composition of  $a\text{-Si}_{3+y/3}\text{C}_y\text{N}_{4-y}$  along the edge SiC-Si<sub>3</sub>N<sub>4</sub>, any material with a composition within the four-phase equilibrium Si<sub>3</sub>N<sub>4</sub>+SiC+C+BN will demix into these two metastable phases with distinct compositions. Analytically this is described by a tie line between both phases through the overall composition of the demixed material. In Fig. 4.44 such tie lines are shown for all materials listed in table 3-2. It can be seen that the thermal stability is high, if the nitrogen content in the Si<sub>3+y/4</sub>C<sub>y</sub>N<sub>4-y</sub> phase decreases, i.e. the SiC content is above a certain value ( Fig. 4-44, Tab.4-2). This is an indication that reaction (4.1) is also retarded because of the increasing mixed coordinated Si by decreasing the nitrogen content of the network of the

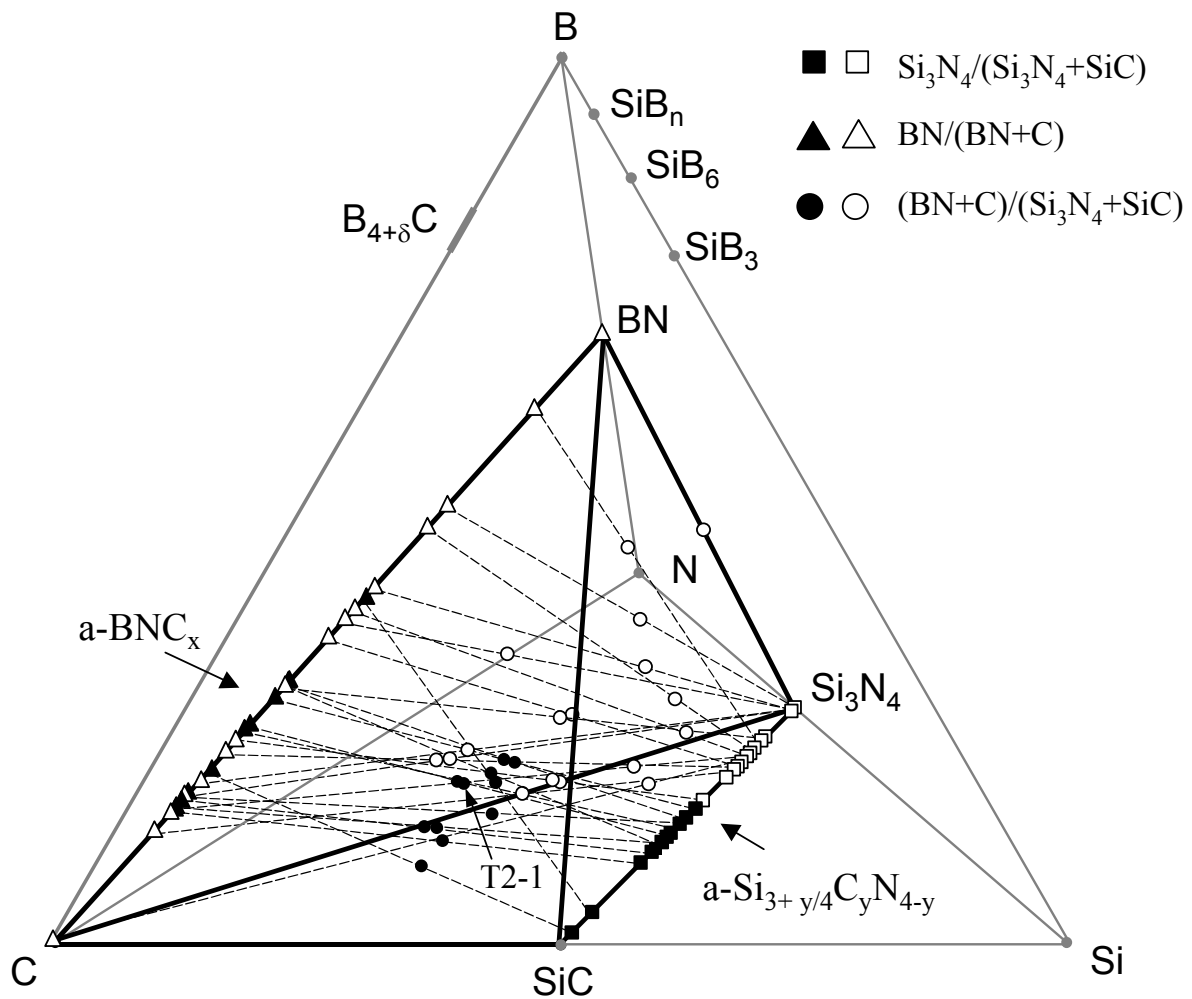


**Fig. 4-44** The quaternary concentration tetrahedron in the system Si-B-C-N with indicated four-phase equilibrium space Si<sub>3</sub>N<sub>4</sub>+SiC+C+BN. The phase amount relations Si<sub>3</sub>N<sub>4</sub>/(Si<sub>3</sub>N<sub>4</sub>+SiC), BN/(BN+C) and (BN+C)/(Si<sub>3</sub>N<sub>4</sub>+SiC) listed in Table 4-2 are depicted. The materials indicated with black (full) symbols are stable at high temperatures up to 2000°C, the other ones shown blank (empty) symbols are not stable.

amorphous  $\text{Si}_{3+y/4}\text{C}_y\text{N}_{4-y}$  phase below a certain value. The increasing stability of the amorphous state of the  $\text{Si}_{3+y/4}\text{C}_y\text{N}_{4-y}$  phase with increasing  $y$  is in accordance with recent calorimetric measurements, which indicate the enthalpies of formation were determined to be  $-90.23 \pm 2.46$  KJ/mol for  $\text{SiC}_{0.6}\text{N}_{1.02}$  and  $-144.05 \pm 3.16$  KJ/mol for  $\text{SiC}_{1.6}\text{N}_{1.33}$  [01Zha].

In any case, inhibiting of reaction (4.1) means that the amorphous state is stable until crystallization starts, i.e. amorphous  $\text{BNC}_x$  phase transforms into a turbostratic structure and the amorphous  $\text{Si}_{3+y/4}\text{C}_y\text{N}_{4-y}$  phase crystallizes into SiC and  $\text{Si}_3\text{N}_4$ . The transformation of  $\text{BNC}_x$  has been found to start already at  $1350^\circ\text{C}$  [01Cai], whereas first crystallization of carbon-rich  $\text{Si}_{3+y/4}\text{C}_y\text{N}_{4-y}$  has been observed only at temperature as high as  $1750^\circ\text{C}$  [00Wei, 01Hör].

The crystallization of  $\text{Si}_{3+y/4}\text{C}_y\text{N}_{4-y}$  results as expected in the formation of the thermodynamically stable phases SiC and  $\text{Si}_3\text{N}_4$ . The formation of  $\text{Si}_3\text{N}_4$  occurs even at higher temperature as  $1841^\circ\text{C}$ , when reaction (4.2) is shifted to the left because of the pressure stabilization of  $\text{Si}_3\text{N}_4$  due to the encapsulation effect. The  $\text{BNC}_x$  phase, which is the basic for the encapsulation effect, is in fact metastable, but its demixing into the stable phases graphite and BN is kinetically hindered strongly due to the low atomic mobility in the  $\text{sp}^2$ -type structures. It decomposes only when C reacts with BN according to reaction u3 at  $2324^\circ\text{C}$  ( $2597\text{K}$ ) (Fig.4.25).

Due to this model as-thermolyzed materials with overall compositions approaching the three-phase tie line triangle  $\text{SiC}+\text{C}+\text{BN}$  should be the most stable one which has been demonstrated recently [01Hör], and this is in accordance with the results of calculation of isothermal sections (Figs.4-19, 4-20, 4-21, 4-22) and phase fraction diagrams (Fig. 4-26, Table 4-2).

In summary, the formation of phases during thermolyses and crystallization of Si-B-C-N precursor can be simplified as shown in Fig. 4-45 and the different degree of thermal stability can be understood qualitatively as follows. High temperature stability up to  $2000^\circ\text{C}$  requires that two effects show up in the materials: (1) significantly decreased carbon activity due to the formation of turbostratic phase  $\text{BNC}_x$  by adding sufficient amount of boron and (2) encapsulation effect because of the embedding of  $\text{Si}_3\text{N}_4$  grains into the  $\text{BNC}_x$  matrix. If the amount of  $\text{Si}_3\text{N}_4$  grains formed in the material is not too high and the grains are nanosized



$\text{Si}_3\text{N}_4$ . Thereby a certain boron content is necessary to enable the formation of a the  $\text{BNC}_x$  phase and to lower the carbon activity.

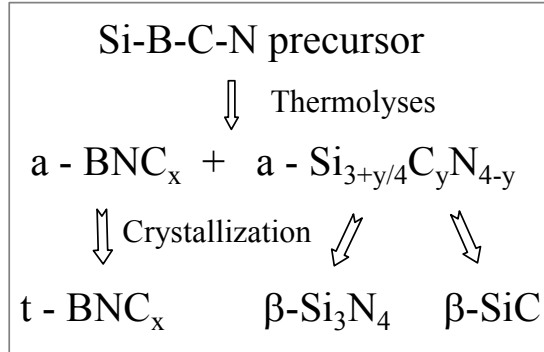


**Fig. 4-45** Phase formation during thermolyses and crystallization of Si-B-C-N precursor.

The mechanisms which are associated with crystallization and phase transition processes of the amorphous into the nanocrystalline state for the precursor-derived ceramics materials are not yet exactly clear. It needs further investigations in order to generalize. But it can be suggested that amorphous ceramics that exhibit a composition within the four-phase equilibrium space  $\text{Si}_3\text{N}_4 + \text{SiC} + \text{C} + \text{BN}$  consist of  $\text{Si}_{3+y/4}\text{C}_y\text{N}_{4-y}$  that can be derived from the structural units of silicon nitride ( $\text{SiN}_4$ ) and carbide ( $\text{SiC}_4$ ) as well as of a matrix phase  $\text{BCN}_x$  present in  $\text{sp}^2$  graphite and hexagonal BN. Crystallization of the  $\text{Si}_{3+y/4}\text{C}_y\text{N}_{4-y}$  phase results in a demixing into  $\text{SiN}_4$  and  $\text{SiC}_4$  units. Further growth of these nuclei leads to the formation of  $\text{Si}_3\text{N}_4$  and SiC nanocrystallites within the surrounding  $\text{BNC}_x$  matrix.

## 5 Phase Equilibria and Constitution in the Si-C-N-H System

Thermodynamic calculations in the Si-C-N-H system have been performed in a number of studies to predict the compositions of ceramic coatings based on  $\text{Si}_3\text{N}_4$  and produced by chemical vapor deposition [73Fis, 80Pal, 81Bad, 84Lar, 91Var, 96Kos]. In the development of ceramic materials for high-temperature applications, Gauckler et al. [79Gau] have calculated phase equilibria in the system Si-C-N-O-H-Ar to predict the production conditions and the understanding of the properties under service conditions. Bill et al and Schuhmacher et al. [00Bil, 98Sch] investigated the transformation of polysilazanes and polysilylcarbodiimides into amorphous Si-C-N ceramics by solid state NMR, IR and mass spectroscopy. In this work, phase equilibrium calculations in the Si-C-N-H system were used for the understanding of the condensation behavior of precursors during thermolysis.

In order to provide a quantitative description of the transformation behavior and the phase formation of amorphous ceramics, such calculations in the Si-C-N-H system were carried out by using the CALPHAD method. As a first estimate these calculations were made and the precondition of a closed system and under the assumption of complete crystallization of the phases, whereas the polymer precursors and the resulting ceramics are amorphous. Nevertheless, important information can be derived from such calculations, as outlined below.

The thermodynamic descriptions of the solid phases and gaseous species of the Si-C-N system as described in Chapter 2.3 have been applied and were combined with the thermodynamic description of the hydrogen containing gaseous species (e.g.  $\text{H}_2$ ,  $\text{CH}_2$ ,  $\text{CH}_3$ ,  $\text{CH}_4$ ,  $\text{C}_2\text{H}_4$ ,  $\text{NH}_3$ ,  $\text{SiH}$ ,  $\text{SiH}_2$ ,  $\text{SiH}_3$ ,  $\text{SiH}_4$ ,  $\text{Si}_2\text{H}_2$ ) as available from the SGTE-database [SGTE]. Since no hydrogen-containing solid compounds are known in this system, the hydrogen-containing ternary system and the quaternary system Si-C-N-H can be calculated by extrapolation from binary edge systems and ternary subsystems.

Calculated isothermal sections of the ternary Si-C-H, Si-N-H, and C-N-H systems at a temperature of 300°C (573 K) are shown in Fig. 5-1.

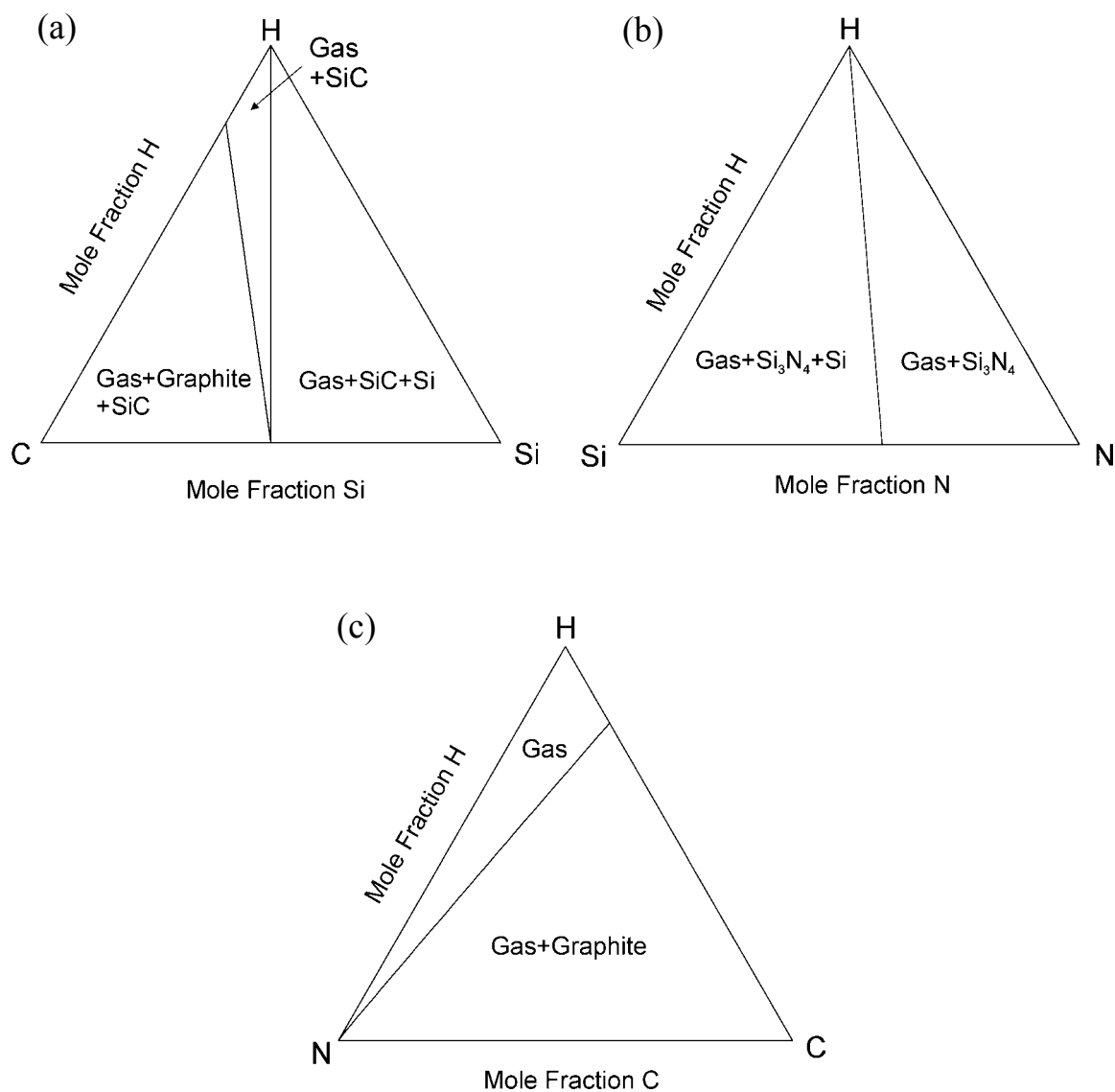


**Fig. 5-1** Calculated isothermal sections of the ternary Si-C-H, Si-N-H, and C-N-H systems at a temperature of 300°C (573 K): (a) Si-C-H system; (b) Si-N-H system; (c) C-N-H system.

The thermolysis of seven different preceramic polymers were experimentally investigated [00Bil, 94Kie]. The composition of these polymer samples determined by chemical analysis and their structural formulae are shown in Table 5-1.

**Table 5-1** Chemical compositions (at.%) and structure formulae of preceramic polymers.

Polymer <sup>a</sup>	Laboratory name	Structure formula	Si	C	N	H
PVS	VT50	$[(CH=CH_2)(NH)_{0.5}SiNH]_n$	11.1	23.1	16.2	49.6
PHMSCD	Sample in [94Kie]	$[(CH_3)(H)SiNCN]_n$	8.3	24.8	16.5	50.4
PHVSCD	MW24	$[(CH=CH_2)(H)SiNCN]_n$	9.9	30.3	21.9	37.8
PMVSCD	Sample in [94Kie]	$[(CH=CH_2)(CH_3)SiNCN]_n$	6.4	29.6	15.2	48.8
PHMS	NCP200	$[(CH_3)(H)SiNH]_n$	11.5	15.7	10.5	62.3
PHVS	MW32	$[(CH=CH_2)(H)SiNH]_n$	10.6	22.9	12.2	54.3
PMVS	MW2	$[(CH=CH_2)(CH_3)SiNH]_n$	8.8	25.5	8.8	56.9

<sup>a</sup> P means poly, H: hydro, M: methyl, V: vinyl, S: silazane, CD: carbodiimide. For details see [98Ald] [95Bil1] and [00Wei].

The hydrogen content of all these precursors are in the range from 37.8 to 62.3 at.%. According to Fig. 5-1 the phase equilibria and phase reactions do not differ significantly with the hydrogen content. Therefore, for simplification, the relative amount of silicon, carbon and nitrogen of the precursor polymers are displayed in a plane at constant hydrogen content of 50 at.% of the calculated quaternary Si-C-N-H as shown in Fig. 5-2. This isothermal section at a temperature of 300°C (573 K) is shown in detail in Fig. 5-3a. It reveals the following phase equilibria: (1) gas+C+Si<sub>3</sub>N<sub>4</sub>, (2) gas+C+Si<sub>3</sub>N<sub>4</sub>+SiC, (3) gas+Si<sub>3</sub>N<sub>4</sub>, (4) gas+Si<sub>3</sub>N<sub>4</sub>+SiC and (5) gas+Si<sub>3</sub>N<sub>4</sub>+SiC+Si. All compositions of precursor polymers investigated here are located in the phase fields (1) gas+C+Si<sub>3</sub>N<sub>4</sub> or (2) gas+C+Si<sub>3</sub>N<sub>4</sub>+SiC. As can be seen from isothermal sections at 300°C (573 K), 500°C (773 K), 700°C (973 K) and 1050°C (1323 K), respectively

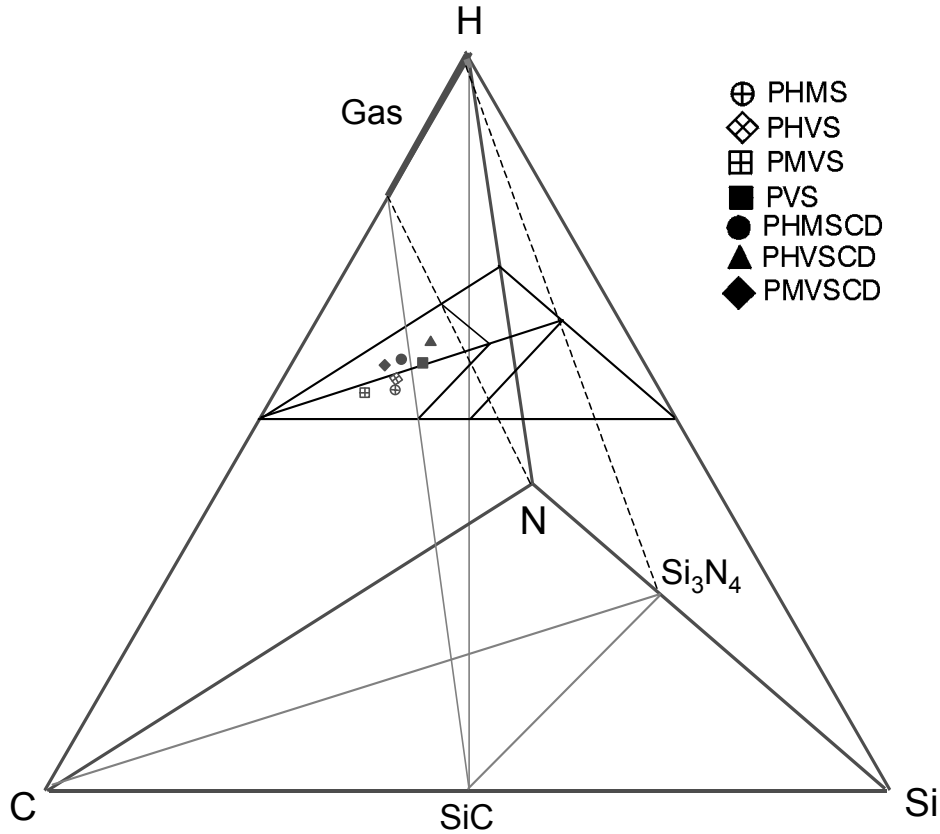


**Fig. 5-2** The quaternary Si-C-N-H concentration tetrahedron at a temperature of 300°C (573 K). A plane of constant hydrogen content of 50 at.% including the compositions of the seven precursor polymers is indicated.

(Fig. 5-3a, b, c and d) the phase equilibrium fields of (1) gas+C+Si<sub>3</sub>N<sub>4</sub> and (2) gas+C+Si<sub>3</sub>N<sub>4</sub>+SiC are extending with increasing temperature, whereas the phase equilibrium fields of (3) gas+ Si<sub>3</sub>N<sub>4</sub> and (4) gas+Si<sub>3</sub>N<sub>4</sub>+SiC shrink due to the progressing of methane decomposition:



The phase equilibrium field of (5) gas+Si<sub>3</sub>N<sub>4</sub>+SiC+Si does not change its extension. At 1050°C (1323 K) methane, which is the main gaseous species at temperatures lower than 800 K, is almost completely decomposed and hydrogen is the dominating gas species. Therefore, at this temperature the phase fields (3) gas+Si<sub>3</sub>N<sub>4</sub> and (4) Gas+Si<sub>3</sub>N<sub>4</sub>+SiC are not extended at all.

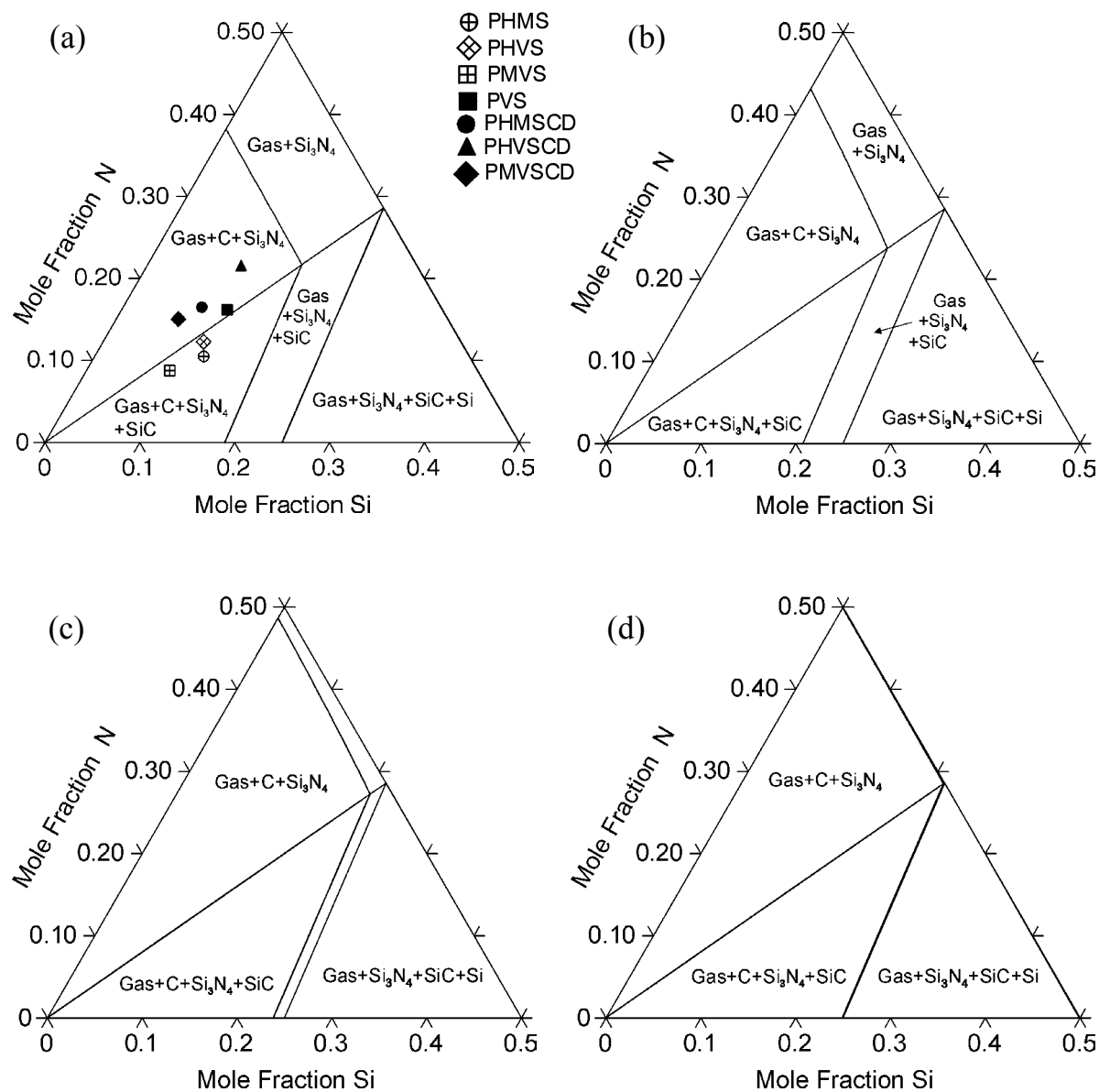


**Fig. 5-3** Calculated isothermal sections at constant hydrogen content of 50 at.% in the Si-C-N-H system: (a)  $T = 300^{\circ}\text{C}$  (573 K) (with compositions of the seven precursor polymers); (b)  $T = 500^{\circ}\text{C}$  (773 K); (c)  $T = 700^{\circ}\text{C}$  (973 K); and (d)  $T = 1050^{\circ}\text{C}$  (1323 K).

According to their compositions the investigated precursor polymers can be separated into two classes: PVS-, PHMSCD-, PHVSCD and PMVSCD with a ratio  $[\text{Si}]/[\text{N}] < 0.75$  located in the three phase field (1) gas+C+Si<sub>3</sub>N<sub>4</sub> and PHMS, PMVS and PMVS with the ratio  $[\text{Si}]/[\text{N}] > 0.75$  located in the four phase field (2) gas+C+Si<sub>3</sub>N<sub>4</sub>+SiC. For all precursors the phase

formation in the temperature range between 27°C (300 K) and 1227°C (1500 K) is illustrated by the phase fraction diagrams (Fig. 5-4) and gas phase composition diagrams (Fig. 5-5) that have been calculated for the precursor compositions given in Table 5-1. In all cases the amount of the gaseous phase decreases with increasing temperature due to the continuous decomposition of CH<sub>4</sub> into H<sub>2</sub> and graphite. After complete degassing of hydrogen, the solids are composed either of Si<sub>3</sub>N<sub>4</sub> and graphite or of Si<sub>3</sub>N<sub>4</sub>, graphite and SiC. Precursor compositions located in the three phase fields (1) gas+C+Si<sub>3</sub>N<sub>4</sub> (precursors PVS, PHMSCD, PHVSCD and PMVSCD) yield as solid phases only Si<sub>3</sub>N<sub>4</sub> and graphite (Fig. 5-4a-d). In these cases some silicon deficit with respect to hydrogen allows the formation of nitrogen containing gas species (N<sub>2</sub>, NH<sub>3</sub>) (Fig. 5-5a-d) until, in the solid product, the ratio [Si]:[N] = 0.75 with the PHMS- PHVS- and PMVS-derived compositions located in the four phase field (2) gas+C+Si<sub>3</sub>N<sub>4</sub>+SiC excess silicon with respect to the atomic ratio [Si]:[N] = 0.75 forms SiC, in addition to Si<sub>3</sub>N<sub>4</sub> and free carbon (graphite)(Fig. 5-4 e-g). With these precursors significant nitrogen partial pressures arise only at temperatures above 627°C (900 K)(Fig. 5-5).

After complete degassing of hydrogen, the composition on ceramics after thermolysis corresponding to the two classes of preceramic compounds described above, are located within the basal Si-C-N plane of the concentration tetrahedron Si-C-N-H. From the calculated phase fraction diagrams (Fig. 5-4) it can be seen that the compositions of solid products calculated in the case of the PVS-, PHMSCD-, PHVSCD- and PMVSCD- derived ceramics should be located close to the tie line Si<sub>3</sub>N<sub>4</sub>-C. The solid phase compositions from PHMS-, PHVS- and PMVS-based materials should be inside the three-phase Si<sub>3</sub>N<sub>4</sub>+SiC+C (Fig. 4-1a).

As pointed out, the calculated [Si]/[N] ratios of the solid phase remain constant within the considered temperature range, but the carbon content increases with temperature. This carbon formation is due to the continuous decomposition of CH<sub>4</sub> to H<sub>2</sub> and graphite with increasing temperature (Fig. 5-5). It has to be emphasized that these calculations were carried out for a closed system as described before. In contrast to this, during thermolysis a continuous loss of gaseous species and a continuous change of the gross composition of the solid material can be

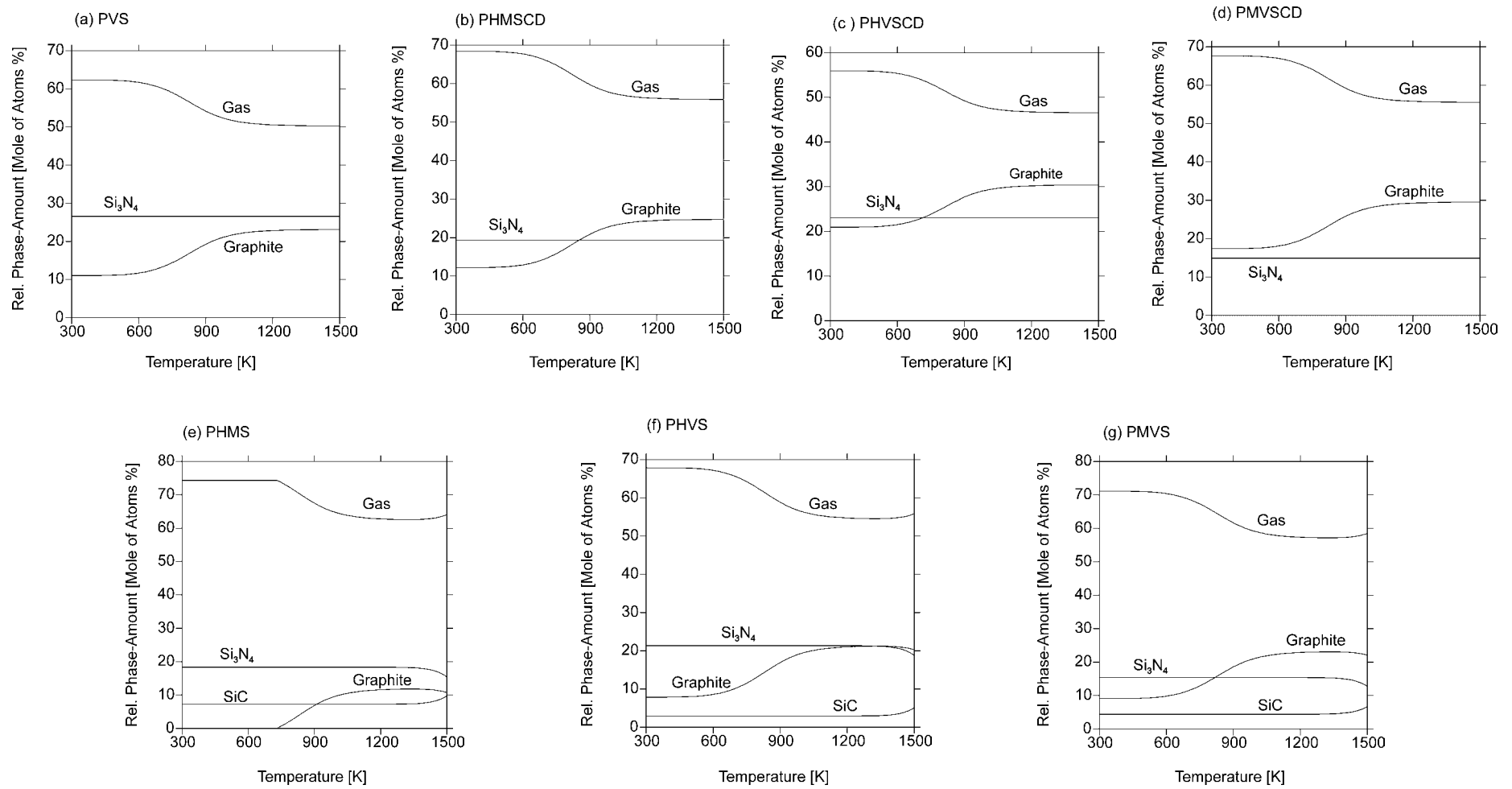


**Fig. 5-4** Calculated phase fraction diagrams for precursor polymer: (a) PVS; (b) PHMSCD; (c) PHVSCD; (d) PMVSCD; (e) PHMS; (f) PHVS; and (g) PMVS.



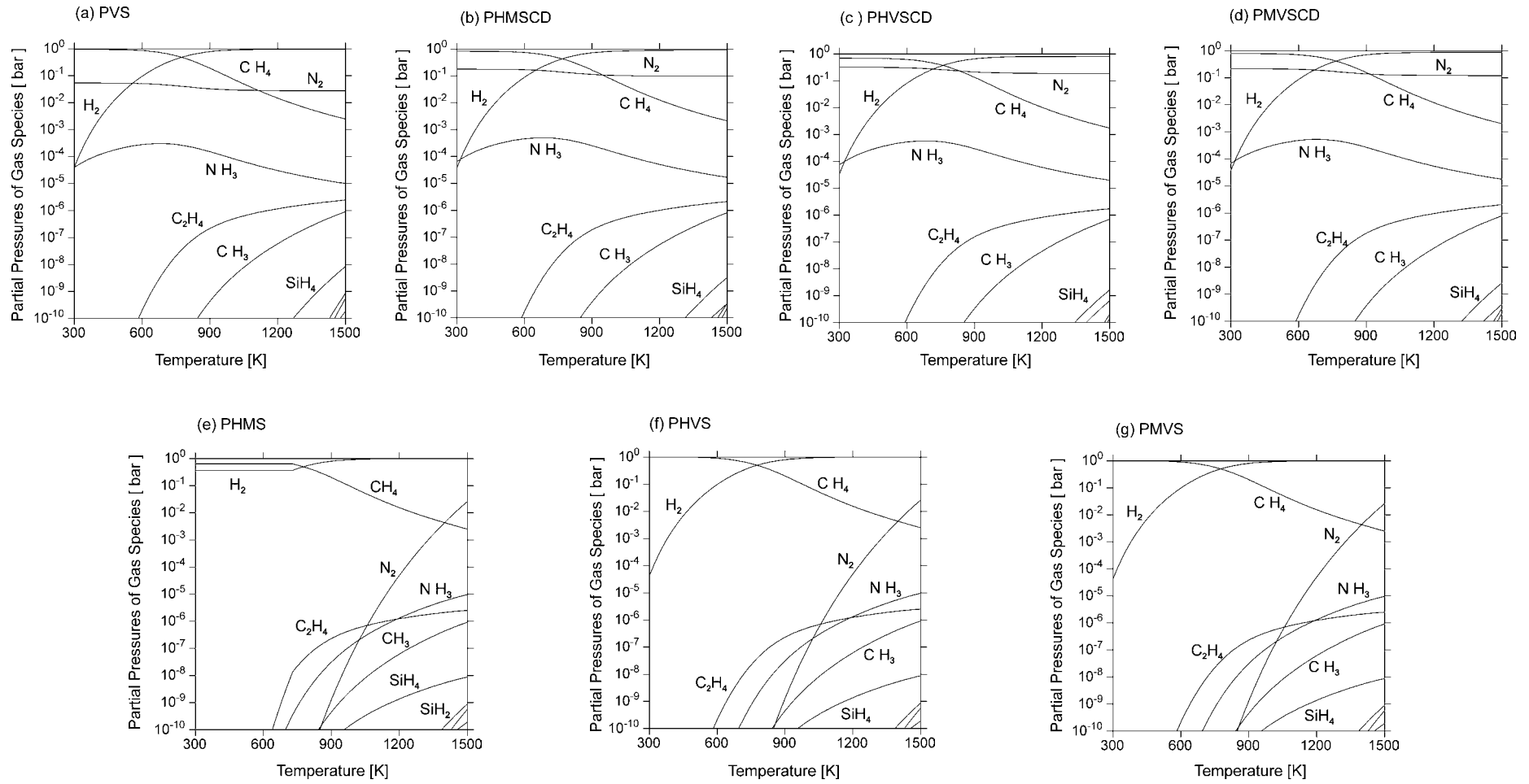


**Fig. 5-5** Partial pressures for the gas phase in equilibrium with precursor polymers: (a) PVS; (b) PHMSCD; (c) PHVSCD; (d) PMVSCD; (e) PHMS; (f) PHVS; and (g) PMVS.

found which is accompanied by the change of the ratio of the gaseous species involved. Owing to the loss of carbon-containing gaseous species during thermolysis the experimentally determined carbon content of the obtained ceramics is shifted to lower values compared to the compositions calculated for 1050°C (1323 K) (at this temperature the precursors were thermolysed). Experimental investigations were in good agreement with the calculated results [00Bil]. Spectroscopic investigations indicate that the decomposition of methane contributes to the formation of carbon during the thermolysis step. Above the temperature of about 337°C (700 K) the amount of methane decreases whereas that of hydrogen increases which is accompanied by the formation of  $sp^2$ -hybridized carbon as revealed by  $^{13}\text{C}$  NMR spectroscopy. These results suggest that the incorporation of free carbon into the ceramic solids is caused by the decomposition of methane.

According to the above-mentioned thermochemical calculations the compositions of the precursor-derived ceramics are located close to the tie line  $\text{Si}_3\text{N}_4$ -C (PVS-, PHMSCD-, PHVSCD- and PMVSCD-derived ceramics) and inside the area defined by the three-phase equilibrium  $\text{Si}_3\text{N}_4$ -SiC-C (PHMS- PHVS- and PMVS-derived ceramics), respectively. The structural investigations of the amorphous ceramics described in [96Sei5, 98Dür, 98Sch, 98Bil, 00Bil, 01Bil, 01Hau] also reveal that the PVS-, PHMSCD-, PHVSCD- and PMVSCD-derived solids consist of  $\text{SiN}_4$  tetrahedra and  $sp^2$ -hybridized carbon units, whereas in the PHMS- and PMVS-based materials  $\text{CSi}_4$  and  $\text{SiC}_x\text{N}_y$  tetrahedra are present beside  $\text{SiN}_4$  and  $sp^2$ -hybridized carbon units, as shown in Table 5-2. In addition, the results in the medium range order clearly exhibit the presence of silicon nitride segregations. The surrounding matrix is enriched in carbon in the case of the compositions located close to the tie line  $\text{Si}_3\text{N}_4$ -C whereas SiC with compositions located inside the triangle  $\text{Si}_3\text{N}_4$ -SiC-C carbon also will be bond to silicon.

**Table 5-2** The structure of the precursor derived amorphous ceramics after thermolysis at 1050°C investigated by X-ray and neutron scattering, solid state NMR, IR and mass spectroscopy [96Sei5, 98Dür, 98Sch, 98Bil, 00Bil, 01Bil, 01Hau].

Precursor	Laboratory name	Structure of amorphous ceramics by thermolysis at 1050°C <sup>a</sup>				
		Si-C-N-matrix			a-Si <sub>3</sub> N <sub>4</sub>	a-sp <sup>2</sup> C
		SiC <sub>2</sub> N <sub>2</sub>	SiCN <sub>3</sub>	CSi <sub>4</sub>	SiN <sub>4</sub>	Csp <sup>2</sup>
PVS	VT50	-	-	-	+	+
PHMSCD	Sample in [94Kie]	-	-	-	+	+
PHVSCD	MW24	-	-	-	+	+
PMVSCD	Sample in [94Kie]	-	-	-	+	+
PHMS	NCP200	(+)	+	+	+	(+)
PHVS	MW32	(+)	+	+	+	+
PMVS	MW2	(+)	+	(+)	+	+

<sup>a</sup> “-” means that the structure is not present, “+” means that the structure is present, “(+)” means that the structure is present, but the signals are very weak.

These results indicate that the structural units of the thermodynamically stable phases are already preformed during thermolysis within the amorphous state on an atomic and medium range scale. Although kinetic aspects like the formation of metastable radical and gaseous intermediate species play an important part, the thermodynamic calculations provide an important base for the correlation of the precursor composition with the architecture of the corresponding amorphous ceramic solids. It is shown that thermodynamic calculations provide a guide for the composition and short-range order in the amorphous microstructure which is in close relation to the structure of the phases crystallizing at higher temperature.

## **6 Thermophysical Properties of Precursor-Derived Amorphous Si-(B-)C-N Ceramics**

Until now less attention has been paid to thermophysical properties of precursor-derived ceramics. Data of thermophysical properties (e.g. thermal expansion, specific heat and thermal conductivity) are important for the determination of the fabrication process and the high-temperature properties of the material in service. For example, a low thermal conductivity is required in applications like heat insulation components in order to reduce fuel consumption.

### **6.1 Thermal expansion**

In this work the thermal expansion for amorphous Si-C-N ceramics derived from the precursors VT50 and NCP200 and the amorphous Si-B-C-N ceramics derived from the precursor T2-1 were estimated. Details about the bulk amorphous ceramics preparation were described in chapter 3.1.

The results for VT50-derived amorphous Si-C-N ceramics in the temperature range from 20°C to 1430°C at a heating and a cooling rate of 5°C min<sup>-1</sup> in nitrogen atmosphere are shown in Fig. 6.1, where the relative length changes  $\varepsilon$  (percent expansion) are plotted as a function of temperature for two heating/cooling thermal cycles. It can be seen that a significant shrinkage occurred during the first thermal cycle, while a more stable length change behavior was achieved during the second thermal cycle. During the first thermal cycle, the specimen expanded linearly up to 1000°C and then shrank drastically at temperatures higher than 1100°C. During cooling the specimen contracted linearly at temperatures lower than 1300°C. The effects in the temperature range between 600°C and 800°C are due to instrumental reasons. The total shrinkage during the first thermal cycle is 2.2%. During the second cycle, the specimen expanded linearly up to 1300°C and shrank slightly at temperatures above around 1400°C. Shrinkage during cooling is linear below 1300°C. The length jump at 780°C is due to instrumental reasons as mentioned above. The total shrinkage during the second cycle is only 0.1%, which is much less than the shrinkage during the first cycle. This unstable

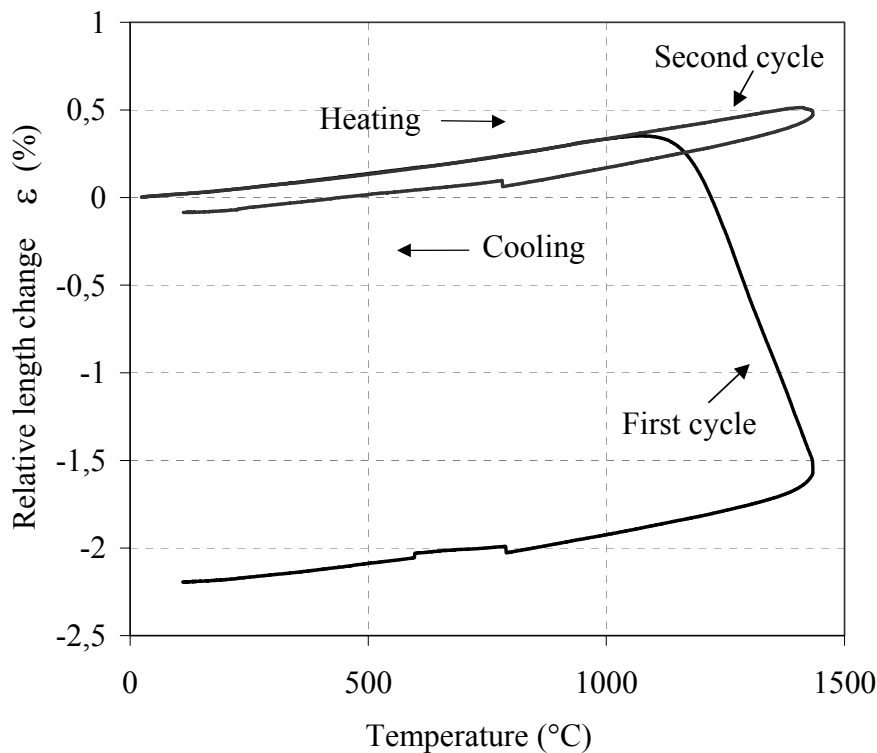


**Fig. 6-1** Thermal expansion behavior of the VT50-derived amorphous Si-C-N ceramics material; relative length changes ( $\epsilon$ , percent expansion) as a function of temperature for two heating/cooling thermal cycles.

thermal expansion behavior is possibly due to the evolution of residual gas during heating above the temperature of thermolysis ( $1050^{\circ}\text{C}$ ) and due to structural changes in the amorphous phases during heat treatment. As mentioned earlier, the VT50-derived amorphous Si-C-N ceramics is prepared by pyrolysis for 4 hours at  $1050^{\circ}\text{C}$  under argon after shaping by plastic forming. The sample shows a porosity of about 17% according to the measurements of light optical microscopy. This porosity originates from the incomplete densification of polymer powder in the green stage and from the evaporation of the gases during the pyrolysis.

In order to achieve a complete degassing and reproducible expansion measurements, the material was heat treated after thermolysis for 10h at  $1400^{\circ}\text{C}$  in nitrogen. The dimensional and mass changes are given in Table 6-1. The length of the specimen shrank from 11.664 mm to 11.373 mm, corresponding to 2.49%. Simultaneously, a mass loss of 0.99% occurred and a density increase of 3.59% from  $1.89\text{ g/cm}^3$  to  $1.95\text{ g/cm}^3$ . Before and after the heat treatment,

the microstructure of the polished surfaces of the ceramic specimens was observed by optical microscopy and is shown in Fig. 6.2. White parts correspond to the solid amorphous phase and black areas to pores. As can be seen from the micrographs, after the heat treatment the porosity is reduced. X-ray diffractometry varying  $2\theta$  from  $10$  to  $80^\circ$  before and after the heat treatment revealed no reflections, which means that there was no crystallization during heat treatment.

**Table 6-1** Changes of length, volume, mass and density, respectively, for the specimen of a VT50-derived amorphous ceramic by heat treatment at  $1400^\circ\text{C}$  in nitrogen for 10 hours.

	Length (mm)	Cross-section (mm)		Volume ( $\text{mm}^3$ )	Mass (mg)	Density ( $\text{g}/\text{cm}^3$ )
Before heat treatment	11.664	3.764	3.423	150.28	283.4	1.89
After heat treatment	11.373	3.728	3.388	143.65	280.6	1.95
Change by treatment	-2.49%	-0.96%	-1.02%	-4.41%	-0.99%	+3.59%

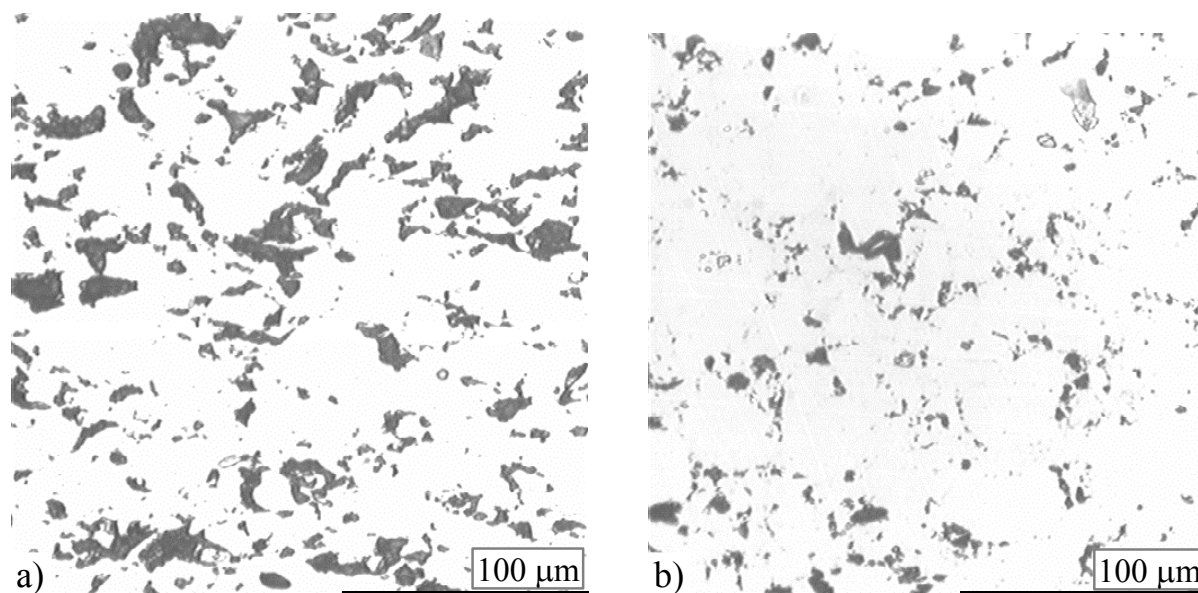


**Fig. 6-2** Light optical microstructure of the VT50-derived Si-C-N amorphous bulk ceramic material before and after the heat treatment at  $1400^\circ\text{C}$  in nitrogen atmosphere for 10h; (a) before heat treatment and (b) after heat treatment.

NCP200-derived Si-C-N ceramic specimens and T2-1-derived Si-B-C-N ceramic specimens were also heat treated at 1400°C for 10 hours in nitrogen atmosphere before being subjected to the thermal expansion measurement. After the heat treatment the specimens were ground to a length of 10 mm. Thermal expansion measurements were carried out with all three types of materials (VT50, NCP200, T2-1) in nitrogen atmosphere using the temperature program as shown in Fig. 6-3. The specimens were heated at 5°C/min from room temperature up to 1500°C, holding 30 min at 1500°C, and then cooled at 5°C to room temperature. Fig. 6-3 shows measured results, where relative length change and temperature are plotted as a function of time for the heating and cooling thermal procedures. Fig. 6-4 represents the relative length changes as a function of temperature for the heating procedure. As can be seen, all three types of materials expanded linearly up to 1450°C. During heating the NCP200-derived ceramic revealed the largest length change. During the 30 min holding at 1500°C the

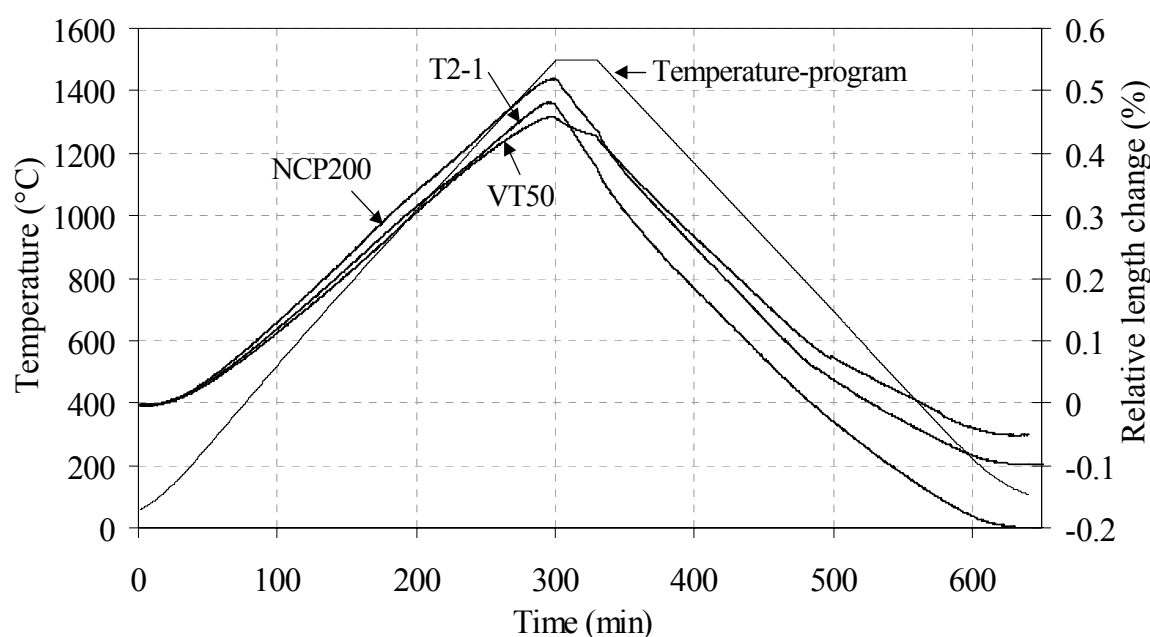


**Fig. 6-3** Thermal expansion measurement of the VT50-, NCP200-derived amorphous Si-C-N ceramics and T2-1-derived amorphous Si-B-C-N ceramic: relative length change and temperature vs. time for the heating and the cooling thermal procedures. Temperature program used for measurements is also indicated.

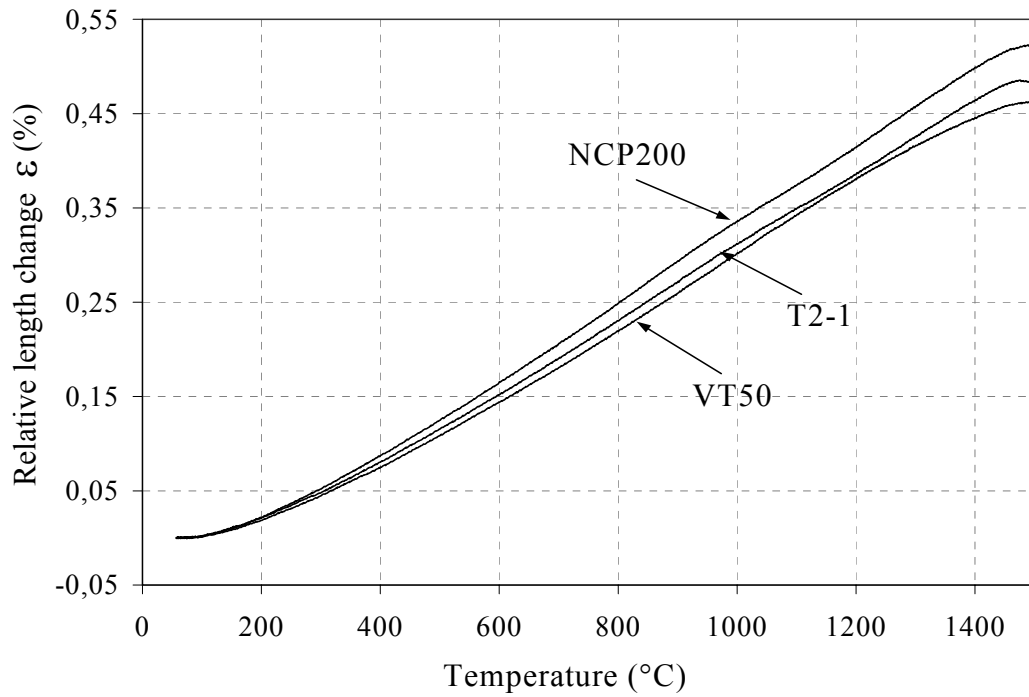


**Fig. 6-4** Temperature dependent relative length changes of VT50, NCP200 and T2-1 specimens, respectively, for the heating procedure.

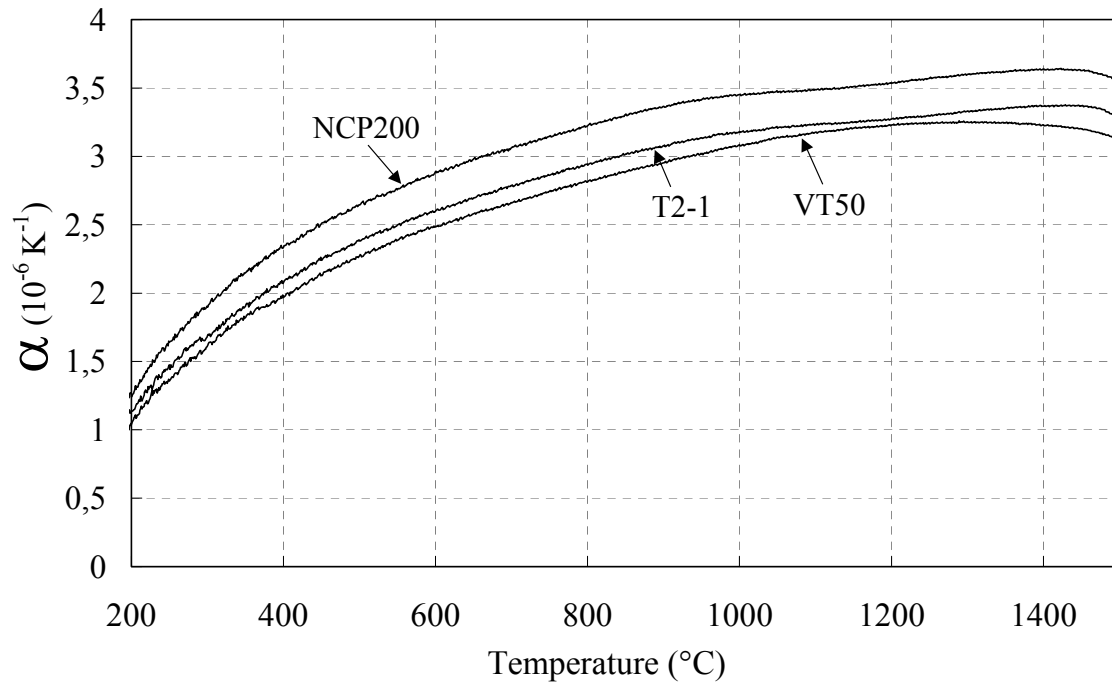


**Fig. 6-5** Linear thermal expansion coefficients vs. temperature for the VT50-, NCP200-derived amorphous Si-C-N ceramics as well as for the T2-1-derived amorphous Si-B-C-N ceramic.



VT50-derived ceramic had the smallest length change of 0.03%, while the specimens of NCP200-derived ceramic and T2-1-derived ceramic revealed a length change of 0.09%. These length changes are due to residual gas evolution in the materials and to some crystallization.

From the expansion data given above, the mean linear thermal expansion coefficient  $\alpha$  was calculated for all three ceramics using equation (3.2). The results were plotted as a function of temperature in Fig. 6-5. The NCP200-derived amorphous Si-C-N ceramics has the largest values in comparison with the VT50-derived Si-C-N ceramic and the T2-1-derived Si-B-C-N ceramic. This is perhaps due to the fact that NCP200-derived amorphous Si-C-N ceramics composites are containing a relatively smaller amount of  $sp^2$  carbon. The thermal expansion coefficients for the three materials increase with increasing temperature. At 400°C and 1000°C the respective values are for the VT50-derived Si-C-N ceramic  $1.98 \times 10^{-6}/K$  and  $3.09 \times 10^{-6}/K$ , for the NCP200-derived Si-C-N ceramic  $2.35 \times 10^{-6}/K$  and  $3.45 \times 10^{-6}/K$ , and for the T2-1-derived Si-B-C-N ceramic  $2.08 \times 10^{-6}/K$  and  $3.18 \times 10^{-6}/K$ . The values (20-1000°C) are about at the same level as those of polycrystalline  $Si_3N_4$  and other non-oxide ceramics, but somewhat lower than that of oxide-type ceramics such as  $Al_2O_3$  and  $ZrO_2$  (Fig. 6-6) [82Sal, 93Rie].

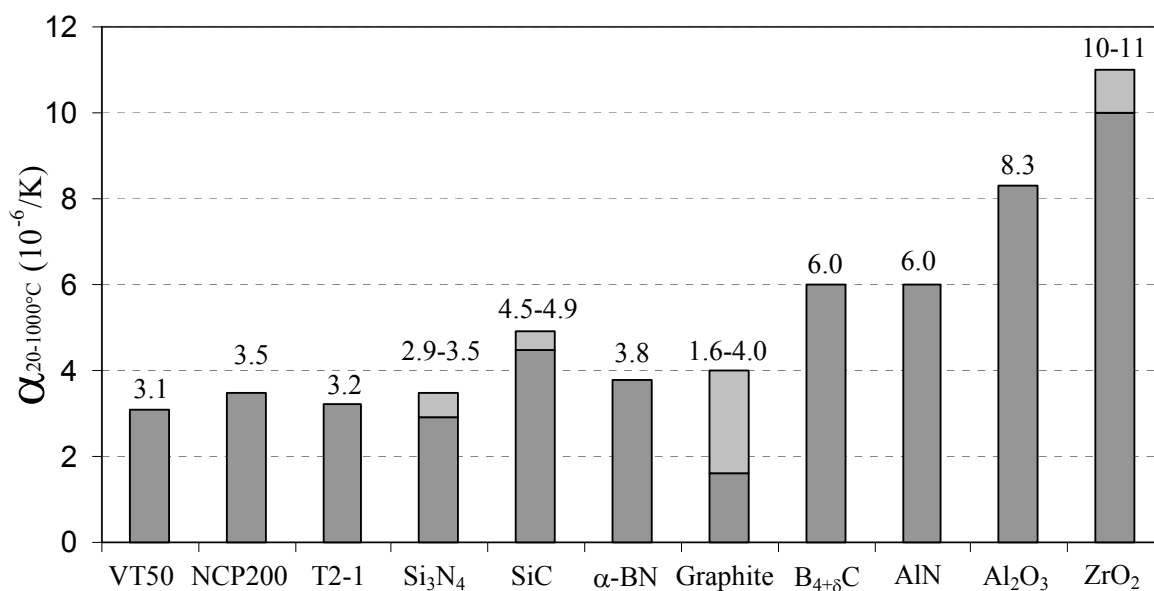


**Fig. 6-6** Comparison of thermal expansion coefficients of precursor-derived amorphous ceramics with that of other ceramics. The data of the other ceramics from literature [82Sal, 93Rie].

The curves in Fig. 6-5 do not show any indication for a glass transition for all three amorphous ceramic materials. Since the glass transition defines glasses, from this point of view, the amorphous precursor-derived Si-(B-)C-N ceramic materials can not be considered to be glasses, although they contain phases which consist of a three-dimension network  $\text{Si}_{3+x/4}\text{N}_{4-x}\text{C}_x$  with a structure which was found to be near-range ordered in very much the same way as e. g. vitreous silica [98Dür, 98Sch, 98Bil, 00Bil, 01Bil].

The glass transition is the phenomenon, in which a solid amorphous phase exhibits a more or less abrupt change in derivative thermodynamic properties (e.g. heat capacity or thermal expansion) from crystal-like to liquid-like values with the change of temperature [84Ell, 93Fel]. Glass is a special sub-set of amorphous materials, which exhibits a glass transition, produced in general by rapid quenching. All glasses are amorphous, but not all amorphous solids are necessarily glasses [84Ell]. Precursor-derived amorphous Si-(B-)C-N ceramic materials are only amorphous solids, but not glasses.

## 6.2 Calculation of the heat capacity

The specific heat of the VT50-, NCP200-derived Si-C-N ceramics and T2-1-derived Si-B-C-N ceramic were calculated using the CALPHAD method on the assumption that these materials are crystallized to stable phases such as  $\text{Si}_3\text{N}_4$ , SiC, graphite and BN. The calculated results are shown in Fig. 6-7.

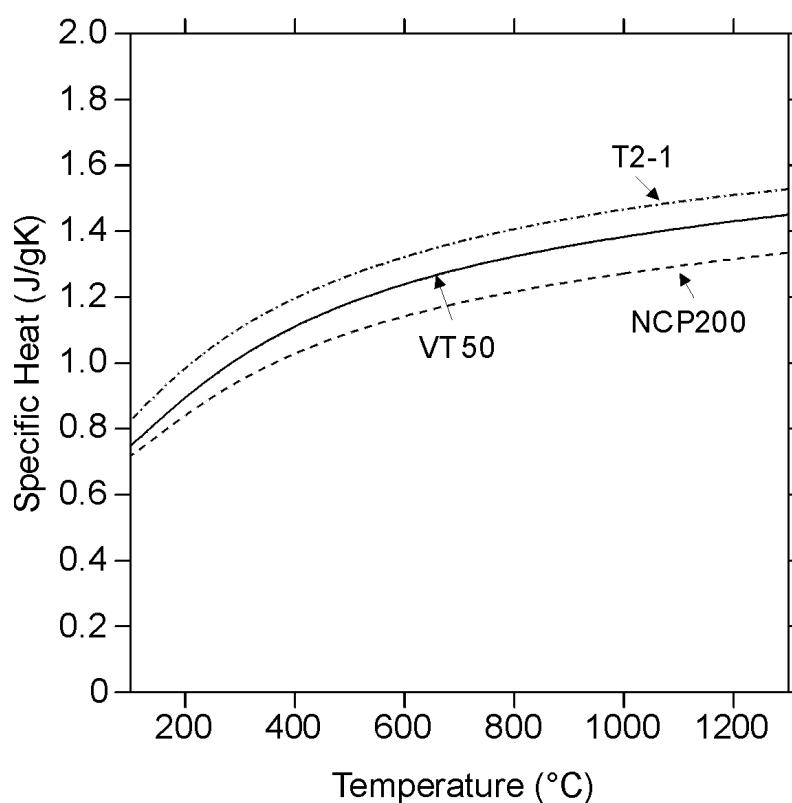


**Fig. 6-7.** Calculated specific heats of the VT50- and NCP200-derived amorphous Si-C-N ceramics as well as T2-1-derived amorphous Si-B-C-N ceramic.

### 6.3 Thermal conductivity

The thermal diffusivity  $\alpha$  of VT50- and NCP200-derived amorphous Si-C-N ceramics and of T2-1-derived amorphous Si-B-C-N ceramic were measured with the laser flash method. As examples, Fig. 6-8 a-c show the measured time dependences of the temperature increase of the rear surface for the VT50-derived ceramic at 500°C, the NCP200-derived ceramic at 550°C and the T2-1-derived ceramic at 560°C, respectively. When the temperature increase reaches the value 100%, this means that the temperature of the rear surface has reached its maximum. From these data the time required to reach half the maximum temperature rise of the rear surface  $t_{1/2}$  was calculated using the computer software, in which the heat losses

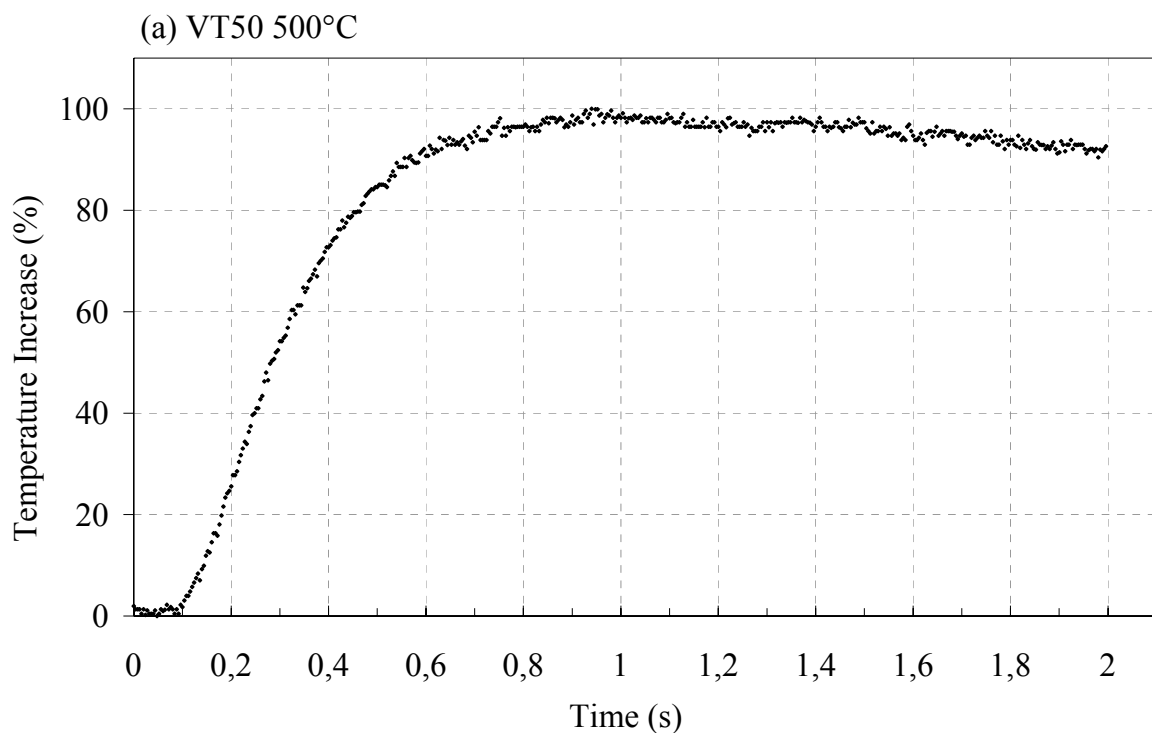


**Fig. 6-8** Measurements of thermal diffusivities of (a) VT50-derived amorphous Si-C-N ceramic at 500°C.

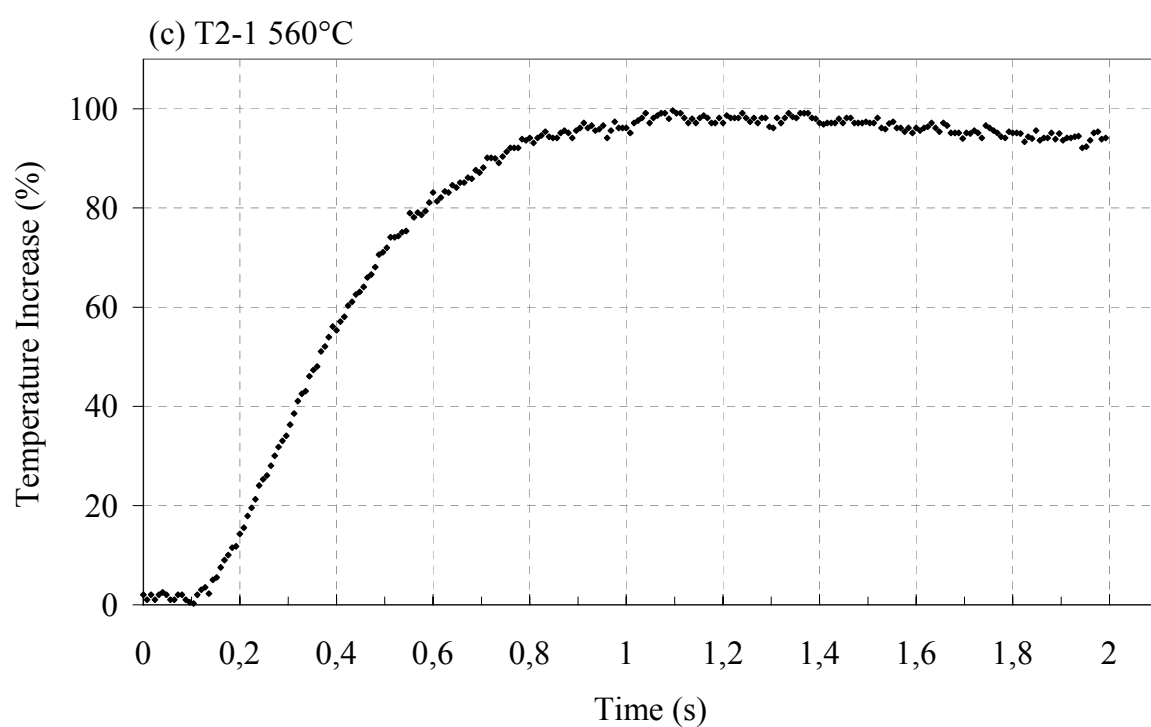
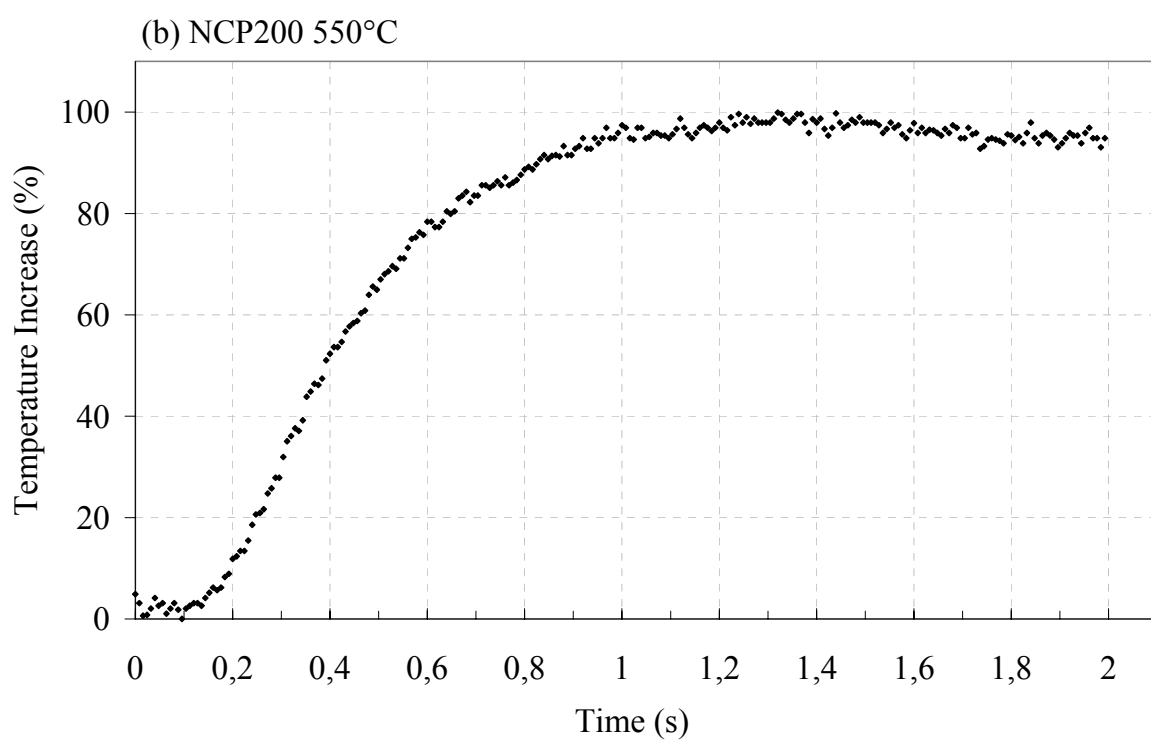


**Fig. 6-8** Measurements of thermal diffusivities of (b) NCP200-derived amorphous Si-C-N ceramics at 550°C; and (c) T2-1-derived amorphous Si-B-C-N ceramic at 560°C.

correction and the finite pulse length correction are taken into account. With the data of the sample thickness  $d$  (see Table 6-2), the thermal diffusivity  $\alpha$  of VT50- and NCP200-derived amorphous Si-C-N ceramics and T2-1-derived amorphous Si-B-C-N ceramic were calculated using equation (3.5). The results are shown in Fig. 6-9.

**Table 6-2** The thickness and density of samples of precursor-derived ceramics used in the measurements of the thermal conductivity.

Samples of precursor-derived ceramics	Thickness $d$ (cm)	Density $\rho$ (g/cm <sup>3</sup> )
VT50	0.1028	2.00
NCP200	0.1021	2.20
T2-1	0.1032	1.77

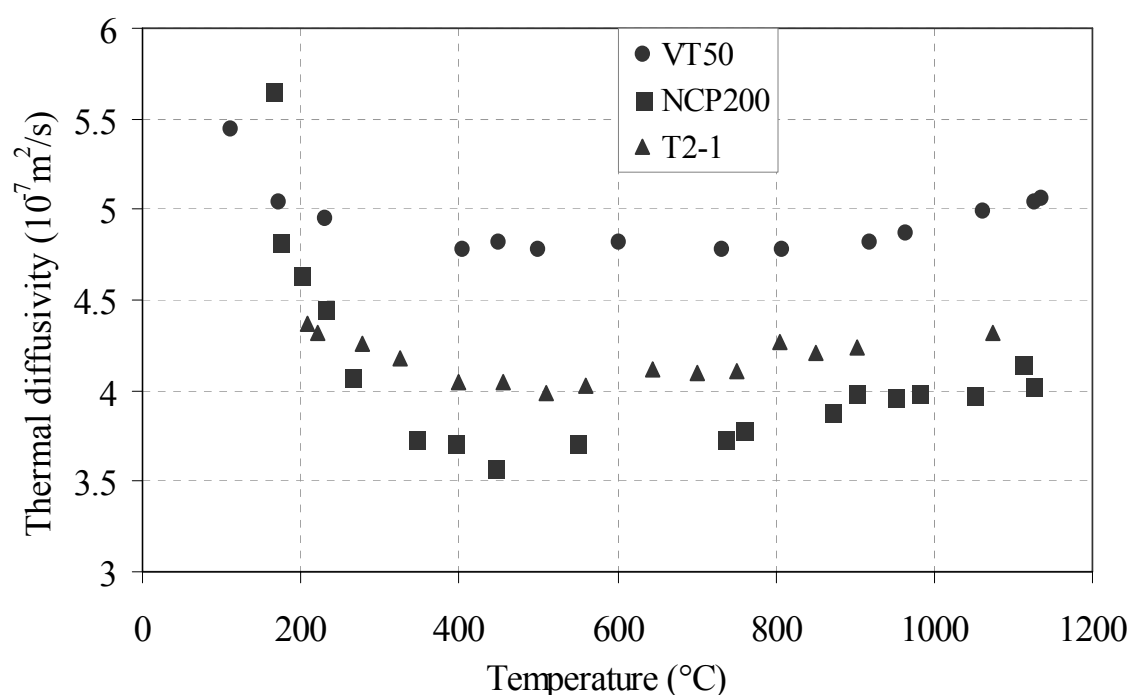


**Fig. 6-9** Temperature dependence of the thermal diffusivity of VT50-, NCP200- and T2-1-derived amorphous ceramics.

From the thermal diffusivity the thermal conductivity was calculated using equation (3.4) and the specific heat  $C_p$  data described in Chapter 6.2 and the density  $\rho$  data measured by the mercury pressure porosimetric method (Table 6-2). The results are presented in Fig. 6-10. The thermal conductivity values for all three ceramics are in the range of 0.77 – 1.43 W/mK over the temperature range between 100 and 1200°C. The absolute values are much lower in comparison with that of polycrystalline  $\text{Si}_3\text{N}_4$ , SiC, BN and graphite. This is perhaps due to the fact that the precursor-derived amorphous ceramics exhibit a bigger amount of porosity and free volume. The free volume and the pores can distinctly decrease the thermal diffusivity and thermal conductivity. The thermal conductivity increases with the rise of temperature in all three materials. These observations were found to be very similar to those obtained in the soda-lime-silica glass [59Kin]. Because during the measurements the samples are heated and the porosities of these samples are decreasing.

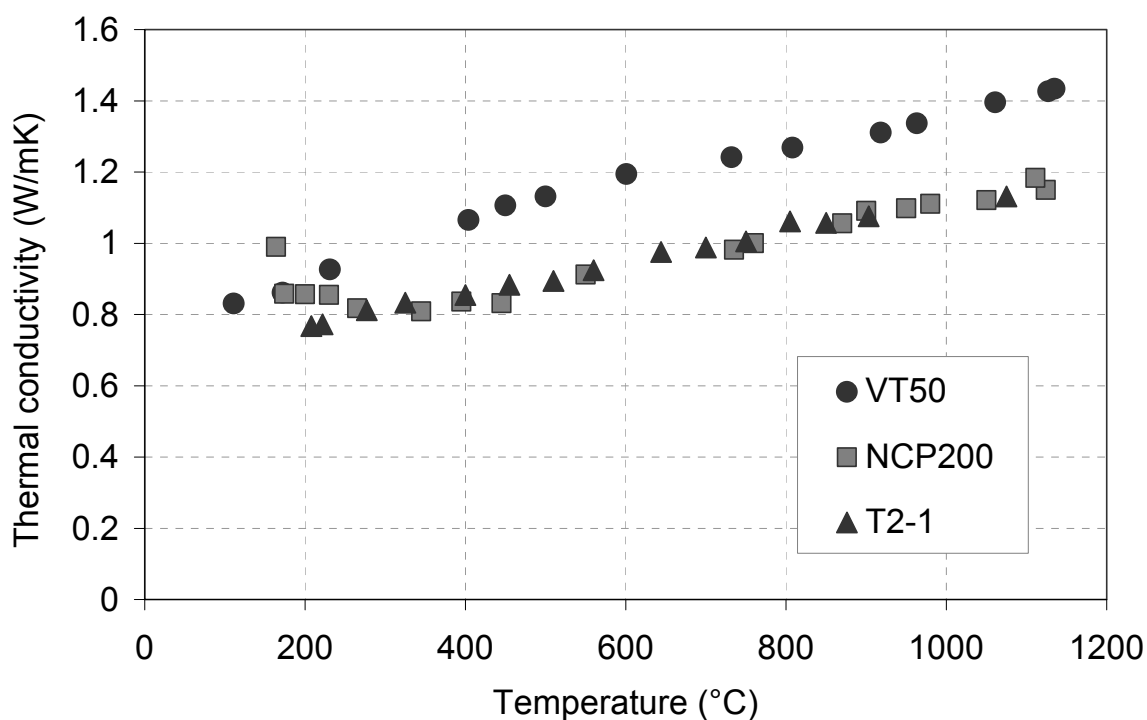


**Fig. 6-10** Temperature dependence of thermal conductivities of the VT50-, NCP200- and T2-1-derived ceramics.

## 6.4 Conclusion

- (1) The precursor-derived Si-C-N and Si-B-C-N ceramics materials shrink at temperatures higher than the pyrolysing temperature due to further gas evolution and changes in the amorphous structure. Heat treatment of the materials is necessary to complete the shrinkage and densification.
- (2) The thermal expansion coefficients of the precursor-derived Si-C-N and Si-B-C-N ceramics are comparable to that of polycrystalline  $\text{Si}_3\text{N}_4$ .
- (3) No glass transition for these amorphous ceramic materials was detected, thus they can not be considered as glasses.
- (4) Thermal conductivities of the precursor-derived ceramics were evaluated and found to be in the range of 0.77 to 1.43 W/mK over the temperature range 100 –1200°C, which are substantially lower than that of polycrystalline  $\text{Si}_3\text{N}_4$ , SiC, BN and graphite.



## **Zusammenfassung (Extended abstract in German)**

In der vorliegenden Arbeit wurde die Konstitution von Keramiken der Systeme Si-C-N und Si-B-C-N umfassend untersucht. Hierzu wurden thermodynamische Berechnungen (CALPHAD-Methode) mit experimentellen Untersuchungen kombiniert. Für die Berechnungen wurden die Computer-Programme THERMO-CALC/PARROT und BINGSS/BINFKF eingesetzt, um das Hochtemperaturreaktionsverhalten der Materialien quantitativ zu erklären und um weitere experimentelle Untersuchungen zu planen. Die Keramiken wurden durch Thermolyse metallorganischer Precursor-Polymere oder aus kristallinen Keramik-Pulvermischungen hergestellt. Die durch Thermolyse hergestellten Si-C-N-Materialien liegen bis ca. 1500°C amorph vor und beginnen erst oberhalb dieser Temperaturen anschließend zu kristallisieren. Bei Temperaturen höher als ca. 1600°C finden Phasenreaktionen statt, die signifikante Masseverluste des Materials bewirken. Eine Vielzahl borhaltiger Si-C-N-Keramiken hingegen beginnt sich erst bei Temperaturen oberhalb von 2000°C zu zersetzen. Auch diese Hochtemperaturstabilität wurde im Detail untersucht. Hierzu wurden verschiedenartige Phasendiagramme und Phasenmengendiagramme für die Systeme Si-C-N und Si-B-C-N berechnet. Die mit der Brutto-Zusammensetzung und Temperatur variierenden Partialdampfdrücke der bei den Reaktionen entstehenden Gasspezies wurden mit Komponenten-Verteilungsdiagrammen berechnet.

Für experimentelle Untersuchungen wurden Si-C-N-Keramiken durch Thermolyse der Precursor-Polymere VT50 (Polyvinylsilazan (PVS), Hoechst AG, Frankfurt) und NCP200 (Polyhydridomethylsilazan (PHMS), Nichimen Corp., Tokyo, Japan) bei 1050°C hergestellt. Die Si-B-C-N Keramiken wurden aus den im PML entwickelten Precursoren T2-1, MW33, MW36, BNCP, BVT50 bei 1400°C thermolysiert. Die resultierenden amorphen Keramiken wurden mit verschiedenen Arbeitsmethoden untersucht. Es wurde die chemische Brutto-Zusammensetzung der Ausgangskeramiken bestimmt. Eine Vielzahl von Proben wurden mit Differential-Thermoanalyse (DTA) und kombinierter Thermogravimetrie (TG) bis zu Temperaturen von 2200°C charakterisiert. Die Auswahl von BN als geeignetem und hinsichtlich der Proben inertem Tiegelmaterial wurde auf der Grundlage von CALPHAD-Berechnungen getroffen. Für Si-C-N Keramiken aus VT50- bzw. NCP200-Precursoren und Si-B-C-N-Keramik aus dem T2-1-Precursor wurden auch thermische

Ausdehnungskoeffizienten mit Differenzdilatometrie und thermische Leitfähigkeiten mit der Laser-Flash-Methode bestimmt. Für die Phasen- und Gefügeanalysen wurden die Röntgendiffraktometrie und die Rasterelektronenmikroskopie (REM) herangezogen. Das REM war für die chemischen Mikrobereichsuntersuchungen mit EDX- und WDX-Analysatoren ausgerüstet. Die Gefüge der aus dem T2-1-Precursor hergestellten Si-B-C-N-Keramik wurden ebenfalls mit hochauflösender Transmissionselektronenmikroskopie (HR-TEM) untersucht.

Das Hochtemperaturverhalten von Si-C-N-Precursorkeramiken wird durch die Reaktion von Siliziumnitrid ( $\text{Si}_3\text{N}_4$ ) und Kohlenstoff zu Siliziumcarbid ( $\text{SiC}$ ) und Stickstoff sowie die Zersetzung von  $\text{Si}_3\text{N}_4$  in flüssiges Silizium und Stickstoff bestimmt. Diese Reaktionen beeinflussen die Stabilität der Si-C-N-Keramiken bei hohen Temperaturen und führen zur thermischen Degradation der Precursorkeramiken. Zur quantitativen Erfassung dieser Hochtemperaturreaktionen im Si-C-N System wurden isotherme Schnitte berechnet. Darüber hinaus wurden die Reaktionspfade für Keramiken aus VT50- bzw. NCP200-Precursoren ermittelt. Deren Reaktionsverhalten wurde zudem durch berechnete Temperatur-Konzentrations-Schnitte und Potenzial-Phasendiagramme ( $\log(p_{\text{N}_2})$ -Temperatur) erfaßt. Aus diesen Daten wurde als Grundlage für die weiteren Arbeiten das Scheil-Reaktionsschema für das ternäre System Si-C-N abgeleitet. Zusätzlich wurden die Gasphasenzusammensetzungen in Abhängigkeit von der Temperatur und der Zusammensetzung der jeweils im Gleichgewicht stehenden kondensierten Proben berechnet. Bei Temperaturen oberhalb von  $2300^\circ\text{C}$  entwickeln neben  $\text{N}_2$  auch die Gasspezies  $\text{Si}_2\text{C}$ ,  $\text{SiC}_2$  und Si signifikante Partialdampfdrücke. Berechnete Phasenmengendiagramme der aus den Precursoren VT50 und NCP200 hergestellten Keramiken wurden im Zusammenhang mit den Reaktionspfaden der Precursorkeramiken diskutiert. Es zeigt sich, dass die Phasenmengendiagramme qualitativ und quantitativ die Ergebnisse der STA-Hochtemperaturuntersuchungen (Bild 1) exakt simulieren. Der einstufige Zersetzungsprozess von VT50 durch die erwähnte Reaktion von  $\text{Si}_3\text{N}_4$  mit Kohlenstoff einhergehend mit 30% Masseverlust durch  $\text{N}_2$ -Abdampfung und der zweistufige Zersetzungsprozess von NCP200 mit 12 bzw. 15 Masse% Verlust durch die zusätzliche  $\text{Si}_3\text{N}_4$ -Zersetzung wurden genau berechnet und die korrelierten endothermen Wärmeeffekte bestimmt. Auch die berechneten Phasenzusammensetzungen wurden durch

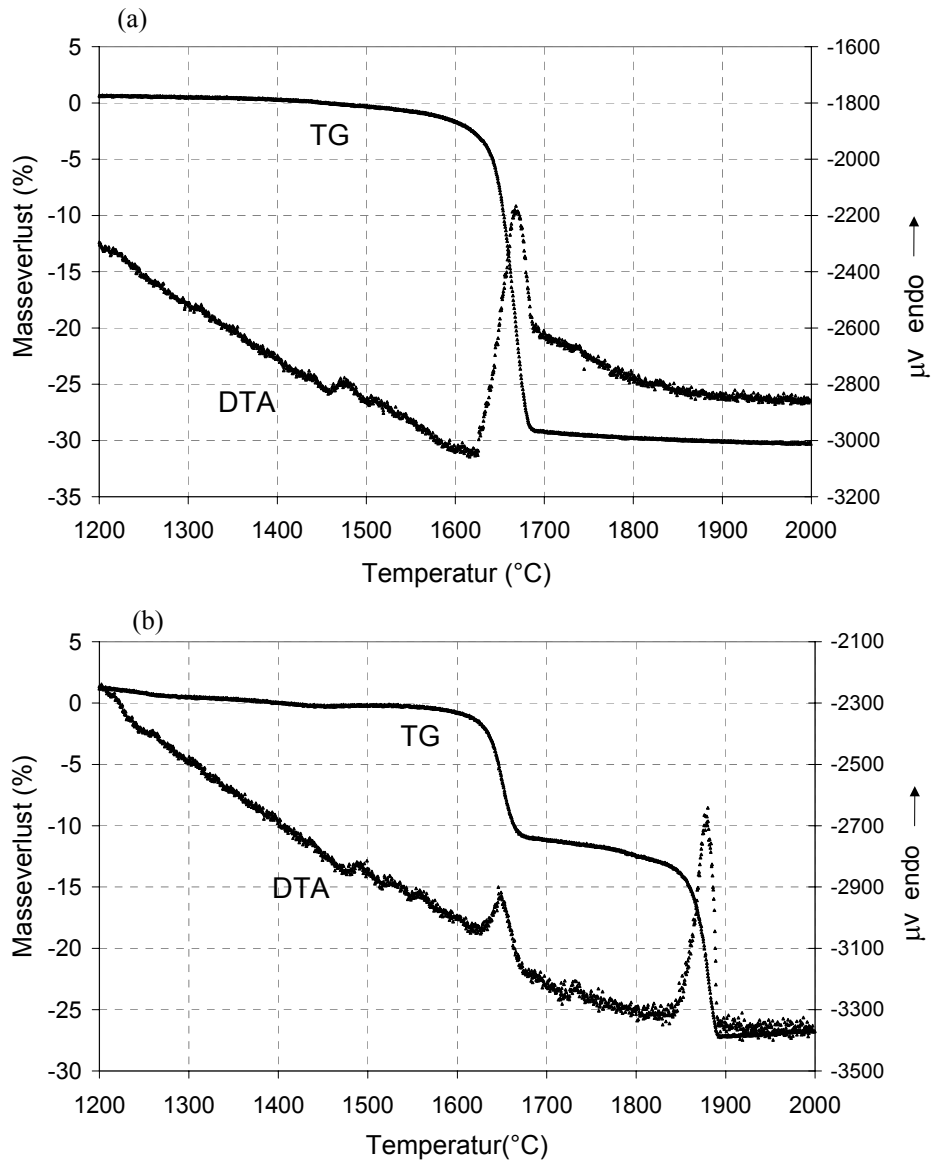


**Bild 1:** DTA/TG Messkurven (STA) für Si-C-N Precursorkeramiken (a) VT50, (b) NCP200, ( $\text{N}_2$ -Atmosphäre, BN-Tiegel, 5K/min).

röntgenographische Analysen und REM/EDX-Untersuchungen der Proben eindeutig bestätigt. Die berechneten Simulationen stimmen mit den experimentellen Ergebnissen überein. Es zeigt sich, dass die CALPHAD-Berechnungen das Hochtemperatur-Reaktionsverhalten der Keramiken quantitativ beschreiben.

Für das quaternäre System Si-B-C-N wurde eine Vielzahl isothermer Schnitte berechnet und die Phasengleichgewichte in Konzentrationstetraedern dargestellt. Zudem wurden isotherme Schnitte bei jeweils konstanten Bor-Gehalten, Temperatur-Konzentrations-Schnitte und

Potenzial-Phasendiagramme rechnerisch ermittelt. Für die Berechnung der Potenzial-Phasendiagramme wurde das bekannte Si:B:C-Verhältnis der ausgewählten Precursorkeramik fixiert und nur das Stickstoff-Potenzial und die Temperatur variiert. Für die Erklärung des Hochtemperaturverhaltens der Precursorkeramiken sind diese Diagramme besonders wichtig. Ein weiterer wichtiger Potenzialdiagrammtyp stellt die Phasengleichgewichte in Abhängigkeit von der Kohlenstoffaktivität und der Temperatur dar. Aus den berechneten Phasendiagrammen wurde das gesamte Scheil-Reaktionsschema des quaternären Systems Si-B-C-N entwickelt.

Für alle B-haltigen Precursorkeramiken, die in dieser Arbeit mit DTA/TG, XRD, SEM, TEM untersucht wurden, und solche aus der Literatur, wurden die zugehörigen Phasenmengendiagramme berechnet. Zusammenfassend wurde festgestellt, dass analog zu den Si-C-N-Materialien eine thermische Zersetzung auch der Si-B-C-N-Materialien durch die Reaktionen von  $\text{Si}_3\text{N}_4$  mit Kohlenstoff und  $\text{Si}_3\text{N}_4$ -Zersetzung zu erwarten ist. Die DTA/TG-Untersuchungen in dieser Arbeit und in der Literatur zeigen jedoch, dass eine Vielzahl von borhaltigen Precursorkeramiken eine Hochtemperaturstabilität unter Inertgas bis 2000°C oder

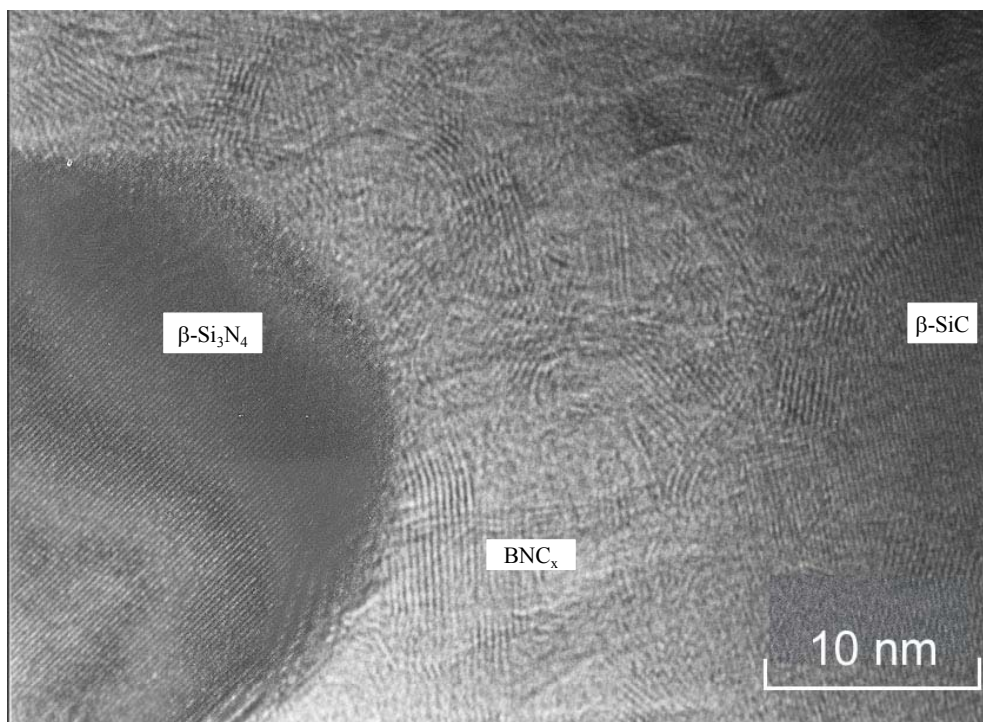


**Bild 2:** Hochauflösende Transmissionselektronenmikroskopie der aus T2-1 hergestellte Precursorkeramik, nach einer DTA/TG-Untersuchung bis 2200°C.

höher aufweist. Die Untersuchungen mit Röntgenographie und HR-TEM zeigen (Bild 2), dass  $\text{Si}_3\text{N}_4$  in den hochtemperaturstabilen Materialien bis zu Temperaturen von  $2200^\circ\text{C}$  nachgewiesen werden kann, also weit oberhalb der für einen Druck von einem bar gültigen  $\text{Si}_3\text{N}_4$ -Temperatur-Stabilitätsgrenze von  $1841^\circ\text{C}$ .  $\text{Si}_3\text{N}_4$ -und  $\text{SiC}$ -Körner sind in eine Matrix von turbostratischem  $\text{BNC}_x$  eingebettet. In dieser  $\text{BNC}_x$ -Phase ist Kohlenstoff gelöst. Freier Kohlenstoff wird nicht gefunden. Aus den Befunden des Gefügebildes der hochtemperaturstabilen Keramik (Bild 2) und der resultierenden Werkstoff-thermodynamischen Auswirkungen wurde die HT-Stabilität erklärt. So nimmt durch die Lösung des Kohlenstoffs in der  $\text{BNC}_x$ -Phase dessen Aktivität stark ab, wodurch die Temperatur der Reaktion von  $\text{Si}_3\text{N}_4$  mit Kohlenstoff ansteigt. Ein weiterer Effekt ist, dass die Matrix aus turbostratischem  $\text{BNC}_x$  einen „Einkapseleffekt“ für die  $\text{Si}_3\text{N}_4$ -Körner bewirkt und durch eine Diffusionsbarriere eine intrinsische Druckerhöhung für Stickstoff aufbaut. Hierdurch wird  $\text{Si}_3\text{N}_4$  thermisch stabilisiert. Das Potenzialdiagramm in Bild 3 zeigt quantitativ den kombinierten Effekt von Druck und Kohlenstoffaktivität auf die Reaktion von  $\text{Si}_3\text{N}_4$  mit Kohlenstoff. Es weist nach, dass die Reaktionstemperatur von  $\text{Si}_3\text{N}_4$  mit Kohlenstoff unter

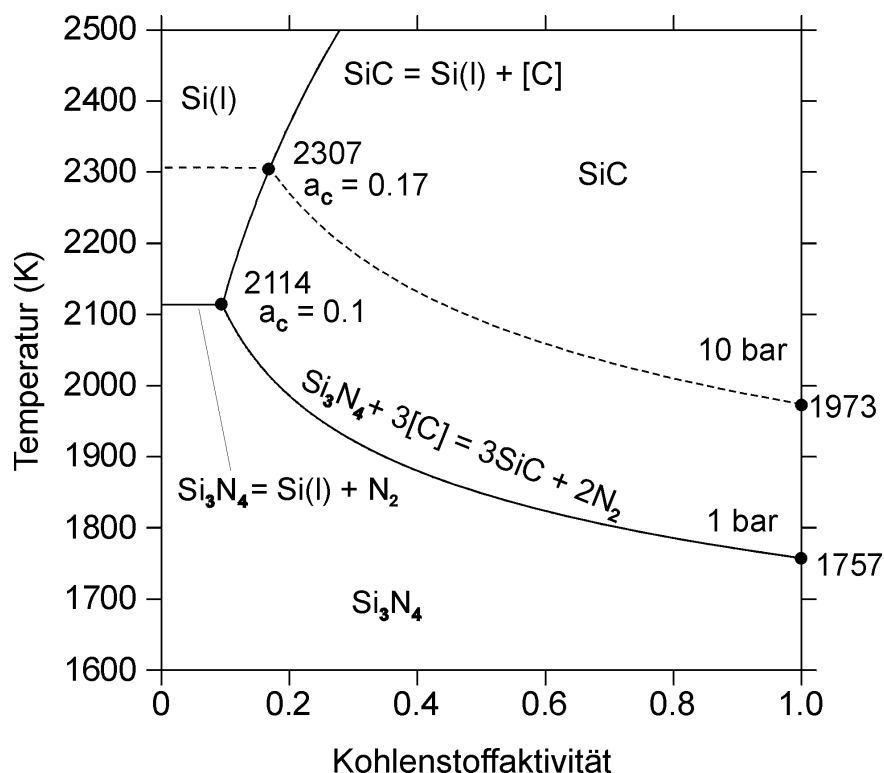


**Bild 3:** Temperatur-Kohlenstoffaktivität Phasendiagramm.

einem internen Stickstoffdruck von 10 bar bei einer von 1 bis 0,17 abnehmenden Kohlenstoffaktivität von 1700°C (1973 K) auf 2034°C (2307 K) steigt. Die Zersetzungstemperatur von  $\text{Si}_3\text{N}_4$ , die durch die horizontale Linie gekennzeichnet ist, nimmt von 1841°C (2114 K) auf 2034°C (2307 K) zu, wenn der Stickstoffdruck von 1 bar auf 10 bar ansteigt.

Es wird deutlich, dass die angenommenen Effekte zu einer Temperaturerhöhung der Reaktion zwischen  $\text{Si}_3\text{N}_4$  und Kohlenstoff sowie zu einer Stabilisierung von  $\text{Si}_3\text{N}_4$  führen und so das Hochtemperaturverhalten der Si-B-C-N-Precursorkeramiken erklärt werden kann. Das hier entwickelte Modell zur Hochtemperaturstabilisierung wird auch durch die Betrachtung von nicht-hochtemperaturstabilen Si-B-C-N-Keramiken unterstützt. Die Phasenmengen-diagramme zeigen, dass diese Materialien einen erheblich höheren relativen  $\text{Si}_3\text{N}_4$ -Phasenanteil aufweisen als die hochtemperaturstabilen Materialien. Auf der Grundlage der geschilderten Annahmen ist davon auszugehen, dass ein zu „geringer Anteil“ an  $\text{BNC}_x$  Matrix und/oder eine nicht vollständige Auflösung von Kohlenstoff bewirken, dass das  $\text{Si}_3\text{N}_4$  dieser Materialien bereits bei niedrigeren Temperaturen reagiert. Durch die Berechnungen isothermer Schnitte wurde abgeleitet, dass Keramiken mit Zusammensetzungen, die in der Mitte des Vierphasengleichgewichts-Bereichs  $\text{Si}_3\text{N}_4+\text{SiC}+\text{BN}+\text{Graphit}$  und nahe beim Dreiphasengleichgewichtsfeld  $\text{SiC}+\text{BN}+\text{Graphit}$  liegen, hochtemperaturstabil sind.

Für die Phasenbildung der Si-(B-)C-N-Precursorkeramiken wurde ein Modell entwickelt, das qualitativ die thermische Stabilität in Abhängigkeit von der Zusammensetzung des Materials beschreiben kann. Danach entmischen sich Keramiken mit einer Zusammensetzung innerhalb des Vierphasen-Gleichgewichtsraums  $\text{Si}_3\text{N}_4+\text{SiC}+\text{C}+\text{BN}$  bei der Thermolyse in zwei amorphe Phasen und zwar in ein ungeordnetes Netzwerk aus  $\text{Si}(\text{C},\text{N})_4$ -Tetraedern mit einer Zusammensetzung  $\text{Si}_{3+y/4}\text{C}_y\text{N}_{4-y}$ , und die bereits beschriebene  $\text{BCN}_x$ -Phase, die vermutlich aus  $\text{sp}^2$ -hybridisiertem Kohlenstoff und hexagonalem BN besteht. SiC-reiche Bereiche der amorphen  $\text{Si}_{3+y/4}\text{C}_y\text{N}_{4-y}$ -Phase sind offensichtlich thermisch sehr stabil und kristallisieren erst bei relativ hohen Temperaturen in  $\text{Si}_3\text{N}_4$  und SiC, die in die mit zunehmender Temperatur turbostratisch kristallisierende Matrix aus der  $\text{BNC}_x$ -Phase eingebettet sind.

Im Hinblick auf ein Verständnis der bei der Thermolyse ablaufenden Kondensationsmechanismen wurde in einem weiteren Teil der Arbeit das System Si-C-N-H berechnet. Dazu wurden die Phasengleichgewichte in dem für die Thermolyse entscheidenden Temperaturbereich zwischen 300°C (573 K) und 1050°C (1323 K) ermittelt und in isothermen Schnitten dargestellt (Bild 4). Außerdem wurden die Phasenmengendiagramme und die sich mit der Temperatur ändernden Zusammensetzungen der Gasphase berechnet und daraus die Reaktionsprodukte der verschiedenen Precursoren bei der Thermolyse abgeleitet. Es zeigt sich, dass aus den thermodynamischen Gleichgewichtsrechnungen mit Einschränkungen auch Aussagen zur Thermolyse von Si-C-N-H-Precursoren gemacht werden können.

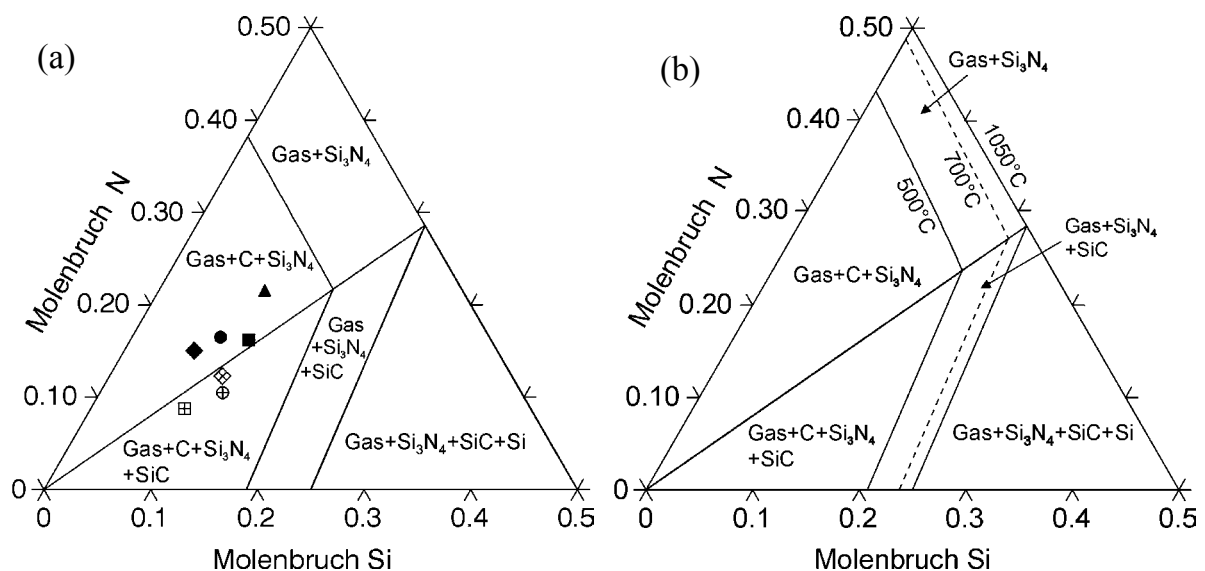


**Bild 4** Berechnete isotherme Schnitte im System Si-C-N-H bei 50 at.% Wasserstoffgehalt bei Temperaturen (a): 300°C, (b): 500°C, 700°C und 1050°C.

Außerdem wurde die thermische Ausdehnung der Si-C-N- und Si-B-C-N-Precursorkeramiken durch Differenzdilatometrie ermittelt (Bild 5). Die Werte sind mit denen von kristallisiertem  $\text{Si}_3\text{N}_4$  vergleichbar. Die amorphen Precursorkeramiken weisen keine Glastransformation auf und sind daher trotz der glasartigen Struktur der  $\text{Si}_{3+y/4}\text{C}_y\text{N}_{4-y}$ -Phase im Sinne der Definition keine Gläser.

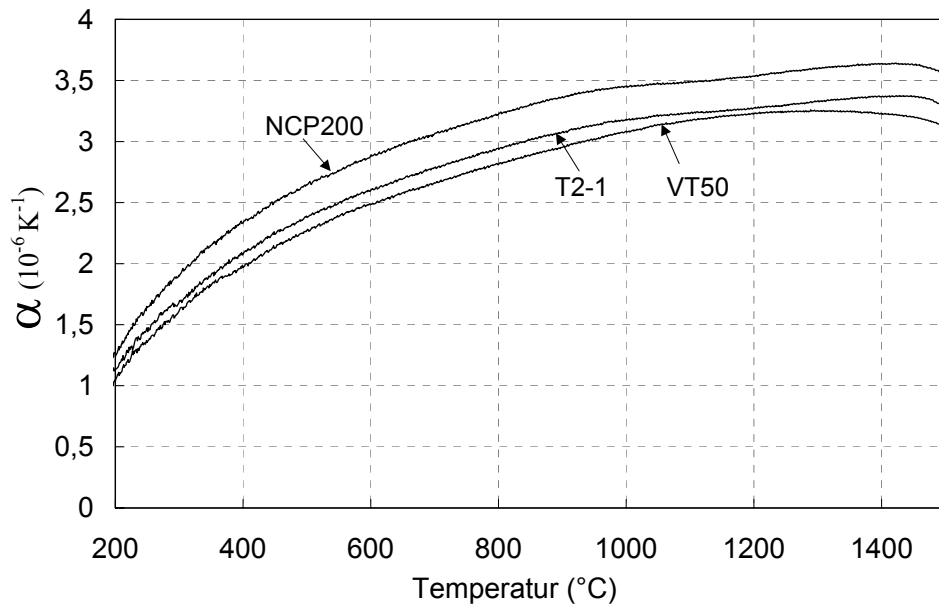


**Bild 5:** Thermische Ausdehnungen von Si-C-N und Si-B-C-N Precursorkeramiken.

Ferner wurden Untersuchungen zur Wärmeleitfähigkeit durchgeführt und dazu die Temperaturleitfähigkeit der Precursorkeramiken mit der Laser-Flash-Methode gemessen, die Wärmekapazitäten der Keramiken thermodynamisch berechnet, und die Probendichten bestimmt. Die daraus abgeleiteten Wärmeleitfähigkeiten liegen im Temperaturbereich von 100 bis 1200 °C zwischen 0,77 und 1,43 W/mK (Bild 6).

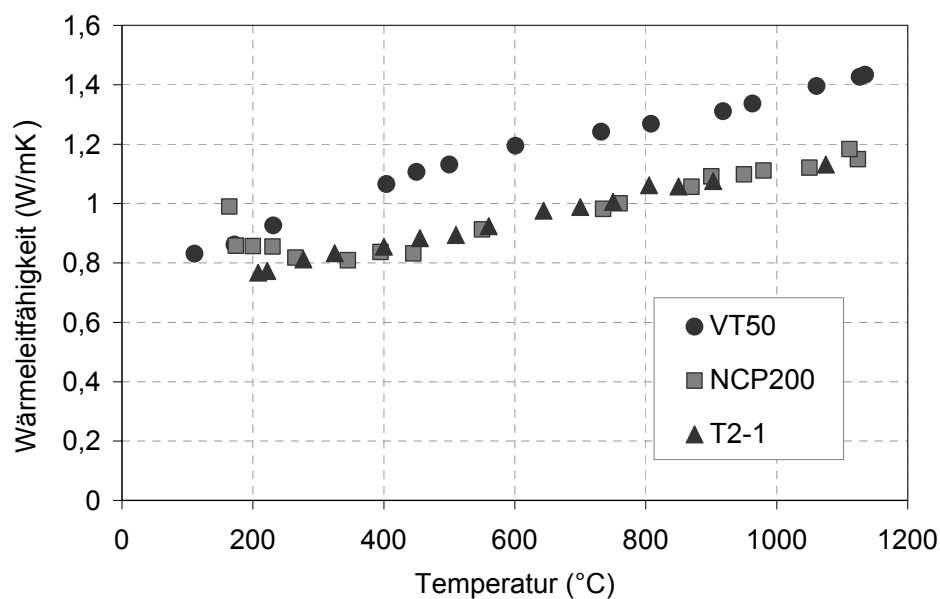


**Bild 6:** Wärmeleitfähigkeiten von Precursorkeramiken.



## References

- [SGTE] Scientific Group Thermodata Europe, Grenoble Campus, 1001 Avenue Centrale, BP66, F-38402 Saint Martin D'Herès, France, <http://www.sgte.org>
- [30Wag] C. Wagner, W. Schottky, "Theorie der geordneten Mischphasen", Z. Phys. Chem., **11** (1930) 163-210
- [36Sch] E. Scheil, "Darstellung von Dreistoffsystemen", Arch. Eisenhüttenwes., **9** (1936) 571-573
- [48Red] O. Redlich, A. T. Kister, "The Algebraic Representation of Thermodynamic Properties and the Classification of Solutions", Ind. Eng. Chem., **40** (1948) 345-348
- [57Gle] O. Gleimser, K. Beltz, P. Neumann, "Zur Kenntnis des Systems Silicium-Stickstoff", Z. anorg. allg. Chem., **291** (1957) 50-66
- [58Tur] E. T. Turkdogan, P. M. Bills, V. A. Tippet, "Silicon Nitrides: Some Physico-chemical Properties", J. Appl. Chem., **8** (1958) 296-302
- [59Kin] W. D. Kingery, "Thermal Conductivity: XIV, Conductivity of Multicomponent Systems", J. Amer. Ceram. Soc., **42** (1959) 617-627
- [60Geb] E. Gebhardt, G. Petzow, "Über den Aufbau des Vierstoffsystems Silber – Kupfer – Kadmium – Zinn IV", Z. Metallkd., **51** (1960) 386-375
- [60Por] K. I. Portnoi, G. V. Samsonov, L. A. Solonnikova, "Alloys of the Boron-Silicon-Carbon System", Russ. J. Inorg. Chem., **5** (1960) 1282-1283
- [61Par] W. J. Parker, R. J. Jenkins, C. P. Butler, G. L. Abbott, "Flash Method of Determining Thermal Diffusivity, Heat Capacity, and Thermal Conductivity", J. Appl. Phys., **32** [9] (1961) 1679-1684
- [62Par] W. J. Parker and R. J. Jenkins, "Thermal Conductivity Measurements on Bismuth Telluride in the Presence of a 2 MeV Electron Beam", Adv. Energy Convers., **2** (1962) 87-103

- [65Sch] H. Schmalzried, "Point Defects in Ternary Ionic Crystals", in H. Reiss (eds.), Progress in Solid State Chemistry, Vol. II, Pergamon Press, Oxford, (1965)
- [66Ras] H. Rassaerts, A. Schmidt, "Thermodynamische Berechnungen im System Silizium-Kohlenstoff-Stickstoff", Planseebericht für Pulvermetallurgie, **14** (1966) 110-114
- [67Kub] O. Kubaschewski, E. L. Evans, C. B. Alcock, "Metallurgical Thermochemistry", Pergamon Press, Oxford, (1967)
- [67Lar] K. B. Larson, K. Koyama, "Correction for Finite-Pulse-Time Effects in Very Thin Samples using the Flash Method of Measuring Thermal Diffusivity", J. Appl. Phys., **38** [2] (1967) 465-474
- [67Pop] P. Popper, "New Electrical Ceramics and Inorganic Polymers", Brit. Ceram. Res. Assn. Special Publ., **57** (1967) 1-20
- [68Gug] E. Gugel, P. Ettmayer, A. Schmidt, "Untersuchungen zum System Silizium-Kohlenstoff-Stickstoff", Ber. Dtsch. Keram. Ges., **45** (1968) 395-402
- [69Sha] P. T. B Shaffer, "The SiC Phase in the System SiC-B<sub>4</sub>C-C" Mater. Res. Bull., **4** (1969) 213-220
- [72Yat] B. Yates, "Thermal Expansion", Plenum press, New York - London, (1972)
- [73Fis] H. Fischer, "Herstellung und Eigenschaften von Siliziumnitridschichten aus Tetramethylsilan", Z. Phys. Chem. (DDR), **252** (1973) 213
- [73Hec] R. C. Heckmann, "Finite Pulse-Time and Heat-Loss Effects in Pulse Thermal Diffusivity Measurements", J. Appl. Phys., **44** [4] (1973) 1455-1460
- [74Plu] W. A. Plummer, "Differential Dilatometry, a Powerful Tool", AIP conference Proceedings No. 17, Thermal Expansion-1973 edited by R. E. Taylor and G. L. Denmann, (1974) 147-158
- [74Ver] W. Verbeek, G. Winter, German Patent 2236068 (1974)
- [74Tay] R. E. Taylor, L. M. Clark III, "Finite Pulse Time Effects in Flash Diffusivity Method", High Temp. – High Press., **6** (1974) 65-72
- [75Cla] L. M. Clark III, R. E. Taylor, "Radiation Loss in the Flash Method for Thermal Diffusivity", J. Appl. Phys., **46** [2] (1975) 714-719

- [75Mug] Y.-M. Muggianu, M. Gambino, and L.P. Bros, *J. Chim. Phys.*, **72** (1975) 85-88
- [76Ber] R. Berman, "Thermal Conduction in Solids", Clarendon Press. Oxford, (1976)
- [76Wil] A. Will, K. H. Kossobutzki, "An X-Ray Diffraction Analysis of Boron Carbide,  $B_{13}C_2$ ", *J. Less Common Met.* **47** (1976) 43-48
- [76Yaj] S. Yajima, K. Okamura, J. Hayashi, "Calculation of the Activation Energy of Solid-State Reactions Using the Moessbauer Effect", *J. Am. Ceram. Soc.*, **59** [7-8] (1976) 324-327
- [77Luk] H. L. Lukas, E. -T. Henig, B. Zimmermann, "Optimization of Phase Diagrams by the Least Squares Method Using Simultaneously Different Types of Data", *CALPHAD*, **1** (1977) 225-236
- [79Gau] L. Gauckler, E. Hucke, H. L. Lukas, and G. Petzow, "Computer Calculations of Heterogeneous Equilibria in the System C-O-H-Si-Ar", *J. Mater. Sci.*, **14** (1979) 1513-1518
- [80Hil] M. Hillert, "Empirical Methods of Predicting and Representing Thermodynamic Properties of Ternary Solution Phases", *CALPHAD*, **4** (1980) 1-12
- [80Pal] E. Palcevskis, J. Grabis, T. Miller, *Latvijas PSR Zinatnu Akad. Vestis Kim Ser.* 1980 No. 3, 286-290; *C. A.* 93 (1980) No. 81448
- [81Azu] T. Azumi, Y. Takahashi, "Novel Finite Pulse-Width Correction in Flash Thermal Diffusivity Measurement", *Rev. Sci. Instrum.*, **52** [9] (1981) 1411-1413
- [81Bad] S. A. Badrak, T. S. Bartnitskaya, I. M. Baryshevskaya, et al., "Use of thermal calculations for evaluating the possible pathways of formation of silicon nitride", *Poroshk. Metall.*, **225** [9] (1981) 66-72
- [81Hil] M. Hillert, "Some Viewpoints on the Use of a Computer for Calculating Phase Diagrams", *Physica*, **103B** (1981) 31-40
- [81Sun] B. Sundmann, J. Ågren, "A regular Solution Model for Phases with Several Components and Sublattices, Suitable for Computer Applications", *J. Phys. Chem. Solids*, **42** (1981) 297-301
- [81Wei] J. Weiss, H. L. Lukas, J. Lorenz, G. Petzow, H. Krieg, "Calculation of Heterogeneous Phase Equilibria in Oxide-Nitride Systems", *CALPHAD*, **5** (1981) 125-140

- [82Luk1] H.L. Lukas, J. Weiss, and E.-Th. Henig, "Strategies of the Calculation of Phase Diagrams", CALPHAD, **6** (1982) 229-251
- [82Luk2] H. L. Lukas, J. Weiss, H. Krieg, E.-T. Henig, G. Petzow, "Phase Equilibria in  $\text{Si}_3\text{N}_4$  and SiC Ceramics", High Temp. - High Pressures, **14** (1982) 607-615
- [82Sal] H. Salmang, H. Scholze, "Keramik", Springer - Verlag, Berlin / Heidelberg / New York, (1982)
- [83DIN] DIN 51 005, Thermische Analyse (TA), Begriffe, Beuth Verlag, Berlin, (1983)
- [83Lan] F. F. Lange, "Fabrication and Properties of Dense Polyphase Silicon Nitride", Ceram. Bull., **62** [12] (1983) 1369-1374
- [84Ell] S. R. Elliott, "Physics of Amorphous Materials", Longman, London and New York, (1984)
- [84Lar] J. F. Lartique, M. Ducarroir, B. Armas, "Calculation of Deposition for  $\text{Si}_3\text{N}_4$  from a  $\text{SiH}_4\text{-NH}_3$  Gas Phase", J. Mater. Sci., **19**(1984) 3079-3089
- [85Sun] B. Sundman, B. Jansson, J.-O. Anderson, "The Thermo-Calc Database System", CALPHAD, **9** (1985) 153-190
- [85Tak] M. Takamizawa, T. Kobayashi, A. Hayashida, Y. Takeda, US Patent, 4 550 151 (1985)
- [86And] J.-O. Andersson, A. F. Guillermet, M. Hillert, B. Jansson, B. Sundman, "A Compound-Energy Model of Ordering in a Phase with Sites of Different Coordination Numbers", Acta Metall., **34** (1986) 437-445
- [86DIN] DIN1341: Wärmeübertragung, Begriffe, Kenngrößen
- [86Luk] H. L. Lukas, E.-Th. Henig and G. Petzow, "A Thermodynamic Optimisation of the Cu-Ag-Pb System", Z. Metallkd., **77** (1986) 360-367
- [87Ans] I. Ansara and B. Sundmann, "The Scientific Group Thermodata Europe", in Computer Handling and Dissemination of Data, P. S. Glaeser, Ed., Elsevier, CODATA Report, (1987) 154-158
- [87Gre] P. Greil, G. Petzow, H. Tanaka, "Sintering and HIPing of Silicon nitride-silicon carbide Composite Materials", Ceram. Int., **13** (1987) 19-25

- [87Kan] R. B. Kaner, J. Kouvetakis, C. E. Warbler, M. L. Sattler and N. Bartlett, "Boron-carbon-nitrogen Materials of Graphite-like Structure", *Mater. Res. Bull.*, **22** (1987) 399-404
- [87Zie] G. Ziegler, J. Heinrich, G. Wötting, "Review Relationships between Processing, Microstructure and Properties of Dense and Reaction-Bonded Silicon Nitride", *J. Mater. Sci.*, **22** (1987) 3041-3086
- [88Car] W. D. Carter, P. H. Holloway, C. White, R. Clausing, "Boron Distribution in Sintered Silicon Carbide", *Adv. Ceram. Mat.*, **3** (1988) 62-65
- [88Nic] K. G. Nickel, M. J. Hoffmann, P. Greil, G. Petzow, "Thermodynamic Calculations for the Formation of SiC-Whisker-Reinforced Si<sub>3</sub>N<sub>4</sub> Ceramics", *Adv. Ceram. Mater.*, **3** [6] (1988) 557-562
- [88Wad] H. Wada, M.-J. Wang, T.-Y. Tien, "Stability of Phases in the Si-C-N-O System", *J. Am. Ceram. Soc.*, **71** [10] (1988) 837-840
- [89DIN] DIN 51 045 (1989) Bestimmung der thermischen Längenänderung fester Körper
- [89Hem] W.F.Hemminger, H.K.Cammenga, "Methoden der Thermischen Analyse, Anleitungen für die chemische Laboratoriumspraxis", Band XXIV, Springer-Verlag (1989)
- [89Kou] J. Kouvetakis, T. Sasaki, C. Shen, R. Hagiwara, M. Lerner, K. M. Krishnan and N. Bartlett, "Novel Aspects of Graphite Intercalation by Fluorine and Fluorides and New B/C, C/N and B/C/N Materials Based On The Graphite Network", *Synth. Metall.*, **34** (1989) 1-7
- [90Pai] R. T. Paine and C. K. Narula, "Synthetic Routes to Boron Nitride", *Chem. Rev.*, **90** (1990) 73-91
- [90Peu] M. Peuckert, T. Vaahs, M. Brück, "Ceramics from Organometallic Polymers", *Adv. Mater.*, **2** [9] (1990) 398-404
- [90Sey] D. Seyferth, H. Plenio, "Borasilazane Polymeric Precursors for Borosilicon Nitride", *J. Am. Ceram. Soc.*, **73** (1990) 2131-2133
- [90Tel] R. Telle, "Structure and Properties of Si-Doped Boron Carbide", in: R. Freer (edt.) *The Physics and Chemistry of Carbides, Nitrides and Borides*, Kluwer, Dordrecht, The Netherlands, (1990) 249-267

- [91Din] A. T. Dinsdale, "SGTE Data for Pure Elements", CALPHAD, **15** (4) (1991) 317-425
- [91Lan] H. Lange, G. Wötting, G. Winter, "Siliciumnitrid - vom Pulver zum keramischen Werkstoff", Angew. Chem., **103** [12] (1991) 1606-1625
- [91Mis] A. K. Misra, "Thermochemical Analysis of Chemical Processes Relevant to the Stability and Processing of SiC-Reinforced Si<sub>3</sub>N<sub>4</sub> Composites", J. Mater. Sci., **26** (1991) 6591-6598
- [91Nar] D. M. Narsavage, L. V. Interrante, "Condensation Polymerization of Tetrakis(ethylamino)silane and Its Thermal Decomposition to Si<sub>3</sub>N<sub>4</sub>/SiC Ceramics", Chem. Mater., **3** (1991) 721-730
- [91Var] A. G. Varlamov, A. A. Shiryaev, Yu. M. Grigor'ev, "Thermodynamic Analysis of the Composition of Condensed Products in the Si-N-C-H System", Izv. Akad. Nauk SSSR, Neorg. Mater., **27** [6] (1991) 1222-1225
- [91Tor] W. Toreki, "Polymeric Precursors to Ceramics - A Review", Polymer News, **16** (1991) 6-14
- [92Bal] H.-P. Baldus, O. Wagner, M. Jansen, "Synthesis of Advanced Ceramics in the System Si-B-N and Si-B-N-C Employing Novel Precursor Compounds", Mater. Res. Soc. Symp. Proc., **271** (1992) 821-826
- [92Bil1] J. Bill, "Herstellung und Eigenschaften keramischer Festkörper in den ternären und quaternären Systemen B-C-N und Ti-B-C-N", Ph. D. Thesis, University of Stuttgart, (1992)
- [92Bil2] J. Bill, R. Riedel, "Boron Carbide Nitride Derived from Amine-Boranes", Mater. Res. Soc. Symp. Proc., **271** (1992) 839-844
- [92Hil] M. Hillert, S. Jonsson, B. Sundman, "Thermodynamic Calculation of the Si-N-O System", Z. Metallkd., **83** [9] (1992) 648-654
- [92Luk] H. L. Lukas, S. G. Fries, "Demonstration of the Use of "BINGSS" with the Mg-Zn System as Example", J. Phase Equilibria **13** (1992) 532-541
- [92Rie] R. Riedel, G. Passing, H. Schönfelder, R. J. Brook, "Synthesis of Dense silicon-based Ceramics at low Temperatures", Nature, **355** (1992) 714-717

- [93Ald] F. Aldinger, H. J. Seifert, "Konstitution als Schlüssel zur Werkstoffentwicklung", Z. Metallk., **84** [1] (1993) 2-10
- [93Fel] A. Feltz, "Amorphous Inorganic Materials and Glasses", VCH Verlagsgesellschaft mbH. D-6940 Weinheim, Germany, (1993)
- [93Hof] M. J. Hoffman, P. F. Becher, G. Petzow, "Silicon Nitride 93 : Proceedings of the International Conference on Silicon Nitride-Based Ceramics", Stuttgart, October 4-6, (1993) (Key Eng. Mater.)
- [93Jha] A. Jha, "Phase Equilibria in the Si-C-N-O System and the Kinetic Analysis of Silicon Carbide Whisker Growth", J. Mater. Sci., **28** (1993) 3069-3079
- [93DIN] DIN1345: Thermodynamik, Grundbegriffe
- [93Rie] R. Riedel, "Nicht-oxidische Keramiken aus anorganischen Vorstufen", Materialkundlich-Technische Reihe 12, Gebrüder Borntraeger Verlag, Stuttgart, (1993)
- [93Su] K. Su, E. E. Remsen, G. A. Zank, L. G. Sneddon, "Synthesis, Characterization and Ceramic Conversion Reactions of Hydridopolysilizanes", Polym. Prep., **34** (1993) 334-335
- [94Bal] H.-P. Baldus, M. Jansen, O. Wagner, "New Materials in the System Si-(N,C)-B and their Characterization", Key Eng. Mater., **89-91** (1994) 75-80
- [94Kie] A. Kienzle, "Darstellung und Verarbeitung borhaltiger elementorganischer Vorstufen zur Herstellung keramischer Materialien in den Systemen SiCB und SiCBN", Ph. D. Thesis, University of Stuttgart, Stuttgart, (1994)
- [94Kuh] U. Kuhlmann, H. Werheit, "Properties of Boron Carbide Related to the Carbon Distribution in the Unit Cell", Proc. 11<sup>th</sup> Int. Symp. Boron, Borides and Rel. Comp., Tsukuba, 1993, JJAP Series, 10 (1994) 94-95
- [94Nei] U. Neidhardt, H. Schubert, E. Bischoff, G. Petzow, "Gas Pressure Sintering of Si<sub>3</sub>N<sub>4</sub> in N<sub>2</sub>/CO/(CO<sub>2</sub>) Atmosphere", Key Eng. Mater., **89-91** (1994) 187-192
- [94Wer] H. Werheit, U. Kuhlmann, M. Laux, R. Telle, "Structure and Optical Properties of Si-Doped Boron Carbide, in: Proc. 11<sup>th</sup> Int. Symp. Boron, Borides and Related Compounds", Tsukuba 1993, JJAP Series 10 (1994) 86-87

- [95Bil1] J. Bill; F. Aldinger, "Precursor derived Covalent Ceramics", *Adv. Mater.*, **7** (1995) 775-787
- [95Bil2] J. Bill, A. Kienzle, M. Sasaki, R. Riedel, F. Aldinger, "Novel Routes for the Synthesis of Materials in the Quaternary System Si-B-C-N and their Characterization", *Adv. Sci. Tech.*, **3B** (1995) 1291-1299
- [95Bir] M. Birot, J.-P. Pillot, J. Dunoguès, "Comprehensive Chemistry of Polycarbosilazanes, Polysilazanes, and Polycarbosilazanes as Precursors of Ceramics", *Chem. Reviews*, **95** [5] (1995) 1443-1478
- [95Fan] P. H. Fang, "On the  $\beta$ -C<sub>3</sub>N<sub>4</sub> Search", *J. Mater. Sci. Lett.*, **14** (1995) 536-538
- [95Hei] D. Heimann, J. Bill, F. Aldinger, "Oberflächenschutz von Si-infiltriertem CFC", in *Arbeits- und Ergebnisbericht (1995)*, SFB 259, Hochtemperaturprobleme rückkehrfähiger Raumtransportsysteme, University of Stuttgart, 95-122
- [95Lim] S.-K. Lim, H. L. Lukas, "Thermodynamische Optimierung des Systems B-C-Si und seiner Randsysteme", in G. Petzow, J. Tobolski, R. Telle (eds.), *DFG, Hochleistungskeramik, Herstellung, Aufbau und Eigenschaften*, VCh, Weinheim, (1995) 605-616
- [95Rie] R. Riedel, H.-J. Kleebe, H. Schönfelder, F. Aldinger, "A Covalent micro/nano-Composite Resistant to High-temperature Oxidation", *Nature*, **374** (1995) 526-528
- [95Roc] P. Rocabois, C. Chatian, C. Bernard, "Thermodynamics of the Si-C system. I. Mass Spectrometric Studies of the Condensed Phases at High Temperature", *High Temp. – High Pressures*, **27/28** (1995/1996) 3-23
- [95Sei] J. Seifert, H. L. Lukas, G. Petzow, "Computational Thermodynamics in Materials Science", *Design Fundamentals of High Temperature Composites, Intermetallics, and Metal-Ceramics Systems*, Edited by R. Y. Lin, Y. A. Chang, R. G. Reddy, C. T. Liu, The Minerals, Metals & Materials Society, (1995) 297-308
- [95Wid] T. Wideman, K. Su, E. E. Remsen, G. A. Zank, L. G. Sneddon, "Synthesis, Characterization and Ceramic Conversion Reactions of Borazine/Silazane Copolymers: New Polymeric Precursors to SiNCB Ceramics", *Chem. Mater.*, **7** (1995) 2203-2212



- [96Bil] J. Bill, "Vom Molekül zur Keramik", Werkstoffwoche '96, Symp. 7, (1996) 235-242
- [96Fra] R. Franke, St. Bender, I. Arzberger, J. Hormes, M. Jansen, H. Jüngermann, J. Löffelholz, "The Determination of Local Structural Units in Amorphous  $\text{SiBN}_3\text{C}$  by Means of X-Ray Photoelectron and X-Ray Absorption Spectroscopy", Fres. J. Anal. Chem., **354** (1996) 874-878
- [96Jal] A. Jalowiecki, J. Bill, F. Aldinger, "Interface Characterization of Nanosized B-Doped  $\text{Si}_3\text{N}_4/\text{SiC}$  Ceramics", Composites Part A, **27A** (1996) 717-721
- [96Kas1] B. Kasper, H. J. Seifert, A. Kußmaul, H. L. Lukas, F. Aldinger, "Entwicklung eines thermodynamischen Datensatzes für das System B-C-N-O-Si" in: F. Aldinger, H. Mughrabi (eds.), Werkstoffwoche '96, 28.-31.05.1996, Stuttgart, Symposium 7, Materialwissenschaftliche Grundlagen, DGM, (1996) 623-628
- [96Kas2] B. Kasper, Ph. D. Thesis, University of Stuttgart, Stuttgart, (1996)
- [96Kos] Z. G. Kostić, P. Lj. Stefanović, P. B. Pavlović, "Thermodynamic Consideration of Si-N and Si-H-N Systems for Silicon Nitride Powder Production in Thermal Plasma", Ceram. International, **22** (1996) 179-186
- [96Gor] W. Gorski, "Dilatometrie-Grundlagen und Meßverfahren", PTB-Bericht, Braunschweig, (1996)
- [96Grö] J. Gröbner, H. L. Lukas, F. Aldinger, "Thermodynamic Calculation of the Al-Si-C System", CALPHAD, **20** (1996) 247-254
- [96Mai] H. R. Maier, F. Schmitz, F. Philipps, "Einsatz des Laserflashverfahren bei keramischen Werkstoffen", IKKM / IPAK Seminar Aachen, (1996)
- [96Rie1] R. Riedel, A. Kienzle, W. Dressler, L. Ruwisch, J. Bill, F. Aldinger, "A Silicoboron Carbonitride Ceramic Stable to 2000°C", Nature, **328** (1996) 796-798
- [96Rie2] R. Riedel, J. Bill, A. Kienzle, "Review Boron-modified Inorganic Polymers-Precursors for the Synthesis of Multicomponent Ceramics", Appl. Organomet. Chem., **10** (1996) 241-256
- [96Rie3] R. Riedel, W. Dressler, "Chemical Formation of Ceramics", Ceram. International, **22** (1996) 233-239

- [96Roc] P. Rocabois, C. Chatillon, C. Bernard, "Thermodynamics of the Si-O-N System:I, High-Temperature Study of the Vaporization Behaviour of Silicon Nitride by Mass Spectrometry", *J. Am. Ceram. Soc.*, **79** [5] (1996) 1351-1360
- [96Sei1] H. J. Seifert, F. Aldinger, "Applied Phase Studies", *Z. Metallkd.*, **87** (1996) 841-853
- [96Sei2] J. Seitz, "Polymer-Pyrolyse-Keramik auf Si/C/N-Basis: Herstellung von Formkörpern, Strukturuntersuchungen und Tribologische Eigenschaften", Ph. D. Thesis, University of Stuttgart, Stuttgart, (1996)
- [96Sei3] J. Seitz, J. Bill, "Production of Compact Polysilazane-Derived Si/C/N-Ceramics by Plastic Forming", *J. Mater. Sci. Letters*, **15** (1996) 391-393
- [96Sei4] J. Seitz, F. Aldinger, "Polymer Derived Ceramics and their Preparation by Powder Technology", International Conference on Powder Metallurgy 4-7 July 1996, Cluj-Napoca, Romania
- [96Sei5] J. Seitz, J. Bill, N. Egger, F. Aldinger, "Structural Investigations of Si/C/N-Ceramics from Polysilazane Precursors by Nuclear Magnetic Resonance", *J. Europ. Ceram. Soc.*, **16** (1996) 885-891
- [97Ald] F. Aldinger, J. Bill, T. Wichmann, "Precursor-Derived Ceramics for Advanced Technologies", Editors: K. Niihara, S. Hirano, S. Kanzaki, K. Komeya, K. Morinaga, 6<sup>th</sup> International Symposium on Ceramic Materials and Components for Engines, Oct. 19-23 1997, Arita, Japan
- [97Bal] H.-P. Baldus, M. Jansen, "Moderne Hochleistungskeramiken - amorphe anorganische Netzwerke aus molekularen Vorläufern", *Angew. Chem.*, **109** (1997) 338-354
- [97Bha] R. T. Bhatt, "Heat Treatment Effects on the Tensile Properties and Microstructure of a SiC/RBSN Composite in Nitrogen", *Ceram. Int.*, **23** (1997) 109-113
- [97Jal] A. Jalowiecki, "Transmissionselektronenmikroskopische Untersuchung der Entmischung und der Kristallisation einphasiger, amorpher Polymer-Pyrolyse-Keramiken", Ph. D. Thesis, University of Stuttgart, Stuttgart, (1997)
- [97Jan] M. Jansen and H. Jüngermann, "A New Class of Promising Ceramics Based on Amorphous Inorganic Networks", *Solid State & Mater. Sci.*, **2** (1997) 150-157

- [97Lüc] J. Lücke, J. Hacker, D. Suttor, G. Ziegler, "Synthesis and Characterization of Silazane-Based Polymers as Precursors for Ceramics Matrix Composites", *Appl. Organomet. Chem.*, **11** (1997) 181-194
- [97Rie] R. Riedel, A. Greiner, G. Miehe, W. Dressler, H. Fuess, J. Bill, "Synthese der ersten kristallinen Feststoffe im ternären System Si-C-N", *Angew. Chem.*, **109** (1997) 657-660
- [97Wei] M. Weinmann, R. Haug, J. Bill, F. Aldinger, J. Schuhmacher, K. Müller, "Boron-Containing Polysilylcarbodi-imides: A New Class of Molecular Precursors for Si-B-C-N Ceramics", *J. Organomet. Chem.*, **541** [1-2] (1997) 345-353
- [98Ald] F. Aldinger, M. Weinmann, J. Bill, "Precursor-Derived Si-B-C-N Ceramics", *Pure & Appl. Chem.*, **70** [2] (1998) 439-448
- [98Bil] J. Bill, J. Seitz, G. Thurn, J. Dürr, J. Canel, B. Z. Janos, A. Jalowiecki, D. Sauter, S. Schempp, H. P. Lamparter, J. Mayer, F. Aldinger, "Structure Analysis and Properties of Si-C-N Ceramics Derived from Polysilazanes", *Phys. Stat. Sol. (a)* **166** (1998) 269-296
- [98Dür] J. Dürr, P. Lamparter, J. Bill, S. Steeb, F. Aldinger, "X-ray and Neutron Scattering Investigations on Precursor-derived  $\text{Si}_{24}\text{C}_{8+d43}\text{N}_{8+d33}$  Ceramics", *J. Non-Crystalline Solids*, **155** (1998) 232-234
- [98Her] M. Herrmann, C. Schubert, "Silicon Nitride/Silicon Carbide Nanocomposite Materials: I, Fabrication and Mechanical Properties at Room Temperature", *J. Am. Ceram. Soc.*, **81** [5] (1998) 1095-1108
- [98Lai] R. M. Laine, A. Sellinger, "Si-Containing Ceramic Precursors", in *The Chemistry of Organic Silicon Compounds*, Vol. 2, Z. Rappoport and Y. Apeloig, eds., J. Wiley & Sons Ltd. London, (1998) 2245-2310
- [98Lei] G. Leitner, "Thermische Ausdehnung - Basis und Anwendung in der Materialforschung", GEFTA Jahrestagung, Stuttgart, 1998
- [98Jün] H. Jüngermann, M. Jansen, "Quaternäre Keramiken im System Si/B/N/C aus polymeren Carbamidsäurederivaten", *Mat.-wiss. u. Werkstofftech.*, **29** (1998) 573-587

- [98Kam] T. W. Kamphowe, M. Weinmann, J. Bill and F. Aldinger, "Preparation of Fibre-Reinforced Si-B-C-N Ceramics by Polymer Precursor Infiltration", *Sil. Ind.*, **63** (1998) 159-162
- [98Kle] Kleykamp, H.: "Gibbs Energy of Formation of SiC: A Contribution to the Thermodynamic Stability of the Modifications", *Ber. Bunsen-Ges. Phys. Chem.* **102** [9] (1998) 1231-1234
- [98Rie] R. Riedel, L. M. Ruswisch, Linan An, R. Raj, "Amorphous Silicoboron Carbonitride Ceramic with Very High Viscosity at Temperatures above 1500°C", *J. Am. Ceram. Soc.*, **81** [12] (1998) 3341-3344
- [98Sau] N. Saunders, P. Miodownik, "CALPHAD (Calculation of Phase Diagrams): A Comprehensive Guide", in: R.W. Cahn (ed.), Pergamon, Oxford, Materials Series Vol. 1 (1998)
- [98Sch] S. Schempp, J. Dürr, P. Lamparter, J. Bill, S. Steeb, F. Aldinger, "Short Range and Medium Range Structure of Amorphous Si-C-N Ceramics by X-Ray and Neutron Diffraction" *Z. Naturforsch.*, **53a** 127 (1998) 127-133
- [98Sch] J. Schumacher, M. Weinmann, J. Bill, F. Aldinger, K. Müller, "Solid-State NMR Studies of the Preparation of Si-C-N Ceramics from Polysilylcarbodiimide Polymers", *Chem. Mater.* **10** [12] (1998) 3913-3922
- [98Sei1] H. J. Seifert, H. L. Lukas, F. Aldinger, "Development of Si-B-C-N Ceramics Supported by Phase Diagrams and Thermochemistry", *Ber. Bunsen-Ges. Phys. Chem.*, **102** [9] (1998) 1309-1313
- [98Sei2] H. J. Seifert, J. Peng, F. Aldinger, "Die Konstitution von Si-B-C-N Keramiken", in J. Heinrich, G. Ziegler, W. Hermel, H. Riedel, (eds.), *Proc. Werkstoffwoche '98, München, Vol. VII, Keramik/Simulation Keramik*, Wiley-VCH, Weinheim, (1999), 339-343
- [98Sri] D. Srivastava, E. N. Duesler, R. T. Paine, "Synthesis of Silylborazines and their Utilization as Precursors to Silicon-Containing Boron Nitride", *Eur. J. Inorg. Chem.*, (1998) 855-859
- [98Wei] M. Weinmann, R. Haug, J. Bill, M. Deguire, and F. Aldinger, "Boron-Modified Polysilylcarbodi-imides as Precursors for Si-B-C-N Ceramics: Synthesis, Plastic-

- forming and High-temperature Behavior” Appl. Organomet. Chem., **12** (1998) 725-734
- [98Wid] T. Wideman, P. J. Fazon, K. Su, E. E. Remsen, G. A. Zank, L. G. Sneddon, “Second-Generation Polymeric Precursors for BN and SiNCB Materials”, Appl. Organomet. Chem., **12** (1998). 681-693
- [98Wil] M. J. Wild, P. Buhler, “On the Phase Composition of Polymethylsiloxane Derived Ceramics”, J. Mater. Sci., **33** (1998) 5441-5444
- [99Bal] P. Baldus, M. Jansen, D. Sporn, “Ceramic Fibers for Matrix Composites in High-Temperature Engine Applications”, Science, **285** (1999) 699-702
- [99Bau] B. Baufeld, H. Gu, J. Bill, F. Wakai, F. Aldinger, “High Temperature Deformation of Precursor-derived Amorphous Si-B-C-N Ceramics”, J. Europ. Ceram. Soc., **19** (1999) 2797-2814
- [99Bil] J. Bill, F. Aldinger, “Precursor-Derived Covalent Ceramic”, in: J. Bill, F. Wakai, F. Aldinger, (eds.), Precursor-Derived Ceramics, Wiley-VCH, Weinheim, New York, (1999) 33-51
- [99Har] P.A.G. O’Hare, I. Tomaszekiewicz, C. M. Beck II, H. J. Seifert, “Thermodynamics of Silicon Nitride. I. Standard Molar Enthalpies of Formation at the Temperature 298.15 K of  $\alpha$ -Si<sub>3</sub>N<sub>4</sub> and  $\beta$ -Si<sub>3</sub>N<sub>4</sub>”, J. Chem. Thermodynamics, **31** (1999) 303-322
- [99Hau] R. Haug, M. Weinmann, J. Bill and F. Aldinger, “Plastic Forming of Preceramic Polymers”, J. Europ. Ceram. Soc., **19** (1999) 1-6
- [99Lia] J.-J. Liang, L. Topor, A. Navrotsky, A. Mitomo, “Silicon nitride: Enthalpy of formation of the  $\alpha$ - and  $\beta$ -polymorphs and the effect of C and O impurities”, J. Mater. Res., **14** (1999) 1959-1968
- [99Jün] H. Jüngermann, M. Jansen, “Synthesis of an Extremely Stable Ceramic in the System Si/B/C/N Using 1-(trichlorosilyl)-1-(dichloroboryl)ethane as a Single-Source Precursor”, Mater. Res. Innovat., **2** (1999) 200-206
- [99Kam] T. W. Kamphowe, “Neue Siliciumorganische Precursoren für Hochtemperaturbeständige Keramische Faserverbundwerkstoffe”, Ph. D. Thesis, University of Stuttgart, Stuttgart, (1999)

- [99Sei1] H. J. Seifert, F. Aldinger, “Thermodynamic Calculations in the System Si-B-C-N-O”, in: J. Bill, F. Wakai, F. Aldinger, (eds.), *Precursor-Derived Ceramics*, Wiley-VCH, Weinheim, New York, (1999) 165-174
- [99Sei2] H. J. Seifert, “Reaction Path Simulations in Multicomponent Materials”, *Z. Metallkd.*, **90** (1999) 1016-1024
- [99Wei] M. Weinmann, T. Kamphowe, J. Bill, F. Aldinger, “Synthese borhaltiger Polysilazane durch Hydrosilylierungsreaktionen von Hydridosilylethylboranen mit vinylierten Polysilazanen sowie deren Überführung in keramische Materialien”, Deutsches Patent Nr. 197 41 460 A 1 (1999)
- [00Bil] J. Bill, J. Schuhmacher, K. Müller, S. Schempp, J. Seitz, J. Dürr, HP. Lamparter; J. Golczewski, J. Peng, H.J. Seifert, F. Aldinger: “Investigations on the Structural Evolution of Amorphous Si-C-N Ceramics from Precursors” , *Z. Metallkd.*, **91** [4] (2000) 335-351
- [00Pen1] J. Peng, H. J. Seifert, and F. Aldinger, “Thermal Analysis of Si-C-N Ceramics Derived from Polysilazanes”, in G. Müller (editor), “Ceramics –Processing, Reliability, Tribology and Wear”, *EUROMAT 99 – Volume 12*, Wiley-VCH, (2000) 120-126
- [00Pen2] J. Peng, H. J. Seifert, F. Aldinger, “Thermal Stability of Precursor-Derived Si-(B-) C-N Ceramics”, in: Bansal Norottam P. and Singh J. P. (eds.) *Innovative Processing and Synthesis of Ceramics, Glasses, and Composites IV*, *Ceramic Transactions*, volume 115, The American Ceramic Society, Westerville, Ohio, (2000) 251-262
- [00Rie] R. Riedel, E. Kroke, Y. L. Li, C. Konetschny, E. Lecomte, C. Fasel, “Silazane Derived Ceramics and Related Materials”, *Materials Science & Engineering Reports*, **R26**, no.4-6, 3 (2000) 97-199
- [00Sch] J. Schuhmacher, “Festkörper-NMR-Untersuchungen zur Umwandlung von Polysilazanen und Polysilycarbodiimiden in Si-(B)-C-N-Keramiken”, Ph. D. Thesis, University of Stuttgart, Stuttgart, (2000)
- [00Wan] Z. C. Wang, T. W. Kamphowe, S. Katz, J. Peng, H. J. Seifert, J. Bill, F. Aldinger, “Effects of Polymer Thermolysis on Composition, Structure and High-

- temperature Stability of Amorphous Silicoboron Carbonitride Ceramics”, J. Mater. Sci. Lett., **19** (2000) 1701-1704
- [00Wei] M. Weinmann, J. Schuhmacher, H. Kummer, S. Prinz, J. Peng, H. J. Seifert, K. Müller, J. Bill, F. Aldinger, “ Synthesis and Thermal Behavior of Novel Si-B-C-N Ceramic Precursors”, Chem. Mater., **12** (2000) 623-632
- [00Wic] T. Wichmann, A. Zern, J. Bill, F. Aldinger, private communication, (2000)
- [00Mül] A. Müller, private communication, (2000)
- [01Bil] J. Bill, T. W. Kamphowe, A. Müller, T. Wichmann, A. Zern, M. Weinmann, J. Schuhmacher, K. Müller, J. Peng. H. J. Seifert, F. Aldinger, “Precursor-Derived Si-(B-)C-N Ceramics - Thermolysis, Amorphous State and Crystallization”, Appl. Organomet. Chem., **15** (2001) 777-793
- [01Cai] Y. Cai, A. Zimmermann, S. Prinz, F. Phillipp and F. Aldinger, “Nucleation Phenomena of Nano-crystallites in As-pyrolysed Si-B-C-N Ceramics”, Scripta Materialia, **45** (2001) 1301-1306
- [01Hau] J. Haug, F. Aldinger, private communication, (2001)
- [01Hil] M. Hillert, “The Compound Energy Formalism”, J. of Alloys and Compounds, **320** (2001) 161-176
- [01Hör] M. Hörz, “Synthese, Charakterisierung und Thermolyse von SiBC(N)-Precursoren durch dehydrierende Kupplungsreaktionen von Tris(hydridosilyl-ethyl)boranen”, Diplomarbeit, University of Stuttgart, Stuttgart, (2001)
- [01Sei1] H. J. Seifert, J. Peng, H. L. Lukas, F. Aldinger, “ Phase Equilibria and Thermal Analysis of Si-C-N Ceramics”, J. of Alloys and Compounds, **320** (2001) 251-261
- [01Sei2] H. J. Seifert, J. Peng, J. Golczewski, F. Aldinger, “ Phase Equilibria of Precursor-derived Si-(B-)C-N Ceramics”, Applied Organometallic Chemistry, **15** [10] (2001) 794-808
- [01Wei] M. Weinmann, A. Zern, F. Aldinger, ” Stoichiometric Silicon Nitride/Silicon Carbide Composites from polymeric Precursors,“ Adv. Mater., (2001), accepted for publication
- [01Zha] Y. Zhang, A. Navrotsky, “Preliminary Results on Drop Solution Calorimetry Experiments of Si-C-N”, private communication, (2001)

- [02Sei] H. J. Seifert, F. Aldinger, “ Phase Equilibria in the Si-B-C-N System”, in: M. Jansen (ed.) High Temperature Ceramics, Structure and Bonding Series, Springer-Verlag, Heidelberg (2002), in print



## Lebenslauf

<b>Personalien</b>	Name	Jianqiang PENG
	Geburtsdatum	22.04.1964
	Geburtsort	Innere Mongolei, China
	Familienstand	Verheiratet, 2 Kinder
<b>Schulbildung</b>	01.1972—07.1977	Grundschule
	09.1977—07.1982	Mittelschule u. Oberschule
	07.1982	Reifeprüfung
<b>Studium:</b>	09.1982—07.1986	Metallphysik an der „University of Science and Technology Peking“ Diplomarbeit mit dem Thema „ODF Texturanalyse von Feiblech aus Si-Stahl“
	10.1995—09.1996	Werkstoffkunde an der Universität Stuttgart
	10.1996—10.1997	Werkstoffwissenschaften an der Technischen Universität Clausthal Diplomarbeit mit dem Thema „Ermittlung röntgenographischer Elastizitätskonstanten keramische Spritzschichten“
<b>Promotion</b>	seit 01.11.1997	Wissenschaftliche Tätigkeit am Max-Planck-Institut für Metallforschung und an der Universität Stuttgart, Abteilung Prof. Aldinger, PML, mit dem Ziel der Promotion
<b>Fortbildung</b>	05.1992—06.1992	Alterung durch Schwingung und Eigenspannungsmessung an der „Dalian University of Technology“
	10.1995—09.1996	Spannungsanalyse und Festigkeitslehre an der staatlichen Materialprüfungsanstalt (MPA) der Universität Stuttgart
<b>Berufstätigkeiten</b>	08.1986—10.1995	Ingenieur am Institut für Metallurgie, der Baotou Eisen- und Stahl Company, China
	seit 01.11.2000	Wissenschaftlicher Angestellter am Max-Planck-Institut für Metallforschung und an der Universität Stuttgart, Abteilung Prof. Aldinger, PML

致谢：

包头钢铁公司

北京科技大学

土左旗察素齐一中

献给我的祖国

彭建强

2002 年 于德国